STATE OF CHARGE DEPENDENT THERMAL RUNAWAY DETECTION OF LITHIUM-ION BATTERY UNDER MECHANICAL ABUSE CONDITIONS

MUHAMMAD BASEER UR REHMAN SHEIKH

A thesis submitted in partial fulfilment of the requirements of the University of Sunderland for the degree of Doctor of Philosophy

March 2018

Abstract

With the high industrial acceptance of lithium-ion batteries as an electric vehicle (EV) energy source, it is necessary to examine these batteries for critical safety issues. The contribution of this research is to investigate the state of charge (SOC) dependent thermal runaway detection of 18650 lithium-ion batteries due to mechanical abuse conditions. To achieve accurate results, an experimental setup was designed to capture temperature variations and deformation of the battery due to loading conditions, where four test protocols were used which were rod, circular punch, three-point bend and flat plate. The numerical simulation model was used for the battery layered model where the concentric layered formation was used for the single battery model. The proposed numerical simulation model integrates both temperature and structural changes.

To ensure accuracy, validation of the numerical simulation model was achieved by comparing these results with experimental results. The validation analysis of battery behaviour shows that the compared results are in good correlation with experimental work and the numerical simulation model can be used for the single battery layered model. Furthermore, numerical simulation analysis of impact load is conducted where results, using quasi-static and impact load, are compared to understand sequential failures and short circuit leading to thermal runaway.

Deformation of cells mimics thermal runaway where various thermal runaway detection strategies are employed in this work, including; force-displacement, voltage-temperature, stress-strain, SOC dependency and separator failure. Results show that a cell can undergo severe conditions even with no fracture or

rupture, which may be slow to develop but they can lead to catastrophic failures. Short circuit displacement was used as an indication of initial failure for all test conditions and mean short circuit displacement was 6.94mm for all test protocols. Numerical simulation results show that with the moderate number of elements where element size is 1mm for active materials and current collectors, better results can be achieved.

Acknowledgments

First and foremost, I would like to give the definitive thanks to Allah for everything he has given me in my life. I would like to thank my supervisor Professor Ahmed Elmarakbi for his guidance, encouragement, efforts and cooperation. I am happy to have him my supervisor who has benefited me a lot. I would also acknowledge the contribution advices of Dr David Baglee and Dr Michael Knowles throughout my research.

I would like to thank all the staff at Automotive and Manufacturing Advanced Practice (AMAP), university of Sunderland, especially Roger Obrien, Adrian Morris, Phil Johnson and John Cheal, who were supportive and encouraging.

I would also thank Brian Britton, from Gestamp ltd. Gateshead, for lending me the load cell for this research.

I do owe special thanks to my parents who are always supporting and encouraging with their best wishes.

I would like to thank my siblings for continuous support and understanding. I would also like to thank my well-wishers, Dr Najla Yousaf Mussa and Dr Muhammad Irfan Alam.

Finally, I would like to give special thanks and acknowledgement for the great and continuous help, patience, and encouragement that I received from my wife.

Table of Contents

List of Figures

List of Tables

Nomenclature

σ_n	Nominal stress
F	Force applied
A	Area of contact
l_c	Length of the cell
b_c	width of the contact
ε_n	Nominal strain
ε_{nr}	Nominal strain for rod test
σ_{nr}	Nominal stress for rod test.
ε_{nt}	Nominal strain for three-point bending test
σ_{nt}	Nominal stress for three-point bending test
ε_{nc}	Nominal strain for circular punch
σ_{nc}	Nominal stress for circular punch test
ε_{nf}	Nominal strain for flat plate test
σ_{nf}	Nominal stress for flat plate test
E_{cf}	Compression modulus for flat plate deformation

ε_{fr}	Failure strain for rod test
σ_{fr}	Failure stress for rod test
ε_{fc}	Failure strain for circular punch test
σ_{fc}	Failure stress for circular punch test
ε_{ft}	Failure strain for three point bending test
σ_{ft}	Failure stress for three-point bending test
ε_{ff}	Failure strain for flat plate deformation test
σ_{ff}	Failure stress for flat plate deformation
F_{r0}	Applied force for 0% SOC rod test
d_{sr0}	Displacement at short circuit for 0% SOC rod test
T_{ir0}	Initial temperature before short circuit for 0% SOC rod test
T_{fr0}	Final temperature for 0% SOC rod test
ΔT_{r0}	Change in temperature for 0% SOC rod test
V_{r0}	Voltage for 0% SOC rod test
ε_{nr0}	Nominal failure strain for 0% SOC rod test
σ_{nr0}	Nominal failure stress for 0% SOC rod test
F_{r25}	Applied force at 25% SOC, rod test

d_{sr25}	Displacement at short circuit for 25% SOC rod test
T_{ir25}	Initial temperature before short circuit at 25% SOC, rod test
T_{fr25}	Final temperature at 25% SOC, rod test
ΔT_{r25}	Change in temperature at 25% SOC, rod test
V_{r25}	Voltage at 25% SOC, rod test
ε_{nr25}	Nominal failure strain for 25% SOC rod test
σ_{nr25}	Nominal failure stress for 25% SOC, rod test
F_{r50}	Applied force at 50% SOC, rod test
d_{sr50}	Displacement at short circuit for 50% SOC, rod test
T_{ir50}	Initial temperature before short circuit at 50% SOC, rod test
T_{fr50}	Final temperature at 50% SOC, rod test
ΔT_{r50}	Change in temperature at 50% SOC, rod test
V_{r50}	Voltage at 50% SOC, rod test
ε_{nr50}	Nominal failure strain for 50% SOC rod test
σ_{nr50}	Nominal failure stress for 50% SOC, rod test
F_{r75}	Applied force at 75% SOC, rod test
d_{sr75}	Displacement at short circuit for 75% SOC, rod test

T_{ir75}	Initial temperature before short circuit at 75% SOC, rod test
T_{fr75}	Final temperature at 75% SOC, rod test
ΔT_{r75}	Change in temperature at 75% SOC, rod test
V_{r75}	Voltage at 75% SOC, rod test
ε_{nr75}	Nominal failure strain for 75% SOC rod test, rod test
σ_{nr75}	Nominal failure stress for 75% SOC, rod test
F_{c0}	Applied force for 0% SOC circular punch test
d_{sc0}	Displacement at short circuit for 0% SOC circular punch test
T_{ic0}	Initial temperature before short circuit for 0% SOC circular punch test
T_{fc0}	Final temperature for 0% SOC circular punch test
ΔT_{c0}	Change in temperature for 0% SOC circular punch test
V_{c0}	Voltage for 0% SOC circular punch test
ε_{nc0}	Nominal failure strain for 0% SOC circular punch test
σ_{nc0}	Nominal failure stress for 0% SOC circular punch test
F_{c25}	Applied force at 25% SOC, circular punch test
d_{sc25}	Displacement at short circuit for 25% SOC circular punch test

T_{ic25}	Initial temperature before short circuit at 25% SOC, circular punch test
T_{fc25}	Final temperature at 25% SOC, circular punch test
ΔT_{c25}	Change in temperature at 25% SOC, circular punch test
V_{c25}	Voltage at 25% SOC, circular punch test
ε_{nc25}	Nominal failure strain for 25% SOC circular punch test
σ_{nc25}	Nominal failure stress for 25% SOC, circular punch test
F_{c50}	Applied force at 50% SOC, circular punch test
d_{sc50}	Displacement at short circuit for 50% SOC, circular punch test
T_{ic50}	Initial temperature before short circuit at 50% SOC, circular punch test
T_{fc50}	Final temperature at 50% SOC, circular punch test
ΔT_{c50}	Change in temperature at 50% SOC, circular punch test
V_{c50}	Voltage at 50% SOC, circular punch test
ε_{nr50}	Nominal failure strain for 50% SOC circular punch test
σ_{nc50}	Nominal failure stress for 50% SOC, circular punch test
F_{c75}	Applied force at 75% SOC, circular punch test
d_{sc75}	Displacement at short circuit for 75% SOC, circular punch test

T_{ic75}	Initial temperature before short circuit at 75% SOC, circular punch test
T_{fc75}	Final temperature at 75% SOC, circular punch test
ΔT_{c75}	Change in temperature at 75% SOC, circular punch test
V_{c75}	Voltage at 75% SOC, circular punch test
ε_{nc75}	Nominal failure strain for 75% SOC, circular punch test
σ_{nc75}	Nominal failure stress for 75% SOC, circular punch test
F_{t0}	Applied force for 0% SOC 3-pont bend test
d_{st0}	Displacement at short circuit for 0% SOC 3-pont bend test
T_{it0}	Initial temperature before short circuit for 0% SOC 3-pont bend test
T_{ft0}	Final temperature for 0% SOC 3-pont bend test
ΔT_{t0}	Change in temperature for 0% SOC 3-pont bend test
V_{t0}	Voltage for 0% SOC 3-pont bend test
ε_{nt0}	Nominal failure strain for 0% SOC 3-pont bend test
σ_{nt0}	Nominal failure stress for 0% SOC 3-pont bend test
F_{t25}	Applied force at 25% SOC, 3-pont bend test
d_{st25}	Displacement at short circuit for 25% SOC 3-pont bend test

T_{it25}	Initial temperature before short circuit at 25% SOC, 3-pont bend test
T_{ft25}	Final temperature at 25% SOC, 3-pont bend test
ΔT_{t25}	Change in temperature at 25% SOC, 3-pont bend test
V_{t25}	Voltage at 25% SOC, 3-pont bend test
ε_{nt25}	Nominal failure strain for 25% SOC 3-pont bend test
σ_{nt25}	Nominal failure stress for 25% SOC, 3-pont bend test
F_{t50}	Applied force at 50% SOC, 3-pont bend test
d_{st50}	Displacement at short circuit for 50% SOC, 3-pont bend test
T_{it50}	Initial temperature before short circuit at 50% SOC, 3-pont bend test
T_{ft50}	Final temperature at 50% SOC, 3-pont bend test
ΔT_{t50}	Change in temperature at 50% SOC, 3-pont bend test
V_{t50}	Voltage at 50% SOC, 3-pont bend test
ε_{nt50}	Nominal failure strain for 50% SOC 3-pont bend test
σ_{nt50}	Nominal failure stress for 50% SOC, 3-pont bend test
F_{t75}	Applied force at 75% SOC, 3-pont bend test
d_{st75}	Displacement at short circuit for 75% SOC, 3-pont bend test

T_{it75}	Initial temperature before short circuit at 75% SOC, 3-pont bend test
T_{ft75}	Final temperature at 75% SOC, 3-pont bend test
ΔT_{t75}	Change in temperature at 75% SOC, 3-pont bend test
V_{t75}	Voltage at 75% SOC, 3-pont bend test
ε_{nt75}	Nominal failure strain for 75%, 3-pont bend test
σ_{nt75}	Nominal failure stress for 75% SOC, 3-pont bend test
F_{f0}	Applied force for 0% SOC flat plate test
d_{sf0}	Displacement at short circuit for 0% SOC flat plate test
T_{if0}	Initial temperature before short circuit for 0% SOC flat plate test
T_{ff0}	Final temperature for 0% SOC flat plate test
ΔT_{f0}	Change in temperature for 0% SOC flat plate test
V_{f0}	Voltage for 0% SOC flat plate test
ε_{nf0}	Nominal failure strain for 0% SOC flat plate test
σ_{nf0}	Nominal failure stress for 0% SOC flat plate test
F_{f25}	Applied force at 25% SOC, flat plate test
d_{sf25}	Displacement at short circuit for 25% SOC flat plate test
T_{if25}	Initial temperature before short circuit at 25% SOC, flat plate test

T_{ff25}	Final temperature at 25% SOC, flat plate test
ΔT_{f25}	Change in temperature at 25% SOC, flat plate test
V_{f25}	Voltage at 25% SOC, flat plate test
ε_{nf25}	Nominal failure strain for 25% SOC flat plate test
σ_{nf25}	Nominal failure stress for 25% SOC, flat plate test
F_{f50}	Applied force at 50% SOC, flat plate test
d_{sf50}	Displacement at short circuit for 50% SOC, flat plate test
T_{if50}	Initial temperature before short circuit at 50% SOC, flat plate test
T_{ff50}	Final temperature at 50% SOC, flat plate test
ΔT_{f50}	Change in temperature at 50% SOC, flat plate test
V_{f50}	Voltage at 50% SOC, flat plate test
ε_{nf50}	Nominal failure strain for 50% SOC flat plate test
σ_{nf50}	Nominal failure stress for 50% SOC, flat plate test
F_{f75}	Applied force at 75% SOC, flat plate test
d_{sf75}	Displacement at short circuit for 75% SOC, flat plate test
T_{if75}	Initial temperature before short circuit at 75% SOC, flat plate test
T_{ff75}	Initial temperature at 75% SOC, flat plate test

ΔT_{f75}	Change in temperature at 75% SOC, flat plate test
V_{f75}	Voltage at 75% SOC, flat plate test
ε_{nf75}	Nominal failure strain for 75% SOC, flat plate test
σ_{nf75}	Nominal failure stress for 75% SOC, flat plate test

Chapter 1: Introduction

1.1 Research background

With the high industrial acceptance of lithium-ion batteries as an electric vehicle (EV) energy source, it is necessary to examine these batteries for critical safety issues. Safety of these batteries is addressed widely with several combinations, and new testing techniques are being implemented to avoid well-known safety concerns which will enhance battery life and lead to better and reliable use in the EV fleet. Abusive conditions for lithium-ion batteries is one of the concerns in this regard where these issues are not discussed in great detail. Abusive conditions for batteries varies and depends on operating conditions as well as environmental impacts (Lotfi, *et al*., 2013; Jeon and Baek, 2011; Wang, *et al*., 2011).

EVs still face criticism due firstly to *range anxiety* where the concern is that a car will run out of charge before it has reached its intended destination. Another issue which has recently received attention in the press is the fact that on several occasions the battery pack has ruptured and exploded. Two battery fires caused Mitsubishi to halt production of the all-electric i-MiEV. It has been suggested that after a small incident the battery pack was slightly damaged and the pack overheated (Morris, 2013).

Recent battery incidents have brought many challenges for the battery manufacturers, in particular, safety. In the USA, the National Highway Traffic Safety Administration (NHTSA), organises safety testing of electrified vehicles where certain measures are taken to evaluate the safety of these vehicles in addition to Federal Motor Vehicle Safety Standards (FMVSS). Safety rating of vehicles is used where crashworthiness of vehicles is tested and assigned these ratings accordingly by NHTSA. The first reported battery incident during testing was reported in 2011, when NHTSA performed a side crash test of a plug-in hybrid electric vehicle, Chevy Volt (Smith, 2012). After the test, when the vehicle was parked in the garage, the battery pack caught fire after one week of the original testing, which did not harm personnel but the battery pack was destroyed. After investigation, the NHTSA report could not replicate the original fire, however, they designed the environment in which original vehicles are tested during evaluation. Similar incidents on a Tesla Model “S” captured media attention and criticism from the users. A series of three vehicle incidents occurred in Tesla's Model “S” where the battery pack caught fire due to crashes. Out of those three incidents, two were the result of a vehicle hitting debris which ruptured battery pack underneath the floor and on one occasion, due to a high-speed vehicle collision, the battery pack caught fire (Lingeman, 2013; Moloughney, 2013). One of the reason for media and public attention was the 5-star rating awarded by NHTSA. Figure 1.1, shows a Tesla Model “S” fire after an incident where the car hit debris. Immediate precautions were implemented by Tesla where a thick firewall was used for battery pack

protection (Musk, 2014). Independent investigators reported these Tesla incidents as the occurrence of thermal runaway, where heat generation of batteries exceeded heat dissipation, and uncontrolled temperature leads to a battery fire. The type of batteries used in the Tesla Model “S” are cylindrical 18650 lithium-ion batteries. Tesla’s model “S” fire after an incident reported in Seppala (2013) is shown in figure 1.1.

Figure 1.1: Tesla model “S” fire after an incident (Seppala, 2013)

Similar battery failures were observed during the current research work, where large format lithium-ion batteries used in other projects caught fire on three separate occasions. On two of the occasions, the batteries used were 90Ah LiFePO4, where, in the first event, the 90 Ah battery was overcharged which affected the battery and after some time the battery started swelling and then a release of gas and smoke was observed. Due to its different nature, no data

about electrical and thermal characteristics is available. On another occasion, the battery module which had 30 batteries connected in series, caught fire, where one of the batteries had a loose connection which caused unbalanced voltages in the module, and after some time the battery plugged in the middle of the module caught fire due to heat generation inside the battery. Figures 1.2 (a, b, and c), show a battery pack fire in the lab.

(a)

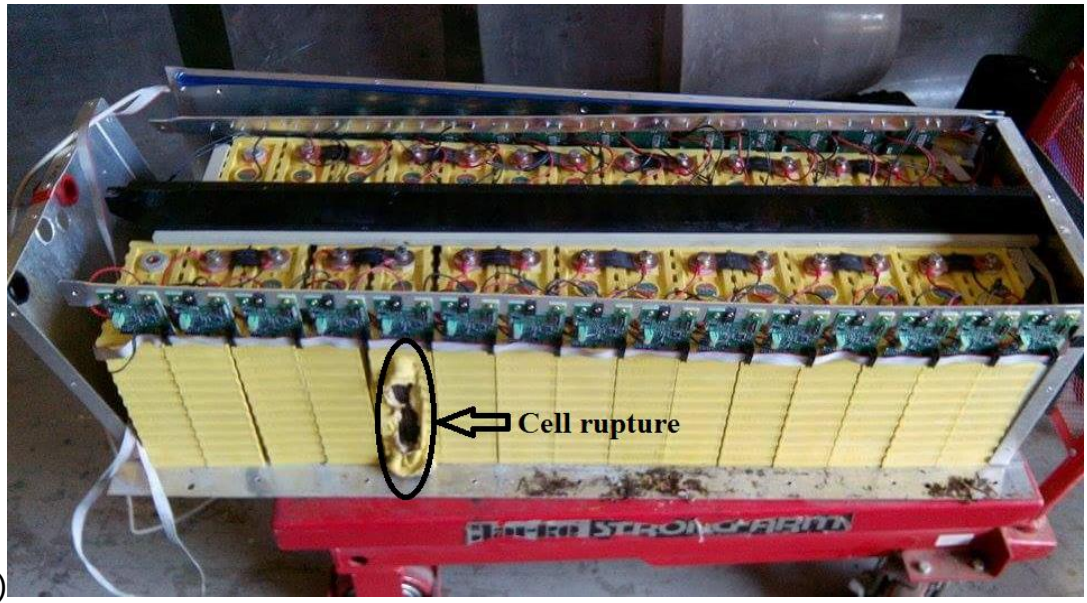

(b)

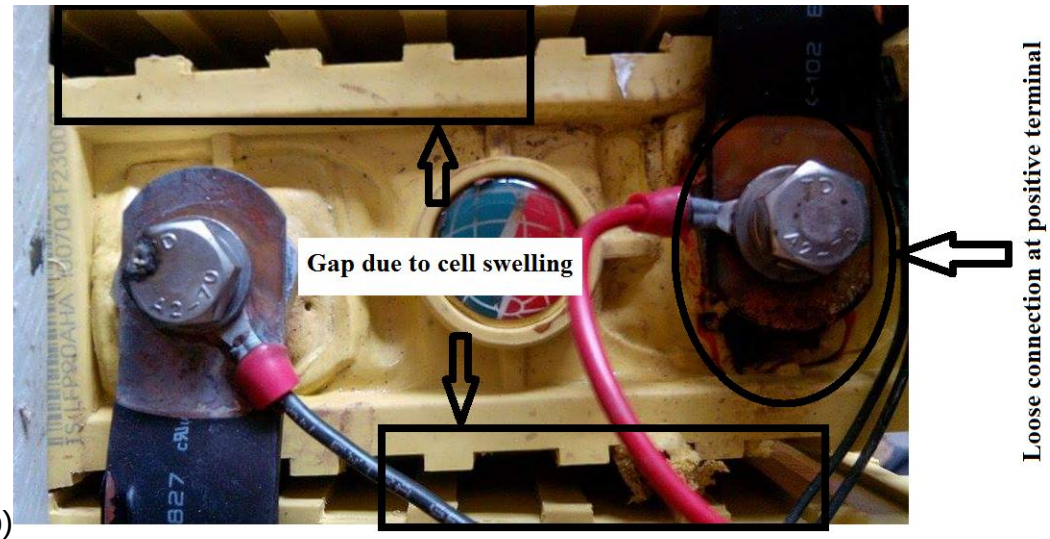

(c)

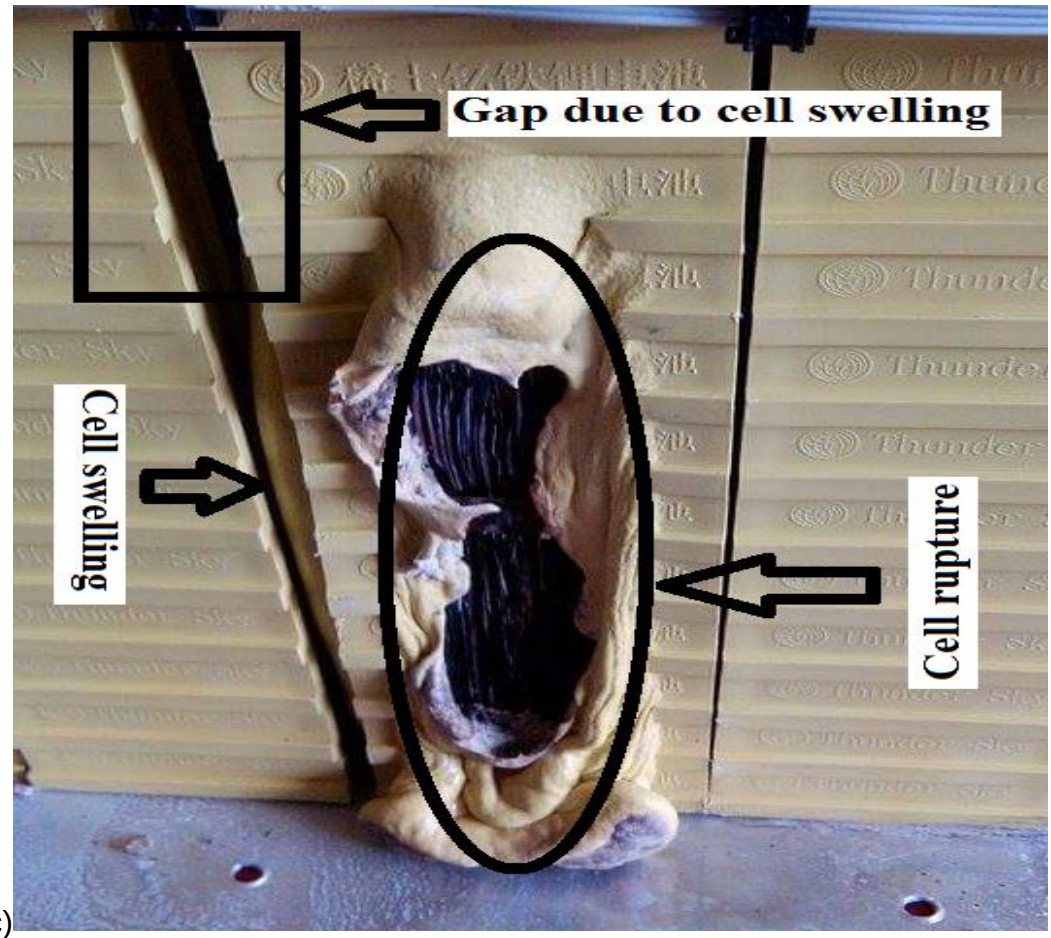

Figure 1.2: (a) Battery module with ruptured cell after fire, (b) loose connection which initiated degradation, (c) casing damage and swelling

Tesla model “S” incidents and battery fire incidents in the lab are few in the examples of battery failure due to abusive conditions. It is also evident that the occurrence of failure and failure response varies due to the type of abuse but in all the above mentioned cases, battery failure led to thermal runaway. Thermal runaway is the event which takes place due to battery failures which is evident from the literature (Liu, *et al*., 2017; Lei, *et al*., 2017; Wang, *et al*., 2016; Escobar-Hernandez, *et al*., 2016; Shan, 2016; Melcher, *et al*., 2016; Mendoza,

et al., 2015) but thermal runaway detection due to operating conditions is not found in the literature.

Available literature indicates various types of battery failures and failure response due to abusive conditions, such as nail penetration, mechanical crush, heating up cells, amongst others. Little research has, however, investigated the Sate of Charge (SOC) dependent thermal runaway failures. Liu, *et al*. (2017), have investigated the effects of the SOC and the charging–discharging process on the thermal runaway of 18650 lithium-ion batteries. In their study, electric heating, used to initiate thermal runaway and effects of SOCs on the thermal runaway, are considered, however short circuit initiation and sequential failures are not considered; in addition the temperature change rate was not involved. The lack of research in this area of research, as well as the vital role of the mechanical failure on the battery safety and stability, directed us to investigate this issue in detail. In this research cylindrical 18650 batteries with lithium cobalt dioxide chemistry are used.

1.2 Overview and research hypothesis

The purpose of this research is to detect early signs of thermal runaway. Thermal runaway of lithium-ion batteries depends on operating conditions, battery capacity and type of abuse. Due to mechanical abuse conditions severity of short circuit leading to thermal runaway varies. While constant monitoring of the battery's behaviour is essential for safety, there is a great

chance of detecting signs of thermal runaway due to state of charge (SOC) dependent mechanical failures.

Current research starts by investigating battery testing techniques, where different techniques are implemented to capture battery data for all stages of testing. Four test protocols including rod, circular punch, three-point bend and flat plate are designed to investigate battery failures due to mechanical abuse conditions, where a quasi-static loading approach is used. Post-failure structural analysis of the battery is an important technique where battery failure patterns, including deformation, crack or fracture are used to understand detailed failures and their effects on battery degradation.

Temperature variations inside individual cells leads to uneven temperature distribution among in-series/parallel connected cells which can lead to permanent damage if not controlled at the cell level. For this purpose temperature analysis using rate of temperature change, short circuit temperature and maximum peak temperature are analysed to understand temperature variations at all stages of battery testing. Voltage and temperature variations are considered an indication of battery degradation in the case of mechanical load.

To validate structural deformation and temperature distribution, various numerical simulation tools are available to researchers but in the current research an LS-DYNA numerical simulation tool is used to analyse mechanical deformation of a battery at different stages of failures. Separator layer failures

are often indicated as early signs of battery failure (Zhang et al., 2016; Zhang et al., 2015b), so in the current research separator failure analysis is conducted for circular punch test and three-point bend test. Experimental work and numerical simulation for validation of experimental results are detailed in this thesis. Based on the above overview following hypotheses are used to detect early signs of thermal runaway.

- At high SOC values, temperature variations will be high compare to low SOC values
- Severity of outcome depends on operating conditions as well as mechanical load type
- High temperature change rate and mean peak temperatures are important to understand initial cell failures
- Numerical simulation approach using concentric layered model can be useful to predict better accuracy due to quasi-static loading

1.3 Research objectives

To understand battery failures and propagation of thermal runaway, the following objectives were set.

- Design of test setup to capture and record maximum battery data due to mechanical failure.
- Quasi-static loading test to understand deformations of battery.

- Force-displacement and voltage-temperature monitoring in the case of different loading conditions.
- SOC dependency of battery, where force applied and displacement concerning SOC are important indicators.
- Implementing finite element analysis (FEA) techniques where mechanical failures are considered to determine deformation and fracture of cells.
- FEA analysis for temperature variations and separator failures in 18650 cylindrical lithium-ion batteries.

1.4 Thesis structure

This chapter covers the background and rationale of this research where safety aspects of the lithium-ion battery are discussed in relation to some EV crashes and their effects. Emphasis is given to highlighting battery safety and initiation of thermal runaway. The following paragraphs cover chapters detailing the research outline.

Chapter two focuses on lithium-ion batteries and their applications for the automotive industry; considering the needs for modelling lithium-ion batteries for efficient and safe operations. Different battery models are considered where the main purpose is to understand more about battery performance estimation in cases of all kinds of abuse conditions. Existing battery models, along with their modelling techniques, relevant results, conclusions extracted from those results and drawbacks will be reviewed in great detail. The literature review will include

critical battery parameters, battery construction, components of battery and battery testing using experimental and simulation techniques. The type of battery with fundamental parameters and experimental set-up will be discussed in chapter three, where all the key experimental sections are included. Battery conditioning to battery testing of all types of equipment will be discussed in depth where the formation of the test set up with particular devices is also discussed. Initial testing results are also presented which mostly link to initial battery testing with various configurations. Battery failures are compared and discussed in detail for further analysis.

Chapter four discusses the significant results from different loading conditions where detail is included of test scenarios and precautions taken for each test. This chapter presents the explanation of individual cell results and their perspective behaviour during each loading condition, with initial and final results of electrical and thermal response in the case of mechanical abuse conditions. All abuse conditions are tested on various cells where different state of charge (SOC) values are used to document effects of SOC on mechanical abuse of lithium-ion batteries. In particular, this chapter identifies parameters useful for failure analysis and thermal behaviour change.

In chapter five, LS-Dyna numerical simulations are discussed with the type of materials used and their parameters. In the beginning, 9 layer single stacks were used for initial model, and then those models were extended for layered model covering the full cell. All quasi-static loading conditions are discussed with layered formations. Layer thickness and contact cards with specified

boundary conditions are also considered. Comparison of simulation results for quasi-static and impact load are also presented where all cases are explained in detail. Several criteria have been chosen to detect early signs of thermal runaway which include cascaded layer failures to individual layer failures. Separator layers are given importance for this purpose. The results are compared with the experimental work to analyse and compare loading conditions and failure associated with applied load.

Chapter six, explains the novel aspects of this study which include major techniques used, results and their impact and limitations of this research. Recommendation for future work is also included in this chapter in great detail.

Chapter 2: Literature Review

This chapter covers the background and available literature related to lithium-ion batteries and their safety. The literature review suggests three main categories on which to focus, which are lithium-ion battery technology, battery testing and validation of results. The first part covers details about battery types used and their unique characteristics whereas in the second part testing of batteries is discussed with various abusive conditions and in the third part battery simulation techniques are discussed. Focus is given to critically discussing available research outcomes which link to this research and citing the results. This chapter clarifies the rationale of this research.

2.1 Introduction

With the growing demand for emission control and environmental friendliness, electric vehicles (EVs) are becoming a reliable choice to tackle emission problems and protect the environment with their safe and reliable propulsion system. Batteries play an important role in EVs which replace the fuel tank with a large battery pack. Battery pack size and weight vary with the type of battery used and the formation of the battery in the EV. Battery structure varies with manufacturer and two common types used are the tunnel formation (where the battery pack is in the shape of a 'T') and floor formation where the battery pack covers the floor, and the tunnel area is removed, giving more comfort to rear seat occupants (Xia, *et al*., 2014). The study of battery types, their properties and their application will help in the understanding of battery characteristics and

behaviour during various operating (Jarett and Kim, 2014) and abuse conditions (Le, *et al*., 2015). Abuse testing of EV batteries is challenging as a real time environment is required to perform static and dynamic testing of batteries. For this purpose specialised test equipment were used which have a number of controls covering all aspects of the battery.

As a result of battery abuse conditions, various degradation phenomena affect battery performance. Thermal runaway is one of the events which occurs when, due to battery failure, battery heat generation increases (Bazinski and Wang, 2015; Le, *et al*., 2015) and heat dissipation is less than heat generation. If heat generation is not controlled at the beginning or within a safe operating window, then the battery can undergo severe damage or catastrophic events which can lead to fire or explosion.

A detailed literature review is discussed in the following sections, where the type of batteries used in the EVs, battery safety, battery modelling and testing are considered. Analytical and finite element models are also discussed.

2.2 Battery safety systems

Safety devices are one of the options being used with lithium-ion batteries according to application requirements. Safety of batteries needs to be addressed at the cell, module, pack and ultimately vehicle level, so the types of safety systems may vary according to the application. Failure at one level can quickly escalate to much more severe failures at a higher level (Wang, *et al*., 2014; Doughty and Roth, 2012). Commonly employed safety devices are a

shutdown separator, cell vent, positive temperature coefficient (PTC) devices, current limiting fuses, diodes and battery management system (BMS) (Kim, *et al*., 2012; Doughty and Roth, 2012). Shutdown separators were used between anode and cathode preventing ionic conduction, which also helped to prevent a cell charge/discharge cycle in the case of an increase in internal temperature. Cell vent is used for the safe release of gases if excessive pressure builds up within cells. Application of specific current interrupt devices is used to provide protection against over-current.

Positive temperature coefficient (PTC) devices are placed in the cell header to limit high current to a safe level. Specifically the excessive current through the device causes internal heating which raises the temperature of the PTC and results in an increase in its resistance (Littlefuse, 2017). Current limiting fuses can be used to replace PTCs when a sustained discharge is not preferred.

Diodes are also being used to prevent inadvertent charging or to steer the discharge current around a weak cell as in a discharge (bypass diode) (Doughty and Roth, 2012).

Battery management systems (BMS) are being used in electric vehicles to protect the cells and battery packs from being damaged, to make the batteries operate within the proper voltage and temperature interval, guarantee the safety and prolong their service life as long as possible, and to maintain the batteries to operate in a state that the batteries may fulfil the vehicle requirements (Woodbank Communications Ltd, 2005).

To provide safe operation and optimum performance, lithium-ion battery packs must be supervised by an electronic BMS that monitors and services each of the individual cells. The features of a BMS depend on the application, but in most cases, functions including data acquisition, battery state determination, electrical management, thermal management and safety management are necessary (Jossen, *et al*., 1999). The design of the battery management system plays an important role in battery life preservation and performance improvement (Bowkett, *et al*., 2013). The advances in lithium-ion battery technology make it possible to power light-duty vehicles by using only electric power stored in a battery (collection of cells). HEV and EV are starting to play important roles in the trend towards vehicle electrification, which is of major interest to the automotive industry. In such trends towards vehicle electrification, it is of special importance to the automotive industry that battery endurance will guarantee proper function over a broad range of environmental and operational variations. The knowledge of battery life and degradation, therefore, becomes crucial to vehicle performance and perceived vehicle quality. The BMS performs many tasks including the measurement of system voltage, current and temperature, the cells' state of charge (SOC), the state of health (SOH), remaining useful life (RUL) determination, controlling and monitoring the charge/discharge characteristics and cell balancing (Spinner, *et al*., 2015a; Spinner, *et al*., 2015b; Bowkett, *et al*., 2013; Dawod, *et al*., 2011; Cao, *et al*., 2008; Moore and Schneider, 2001; Kutkut, and Divan, 1996). Some of the key features of lithium-ion batteries discussed by Chanson and Wiaux, 2013 are

important as the reference for the battery management system and battery protection using the mechanical and electrical design of battery pack. Battery chemistry is also important to understand safety concerns, where different chemistries are available and used depending on the applications.

2.3 Battery chemistry

Batteries are divided into different types according to their chemistry. Batteries with similar chemistry exhibit some unique characteristics and differ from each other. In EVs batteries having long calendar life, long cycle life, and high capacity, fast charge and discharge rate and light weight are selected for powering vehicles. Lithium-ion batteries are common power source for EVs and fulfil the desired power and energy requirements for EV applications. In this section lithium technology is discussed with respect to their chemistry and performance. Focus is given to battery type and chemistry mostly used in the EV fleet.

In lithium battery cells, lithium intercalation compounds are used as positive and negative electrodes (Yiu, 2011). These batteries follow the same chemical principles and designs as others with dominating lithium technology (Nguyen and Taylor, 2004). The lithium family is further divided with respect to cost, specific energy, specific power, safety, performance and life span. As shown in figure 2.1 (Battery university, 2017), each type has its advantages and shortcomings but selection of battery type depends on application and specific requirements.

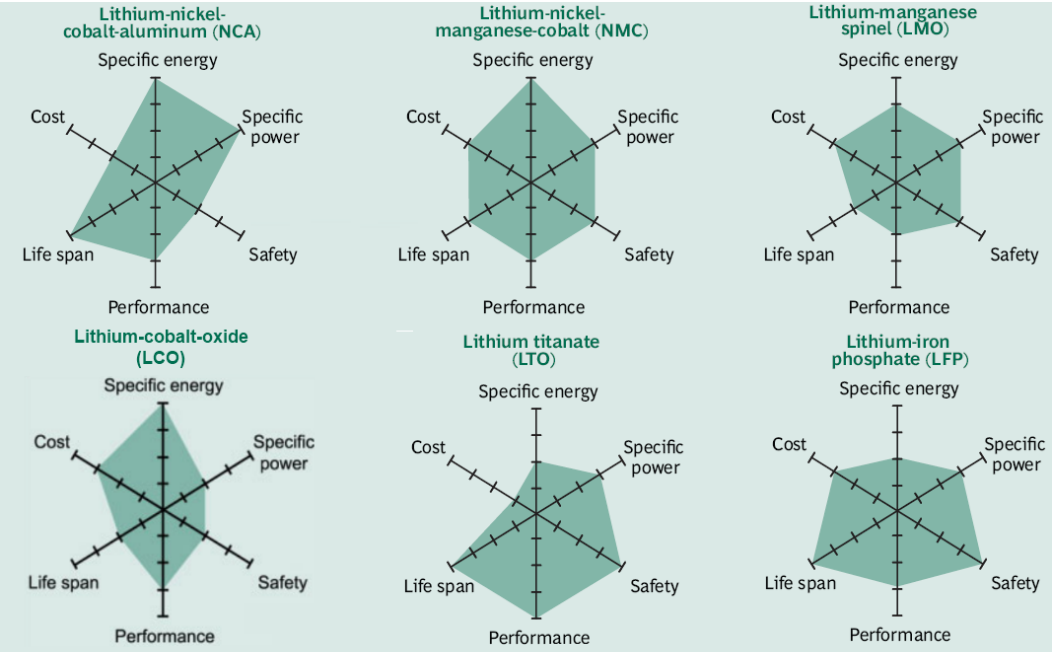

Figure 2.1: Comparison of Lithium-ion batteries for EV applications (Battery University, 2017)

2.4 Lithium-Ion battery and applications

Among different types of batteries used in the automotive industry lithium-ion batteries are growing popular due to their high energy density, high galvanic potential, and low self-discharge and low weight (Tang, *et al*., 2017; Finegan, 2016; Doughty, 2012). Furthermore, lithium-ion batteries have high power and higher open circuit voltage (Lu, *et al*., 2013; Budde-Meiwes, *et al*., 2013; Kizilel, *et al*., 2009; Smith, *et al*., 2007). These batteries are a common power source for many portable devices and the latest battery electric vehicles (BEVs), Nissan (Leaf) and Tesla (Model 'S' and Roadster) are among the main automotive manufacturers using lithium-ion batteries for their fleets. Extended range electric vehicles (E-REV) such as Chevy Volt (Yiu, 2011; Kizilel, *et al*.,

2009), have used similar battery technology. Lithium-ion cylindrical and prismatic cells are shown in figure 2.2.

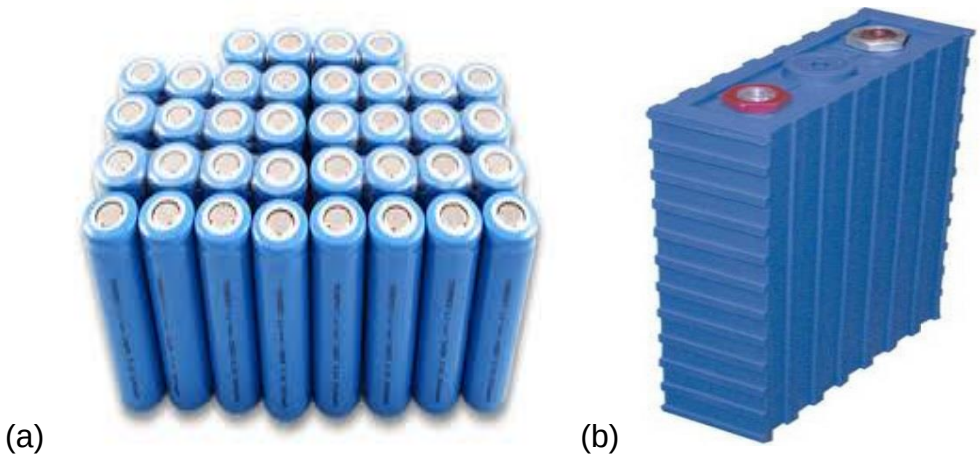

(a) (b)

Figure 2.2: Lithium-ion battery (a) 18650 cylindrical cell (b) prismatic cell (Battery University, 2014)

Both the Tesla Model “S” and Model “X” EVs get their electrical energy from the lithium-ion 18650 cylindrical cell. Each battery pack for the Tesla cars uses around 7000 of these cells connected in series and parallel (Battery University, 2014). A schematic of a lithium-ion battery is shown in figure 2.3.

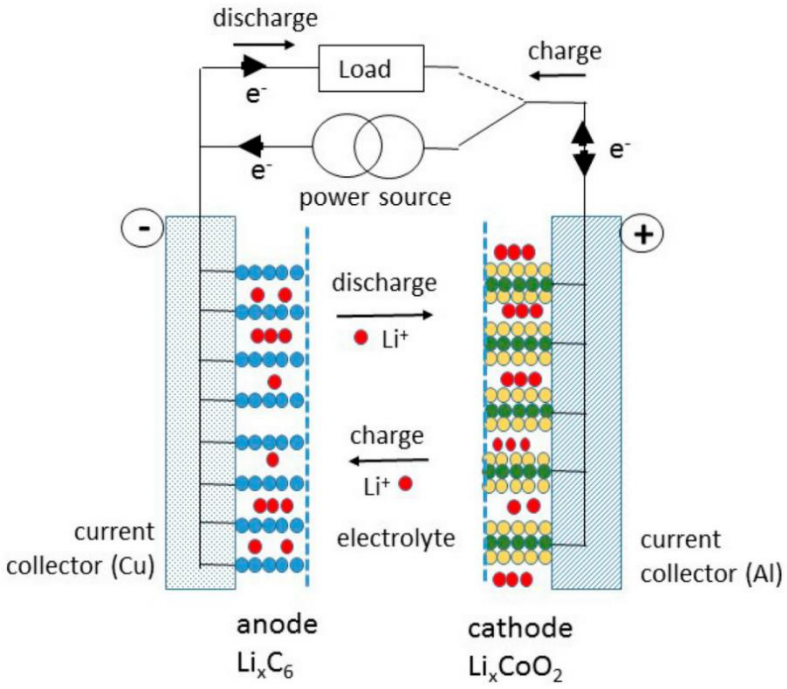

Figure 2.3: Schematic of Lithium-ion battery (Julien, *et al*., 2016)

EV manufacturers have used various types of batteries for their fleets. Choice of the battery depends on several aspects including power draw, capacity, and thermal stability (He, *et al*., 2012) and crash safety. Crash safety or crashworthiness of the lithium-ion battery is a crucial aspect as high battery content in EV battery packs poses some safety risks (electricity damage, battery pressure, combustion, electrolyte splash and heat damage) following a crash which raise safety, durability, uniformity and cost concerns which impose limitations on the wide application of lithium-ion batteries in vehicles (Zhao, *et al*., 2014; Albright and Al-Hallaj, 2012; Lisbona and Snee, 2011; Kizilel, *et al*., 2009). Due to the chemical properties of lithium-ion batteries, they can adapt higher temperatures quickly (Shi, *et al*., 2016), and these higher temperatures can trigger exothermic chemical decomposition of lithium-ion battery component

materials (Miller, 2009; Kim, *et al*., 2007; Nguyen and Taylor, 2004) that lead to further temperature rise and possibly catastrophic failure of the lithium-ion battery system (Lopez, *et al*., 2015) and thermal runaway. Temperature variations of lithium-ion batteries depend on the operating conditions. Under normal operating conditions temperatures of these batteries can be easily controlled to remain in the safe range, whereas stressful conditions such as high power draw at high cell/ambient temperatures as well as defects in individual cells may steeply increase local heat generation (Liu, *et al*., 2017; Bazinski and Wang, 2015; Spinner, *et al*., 2015b; Siguang and Chengning, 2009).

A few of the failure scenarios of lithium-ion batteries are overcharge of an individual cell or the entire battery pack, an internal short circuit (ISC) of cells resulting from a latent defect due to an internal foreign object, separator wear out, dendrite growth, crushing or penetration of a cell, an external short circuit of a cell module or pack, and/or exposure to abnormally high temperatures (Richardson, *et al*., 2014; Chen and Evans, 1996), due to fire or failure of neighbouring components (Smith, *et al*., 2010; Kim, *et al*., 2009; Santhanagopalan, *et al*., 2009; Kim, *et al*., 2007; Spotnitz, *et al*., 2003)

Although all the above-mentioned failure scenarios affect the performance of lithium-ion batteries and cause temporary or permanent damage, some of the abusive conditions can cause severe failures resulting in catastrophic events. Hu, *et al*. (2011) and Sahraei, *et al*. (2010) mentioned electrical integrity, thermal integrity and mechanical integrity which are interrelated aspects of

battery safety, which give new dimensions for the safety analysis of batteries and emphasis on considering all aspects of maximum parameters. Sahraei, *et al*. (2012a) discussed short circuit occurrence and concluded that electric short circuit is a necessary but not sufficient condition for the occurrence of thermal runaway after mechanical abuse. Chemistry of the cell, resistance of separator to heat, size of the fractured part and rate of heat transfer, which all play a role in processes leading to a thermal runaway. If the cell has not gone to thermal runaway right away it can still go into a slow process of electrochemical reaction, releasing gases that eventually could lead to a catastrophic event (Sahraei, *et al*., 2012a). The above statement about the occurrence of thermal runaway supports the argument by Hu, *et al*. (2011) and Sahraei, *et al*. (2010), which is further investigated in following sections, where research will be discussed with regards to the rationale, significant results and methodologies.

Lithium-ion batteries have revolutionised the portable electronics industry by offering significantly higher energy density and specific energy, compared to other battery technologies, which is now transitioning from its pigeonhole in portable applications to become a factor in the transportation and stationary storage markets (Battery University, 2014). The lithium-ion battery is the winning type of rechargeable battery of the decade and there are hundreds of manufacturers of these batteries. Most of the existing manufacturers of li-ion batteries use lithium ion phosphate (LFP) active cathodes because of advantages such as no materials subject to severe price hikes, low cost materials overall and easier patent position. They also have good temperature

performance that can be reflected in greater safety (Albright and Al-Hallaj, 2012). For cylindrical 18650 cells various chemistry is used, but limited detail is available as manufacturers have not mentioned these details in their data sheets. A cylindrical 18650 lithium-ion battery layered model is shown in figure 2.4.

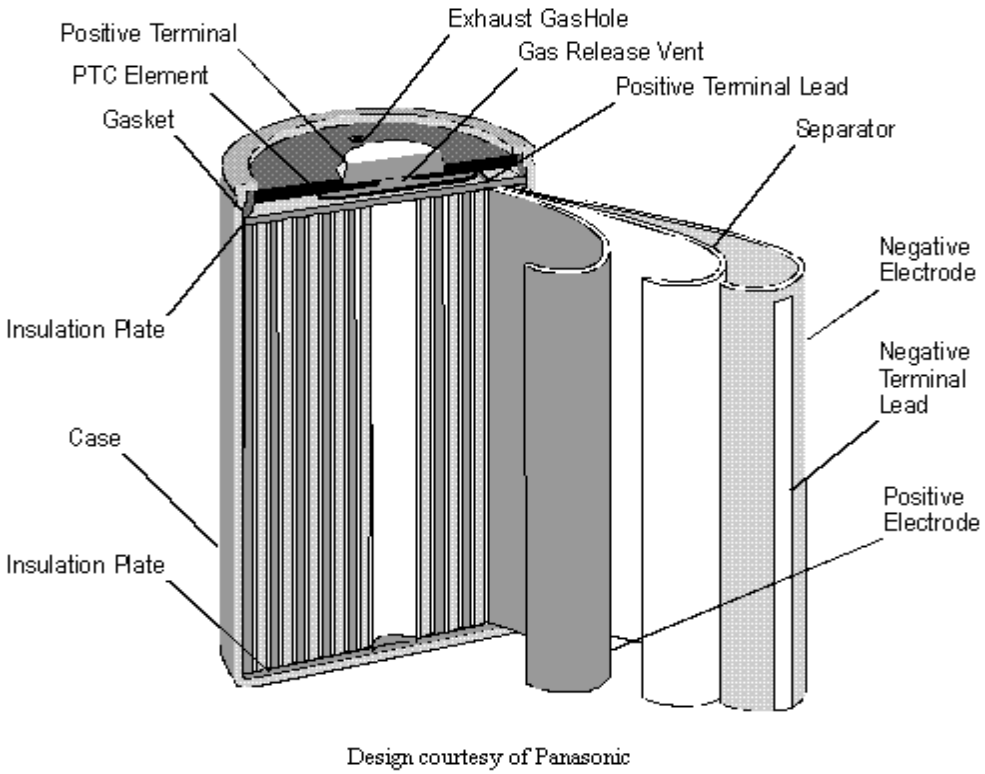

Figure 2.4: 18650 cylindrical lithium-ion battery layered model (Battery University, 2017)

Within the battery domain, a number of technologies, old and new, are competing for industry dominance in the short- and long-term. The immediate battle in many applications seems to be lead acid versus lithium-ion. Lithium-ion batteries are considered an enabling technology for many portable applications

but have yet to see widespread adoption in the stationary market compared to lead acid batteries (Battery University, 2014).

A lithium-ion battery pack is considered more compact as well as lightweight compared to various other battery packs used in EV fleets. The safety of a lithium-ion battery is a crucial aspect as a number of cells are connected to form a battery pack where damage or fault to a single cell can cause failure to surrounding cells and can lead to temporary or permanent damage to a large battery pack. Safety aspects of lithium-ion batteries are discussed in the following sections where focus is given to single cell characteristics; however failures of multiple cells and battery pack are also considered.

2.5 Lithium-Ion battery safety for electric vehicles

Research on battery safety is limited, and the standard aspect of battery testing carried out by several researchers is short circuit initiation of the lithium-ion battery when a battery encounters any external or internal abuse. A short circuit occurrence can be considered an initial failure to a battery as it leads to changes in electrical and thermal parameters. Mechanical damage to EV batteries can disturb both electrical and thermal stability which may cause the movement, pressing, short-circuit, cracking, leakage, thermal shock, explosion and burning (Wang, *et al*., 2011) which depend on types of crash/impact and operating conditions.

Safety analysis of electric vehicle batteries involves many challenges and a complete understanding of battery chemistry, material properties, thermal modelling of batteries, and battery performance under normal to extreme conditions, battery abusive conditions, battery behaviour after temporary or permanent damage is necessary to develop a test model. Compactness of a Li-ion battery pack gives rise to safety issues due to potential overheating, and research shows that under stressful conditions such as high power draw at high cell/ambient temperatures as well as defects in individual cells may steeply increase local heat generation (Kizilel, *et al*., 2009) which leads to thermal runaway.

Literature available in these subjects is critically reviewed to set grounds for research and gain useful knowledge. In the next sections of this literature review, results from the studies are discussed to show the effectiveness of the proposed remedial concepts in thermal runaway detection after mechanical abuse.

2.5.1 Lithium-ion battery hazards

Chemistry of lithium-ion cells includes hazardous materials such as lithium metal and flammable solvents, these can lead to exothermic and runaway reactions above a defined temperature (Shan, 2016; Shi, *et al*., 2016). Lisbona and Snee, (2011) reviewed hazards associated with primary lithium and lithium-ion batteries and mentioned a number of incidents related to lithium-ion cells during transport, storage and recycling operations. They linked these events to

incorrect handling, storage and packaging practices which may lead to mechanical damage, water ingress, and internal or external short-circuit of charged batteries. Researchers further divided side reactions into parts and mentioned temperature increase, heat generation and overcharging of metal lithium cells due to the low melting point of lithium metal (180°C), all of which can originate hazards associated with lithium-ion cells. Authors concluded that reactions between the organic solutions and the electrode surface occur when the temperature of the cell increases, particularly if the solid electrolyte interface (SEI) is disrupted (Lisbona and Snee, 2011).

2.5.2 Thermal runaway

Excessive heat generation in lithium-ion cells leads to a runaway reaction also called thermal runaway reaction (Escobar-Hernandez, *et al*., 2016; Le, *et al*., 2015). Thermal runaway happens due to internal or external abuse of lithium-ion batteries which affect battery chemistry.

Thermal runaway and heat effects are linked to the state of charge and depend on cell type, load applied and history of cell, described as the higher the charge voltage the lower the onset temperature (Sahraei, *et al*., 2012b) Thermal runaway events can occur due to abusive conditions as shown in figure 2.5, which is further detailed in figure 2.6.

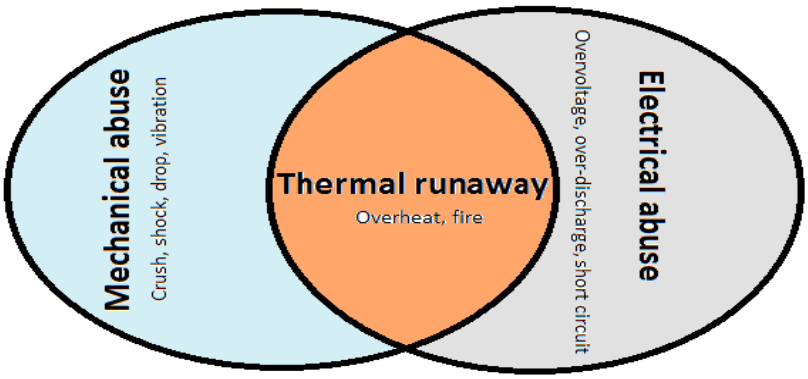

Figure 2.5: Triggers of thermal runaway

Mechanical or electrical abuses individually or together can lead to thermal runaway. Figure 2.6, shows variety of causes, processes and effects which can happen in lithium-ion cells. These can be related or can trigger each other.

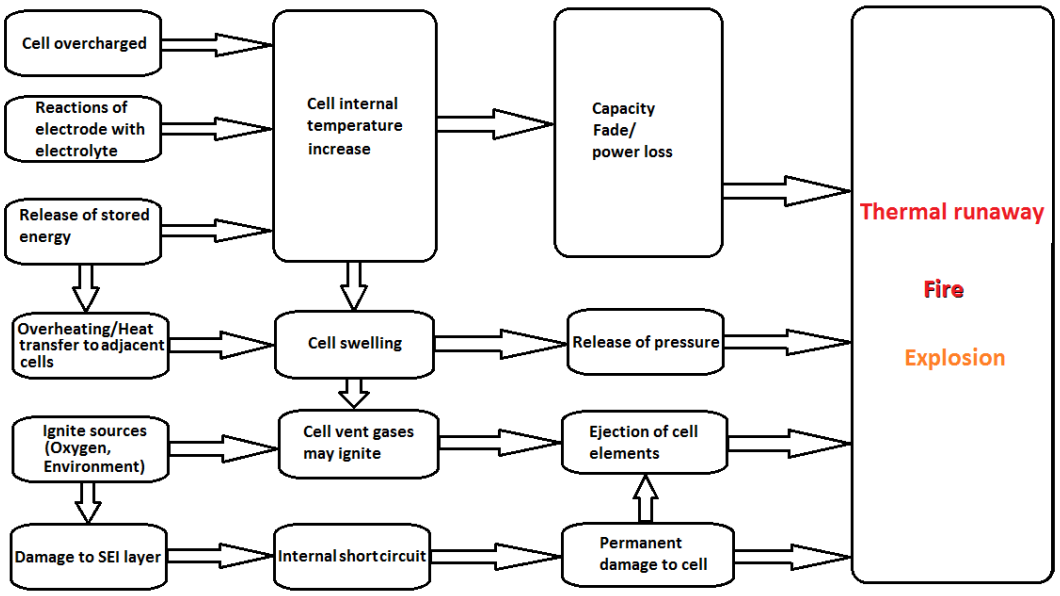

Figure 2.6: Causes, processes and effects which trigger thermal runaway (Liu, et al., 2017; Sheikh, et al., 2017; Shi, et al., 2016; Li, et al., 2013; Lu, et al., 2013; Wong, et al., 2012; Tobishima and Yamaki, 1999).

Thermal runaway in lithium-ion batteries can occur due to various operating conditions which include the exothermic reaction of chemicals (Liu, *et al*., 2017; Shi, *et al*., 2016; Wong, *et al*., 2012), overcharge of batteries (Lu, *et al*., 2013; Tobishima and Yamaki, 1999), discharge rate, the rate of heat transfer from the battery to the surroundings (Li, *et al*., 2013),short circuit (Sheikh, *et al*., 2017), and over discharge (Lu, *et al*., 2013). Thermal runaway detection is of important concern to avoid greater damage and to ensure safe operation of electric vehicles.

2.6 Lithium-ion battery testing and characterisation

Battery testing can be divided into two parts where the first is to characterise batteries by applying different operating conditions including charge/discharge, temperature and internal abusive conditions. In the second part, advanced battery testing tools can be used to test batteries up to their maximum potential by applying stress on batteries.

To characterise a lithium-ion battery, different testing techniques are used by researchers (Mendoza, *et al*., 2017; Lei, *et al*., 2017; Drake, *et al*., 2015; Zhang, *et al*., 2014; Kim, *et al*., 2014). Some of the methods used, employ advanced equipment and tools including universal battery testers, advanced power supplies, accelerating rate calorimeter (ARC) (Mendoza, *et al*., 2017; Zhang, *et al*., 2016), thermal chambers, IR thermography, high resolution cameras, amongst others where some of these techniques are combined with basic lab-based techniques, including characterization at different charging and

discharging rates, variation of applied current and voltages, capacity estimation at different operating temperatures and cell temperature estimation using thermocouples (Kim, *et al*., 2014; Zhang, *et al*., 2014). Literature is studied to analyse these techniques and their implementation for characterization and cell thermal behaviour.

Dubbary, *et al*. (2011) examined two types of large format (>10Ah) LFP cells to check ageing mechanisms. For this purpose, authors selected different charge and discharge rates of 25°C and 60°C. Results were analysed using incremental capacity analysis (ICA) along with other electrochemical techniques. Authors mentioned the cells degraded at 60°C and emphasised degradation is more complicated than those reported in the literature. Results from their work show that at 25°C with C/10 rate cells higher capacity was delivered compared to C/2 rate. In another comparison at voltages below 2.75V, cells exhibited the same results. At 60°C one of the cells delivered the same capacity at C/10 as at 25°C but at C/2 rate capacity decreased (9.9Ah) significantly which is 89% of its capacity at 25°C. Authors concluded low capacity retention at C/2 was due to the capacity cut-off in the charging régime where cells were allowed to charge up to 10Ah. Haruna, *et al*. (2011) worked on high energy density and long-life scan lithium-ion cells, where cell chemistry consisted of positive electrodes containing a lithium manganese spinel or a mixture of it with a layered-manganese based material and negative material containing hard carbon material. They developed 8Ah-class cells with this chemistry which showed that their lives were long enough to withstand a cycling

load for ten years of use. They used an isothermal box to cycle 8 Ah cells at 25°C using a regenerative charge/discharge cycler. They charged cells at 4A to 4.2V in the constant current-constant voltage (CC-CV) mode for 3 hrs. The discharge current was 4A and the cut-off voltage was 2.7V. The rest time between charge and discharge or discharge and charge was 20min. They stored cells at 25°C and 50°C in an isothermal box after being charged to 3.9V to 4.2V to estimate capacity fade for 30 to 60 days. Authors concluded capacity fading is explicitly dependant on the temperature and cell voltage. The higher the storage temperature or cell voltage, the greater the capacity fading, where temperatures are affected more than voltage (Haruna, *et al*., 2011).

To better represent thermal behaviour during charge and discharge of low capacity lithium-ion cells (Jeon, 2014) numerical simulation was conducted using cylindrical 18650 batteries. Authors used two different models, where a porous electrode model was used for lithium content inside particles, and a thermo-electric model was used to predict temperature distribution inside the cell. The charge capacity was predicted at rates of 0.5C, 1C and 2C. Authors predicted that the capacity increases at low charge rates and decreases at high charge rates; also discussed by Dubbary, *et al*. (2011) and Haruna, *et al*. (2011). Authors mentioned that solid phase diffusion limitation plays a significant role at high charge rates. Similar to charge capacity, the discharge capacity was predicted at rates of 0.5C, 1C and 2C. Results showed that capacity decreases at high discharge rates but increases at low discharge rates (Jeon, 2014).

Results from above experimental work suggest that the increase in temperature during discharge is higher than that during charge; also temperature difference between charge and discharge is decreased with increasing C-rates. Authors also mentioned at a rate of 1C, the discharge temperature increases with a waving region at the beginning, whereas the charge temperature increases until a certain point and then decreases. The thermal behaviour is closely related to the change in entropy and applied current (Jeon, 2014).

2.7 Internal temperature measurement of lithium-ion batteries

Temperature plays a significant role for lithium-ion battery performance estimation, ageing and safety. Temperature measurement inside the cell is ideal for better estimation of thermal properties, but it is difficult especially for sealed cells (Zheng, *et al*., 2017; Zhang, *et al*., 2014; Koo, *et al*., 2014; Richardson, *et al*., 2014; Ji, et al., 2013). Insertion of measurement equipment in the cell may exhibit unfamiliar properties and require high-level care. Internal temperature measurement tests conducted by Li, *et al*. (2013) and Forgez, *et al*. (2010) are discussed in this section.

To understand thermo-electrochemical reactions battery internal temperature understanding is valuable (Spinner, *et al*. 2015b, Kim, *et al*., 2014) and is also useful to validate simulation models and to refine battery thermal design. Battery temperature measurement can be classified into three types concerning location of temperature measurement (Li, *et al*., 2013).

In the first type, temperature sensors are located outside individual cells. Further, as explained by Mayyas, *et al*. (2011) and Sabbah, *et al*. (2008) one-point temperature measurement on the cell surface is used to present an overall state of the cell.

In the second type, a single temperature sensor was mounted on top of the cell and sealed inside as mentioned by Jasinski, (1974). Li, *et al*. (2013) criticised that in the second method no temperature sensor was placed between the electrodes which made it difficult to monitor internal temperature and temperature distribution inside the cell. First and second for temperature measurement is for single location temperature measurement as no contact between internal layers or electrode is formed and temperature measurement is for base temperature which can be used for small-scale applications, including small electronics products such as cell phones and laptops where associated error may be negligible. But in large format traction batteries temperature variations develop at different locations inside the battery, the non-uniform temperature distribution may cause local hot spots which affects cell durability and raises safety problems (Li, *et al*., 2013).

So they proposed a third type where sensors were inserted deep inside the cell to obtain internal temperatures. These three types are useful to build test rigs where temperature measurement at different locations is vital. The first and second type can be better implemented to measure surface temperature in the case of a crash where crash location varies. Temperature variations are monitored by using three thermocouples each on a cell's positive terminal,

negative terminal and mid-surface. To further understand surface and internal temperature measurement, research conducted by Forgez, *et al*. (2010) has been reviewed, where authors used thermal modelling of the $LiFePO_4$/graphite lithium-ion battery to determine heat transfer coefficients and heat capacity from simultaneous measurements of the surface temperature and the internal temperature of the battery while applying 2Hz current pulses of different magnitudes. They used thermocouples for internal temperature measurements, thermal steady state temperature measurements were used for heat transfer coefficients, and heat capacity was determined from the transient part. Results showed that accuracy during complete charge/discharge of the battery is within 1.5°C. Also, the model allows for simulating the internal temperature directly from the measured current and voltage of the battery, but this research does not address the comparative study on different batteries which is equally significant to understand heat transfer coefficient and heat capacity.

The calorimeter is used for internal temperature measurement of lithium-ion batteries to get significant results of temperatures of batteries at different positions by inserting thermocouples inside batteries. Results are discussed in the following sections.

2.7.1 Adiabatic calorimeter used for internal temperature measurement of battery

Adiabatic calorimeter and accelerating rate calorimeter (ARC) are used to measure thermal characteristics of batteries (Lei, *et al*., 2017; Mendoza, *et al*., 2017; Zheng, *et al*., 2016; Shah, *et al*., 2014;). Li, *et al*. (2013) used an

adiabatic calorimeter to perform constant-current discharge experiments under a series of discharge rates on sensor embedded 5 Ah and 25 Ah cells. Where for 5 Ah cell four thermocouples were affixed on corners of separator and 1 in the middle of the cell for 25 Ah cell 12 thermocouples are affixed inside with separator, and 12 thermocouples are affixed on the surface of the cell with the corresponding location as for separator. Results of the adiabatic calorimeter (cells placed middle of the cavity to avoid direct contact with the wall), natural convection (cells placed in the room without ventilation) and forced convection (cells placed in environment chamber equipped with heater and refrigeration compressor), were compared and concluded with following findings (Li, *et al*., 2013).

(1) Internal temperature could differ from the surface as much as 1.1°C, even for a thin laminated cell.

(2) The time constants of thermal response at the internal locations are generally dozens of seconds larger than on the surface.

(3) The internal variation in the plane direction reaches above 10°C under adiabatic 1.5C discharge, much larger than in the through-plane direction, indicating the in-plane heat conductivity needs improvement.

(4) Forced convection is effective to suppress the temperature rise as well as the variation.

Findings by Li, *et al*. (2013) are useful for implanting sensors/microchips in single cells to extract multiple physic-electrochemical signals simultaneously,

but temperature variation and their ratios are detailed for specific tests which vary when complete cell temperature variation is taken into account. This research also considers high capacity cells which are interesting to understand but out of the scope of testing cylindrical cells. So in the next section ARC results on cylindrical 18650 cells are discussed.

2.7.2 Thermal characteristics of lithium-ion cells using ARC

Mendoza, *et al*. (2017); Lei, *et al*. (2017); Zheng, *et al*. (2016) and Mendoza, *et al*. (2015) used accelerated rate calorimeter (ARC) for thermal runaway analysis. Ishikawa, *et al*. (2012) also analysed thermal characteristics of cylindrical lithium-ion cells using accelerated rate calorimeter (ARC) and electrochemical impedance spectroscopy (EIS) measurements. This method integrates both calorimeter and spectroscopic results where authors used mapping of thermal runaway characteristics (cells tested at different states of charge SOCs), high temperature storage test (temperature ranges from 70°C to 100°C), calculation of thermal deterioration activation (estimated from the discharge capacities before and after high temperature storage) and calculation of charge/discharge activation energy (EIS measurements were recorded). They presented the following results from their experimental work.

(1) By mapping the thermal runaway, it was possible to clarify the SOC dependence on the temperature in the self-heating domain.

(2) The lowest deterioration activation energy value and the lowest frequency factor value were obtained at the SOC of 66% at the SOC of 0° and

87%. The value of the deterioration activation energy and frequency factor tended to increase when there was an imbalance of lithium-ions between the anode and cathode.

(3) The charge/discharge activation energy was obtained from the recorded EIS measurements. The lowest charge/discharge activation energy value was found at the SOC of 22%.

Although the above results are significant as they discuss SOC dependent thermal properties and their effects on a cell but less detail was included about the specific location which is equally important when thermal properties vary.

Review of internal temperature measurement was conducted, and it was concluded that by incorporating more thermocouples at different surface locations better temperature measurements can be achieved at surfaces, which will be implemented in this research.

2.8 Battery performance indicators

The battery safety system is designed to reduce the probability of failure and the severity of outcome if an event occurs. According to Cho, *et al*. (2012), it is, therefore, essential that EV batteries are designed to be tolerant of abusive conditions such as crush from a collision with another vehicle or a foreign object. Also, the author states that safety systems must be incorporated into battery management systems to reduce the probability of single cell failure and preclude propagation of failure to adjacent cells. Kim, *et al*. (2012) stated that many of the problems associated with the battery management system are that

they are not designed to examine the inherent uncertainties of battery dynamics, especially after a change to physical battery structure or a chemical change/reaction which could lead to thermal runaway (Gu and Wang, 2000).

2.8.1 Battery thermal behaviour

Kalnaus, *et al*. (2017); Lopez, *et al*. (2015); Kim, *et al*. (2012); Lotfi, *et al*. (2013); Xu, *et al*. (2010); Doughty and Peter, (2012); Yang, *et al*. (2005) have examined Lithium ion cell thermal behaviour for charge and discharge under normal conditions and possible thermal runaway; however no signs of extreme mechanical conditions were found which are necessary to investigate behaviour of the cells following an impact, and would allow improvements to be made to the safety of the design of the vehicles and the batteries. Furthermore, this will allow a baseline for 'normal' thermal behaviour to be developed supporting the detection of abnormal conditions which could indicate thermal runaway. Rad, *et al*. (2013) and Wang, *et al*. (2005) dealt with battery modelling using various techniques, such as heating up batteries (Oven test), nail penetration, battery crush, overcharge, over discharge, internal and external short circuits which were also found in Bandhauer, *et al*. 2011; Ramadesigan, *et al*. 2012. A small number of researchers investigated the relation between the battery testing and simulation. Recent safety issues after EV collision raised the need for detecting the onset of thermal runaway to protect occupants and minimise damage to the vehicle and battery pack. Thermal runaway can spread quickly in the case of a

crash/impact to the battery where battery electrochemistry, structural deformation and impact location play a significant role. In this research, collision induced issues are discussed in detail and factors which fuel these problems are identified.

2.8.2 Battery mechanical behaviour

To better understand battery properties due to abuse conditions, a model is required to represent battery operation which also integrates electrical, thermal and physical behaviour due to impact. In this research the cylindrical lithium ion cell is investigated using a finite element model (FEM) for its material properties and possible structural deformation.

Battery abusive testing, as detailed by Tang, *et al*. (2017); Zhang, *et al*. (2017); Shi, *et al*. (2016); Lopez, *et al*. (2015); and Lamb and Orendorff (2014) are used for safety analysis and prediction of failures. Sahraei, *et al*, (2012a) have examined the 18650 lithium-ion battery abuse response using different loading conditions and simulation. In their study the model is simulated for all loading conditions with various steel casing thicknesses. An 18650 cylindrical cell layer model has not, however, been considered; also, regarding the state of charge (SOC), induced changes are not found. The lack of research to investigate battery behaviour in detail, as well as the role of testing batteries for early detection of thermal discrepancies for EV safety and stability, has encouraged the investigation of this significant issue in great detail.

Failure of a lithium-ion battery can occur due to internal or external abuse conditions, triggers for external abuse conditions are crash/impact, charge/discharge discrepancies and thermal abuse. Internal abusive conditions are considered to be internal short-circuit, excessive heating due to resistance build-up and failure of internal battery components (Sahraei, *et al*. 2012b; Somasundaram, *et al*. 2012).

Large battery cells mostly used in automotive applications are considered good for ease of assembly into battery modules due to less number of cells required to achieve desired capacity for applications, but these cells have low thermal stability compared to smaller cells. As larger cells have high energy content stored and have low surface to volume ratio resulting in a reduced cooling area per volumetric heat generation, they can attain thermal runaway situations earlier compared to their smaller counterparts (Kim, *et al*. 2007). Battery packs for electric vehicles (EVs) consist of battery modules, and each module consists of several numbers of cells dependent on the cells used and size of battery pack required.

2.8.3 Electrical, mechanical and thermal integrity of battery

Mechanical damage of lithium-ion batteries is considered a high risk for EV safety and reliability although much focus is given to vehicle structure, and protective fire walls but research on the mechanical integrity of lithium-ion batteries in the case of abusive conditions is limited. Melcher, *et al*. (2016); Zhao, *et al*. (2014); Sahraei, *et al*. (2012a) have discussed short circuit

detection in 18650 cells due to mechanical abuse conditions, where both experimental and simulation work shows good correlation, but thermal effects due to mechanical abuse are not discussed in detail which is equally important to understanding the triggers of thermal runaway in the case of abusive conditions. A framework for mechanical, electrical and thermal solvers, proposed by L'Eplattenier, *et al*. (2013) is shown in figure 2.7.

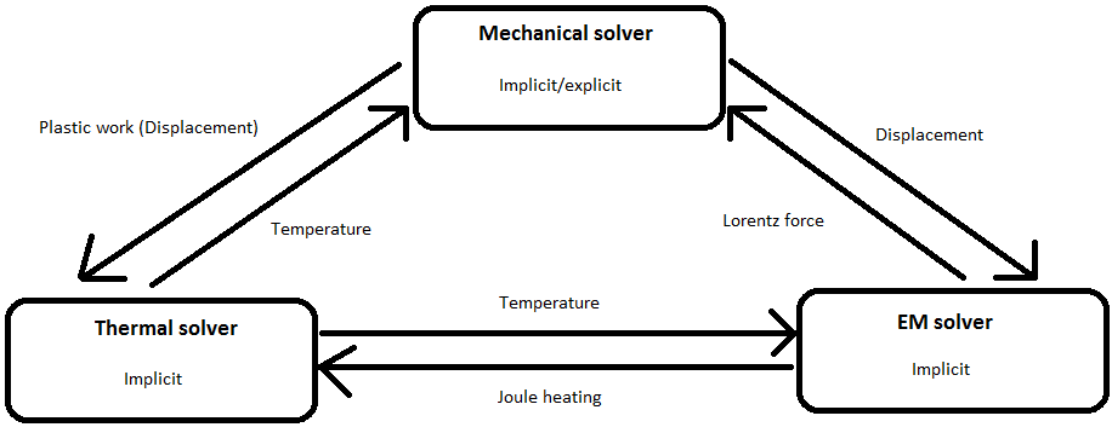

Figure 2.7: Mechanical, Electrical and thermal solver framework (L'Eplattenier, *et al*. 2013)

Electrical, thermal and mechanical integrity are three interrelated aspects of EV battery safety so better understanding of all of these is required to achieve maximum safety. Mechanical integrity is considered crucial in the case of loading conditions as it tends to develop crack/deformation in a battery which can lead to battery structure failure, short circuit or thermal runaway. In most of the cases, the electric short circuit is considered the initial failure state as it causes immediate electrical and thermal changes in the cell; however this

condition alone is not enough for the thermal runaway occurrence. Other factors which influence thermal runaway as investigated by researchers are chemistry of the cell, resistance of separator to heat, the size of the fractured part and rate of heat transfer. If the cell has not gone to thermal runaway right away, it can still go into a slow process of electrochemical reaction, releasing gases that eventually could lead to a catastrophic event (Sahraei, *et al*. 2012a).

2.9 Modelling of lithium-ion batteries

To ensure safety and enhance the performance of lithium-ion batteries, different modelling techniques and models are investigated by researchers which varied from basic equivalent circuit model to thermal modelling of batteries (Soylu, *et al*. 2017; Wang, *et al*. 2017; Yang, *et al*. 2017; Grandjean, *et al*. 2017; Gao, *et al*. 2017; Zhang, *et al*. 2017; Jiang and Peng, 2016; Westerhoff, *et al*. 2016; Wu, *et al*. 2016; Sung and Shin, *et al*. 2015; Hussein, 2015; Taylor, 2014; Gomez, *et al*. 2011; Hu, *et al*. 2012). Based on the dynamic characteristics and working principles of the battery, the equivalent circuit model was developed by using resistors, capacitors and voltage sources to form a circuit network (Grandjean, *et al*. 2017; Gao, *et al*. 2017; He, *et al*. 2011). Battery dynamic models aim to describe the electrical, thermal and operational properties of lithium-ion cells. Three commonly used battery models which accounted for details about electrical and thermal properties are as follows.

- Artificial Neural Network (ANN) Models (Soylu, *et al*. 2017; Wang, *et al*. 2017; Hussein, 2015; Taylor, 2014; Cai, *et al*. 2000).

- Electrochemical Models (Zhang, *et al*. 2017; Yang, *et al*. 2017; Jiang and Peng, 2016; Westerhoff, *et al*. 2016; Sung and Shin, 2015; Doyle, *et al*. 1993)
- Equivalent Circuit Models (Grandjean, *et al*. 2017; Gao, *et al*. 2017; Wu, *et al*. 2016; Saw, *et al*. 2014).

ANN models benefit from being able to adaptively learn cell or batteries' characteristics. The disadvantage of such models is the need for significant amounts of data to train and validate the model. Electrochemical models attempt to explain and predict the chemical reactions which occur at the electrodes and the resultant electrical behaviour at the terminals. Developing such models requires a detailed understanding of the physical and chemical composition and structure which is often difficult to obtain due to commercial restrictions.

Equivalent circuit models use networks of elementary idealised electrical components (e.g. resistances, capacitances, ideal voltage current sources, amongst others) to replicate the behaviour of the cells or battery in question. The advantage of an equivalent circuit model is that, once the correct model structure has been determined, the parameters of the model can be determined by various techniques utilising experimental data.

Various types of equivalent circuit model have been identified (He, *et al*.,2011).These are briefly summarised below.

Internal resistance model (aka RInt model): this simple model consists of an ideal voltage source equivalent to the open circuit voltage of the cell, in series

with a resistance. This model forms a useful first approximation of the behaviour of many battery types but fails to capture many aspects of the performance of real cells.

RC model: this model uses two capacitors and three resistors to simulate the charge/discharge behaviour and surface effects within the cells.

Thevenin model: this model adds a parallel RC network in series with the internal resistance model to replicate the dynamic behaviour of batteries and cells.

PNGV model (Partnership for new generation vehicle): this model builds on the Thevenin model by adding the series capacitor to account for variations in open circuit voltage.

Dual polarisation (DP) model: this model has been developed to specifically account for the behaviour of lithium-ion batteries concerning polarisation and variations in the open circuit voltage and the internal impedance of the battery which occurs as the state of charge (SOC) changes during charging/discharging.

2.10 Thermal management of lithium-Ion batteries

Thermal management of Li-ion batteries is critical for high-power applications; it is vital to safety and to enhance battery performance and extend the life cycle. The operating temperature controls the electrochemical performance of the Li-ion battery. One of the side effects of exposure to high temperature is premature ageing and accelerated capacity-fade (Leng, *et al*. 2015). Designing

the thermal environment is critical in Li-ion technology; therefore efficient thermal management that continuously regulates battery operating temperature is essential to safety and optimal performance in high temperature and high discharge Li-ion applications. Resolving the thermal management issues with Li-ion batteries will benefit their use in electric and hybrid electric vehicles (Al-Hallaj, *et al*. 2005).

Temperature control of lithium-ion batteries is the key to developing a good thermal management system which enhances performance and increases life cycle. To understand thermal issues associated with lithium-ion batteries, heat generation inside the cell and the effect of operating conditions are considered important parameters. Improper thermal management of batteries can cause power/capacity fade, thermal runaway, electrical imbalance among multiple cells in a battery pack and low-temperature performance (Lotfi, *et al*. 2013).

Albright and Al-Hallaj, (2012) concluded that temperature does have an influence on the performance degradation of lithium-ion batteries and further explained high-temperature effects nearly all as positive electrode and electrolyte chemistries and if heat is not dissipated, then it can lead to thermal runaway. In the next section heat generation in lithium-ion batteries is discussed in detail with governing equations for temperature increase and uniform temperature.

2.11 Analytical approach for heat generation in lithium-ion battery

Heat generation in lithium-ion batteries is a complex process which includes electrochemical changes of batteries due to operating conditions and temperature. In this section operating conditions including charge/discharge rate, resistive heat generation inside cell and operating time are discussed which help to numerically analyse lithium-ion batteries. Temperature variations inside individual cells can cause uneven temperature distribution among series/parallel connected cells which can lead to permanent damage if not controlled at cell level. Most thermal management systems are designed to control propagation of heat generation and operation at cell level. In this thesis temperature variation is considered and phenomena which affect temperatures and their numerical validation is investigated using available research.

Some of the factors that influence heat generation rates are battery type, working status (SOC) and ambient temperature, however these factors vary with different driving conditions of vehicles. Heat generation in lithium-ion batteries consists of three parts: chemical reaction heat, polarization heat and joule heat (irreversible) (Zhao, *et al*. 2014; Cho, *et al*. 2012). Causes of heat generation in lithium-ion batteries are considered and governing heat generation equation due to joule heating and entropy changes (reversible) proposed by Bandhauer, *et al*. (2011) and Bernardi, *et al*.,(1985) are given.

$$q = I(U\text{-}V)\text{-}I(T\frac{du}{dt}) \tag{2.1}$$

Eq. (2.1) sets the ground for SOC dependent heat generation but heat capacity inclusion is required as batteries exhibit different characteristics due to materials

used, so two governing equations for heat capacity of battery are considered. Each is for heat capacity during uniform temperature and temperature rise.

Bandhauera, *et al*. (2011) presented heat generation equation using an energy balance on the battery where the temperature of the battery is allowed to rise during operation. Heat generation equation is as follows.

$$q = MC_p\frac{dT}{dt} + hA\,(T_{surf} - T_{well}) \tag{2.2}$$

Where first term is heat stored inside the battery and second term is heat transferred from the surface of the battery to the constant temperature well.

Heat generation of the battery is an important factor which influences other parameters and approximation of heat generation at the cell level is important as described by Braun, *et al*. (2012); Vilayanur, *et al*. (2010) and Onda, *et al*. (2006). The safety and performance of lithium ion batteries are highly dependent upon the materials that are used to produce the batteries (Chanson and Wiaux, 2013) as well as on battery size, design, quality and energy content (Finegan, *et al*. 2015; Golubkov, *et al*. 2014). Abuse of batteries to cause damage to batteries are carried out to analyse safety issues, especially when the deployment of the batteries is large (Zhang, *et al*. 2016; Finegan, *et al*. 2015; Zhang, *et al*. 2015a, Zhang, *et al*. 2015b). Potential damage includes cell rupture, the release of debris (leakage) and test box damage (Orendorff, *et al*. 2016).

Assumptions based on past research are that the cell voltage could be used to identify the initiation of mechanical failure (Zhang, *et al*. 2015a). Tension

(stress: strain ratio) causes an initiation of cut-off (Orendorff, *et al*. 2016; Zhang, *et al*. 2015b). Rigid rod test calibrates with hemispherical punch test results, so the hemispherical punch was not used in the current research (Sahraei, *et al*. 2012a).

The objective of the current research is to detect signs of thermal runaway in lithium-ion 18650 battery due to mechanical abuse conditions. Thermal runaway is the event causing problems to users for many years, and some of these issues include sudden failure or slow propagation of failure, however like other industries the automotive industry has also suffered from some serious issues of thermal runaway in EV. Wide use of lithium-ion batteries in EV requires crash safety analysis of these batteries, however, many experiments have been conducted and analysis done to find the causes of thermal runaway (Abraham, *et al*. 2006; Selman, *et al*. 2001), where various lab equipment is designed and used for this purpose including various types of calorimetry, impedance spectroscopy (Abraham, *et al*. 2008), state of the art chambers, amongst others.. All of these serve the purpose of detecting battery irregular behaviour including degradation and thermal runaway events due to abuse conditions (Roth and Doughty, 2004), but thermal runaway occurrence due to loading conditions where structural integrity is effected is not considered in detail. Some researchers did, however, conduct mechanical failure analysis of the battery, but the thermal analysis was not carried out. Mechanical abuse conditions of lithium-ion 18650 batteries are discussed in the next section

where different research and outcomes with possible improvements are discussed.

2.12 Mechanical failure analysis of 18650 lithium-ion battery

Analytical and numerical simulation approaches are commonly used for battery analysis, especially thermal behaviour of batteries. In this section mechanical failure analysis of battery following analytical and numerical approaches are discussed. Analytical approach to estimate heat generation of lithium-ion battery is detailed with useful equations; however for numerical simulation approach various tools are discussed and focus is given to LS-DYNA simulation tool.

Xu, *et al*. (2016) and Sahraei, *et al*. (2012a) used compression and bending tests to detect short circuit of 18650 cells using mechanical loading where impact velocities were 5mm/min and 1mm/min respectively. Force-displacement relationship shows good approximation where sudden voltage drop and temperature rise occurred which is an indicator of short circuit. Sahraei, *et al*.,(2012a) further verified experimental results using simulation results where stress location at jellyroll shows the onset of the short circuit. This work provides a good base for battery investigation using mechanical abuse but limited results of temperature variations, voltage change and SOC dependency pave the way to improve these results using a better simulation model which includes thermal effects as well. Xu, *et al*. (2016) investigated state of charge (SOC) dependent mechanical integrity behaviour of lithium-ion 18650 cells, where flat plate

compression and bend load were used to check cell behaviour at different SOC values. Authors found that mechanical hardening mechanism occurred at high SOC for the compression test, whereas in bending test bending modulus increased with SOC and failure modulus linearly decreased. This research achieved similar results as by Sahraei, *et al*. (2012a) where four loading conditions were used for mechanical abuse analysis of 18650 cells except simulation results which were not considered.

So far available mechanical abuse testing of 18650 lithium-ion cells is limited to certain aspects and need more investigation. Review suggests that there are various ways to carry out impact analysis of lithium-ion 18650 cells (Zhang, *et al*. 2017; Lopez, *et al*., 2015; Lamb and Orendorff, 2014) which can be further extended to battery pack crash analysis with real-time data. Validation of loading conditions and results can be achieved using various simulation techniques which are further explained in the following section.

Short circuit occurrence is an indication of failure in the battery (Guirong and Henghai, 2012; Maleki and Howard, 2009), but not an absolute condition for the occurrence of thermal runaway in the case of mechanical failure. Thermal runaway is defined as likely to occur after SOC dependent temperature cut-off points, this phenomenon is explained with respect to voltages, Al-Hallaj, *et al*. (1999) mentioned that OCP (Open circuit potential) increases the onset of thermal runaway taking place at lower temperatures, and explained three voltage settings and temperatures at thermal runaway with those settings. Thermal runaway reported to occur at 104°C when cell has OCP of 4.06V,

109°C at 3.0V and 144°C at 2.8V. More in depth temperature due to electrochemical reaction is discussed by Yang, *et al*. (2006), where authors explained at 85°C SEI on graphite negative electrode exothermally decompose and separator layer melt at (130°C to 190°C) and aluminium current collector can be melted at 660°C, although these results depend on slow build-up of degradation phenomena but give good idea to investigate thermal runaway occurrence in the case of short circuit, however to detect onset of thermal runaway in the case of mechanical abusive conditions, complete understanding of load applied and time of load on the cell is required, where SOC dependency is a major factor in this regard.

Wang, *et al*. (2017a) and Wang, *et al*. (2017b) explained thermal runaway risk (TRR) score from “0” to “100”, three conditions are explained for battery failure where two of the conditions directly link to occurrence of thermal runaway and voltage and temperature relationship is considered for detection of thermal runaway. Onset of short circuit is linked to thermal runaway due to unwanted electrode connection either by mechanical, electrical or thermal abuse, where immediate variations cause disturbance to the system. Onset of short circuit and possible thermal runaway is explained in next chapter where quasi-static loading is applied and temperature and voltage variations are recorded for the duration of tests, as this phenomenon is not described in detail, however thermal runaway is linked to short circuit occurrence but type of short circuit, possible short circuit formations and failure intensity are not in the literature.

2.13 Numerical simulation approach

Lithium-ion battery is considered a complex energy source when it comes to model battery dynamic characteristics. To analyse the transient behaviour of batteries, finite element analysis (FEA) is an efficient method as mentioned in the literature (Marcicki, *et al*. 2017; Wang, *et al*. 2016; Xia, *et al*. 2014; Trattnig, *et al*. 2014; Wierzbicki, *et al*. 2013; Sahraei, *et al*. 2012a; Sahraei, *et al*. 2012b; Yeow, *et al*. 2012; Martínez-Rosas, *et al*. 2011; Guo, *et al*. 2010; Cheng, *et al*. 2009). Tourani, *et al*. (2014) conducted electrochemical modelling of lithium-ion cells and explained 1D modelling is useful for cell level study whereas 2D thermo-electro model considers component material improvement where current distribution and temperature distribution is considered. Energy conservation equation or heat transfer mathematical model is considered for FEM model which consists of average density, average specific heat, thermal conductivities in x, y and z-direction and heat generation rate per unit volume. Abaqus, Ansys and LS-DYNA are popular software tools used for finite element analysis (FEA), although some differences among them make them suitable for specific applications as they have different solution procedures and time integration methods.

2.13.1 LS-DYNA simulation tool

LS-DYNA is useful for impact simulation and is widely used by engineers in various projects where automotive applications including crash analysis and structural behaviour analysis are benefiting the automotive industry. In recent

years LS-DYNA has been extensively used for collision induced simulation of batteries where different simulation scenarios are considered to predict battery behaviour in the case of crash/impact.

Zhang, *et al*. (2015a) used a representative sandwich (RS) model of battery to predict short circuit in the cell where thicker layers of anode, cathode, separator, anode current collector and cathode current collector are used. LS-DYNA numerical simulation tools are used where spherical indenter is used for mechanical load and symmetry model is used for computation efficiency. Zhang, *et al*. (2015a) used separator failures as indications of short circuit and mentioned failure of separator layer will occur well in advance before other layers fail. Failure strain is considered, and current density is used for electrical failure analysis. Although results are significant, due to thickness of layers battery mechanical integrity might be affected. Zhang, *et al*. (2015b) presented coupled mechanical-electrical-thermal simulation model, where quasi-static loading using spherical indenter was used on RS model of battery, a much more detailed model was presented which accounts for stress-strain failures of individual layers and then those layer properties were used for symmetry model. Mechanical failure is explained in great detail with strain failure but electromagnetic solver (EM) is not discussed in detail. Current density variations due to mechanical failure were used for onset of short circuit. Due to thicker layers to form (RS) model, overall thickness of layers is increased which is useful to predict failure response at limited scale but when it comes to investigation of individual layers for failure response it is difficult to achieve

accuracy as material properties of layers change with the change in dimensions. To achieve accuracy due to battery abuse behaviour detailed layered model will be useful where layer formation is same as provided in battery data sheets; however thickness may increase to achieve computational efficiency.

2.13.2 18650 lithium-ion battery simulation

FEA is widely used for battery modelling and most commonly used formation found in the literature (Marcicki, *et al*. 2017; Zhang, *et al*. 2015a; Zhang, *et al*. 2015b) is pouch cell or prismatic battery model where layers were modelled to analyse failure response. Sahraei, *et al*. (2012a) used lumped model to simulate 18650 lithium-ion battery where all layers (anode, cathode, separator, anode current collector and cathode current collector) are lumped in single jellyroll model and steel casing using LS-DYNA shell elements was developed to predict onset of short circuit. Location of stress, force and displacement criteria are considered to document short circuit. Saharei, *et al*. (2012a) also proposed battery delamination but apart from delamination geometry no detail was given. A more detailed layered model is required to understand individual layer failures and crack development due to mechanical failure.

2.14 Summary of the findings and implications for current research

A thorough literature review is conducted in this chapter which focuses on battery modelling and testing where different test techniques are discussed with significant results and limitations of those results. Also in this chapter, the

application of abuse testing of lithium-ion batteries, their importance, finite element methods (FEM) for short circuit prediction using both experimental results and finite element analysis results are discussed. From the literature it is clearly evident that abusive conditions of lithium-ion battery vary with various operating conditions, which is evident from results mentioned above with citations. Literature on mechanical abuse testing of 18650 cylindrical lithium-ion cell is limited and does not cover many aspects which are equally important for battery integrity, which leads to finding alternative methods to detect early signs of thermal runaway in case of abusive conditions, which are discussed in the remainder of the thesis in detail.

Although the principle aim of this research is to detect early signs of thermal runaway due to abusive conditions, studies using same testing techniques including both experimental and FEM modelling but different area of study are also discussed in this chapter, therefore, the literature review is not confined to thermal runaway detection. In the literature LS-DYNA numerical simulation tool for battery modelling is used frequently due to its explicit analysis technique which is required to achieve closer values and validation of results using modelling approaches and to minimize limitations. Detailed LS-DYNA battery model can be implemented by incorporating number of parameters and boundary conditions but the major task will be to achieve computational efficiency which can lead to integration of single cell into battery pack development.

In this research experimental testing and numerical simulation methods are used for the following reasons

1. Literature suggests good correlation of experimental results and simulation model, where parameters obtained from experimental work are useful in this regard.
2. Short circuit initiation is observed where various detection strategies are employed.
3. Test protocols are useful to monitor temperature variation of 18650 batteries due to different loading conditions where short circuit leading to thermal runaway is discussed in the current research.
4. LS-DYNA numerical simulation tool is used to validate experimental results.

In this research experimental setup is designed to cover the gap found in the literature where in the literature, thermal runaway detection strategies are not found. Short circuit initiation is found to be one of the battery failures due to mechanical abuse but short circuit leading to thermal runaway is not found. State of charge (SOC) dependent mechanical failure is also found in the literature but further investigation of these failures which can lead to severe failures is not found. In this research detailed analysis of mechanical testing are used to observe cell level failures where sample time, applied force, displacement, (SOC) and stress-strain failures are considered.

Chapter 3: Experimental Methodology and Preliminary Results

3.1 Introduction

To better understand battery behaviour, battery testing and characterization approaches are used which also investigate the effect of mechanical loading on electrical, thermal and mechanical behaviour. When an EV is involved in a crash, it differs from a conventional vehicle crash as an EV crash includes the battery pack which contains a high energy content and, due to the high battery pack weight, the vehicle's overall weight increases which impose weight limit for protection across battery packs. In these conditions, heavy protection firewalls are not suitable for vehicle performance, so the battery pack is protected with an efficient light weight material protection sheet, but when an extreme crash happens, this protection sheet can undergo various shapes of impact. These can be either sharp edges or uneven shapes. In this research mechanical abuse conditions are comprised of quasi-static loading where four test protocols which are rod, circular punch, three-point bend and flat plate are used to investigate thermal runaway events at various SOCs. Numerical simulation method is used to validate results which are discussed in chapter 5.

Different types of loads are used in this research which serve the common purpose of detecting an onset of short circuit and respective thermal and mechanical behaviour. Temperature variations due to SOC, and the force-displacement relationship are considered, which vary at different loading conditions. Open Circuit Voltage (OCV) is reported for the duration of each

experiment; continuous voltage measurements are recorded during each loading test. This chapter covers details of the test setup, equipment and devices used, preparation of cells for the test, techniques used to conduct tests and initial results of the experiment.

3.2 Description of experimental work

In the current research two sets of experiments are used, where the first experiment is used for cell conditioning using charge, discharge and continuous monitoring of temperature and open circuit voltages (OCV), as voltage and temperature variations are important to understand short-circuit induced thermal runaway. In the second experiment a controlled chamber is designed using polycarbonate sheet which is good for fire resistance and provides maximum protection to equipment and personnel. A calibrated mechanical press with a load cell is used which is equipped with a data logger, thermal camera and laptop (PC) to capture and record data when different loading conditions are applied on initially conditioned cells. The onset of a short circuit is an important criterion to detect signs of thermal runaway in the case of mechanical abuse. Both experimental setups are discussed in detail in this section. Failure of components or apparatus is mentioned when they occur during testing of cells.

3.3 Battery conditioning

Lithium-ion batteries are considered safe when used under manufacturer described conditions but excessive charge/discharge and inappropriate handling can cause battery degradation or initiate internal failures before they

are used in actual applications so in this experiment a unique set up is designed to condition batteries which use a constant current-constant voltage (CC-CV) charging régime and controlled DC load to discharge at a desired level.

3.3.1 Test equipment setup

Initially, batteries are tested for their charge/discharge behaviour to ensure batteries are in a good condition and to understand and observe temperature variations in individual cells as an unbalanced cell can cause propagation of failure in adjacent cells. Results obtained in this experiment are compared with other cells to make sure cells are in a healthy condition to use in further experiments. To avoid stress conditions, low charge rates are applied on all cells. In most of the cases, charge time varies because of initial charge states. The test setup is shown in figure 3.1, and explained in detail in the following sections.

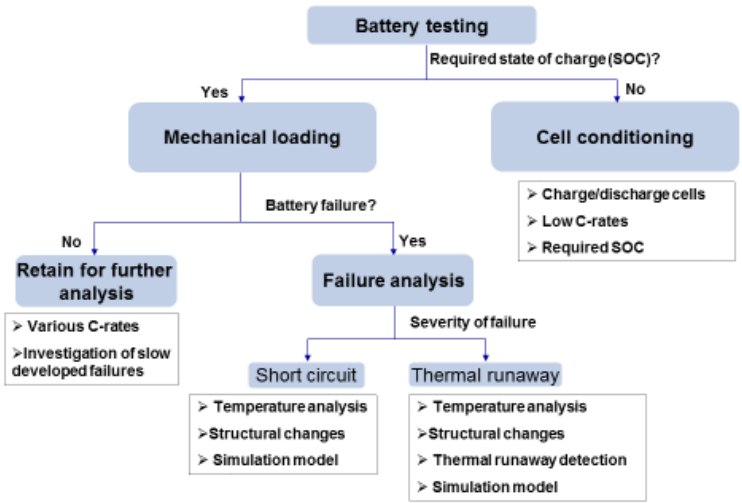

Figure 3.1: Battery testing hierarchy

A Chroma Programmable power supply 62100H-30 is used due to its high commercial acceptance and usage in battery testing experiments, which fulfils most of the battery charging and balancing requirements from small capacity cells to large commercial cells. 62100H-30 has an output voltage range of 0-30V with line regulation of +-0.01% of full scale and load regulation of +-0.02% of full scale, output current range of 0-375A with line regulation of +-0.05% of full scale and load regulation of +-0.1% of full scale and output power of 11.25 kW. With high precision readings, this power supply accounts for voltage and current temperature coefficients which are 0.04% of Vmax/˚C and 0.06% of Imax/˚C for voltage and current respectively.

A Chroma DC electronic load 63205 is used for constant current (CC), constant voltage (CV) discharge which also has constant power and constant resistance discharge options but we didn't use these functions for the current experiment. DC load has a power rating of 6.5kW, the current rating of 0-180A with a resolution of 52mA and accuracy of 0.1%+0.2% full scale. DC load has a voltage rating of 0-80V with a minimum operating voltage of 1V at 80A and resolution of 2mV with an accuracy of 0.05%+0.1% full scale.

A Chroma digital multimeter 12601 is used in this experiment which has the additional option of data logging on PC using software which can measure 11 types of measurements including voltage, current, resistance and temperature using thermocouples. In this experiment K-type thermocouples with a range of -200˚C ~ 1372° and an accuracy of ± 1.5˚C are used with the multimeter to constantly monitor the surface temperature of cells.

A Chroma power supply 62100H-30, DC electronic load 63205 and digital multimeter 12601 are interconnected and then further connected to PC using an RS-232 interface to log data at certain time intervals and avoid apparatus setting every time as most of the settings can be changed using software. The arrangement of apparatus for this experimental setup is shown in figure 3.2.

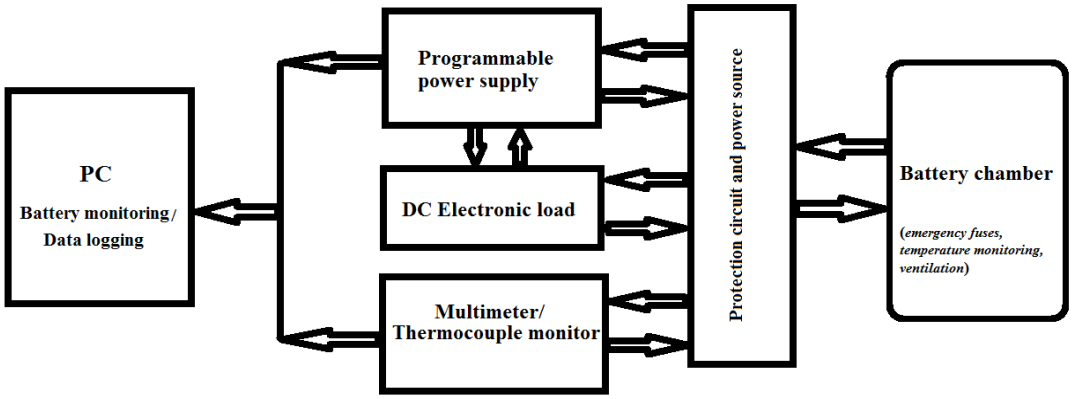

Figure 3.2: Arrangement of apparatus for Initial test

3.3.2 Cell selection and assumptions

Cells used in this research are Samsung 2200mAh lithium-ion cells from Samsung, Korea. The cell has dimensions of 18mm diameter and 65mm length with $LiCoO_2$/graphite chemistry. Low capacity cells are chosen to avoid severe conditions during cell conditioning and actual tests. Figure 3.3(a) shows 18650 Samsung 2200mAh cell.

These cells have a steel casing of thickness ~0.30mm and spiral wound layers of the anode, cathode, separator, anode current collector and cathode current collector as shown in figure 3.3(b).

(a)  (b) 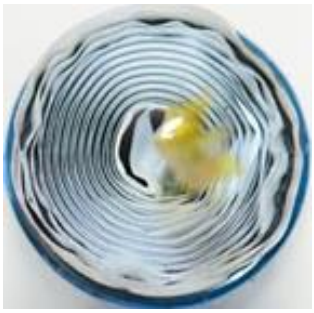

Figure 3.3: (a)18650 Samsung 2200mAh cell, (b) Spiral wound layers of 18650 cylindrical cell

Cell temperatures are not fixed so the temperature variations are the result of natural heat up and cool down. According to Doerffel, (2007) accurate measurement of cell temperatures is difficult as *in situ* measurement is not possible in all applications, so temperature measurement at cell terminals was proposed where the negative electrode has a high thermal conductivity compared to the positive electrode and this method gives a better accuracy of temperature compared to measuring on the surface.

3.3.3 Test régime

The cells are charged and discharged at three different C-rates 0.3C, 0.5C and 1C. Self-discharge is ignored due to the frequency at which the cells are used.

To achieve accuracy and consistent results, constant current (CC), and the constant voltage (CV) régime is used to condition all the cells used in this research. The discharge portion of the test cycle is performed at a constant current. The test protocol for each charge/discharge rate is as follows (Sheikh, *et al*., 2015):

1. Step 1 – Rest for 1 minute.
2. Step 2 – Charging. The cell was charged at the specified rate until a cut-off voltage is reached. This voltage was maintained until the current dropped to 0.01C (i.e., 22mA for these cells) (Doerffel, 2007).
3. Step 3 – Discharge. The cells were discharged at the specified rate until the voltage dropped to cut off voltage.
4. Step 4 – Rest for 1 minute

All batteries were stored in a battery chamber for 48 hours so that they could attain an equilibrium state and the OCV become stable during this period. The chamber used for battery testing and installation is discussed in the next section.

3.4 Battery chamber installation

The battery chamber is specially designed for this experiment which includes ventilation, isolated bottom surface to avoid contact with metal, fan controlled exhaust to maintain temperature, and protection fuses to avoid damage to equipment in case of abuse conditions including short circuit, over-charge, over-discharge or unexpected load conditions. An alarm function is also used from the power supply and DC load to avoid damage. An emergency alarm in case

of smoke/fire in the test chamber was installed for further safety of personnel and equipment. A thermometer was installed inside the chamber to constantly monitor temperatures. Battery chamber with setup is shown in figure 3.4.

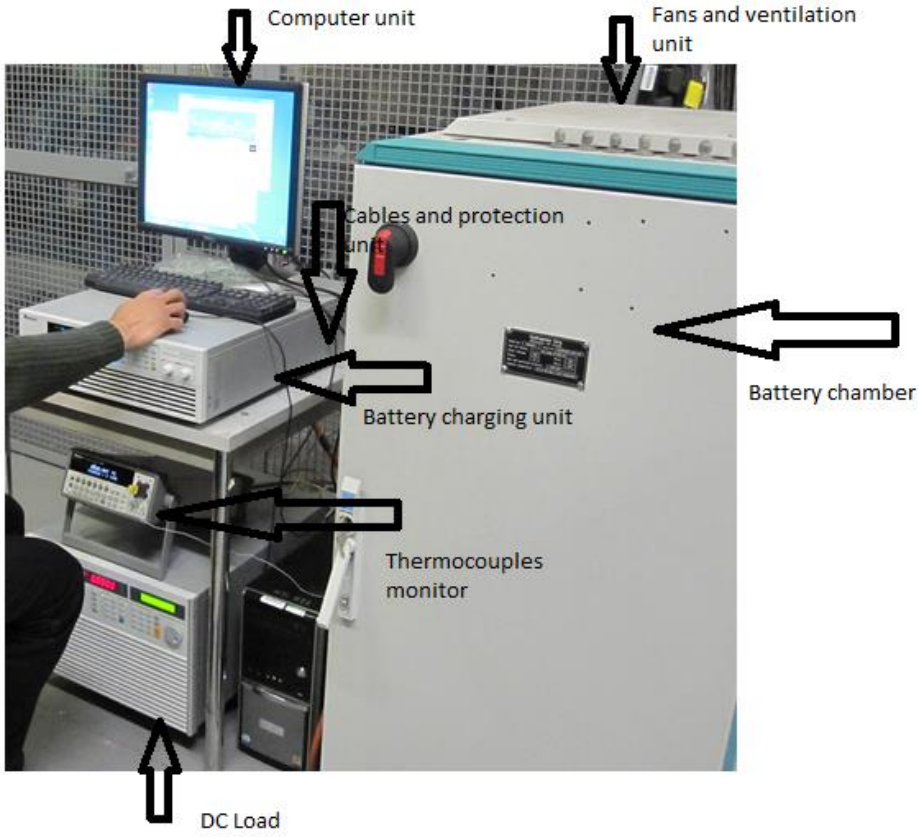

Figure 3.4: Battery chamber and initial conditioning unit

Before experimental work, the temperature of the cell and test components are maintained in the chamber so that supporting plates and wedges would not act as a medium for the cell to dissipate heat which could affect battery heat distribution and result in unrealistic temperature variations. The experimental set up for the mechanical load with the equipment used and the rationale for setup are discussed in the following sections.

3.5 Mechanical loading setup

A specialised test setup had been designed to conduct experimental work where every possible precaution was taken to achieve maximum accuracy and ensure safety of personnel and equipment. A rigid wood base was used to fix the mechanical press to absorb shock and protect against movement. The mechanical press was equipped with a 100kN load cell to record force applied, load cell is capable of both tensile and compression testing with output of 2mV/V with very low deflection. A Datum XL100 data logger with 8 channels was used for load cell, thermocouples and voltage data logging. A power supply for load cell was used which is accurate enough to constantly provide required voltage for load cell without fluctuations. FLIR infrared thermal camera was used to capture and record test data where the reference temperature was set for the cell so that temperature of equipment did not affect the results. A laptop was used to record all test data with a unique test number and test conditions. A polycarbonate sheet with a thickness of 3mm was used to protect equipment and personnel from hazardous situations which might happen in the form of cell ignition or fire. Experimental setup is shown in figure 3.5.

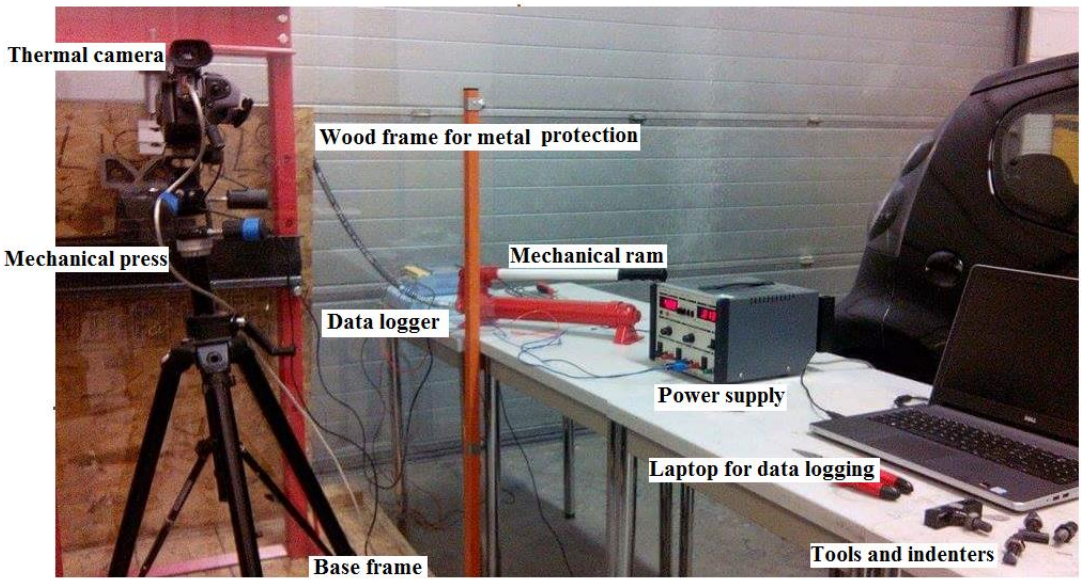

Figure 3.5: Mechanical loading setup

Mechanical abuse tests were applied to 18650 cylindrical lithium battery cells. Displacement (mm), Force (N); Temperature (°C), Voltage (V) and Stress (MPa) measurements were recorded after loading was applied to the batteries.

3.6 Description of testing protocol

In this section, the test procedure is discussed in great detail where loading conditions, type of testing, individual cells' behaviour and significant results are discussed. The trials were run in four different states of charge SOC (0%, 25%, 50% and 75%) with five repeated tests to evaluate thermal runway of 18650 lithium ion battery. Tang, *et al*. (2017); Xu, *et al*. (2016); Melcher, *et al*. (2016); Spinner, *et al*. (2015b) and Sahraei, *et al*. (2012a) have also worked on 18650 lithium-ion batteries, where Saharei, *et al*. (2012a) used constant SOC of 10%, and temperature variations were not considered. In current research

temperature variations with SOC is considered which varied at different loading conditions. Repeated tests showed similar results, values are compared with each test and mean values are used for further analysis.

Thermal properties of the loading tests are reported with an infrared camera to observe the initial hot spot and crack location, where thermal properties are observed as stable conditions, changed to under stress conditions. Thermal images at different SOC values are taken where sampling time is crucial to judge short circuit occurrence.

Thermal runaway is evaluated by reporting the amount of displacement in millimetres after impact is exerted on 18650 lithium-ion batteries with rapid change in thermal properties. The high rate of change of temperature causes a sudden voltage drop which was evident in this research and discussed in detail on different abuse conditions. The temperatures were measured at three sites on the surface of each battery. The method of thermocouple attachment on the battery was implemented because it is a more practical method than, for example the use of adiabatic Accelerating Rate Calorimetry (ARC) that requires access to an adiabatic calorimeter and causes gas release (Orendorff, *et al*., 2016). Attaching the thermocouples to three locations of the battery cell allowed the top, bottom and mid-surface battery sections to be evaluated for temperature changes (Sahraei, *et al*., 2016). Thermocouples are attached to the surface of each battery at the positive charge terminal end (+ve), the mid-surface and the negative charge terminal (-ve).

3.6.1 Rod test

Rod with diameter 11.70mm and length 33.20mm was used, which is 'T' shaped and the material used is alloy steel. A rigid base plate is placed beneath the cell which is tightened from the bottom and fixed on a mechanical press. The rod indenter is calibrated with the load cell using a specialised design adapter to make sure the rod is fixed and does not give inertial forces during compression of cell. Insulated sheet was used to avoid heat transfer which may occur when indenter/bottom plate established contact with the cell which is thermally active.

In the 0% SOC rod test, the onset of a change began at approximately the same time for all the thermocouples at about 8.51mm displacement for +ve terminal and mid surface but occurred a few seconds earlier for –ve terminal when the displacement is equal to 8.389mm. Test setup is shown in figure 3.6 (a,b).

(a)

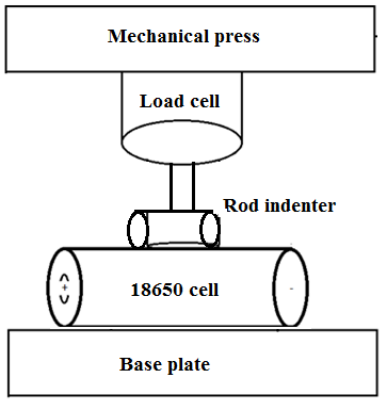

(b)

Figure 3.6: (a) Line diagram of rod test, (b) Experimental setup for rod test

The temperature for –ve terminal showed an approximately 90°C increase when the largest displacement amount was observed. The OCV was 3.43 V when the experiment started but after 336 seconds the dropped to approximately 0.08 V. The force measured at 12.776 kN. In 25% SOC with rod loading the highest temperature was 68.2°C at the largest displacement of approximately 7.794 mm and voltage rapidly decreased to zero within a few seconds.

The rod test for the lithium-ion battery cells in 50% SOC did not show a dramatically changed displacement. The largest displacement caused by the rod in a 50% SOC environment measured approximately 7.569mm, at that point +ve terminal temperature equalled about 22.2°C, the mid surface temperature equalled about 23.5°C and -ve terminal temperature equalled about 31.5°C, after which the displacement remained the same, so that this test was discarded and not considered for further analysis in this thesis. For a better understanding of the results mean values of force and displacement at various SOCs were compared as shown in figure 3.7.

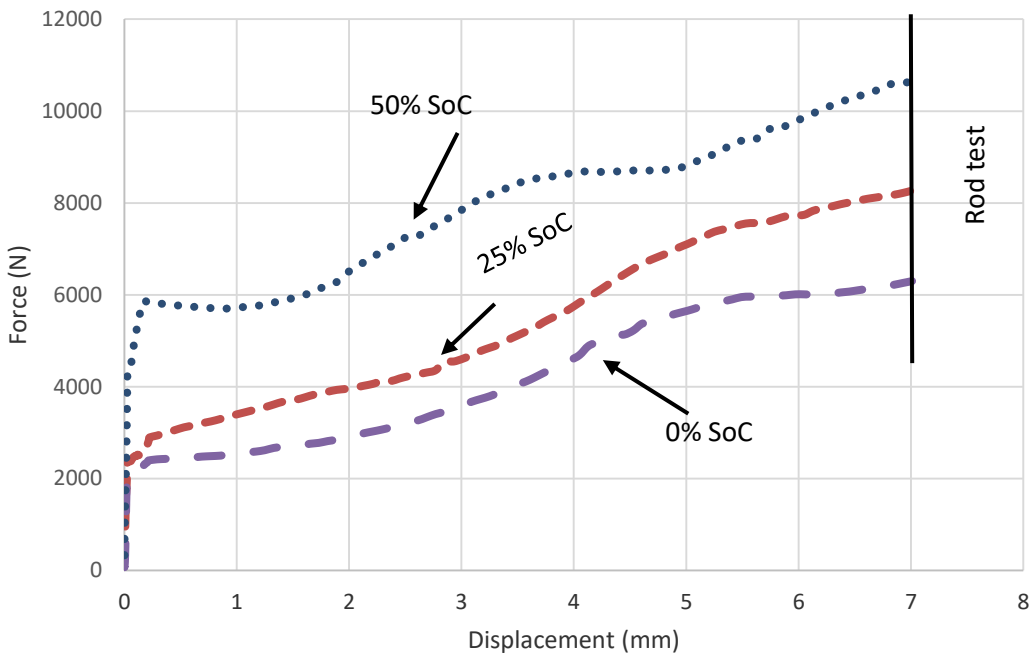

Figure 3.7: Rod test, force and displacement at different SOCs

As described above, the displacement varies at various SOCs therefore to generalise results and achieve accuracy. Displacement cut off point is set to 7mm to check applied force and displacement response due to SOC. At high temperatures, the battery casing which is made of steel and current collectors made of copper and aluminium became softer which is also mentioned by Xu, *et al*. (2016); Scapin, *et al*. (2014) and Chen, *et al*. (2004). As shown in figure 3.7, low force is required for 0% SOC which is due to the very little electrochemical reaction, in the cell and applied force is higher at higher SOCs which is due to hardening of cell layers as the electrochemical reaction took

place with lithium insertion and transport. This phenomenon was observed for other loading conditions; however this is not the ultimate scope of this research.

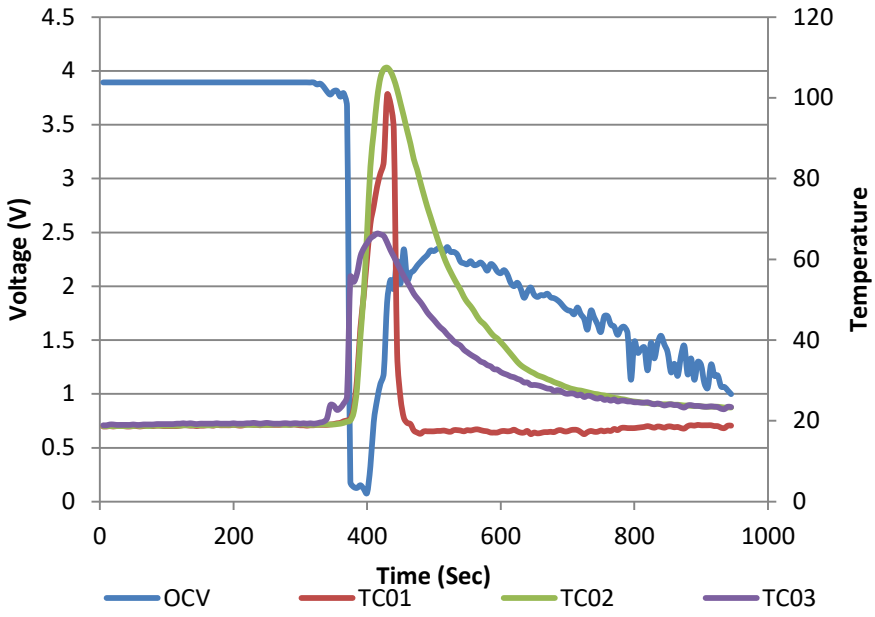

Figure 3.8: Rod test, Voltages Vs Temperature at 75% SOC for complete test

Further analysis was done to understand the effects of SOC on short circuit occurrence and sudden voltage drop observed at high SOCs compared to lower values of SOCs. A similar phenomenon was observed by Xu, *et al*. (2016) where loading type was flat plate and three-point bend. Voltage drop due to short circuit occurrence was discussed by Sahraei, *et al*. (2012a) but the effect of SOCs on short circuit are not considered in great detail, however, the onset of short circuit with respect to peak force and voltage drop is discussed. Times for short circuit occurrence and voltage response are shown in figure 3.9.

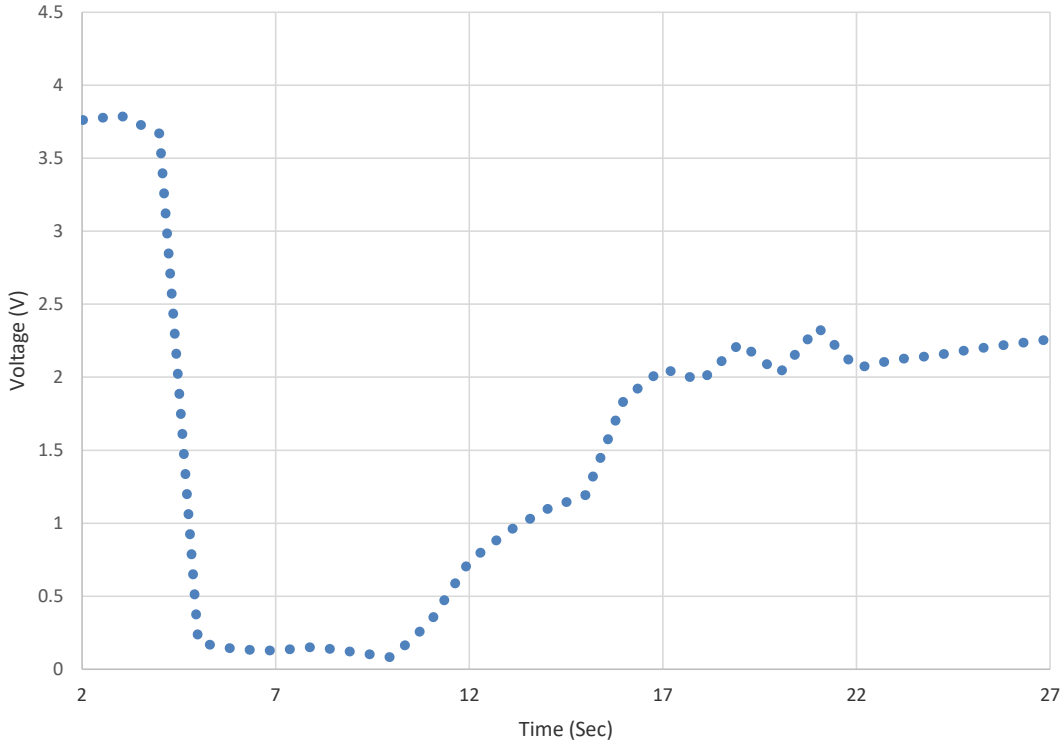

Figure 3.9: Short circuit occurrence at 75% SOC, rod test

Localised time duration of short circuit occurrence, where voltage dropped to nearly zero and stabilised itself to nearly cut off voltage shows deformation of one or more than one layers and the voltage increase after short circuit is due to release of applied force which allowed layers to relax. Applied force with respect to time is shown in figure 3.10, where at 25% SOC force drops at around 300 sec which is the time of short circuit and is due to release of load.

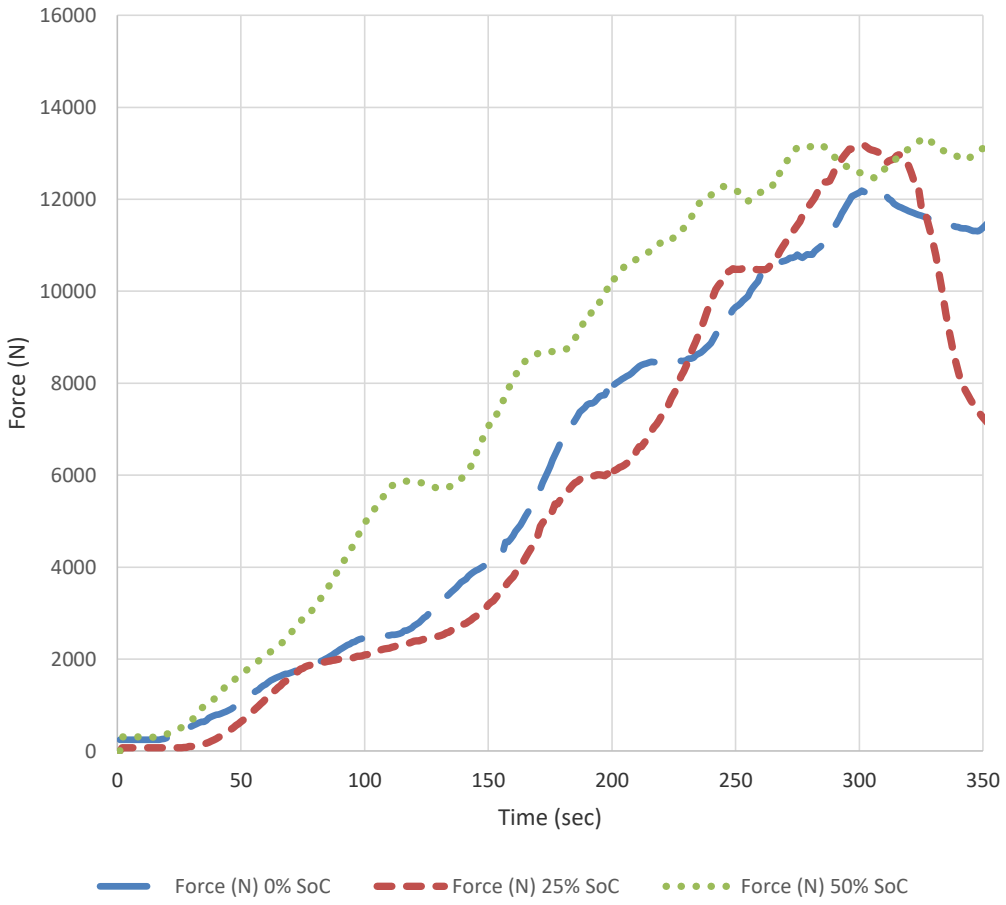

Figure 3.10: Rod test, Force values at different SOCs

The above phenomenon is further explained in figure 3.11, where it can be seen that higher the initial SOC requires higher force as layers become stiff due to electrochemical reaction, where the higher the potential the higher the stiffness of layers which are also reported by Xu, *et al*. (2016) and Sahraei, *et al*. (2012a).

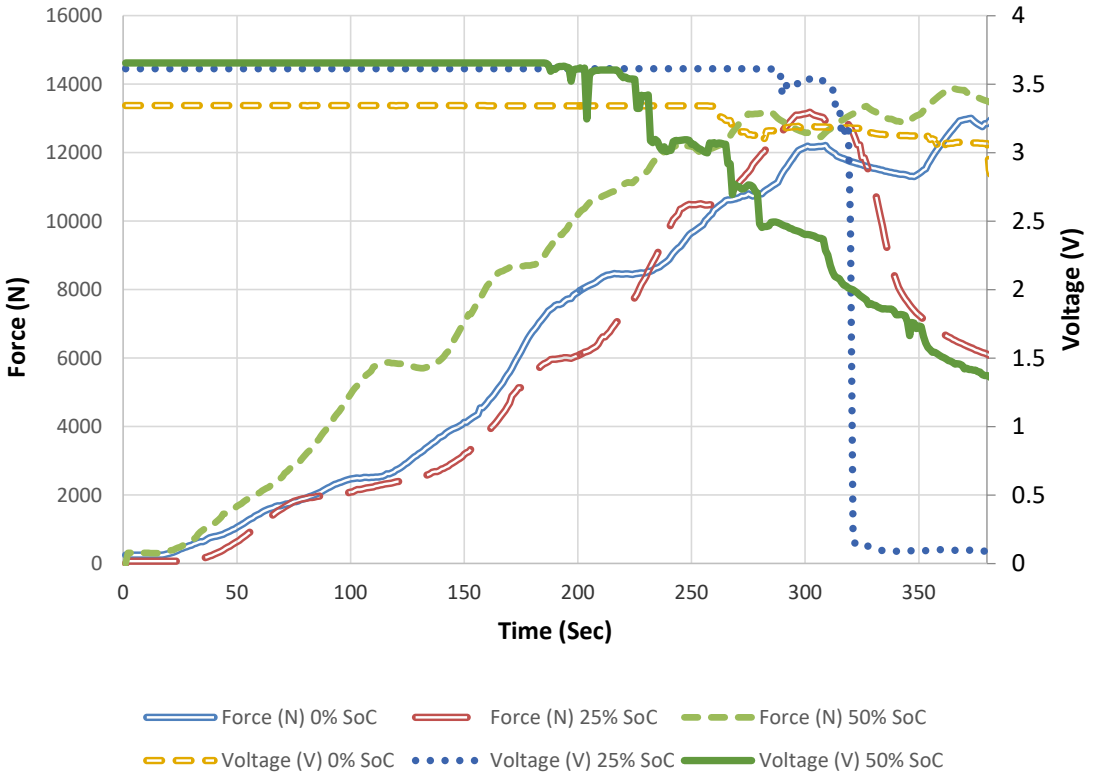

Figure 3.11: Significant rod test results for force and voltage

To conclude, the rod test results were compared for 75% SOC, which is evident in Hooper, *et al*. (2016) where high cell degradation occurs at 75% SOC, so repeated tests were used to achieve better accuracy at initially conditioned 75% SOC cells. Results obtained are shown in figure 3.12.

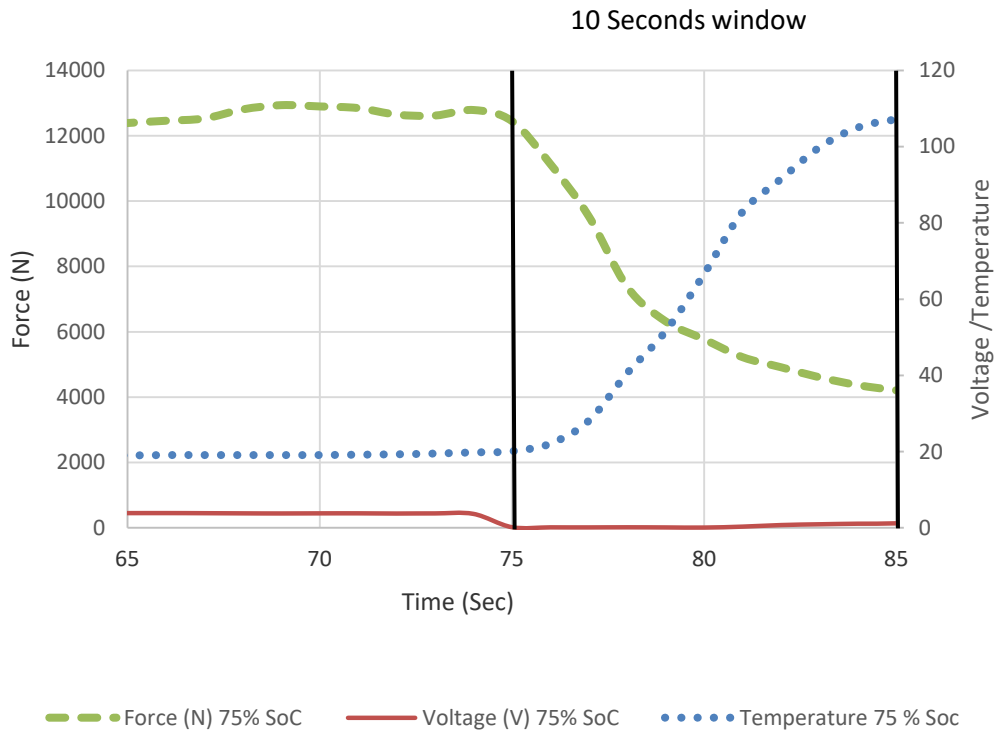

Figure 3.12: Rod test, force, temperature and voltage values at 75% SOC

As shown in figure 3.12, within ten seconds of short circuit occurrence where force was released the voltage dropped to nearly zero and the temperature increased at the rate of 540°C/minute, which is important to detect early battery degradation as individual battery cells with such a high temperature rise can cause adjacent cells to degrade or imbalance temperature distribution within the module or pack. These results are further explained in the next chapter where crack initiation and initial hotspots due to mechanical failures are discussed.

3.6.2 Circular punch test

A circular punch with outside diameter 15mm, height 24.50mm and inside diameter 11.70mm was designed with alloy steel material using the same safety precautions for testing as for rod test. A rigid flat plate was used for the base which was fixed on a mechanical press. Test conducted with the circular punch is discussed in the following sections.

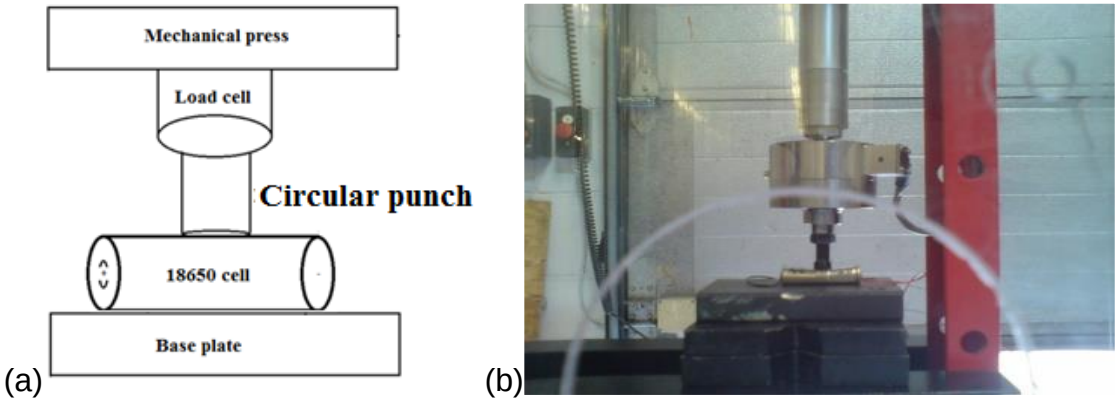

Figure 3.13: (a) Line diagram circular punch test, (b) Experimental setup for circular punch test

Initially at 0% and 25% SOCs circular punch test did not show major changes in voltage and temperatures. Repeated tests exhibited similar behaviour which might have been due to low potential and electrochemical reaction which is slow to proceed to a similar phenomenon as detailed by Jian, *et al*. (2016), where the electrochemical process is considered to have a finite current value or non-zero current value which means it would have some internal resistance which is also at non-zero value so that initial voltage value, which represents OCV, may have a slightly different value compared to the measured value but

where the voltage (OCV) would be dependent on SOC as reported in this thesis. To understand voltage and SOC dependence in circular punch test high SOC values of 50% and 75% were used and concluded with significant changes as shown in figure 3.14.

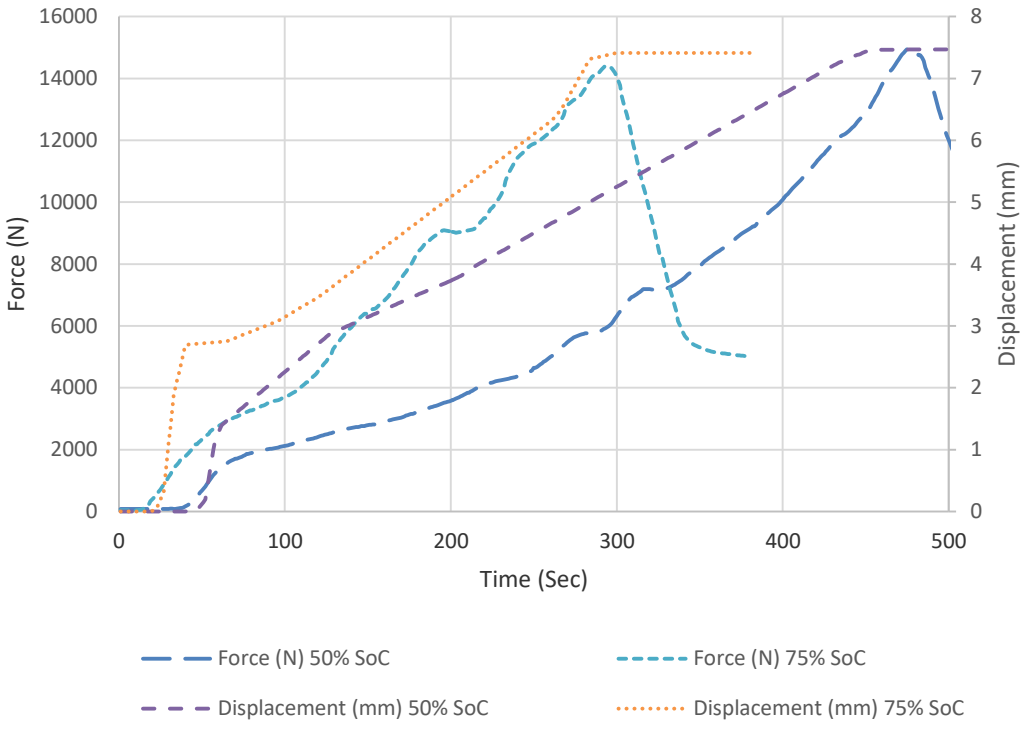

Figure 3.14: Circular punch, force Vs displacement at 50% and 75% SOC

Low current values were used to condition cells as mentioned at the beginning of this chapter to control Li insertion/extraction rates among the particles of the electrodes. As mentioned by Roscher, *et al*. (2011) inhomogeneity can occur in the particles' Li content due to very high current rates which can force transfer of ions from lithiated to delithiated particles. The under mentioned controlled environment of 50% and 75% SOC cells were tested and found that high SOC

cells (75% in circular punch case) tended to attain short circuit earlier compared to their low SOC counterparts due to softening of the metal layers (current collectors and casing) and at the same force voltage dropped to zero and force released due to cell deformation. The deformation value was lower than 50% SOC which exhibited hardening of layers as show in figure 3.14. Force and voltage relation with respect to time is shown in figure 3.15.

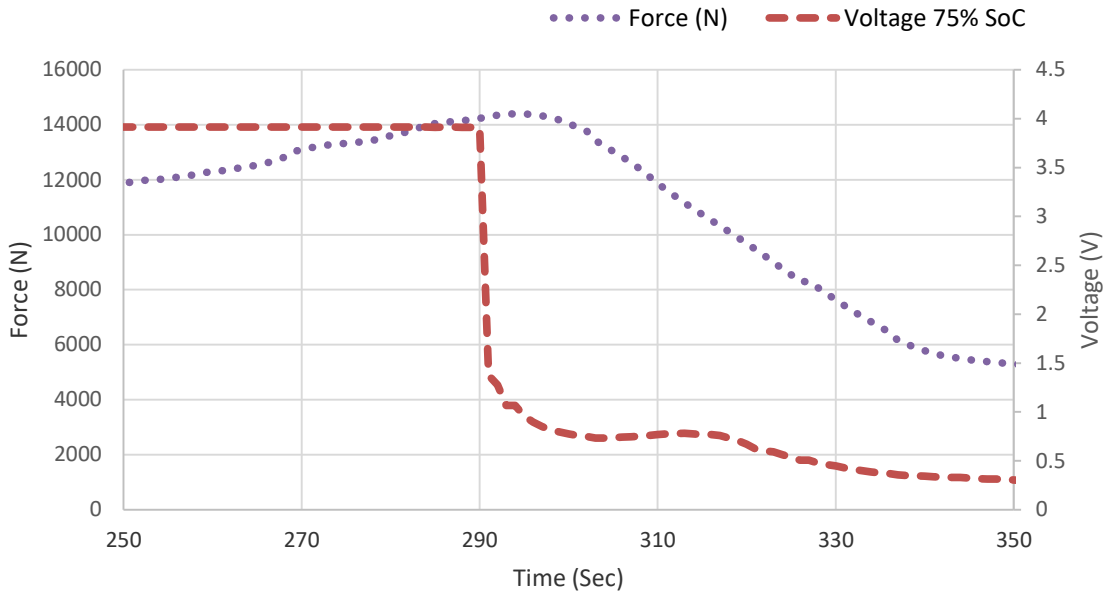

Figure 3.15: Circular punch, force and voltage relation at 75% SOC

Contact area is important when discussing internal shorting due to external force applied where layers become closer and shrink in the case of separator and break in the case of active materials which are low density. Active materials use coatings where anode with graphite coating and cathode with $LiCoO_2$ coating was used in 18650 cylindrical cells discussed in this work. As shown in figure 3.15, short circuit occurred at around 14 kN force where the potential

difference was around 0.2V. Layers exerted high force before going into damage zone and making contact with current collectors. The mechanism of internal short circuit was discussed by Guo, *et al*. (2016) and is as shown in figure 3.16.

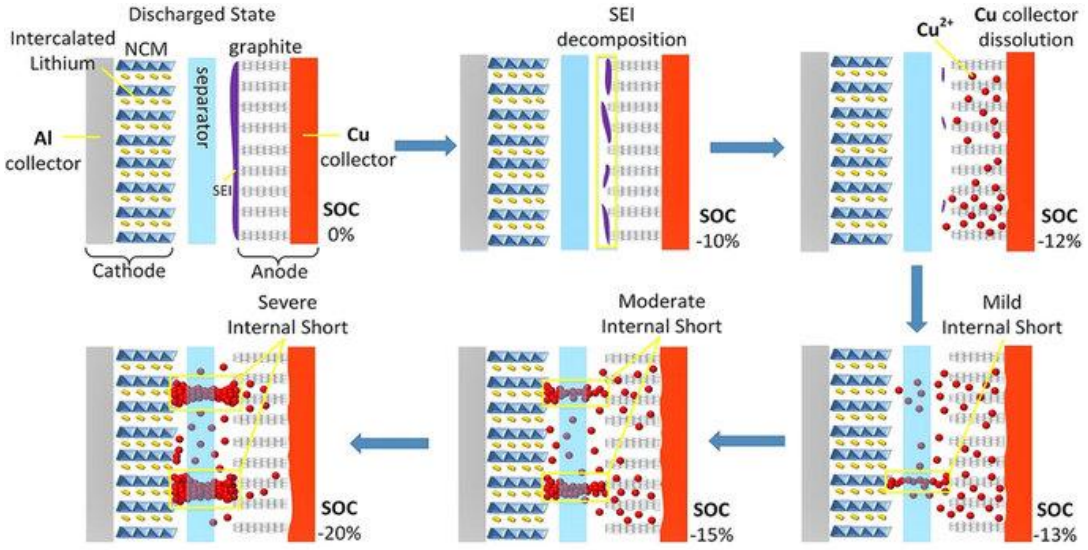

Figure 3.16: Internal short circuit occurrence due to over-discharged process (Guo et al., 2016)

Internal short circuit with respect to SOC is explained by Guo, *et al*. (2016) where internal short circuit due to over-discharge cells is considered, but in current research short circuit initiation due to deformation of layers is discussed which can be more catastrophic if this happens in the battery pack or module where cells are connected in series/parallel and initiation of short circuit in one or more cells can attain higher temperatures and SOC can go as low as -20% as shown in figure 3.16. Thermography results are discussed in detail to analyse this phenomenon in the next chapter.

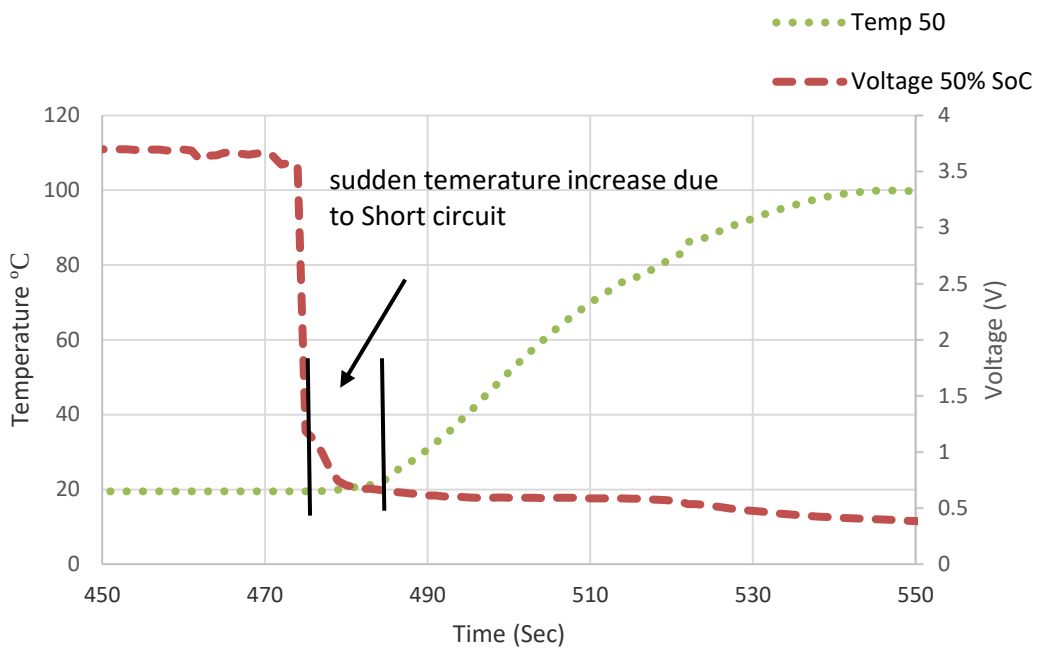

Figure 3.17: Circular punch, voltage and temperature relation at 50% SOC

Xu, *et al*. (2016) and Guo, *et al*. (2016) discussed short circuit occurrence of lithium-ion batteries where Xu, *et al*. (2016) tested SOC dependent mechanical integrity of lithium-ion batteries and Guo, *et al*. (2016) discussed over-discharge induced internal short circuit, but in both pieces of research thermal effects were not considered in detail where temperature increased after short circuit occurrence as shown in figure 3.17, where temperature rose to 100°C within a minute which is much slower compared to temperature increase rate of 540°C/minute in case of rod test.

3.6.3 Three-point bend test

Three-point bend test is performed on 18650 lithium-ion cells to check mechanical integrity of these cells where cells tend to bend in a way with much

of the stress exerted on the mid bottom surface. Three-point bend tests are not commonly used for these types of batteries in the literature and very little evidence was found (Xu, *et al*. 2016; Sahraei, *et al*. 2012a), for these tests but the type of indenter and support varied in dimensions. Three-point bend test holder and indenter are discussed in this section.

Specific cell holder and sharp edge indenter were designed, where dimensions for cell holder were 88mm length, 56mm width and cell holder cuts of 19.7mm. Cell holder supports were welded to 4mm thick bottom rigid plate and the gap between both holder plates was 42mm as shown in figure 3.18. Indenter has cone shape with length 7.4mm and thickness of 1mm, where total length of indenter was 24.50mm and rod diameter of 11.70mm. The same assembly protocol was used as when rod test and circular punch were used. Detailed experimental results are discussed in the following sections.

Sharp edge of thickness 1 mm is chosen for this research because it differs from nail penetration where short circuit initiation occurred due to nail penetration (NHTSA, 2017; Zhao, *et al*. 2015; Christopher, *et al*.,2014; Feng, *et al*. 2014;) deep into the layers and showed high temperature change as all layers were in contact with nail, but in the current research sudden loading conditions were calculated which could be the result of initial deformation of separator layers or current collectors coming into contact where, due to energy absorption after short circuit forces, drop down to low values and impact becomes quasi-static. Experimental set up is shown in figure 3.18(a,b).

(a)

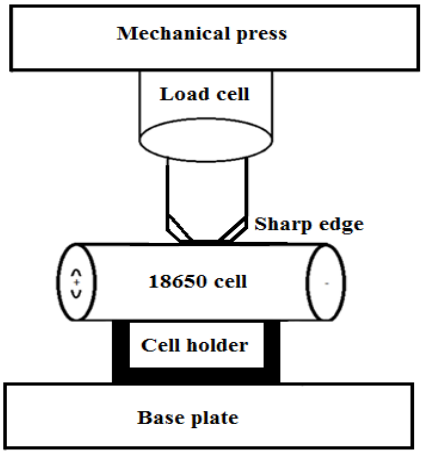

(b)

Figure 3.18: (a) Line diagram for Three-point test, (b) Experimental setup for Three-point bend test

For three-point bend test with sharp edge of 1mm, maximum force applied to initiate short circuit for 75% SOC is 2.98 kN. Lower force values were recorded at other SOCs. Temperature increase and voltage drop were recorded for all tests as shown in figure 3.19.

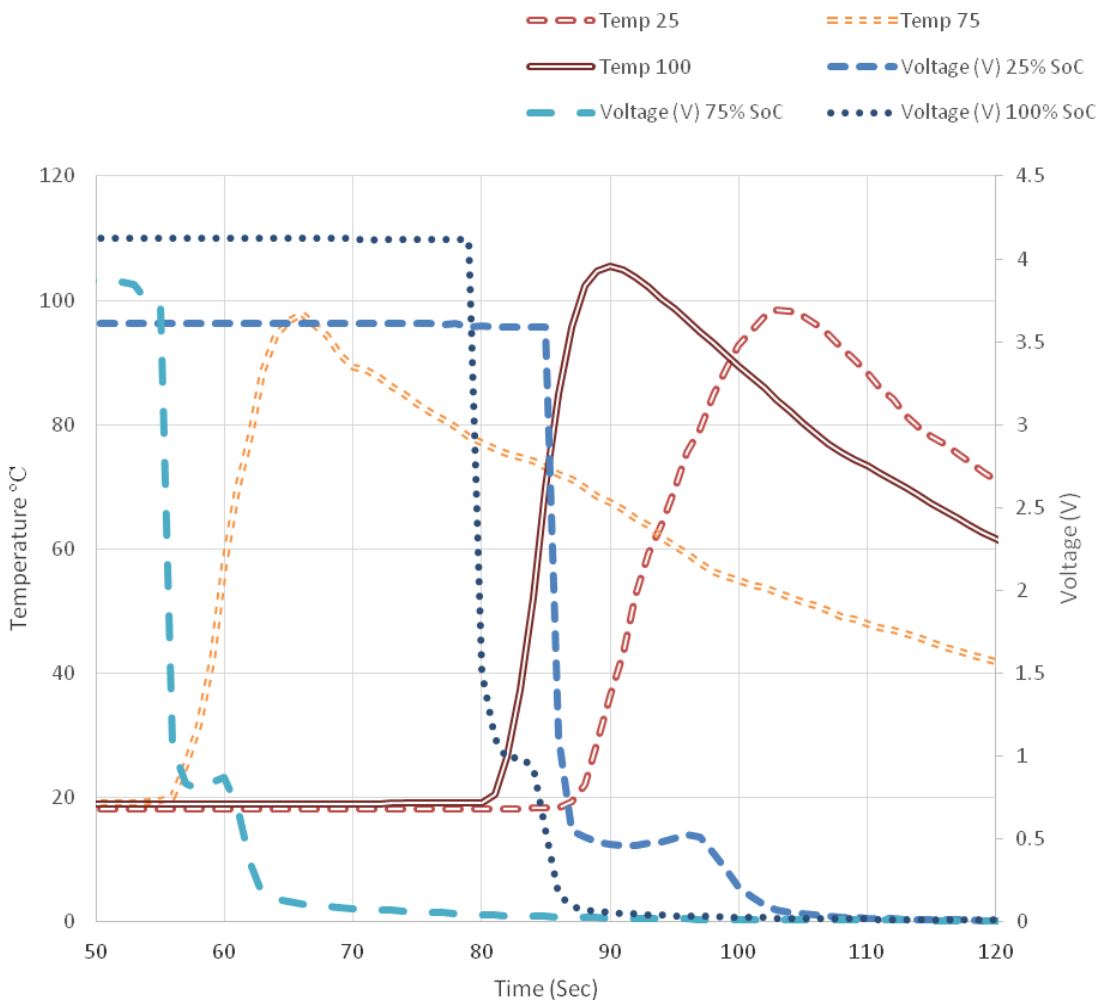

Figure 3.19: Three-point bend test, voltage and temperature relation

The 100% SOC test which is only used for three-point bend test, the temperature rose to 110°C with force 3kN and displacement of 7.7mm at the instant of short circuit. Temperature rise is sudden and rose at the rate of 700°C/minute. Sharp edge crack on sides and mid surface were recorded and tension at bottom was recorded which showed steel material stiffness at the time of impact. Similar results were observed for 25% SOC and 75% SOC, although 50% SOC was ignored due to inconsistent results during repeated

tests. Force-displacement behaviour at short circuit was shown in figure 3.20. Faster voltage drop in low SOC was observed which was due to immediate short circuit development in these cells.

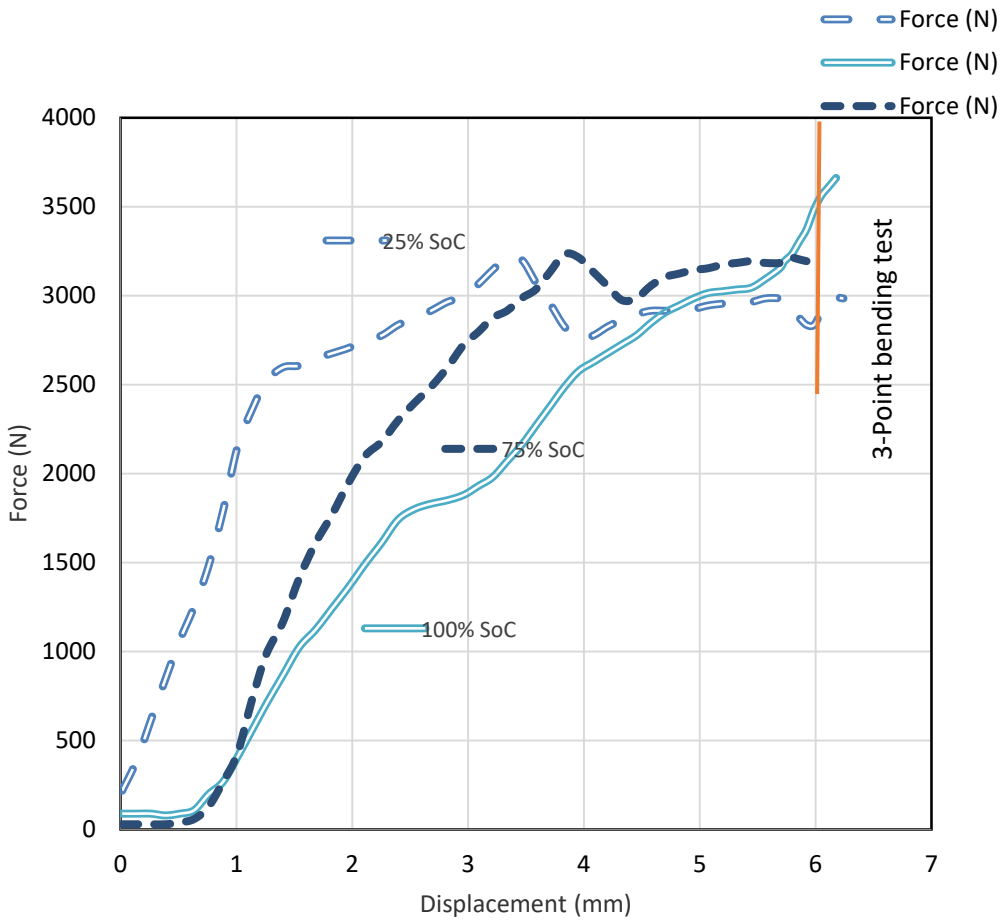

Figure 3.20: Three-point bend test, Force and displacement relation at different SOCs

As shown in figure 3.20, initially the cell experienced an elastic region but fracture occurred at a force of 2.5kN for 25% SOC and at 3.2kN cell started to deform and undergo deformation which is the initiation of short circuit for this test. 75% more force was required for initial fracture which was 3.2kN and

permanent deformation occurred immediately after initial fracture at 3kN and cell experienced short circuit. For 100% SOC cell experienced fracture at 1.8kN but did not undergo short circuit until applied force was 3.5 kN. Buckling of steel casing was observed from 100% SOC where force varied due to softening of steel casing but did not achieve permanent deformation. A similar phenomenon is mentioned by (Xu, *et al*. 2016).

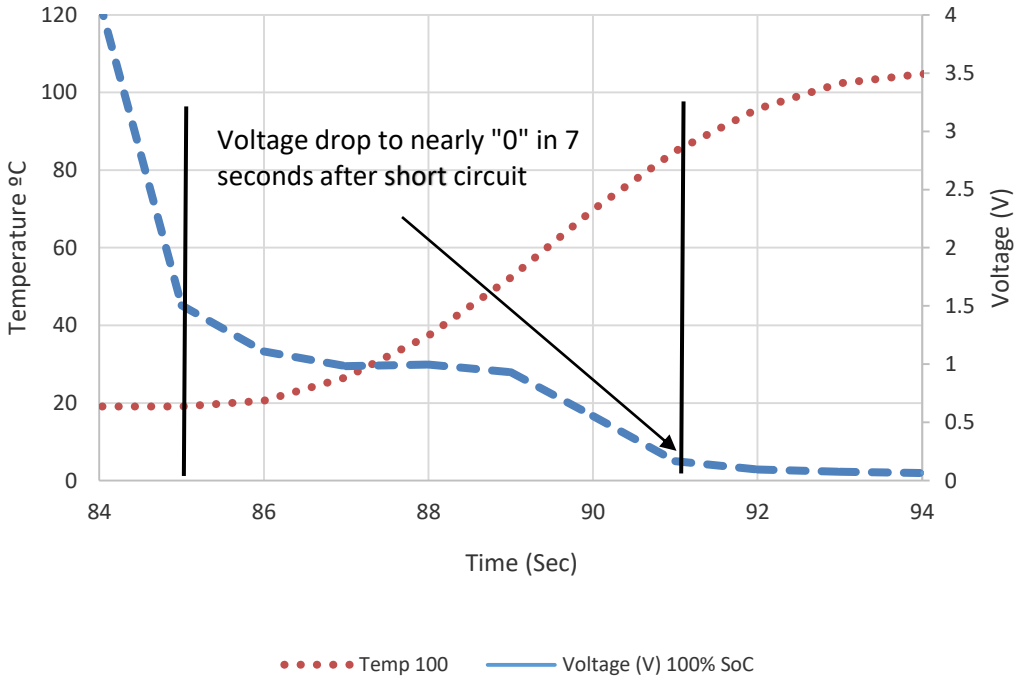

Figure 3.21: Sudden voltage drop as a result of short circuit due to bending

As explained above, short circuit occurrence will be slow in high SOC cells but temperature variation will be high in these cells as high energy content is stored. Rate of temperature change may vary which depends on many factors including, area of fracture and place of temperature measurement. In figure 3.21, voltage drop due to short circuit with 100% SOC is shown. It was

observed that it took 7 seconds to attain the voltage drop to nearly zero value following the high temperatures attained. This phenomenon will be further investigated in the next chapter where more thermal and electrical parameters will be involved to detect early signs of short circuit which can lead to thermal runaway. Due to similarity and consistent results, 75% SOC tests for three-point bend will be further investigated.

3.6.4 Flat plate deformation test

Flat plate deformation test was conducted using flat plate adaptor of length 70mm and width 20mm which was fixed to load cell. The bottom plate was a rigid plate with much higher dimensions than the indenter. No cell support was used for this test. Electrolyte leakage occurred in flat plate deformation as batteries underwent large mechanical failures.

Four environments were used when measuring the displacement occurring due to flat plate compression: 0%, 25%, 50% and 75% SOC. The compression was caused by the two flat plates each measuring 20 mm x 70 mm as shown in figure 3.22 (a,b).

(a)

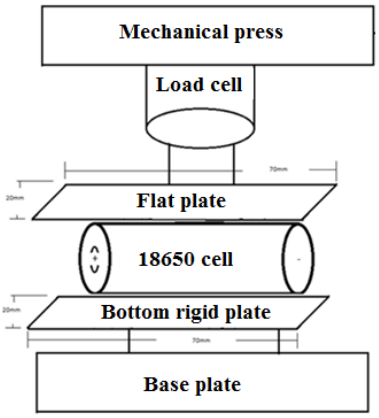

(b)

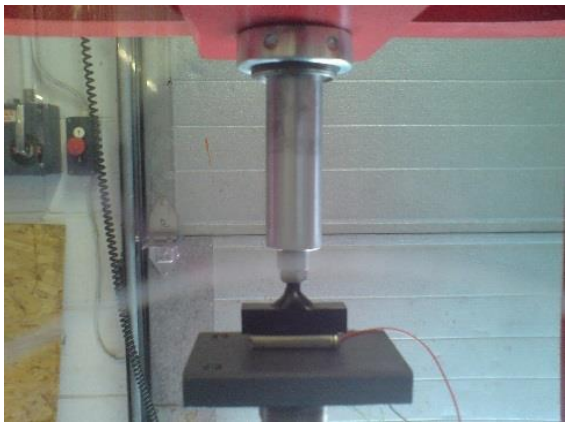

Figure 3.22: (a) Line diagram for plate plate test, (b) Experimental setup for Flat plate test

During flat plate compression test first temperature peak started to form at the same time for each surface location under the condition of 0% SOC, but the peaks for the buckling of the shell and the shell fracture occurred very close. The flat plate compression results for the 25% SOC environment over time showed an unusual shape. High temperatures were recorded as shown in figure 3.24.

The flat plate compression results for the 50% SOC environment show that the maximum displacement occurred at 6.450 mm. The curve began its increase close to a temperature of 90°C, after the peak for all three thermocouples attached at top, mid and bottom of cell had displacement measurements of 6.36mm to 6.45mm. The curves descended to their initial level so that by 6.45mm all the sections of the battery lost voltage.

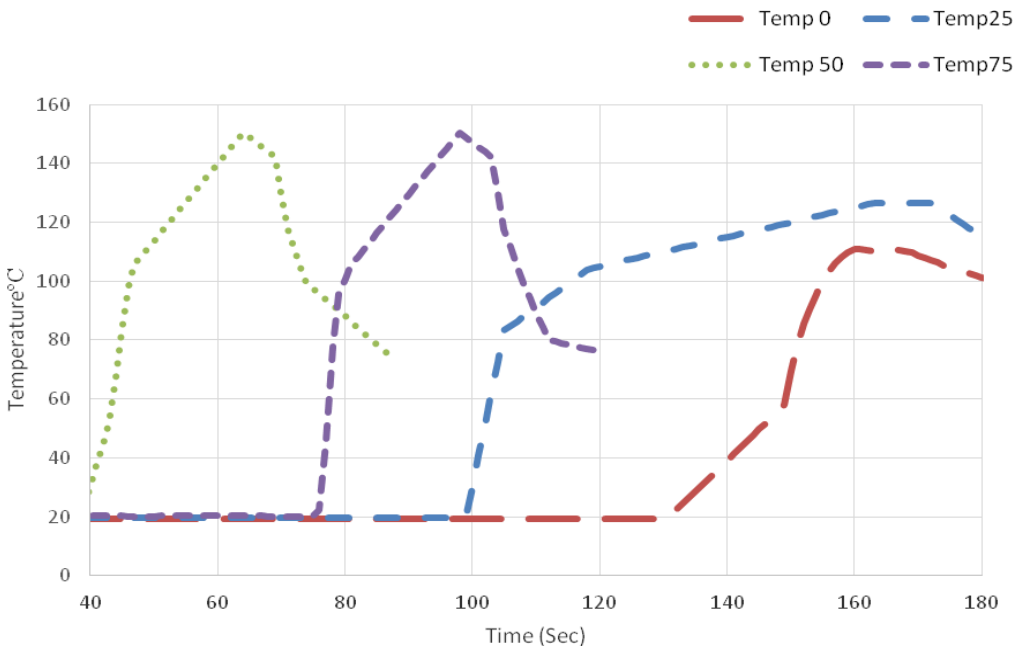

Figure 3.23: Flat plate temperature variations at various SOC

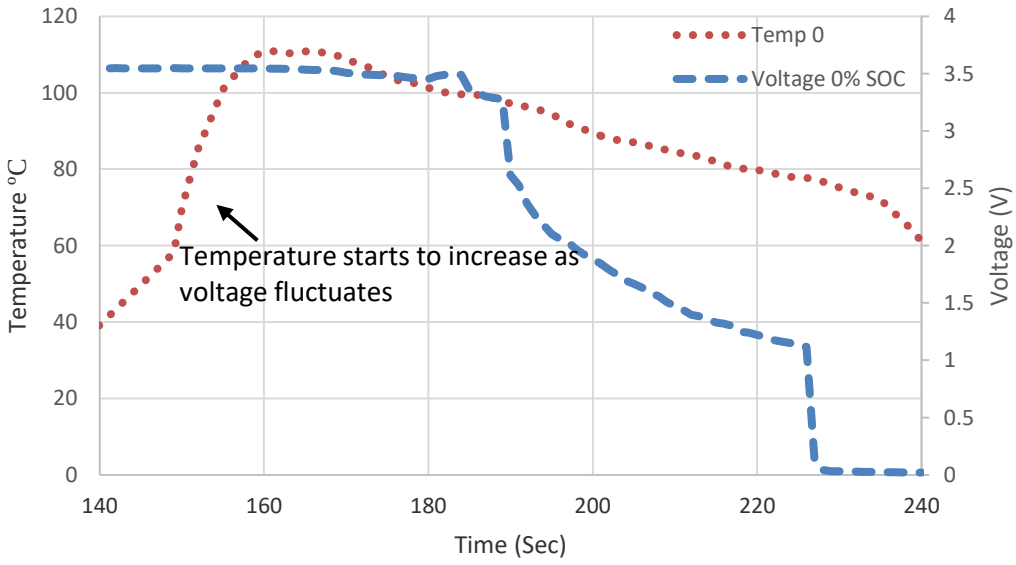

Figure 3.24: Flat plate, 0% SOC temperature and voltage variations at short circuit

As shown in figure 3.24, voltage and temperature variations were different in flat plate compression as maximum cell area was impacted with this type where cell temperature increased immediately after load applied, although some voltage fluctuations were observed which indicated changes in cell's internal chemical properties where current collectors and active materials were in direct contact. These types of cell fractures were not observed on the steel shell casing but endcaps were affected as at the high force endcaps started to become detached and electrolyte leakage occurred. This indicates flat plate deformation can cause cells to undergo internal damage even though there are no signs of external rupture or damage; however change of shape is observed due to this type of loading where the cell changes from circular shape to elliptical shape. Voltage variations for 75% SOC is shown in figure 3.25.

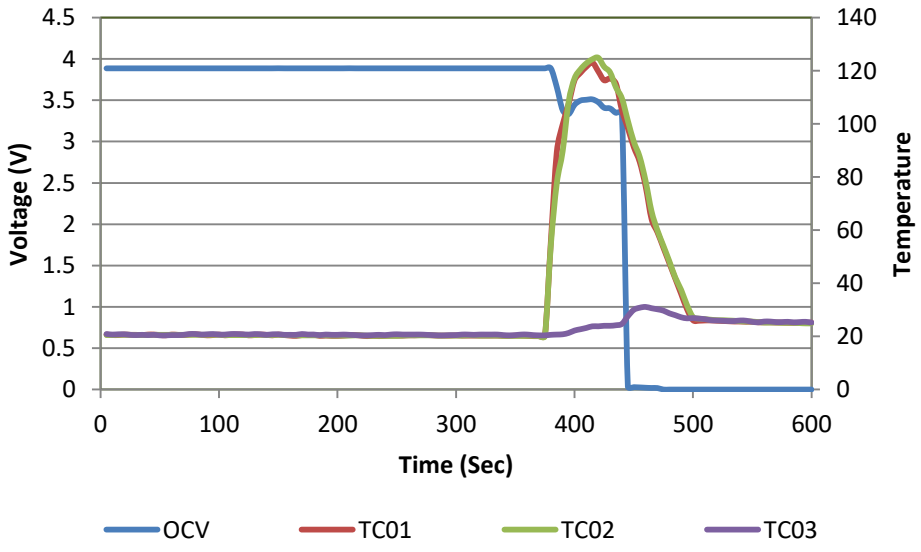

Figure 3.25: Voltage variations at 75% SOC with respect to time at short circuit

The abrupt ascent of the three sections of the lithium ion battery cell is shown as a 90°C increase where the maximum displacement measures 7.331mm. The shape of the curves are similar at the lowest level, mid-surface and -ve at the highest level as the curves move from the first peak at a range between 100°C to 120°C for thermocouples +ve, mid-surface and –ve at 7.329 mm; and then to the second peak ranging from 125°C to 160°C for +ve, mid-surface and -ve in the 75% SOC environment under flat plate compression. The second peak occurs at 7.263 mm for all three thermocouple sections of the lithium-ion cell. The results are far more dramatic for this type of compression than for the rod caused displacement. These testing and relevant results are further detailed in next chapter.

3.7 Summary

Short circuit leading to thermal runaway is evaluated in this chapter where test setup and protocols are discussed in detail. All tests showed significant results where short circuit occurrence and time of temperature increase and voltage drop with drop in force were evaluated. Repeated tests were used for accuracy (accurate mean values are used for analysis). Due to the nature of the experiment, several cells were tested for each test protocol but due to the limitations of this thesis significant results were discussed and conclusions drawn from those results. As discussed and shown in above sections, all loading conditions have their significance in this work, where the ultimate goal is to detect early signs of short circuit which may lead to thermal runaway due to quasi-static loading conditions. The three-point bend test showed short circuit

occurrence due to low applied force; however flat plate deformation showed less displacement. In rod, circular punch and flat plate deformation tests, significant temperature changes were observed which vary with varying SOC. Results obtained and discussed in this chapter are further discussed in the next chapter where crack initiation due to impact, crack location and governing mathematical equations and results are discussed in detail.

Chapter 4: Experimental Analysis and Results

4.1 Introduction

Initial battery failures due to all four loading conditions were discussed in previous chapters where full recovery zones for cells were not evident during the testing, however partial recovery on a few of the tests was observed which will be explained in detail to discuss cell characteristics before and after recovery.

Results from the previous chapter are concluded for short circuit displacement, and the stress-strain relation is discussed for each test condition with the stored capacity which is expressed as SOC. Structural analysis for each test type is detailed with failure pattern and behaviour, where cell deformation with the initiation of buckling, crack, or fracture is considered. Temperature variations, particularly in the onset of short circuit and possible thermal runaway, are discussed where results from the thermal camera were used with sample time and contour plot of temperature change.

4.2 Displacement analysis

Initial analysis focused on exploring how displacement relates to the onset of the short circuit in the batteries, where figure 4.1 shows displacement vs. SOC at the point of the short circuit, where the short circuit is defined as the moment that the cells' voltage began to drop. Short circuit occurrence for flat plate took place at relatively low displacement for 0% SOC, but the highest displacement

of approximately 7mm is observed for 75% SOC, which is the highest SOC in this loading condition. These phenomena are also mentioned by Xu, *et al*. (2016) and considered as stiffening of internal layers.

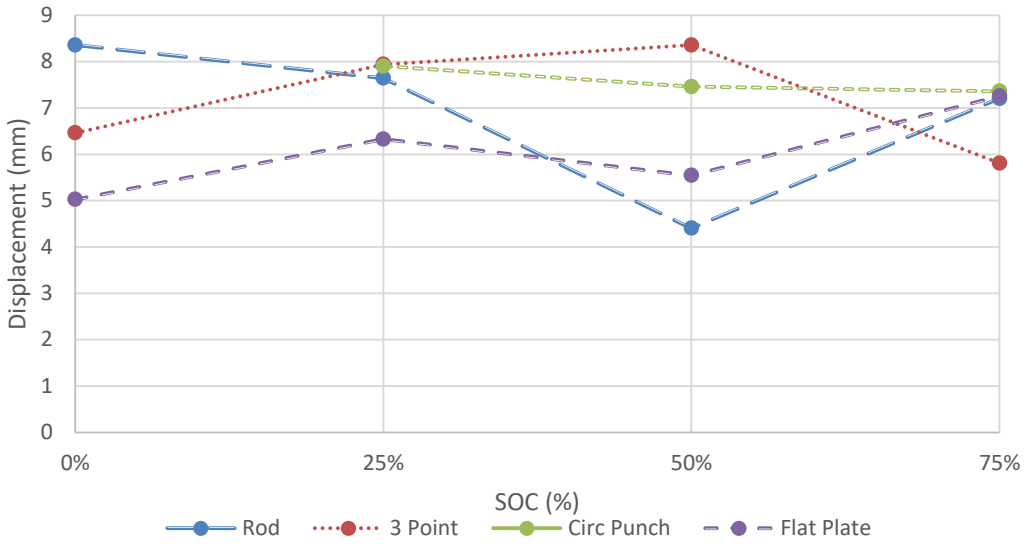

Figure 4.1: Displacement Vs SOC at short circuit

Circular punch test showed similar behaviour at 50% and 75% SOCs, where the amount of displacement at the short circuit is the same, however at 25% SOC, and high displacement value was observed for short circuit occurrence. Three-point bend test showed a linear increase of displacement with increasing SOC except at 75% SOC where short circuit occurred when sharp edge travelled less distance. For rod test, unusual behaviour was observed where linearly decreasing displacement with increasing SOC was observed except 50% SOC where the low value was observed. By repeating test much higher values were observed, which are shown in figure 4.1. This finding is significant to

understand displacement behaviour of cells, which is further detailed as displacement range for short circuit occurrence due to quasi-static loading. For flat plate tests displacement range for all tests, scenarios are 5mm to 7mm, which shows battery cells are safe below 5mm displacement during flat plate deformation, given that same test protocol used here was used for testing. Displacement range is 7mm to 8mm for rod test and circular punch tests except for 50% SOC rod test which exhibits low travelled distance of indenter. For three point bend test this range was 6mm to 8.3mm.

4.3 Temperature analysis

Mean peak temperatures at short circuit instance are shown in figure 4.2.

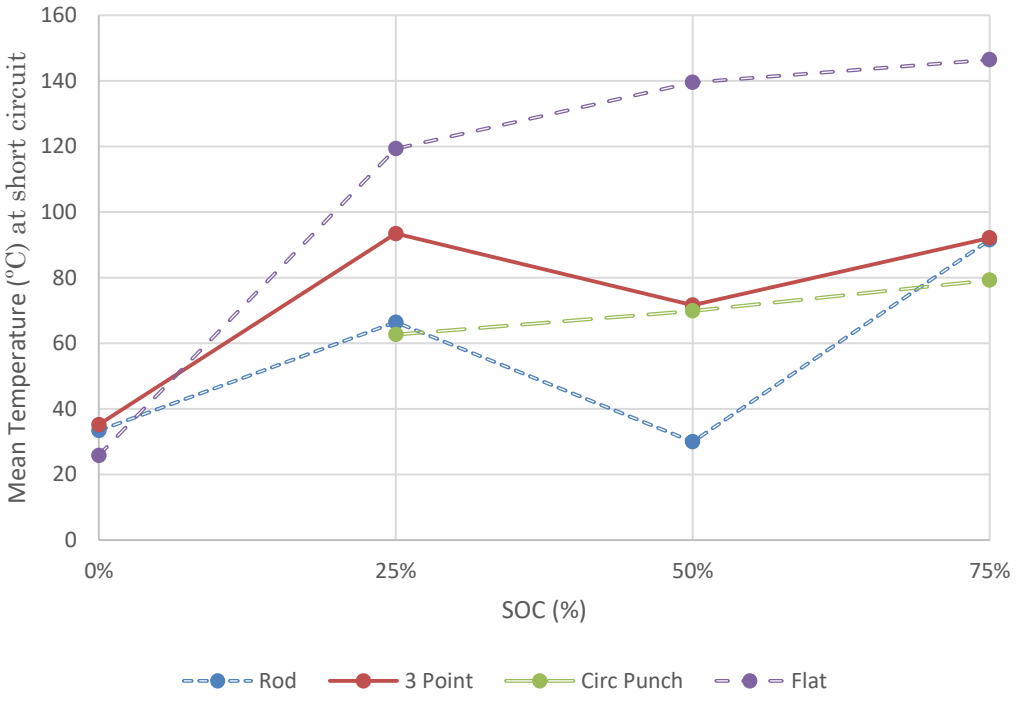

Figure 4.2: SOC Vs mean peak temperature

Figure 4.2, presents the mean maximum temperature for each loading condition by SOC. The temperature at short circuit occurrence has low values for low SOCs for all cells, and these values changed with the change in SOC. There is a positive trend where increases in SOC increase maximum temperature recorded at the point of the short circuit. The trends for three-point bend, rod and circular punch tests are similar, but the trend for the flat plate is much steeper.

A model is fit with the following formula to predict the maximum temperature of a cell following the short circuit in the flat plate test.

$$\text{Ln (Max Temp)} = 3.739 + (0.008 + 0.01982)*\text{SOC} + (-0.056) \qquad (4.1)$$

Where Max Temp is the temperature in °C, SOC is the percentage state of charge out of 100.

Temperature change rate which is the maximum change at the instant of short circuit is discussed below where temperature change rate varies regardless of maximum temperature so that temperature change rate is observed to explain the propagation of temperature change immediately after short circuit where load is released and mean values are used for analysis as shown in figure 4.3.

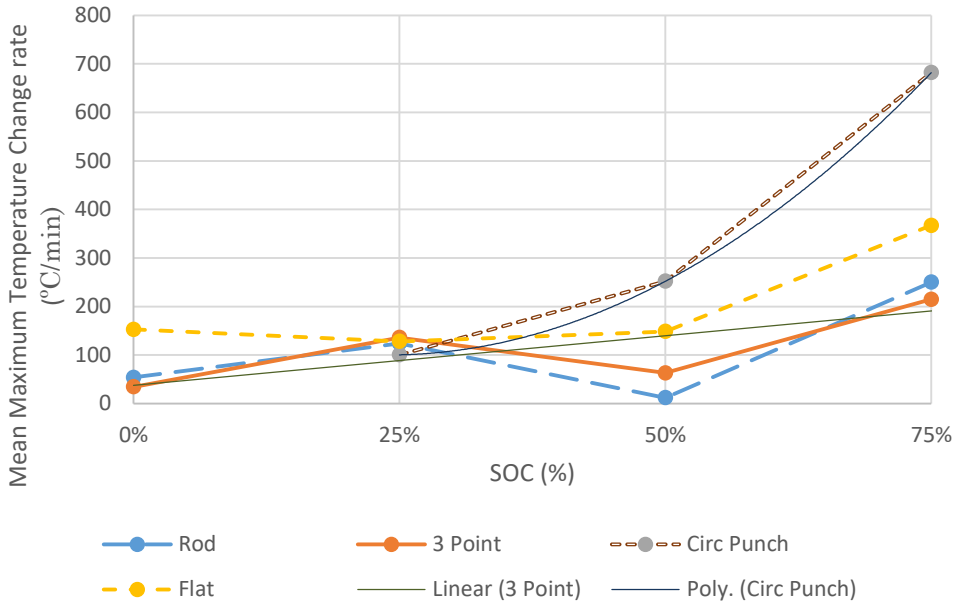

Figure 4.3: Mean maximum temperature change rate for all tests

SOC against mean peak temperature change (degrees/min) is presented in Figure 4.3, Similar to above, it would appear there is generally a positive relationship between rate of temperature change and SOC, but there seems to be less effect from test type, although circular punch is steeper than the other three test scenarios. Based on the previous analysis of displacement at short circuit, it can be concluded that it is likely that displacement has less effect on temperature if all conditions are not considered; therefore, models predict the temperature will include SOC and test type as predictor variables. Detail of all the values obtained are given in the next section with hotspot and local temperature change at the location of the short circuit.

A linear model predicting maximum temperature change is also used following the methods of the previous model. The final model for circular punch is:

$$\text{Max Temp Change} = 62.66 + (2.037 + 9.595)*\text{SOC} + (-299.46) \quad (4.2)$$

Where maximum temperature change is degrees/minute, C is 1 for circular punch loading conditions, and SOC is the state of charge out of 100. This model predicts the maximum temperature change concerning SOC.

Both models developed predict that thermal runaway of the cell can occur when the SOC is greater than 25% for the flat plate. In this scenario, it is predicted that the temperature will exceed 80ºC, beyond the safe operating temperatures of the cell, and can begin thermal runaway. Extrapolating this finding to a bank of cells to find how much neighbouring cells would heat up is difficult. An additional difficulty is that a loading condition like the flat plate would have difficulty occurring in a bank of cells without also crushing the entire bank.

It is worth noting that the first model does predict maximum temperatures of 320ºC for a 75% charged cell in a flat plate loading condition, four times the maximum safe operating threshold which is also evident from thermal camera results described later in this chapter. This high temperature could potentially lead to thermal runaway on neighbouring cells, however this provides grounds for predicting safety criteria, and thermal runaway occurrence may vary with operating conditions and impact speed which is explained earlier in this chapter. Additionally, Sahraei, *et al*. (2012a) noted that there are many factors of the cell which may lead to thermal runaway including chemistry of the cell, resistance of the separator to heat, size of the fractured part, rate of heat transfer and if a damaged cell does not go to thermal runaway there is a slow process of electrochemical reaction releasing gases that could lead to other failure events,

and that the dead cell inside the battery pack can also distort the electrical balance of the pack leading to other consequences.

4.4 Immediate and post-failure analysis

Short circuit occurrence is reported immediately at the point of short circuit, compared to some of the studies provided in the literature with the high-temperature change due to the maximum affected area and deep penetration of object, causing high internal resistance increase and severe short circuit occurrence. Similar phenomena were widely addressed using nail penetration tests, where primarily disturbance is created to affect electrochemical reactions inside cells.

Detailed results are presented in this chapter and previous chapter, where force vs. displacement for all test scenarios is presented, and voltage vs. temperature is presented. Most of the batteries appear to have experienced short circuit followed by temperature increases.

For the all test scenarios, nominal stress and nominal strain behaviour are calculated using equations 4.3 to 4.6 as follows,

$$\sigma_n = \frac{F}{A} \tag{4.3}$$

Where F is the force applied as shown and discussed in this chapter and previous chapter, A is the area of contact which is given by Xu, *et al*. (2016) as follows,

$$\mathrm{A} = l_c b_c \tag{4.4}$$

Where l_c is the length of the cell and width of the contact b_c , is calculated by Eq. 4.5, as given below,

$$\mathrm{b_c} = 2Rarc\,cos\left[\frac{R-s/2}{R}\right] \tag{4.5}$$

Where “R” is the radius of the cell and “s” is the displacement of the indenter used, so the nominal stain ε_n can be obtained using Eq. 4.6, given as follow

$$\varepsilon_n = \frac{s}{2R} \tag{4.6}$$

All the analyses mentioned in this section are discussed with each test protocol in the following section and the conclusion of analysis is presented in the later section.

4.4.1 Rod test

4.4.1.1 Immediate failure analysis

In this section first instances of short circuit with observed values are discussed where the initial and final time of observation and final voltages are detailed. This section serves the purpose of including detail values in the form of a table so that these values can be referred to in particular sections. Numeric values used in this section are useful to relate short circuit occurrence with other failures as mentioned throughout this chapter. Nomenclature according to loading scenario and % SOC are used and first later of each test case is used with the parameter as given in tables 4.1 to 4.16. For rod test “r” is used, where

t_{r0} represents time of short circuit occurrence at 0% SOC, F_{r0} represents applied force, d_{sr0} represents displacement at short circuit for 0% SOC, T_{ir0} represents initial temperature before short circuit occurrence at 0% SOC, T_{fr0} represents final temperature, ΔT_{r0} represents change in temperature, V_{r0} is used for voltage, ε_{nr0} represents nominal failure strain for 0% SOC rod test and σ_{nr0} represents nominal failure stress for 0% SOC. The same nomenclature is used for all loading conditions except the test case initial which is denoted as *r,c,t* and *f*. Three points of interest for test time (t) and voltage (V) are given for all the test cases in the detailed analysis, where tables provide these values.

For 0% SOC rod test short circuit started at the force (F_{r0}) of 10.32 kN with initial short circuit displacement (d_{sr0}) 8.389mm and temperature change (ΔT_{r0}) is 5.3˚C within 5 sec of occurrence. Cell took 2 minutes before being completely drained and a slow increase of temperature was observed which was discussed earlier in this chapter. Initial voltage (V_{r0}) is 3.343 V, all the values obtained from this test are given in Table 4.1.

Time (s) t_{r0}	Force (kN) F_{r0}	Displacement (mm) d_{sr0}	Initial temp (°C) T_{ir0}	Final temp (°C) T_{fr0}	Change in temp (°C) ΔT_{r0}	Voltage V_{r0} (V)	Nominal failure Strain ε_{nr0}	Nominal failure stress, σ_{nr0} (MPa)
280	10.32	8.389	20	25.3	5.3	3.343	0.4661	8.754
384						3.341		
405						0.07		

Table 4. 1: 0% SOC rod test results at short circuit development

High force (F_{r25}) is required for 25% SOC, where relatively low displacement (d_{sr25}) is observed and high-temperature change (ΔT_{r25}) is observed for first 10

sec where ΔT_{r25} is 47.7˚C. As detailed in table 4.2, short circuit occurrence for 25% rod test happened at nearly same loading time as 0% SOC, but temperature response is high and initial voltage (V_{r25}) took 40 sec to reach the voltage below cut off point.

Time (s) t_{r25}	Force (kN) F_{r25}	Displacement (mm) d_{sr25}	Initial temp (°C) T_{ir25}	Final temp T_{fr25} (°C)	Change in temp ΔT_{r25} (°C)	Voltage V_{r25} (V)	Nominal failure Strain ε_{nr25}	Nominal failure stress, $\sigma nr25$ (MPa)
286	11.80	7.794	21	68.28	47.7	3.612	0.416	10.419
320						3.45		
325						0.13		

Table 4. 2: 25% SOC rod test results at short circuit development

At 50% SOC short circuit time (t_{r50}) applied force (F_{r50}) is identical to 25% SOC; however, slightly low displacement is observed and temperature change (ΔT_{r50}) is 65.7˚C. Similar failure stress (σ_{nr50}) and strain (ε_{nr50}) behaviour are observed, where it took 39 sec to enter into severe failure modes. Table 4.3 gives values of 50% SOC rod test.

Time (s) t_{r50}	Force (kN) F_{r50}	Displacement (mm) d_{sr50}	Initial temp (°C) T_{ir50}	Final temp T_{fr50}	Change in temp ΔT_{r50}	Voltage V_{r50} (V)	Nominal failure Strain ε_{nr50}	Nominal failure stress, $\sigma nr50$ (MPa)
217	11.9	7.569	20.1	85.8	65.7	3.654	0.4205	10.676
256						2.99		
487						0.20		

Table 4. 3: 50% SOC rod test results at short circuit development

Similar to observations for 0%. 25% and 50% SOCs, 75% SOC rod test behaviour is observed in detail where cell showed stiffness and required the

high force (F_{r75}), to initiate short-circuit phenomena. Initial voltage (V_{r75}) was 3.894 V and it took 65 sec to completely lose charge. Temperature change (ΔT_{r75}) was 86.2˚C; significant results are given in table 4.4.

Time (s) t_{r75}	Force (kN) F_{r75}	Displacement (mm) d_{sr75}	Initial temp (°C) T_{ir75}	Final temp T_{fr75} (°C)	Change in temp ΔT_{r75} (°C)	Voltage V_{r75} (V)	Nominal failure Strain ε_{nr75}	Nominal failure stress, $\sigma nr75$ (MPa)
310	12.25	6.971	21.3	107.5	86.2	3.894	0.387	11.490
325						3.875		
375						0.182		

Table 4. 4: 75% SOC rod test results at short circuit development

After initial comparison 75% SOC is selected for thermal analysis as 25% and 50% SOC cells showed identical behaviour contrary to 75% SOC cell where displacement (d_{sr75}) and final temperature (T_{fr75}) showed significant changes, which can be used to analyse initial hotspot for thermal runaway detection.

4.4.1.2 Nominal stress-strain analysis

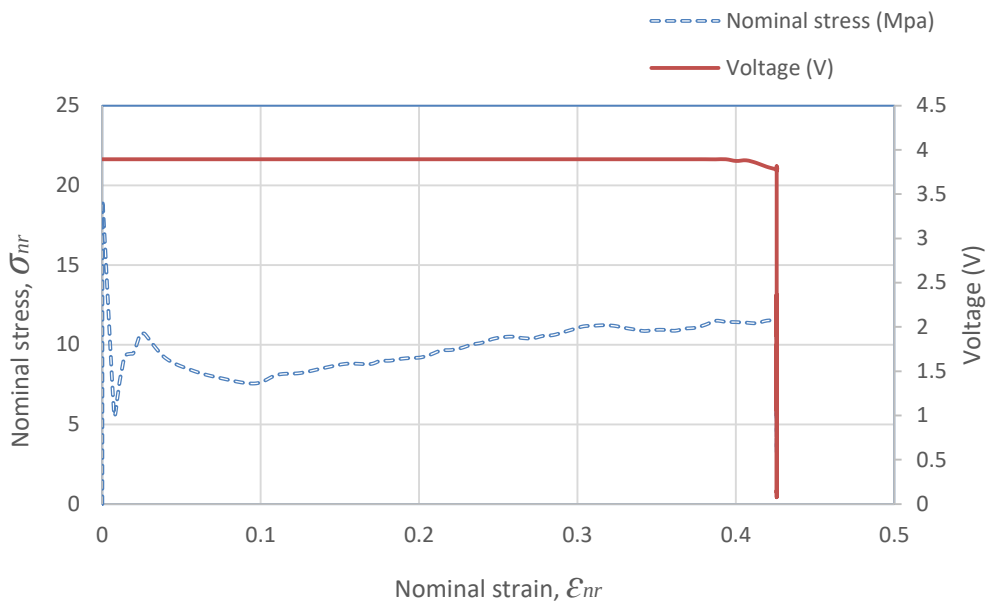

Figure 4.4: Rod test at 75% SOC, Nominal stress-strain and voltage-strain curve

As shown in figure 4.4, nominal stress-strain and voltage behaviour were observed, where ε_{nr} represents nominal strain for rod test, and σ_{nr} represents nominal stress for rod test. Cell permanent failure occurred at the nominal strain of 0.42 and nominal stress of 11.5 MPa, failure stress and strain is also calculated for each test case, where the cell with higher SOC is chosen to detect failure strain.

For the rod test failure strain showed the linear relationship and had adjusted R square fit of 0.8449, as shown in figure 4.5, where εfr represents failure strain for rod test.

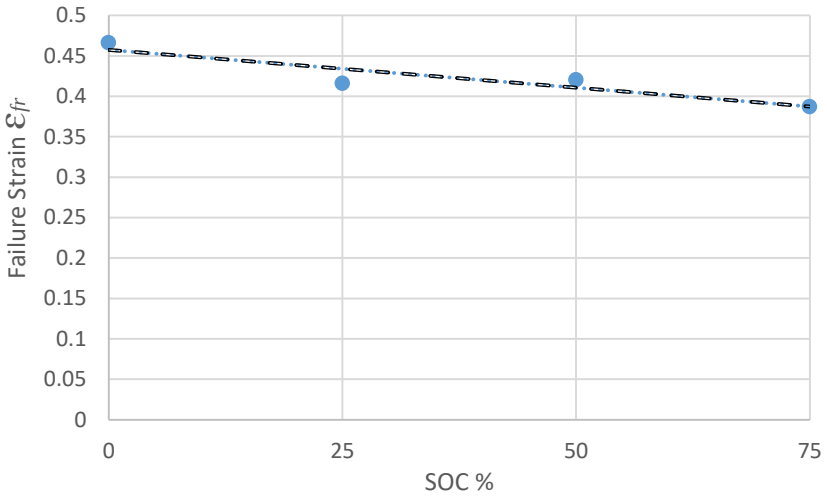

Figure 4.5: Nominal failure strain for rod test

Governing equation due to linear fit is given as follows,

$$\varepsilon_{fr} = 0.4573 - 0.0009\text{SOC} \tag{4.7}$$

Failure strain for rod test has linearly decreasing curve, where at 0% SOC failure strain is relatively high and for 25% and 50% SOCs failure strain has identical values which show for 25% and 50% SOCs electrochemical changes inside cell did not affect mechanical integrity of cell and cell failures showed identical results. This phenomenon is further investigated using failure stress of this testing type.

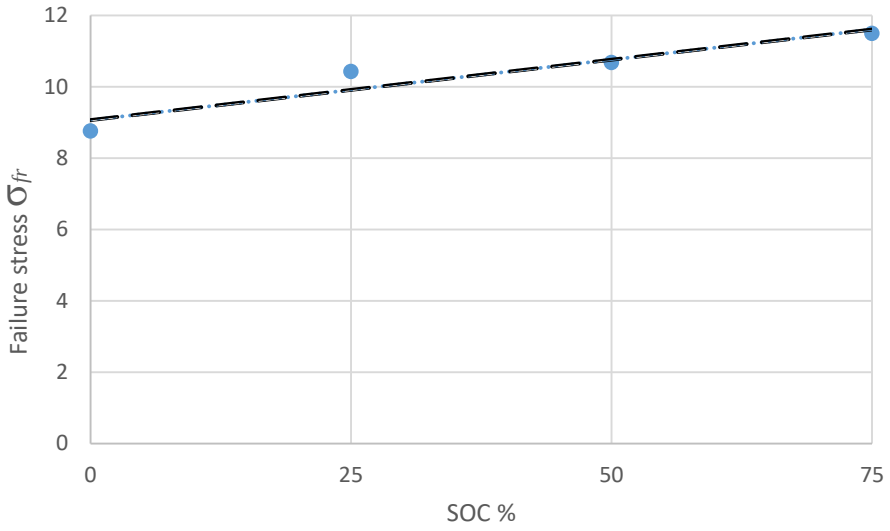

Figure 4.6: Nominal failure stress for rod test

$$\sigma_{fr} = 9.065 + 0.0339\text{SOC} \tag{4.8}$$

Eq. (4.8) Can be used for rod test failure stress, where σ_{fr} represents failure stress for rod test; as shown in figure 4.6, with the increasing SOC failure stress increases which are directly linked to the electrochemical behaviour of cells where cell stiffness increases as SOC increases. Failure stress is relatively low at 0% SOC and high at 75% SOC, but identical behaviour is noticed at 25% and 50% SOCs where failure stress is almost the same, which shows cells can behave in similar ways for different SOC values, however, themal analysis may provide opposite results as thermal variations depend on individual layers' behaviour.

4.4.1.3 Post-failure structural analysis

The post-failure structural analysis is conducted to understand failure location with various SOC and loading conditions. Terminal shapes, crack locations, the

formation of the crack, top and bottom cell geometries are shown and explained in this section. As shown in figure 4.7, in rod test due to load at centre location, cell deforms drastically, and buckling of layers occurred.

Figure 4.7: Cell physical changes, (a) Top view, (b) buckling of top, (c) side view, (d) buckling of side

It can be seen that formation of crack did not occur in rod test when cell experienced short circuit, however, immediate short circuit initiation and voltage drop without structural damage shows internal layer damage where current terminals are intact and no cell swelling, smoke or fire is observed. An almost similar pattern is observed at all SOCs, so cell labelling is not used.

Results obtained by the infrared thermal camera are discussed below.

4.4.1.4 Post-failure temperature analysis

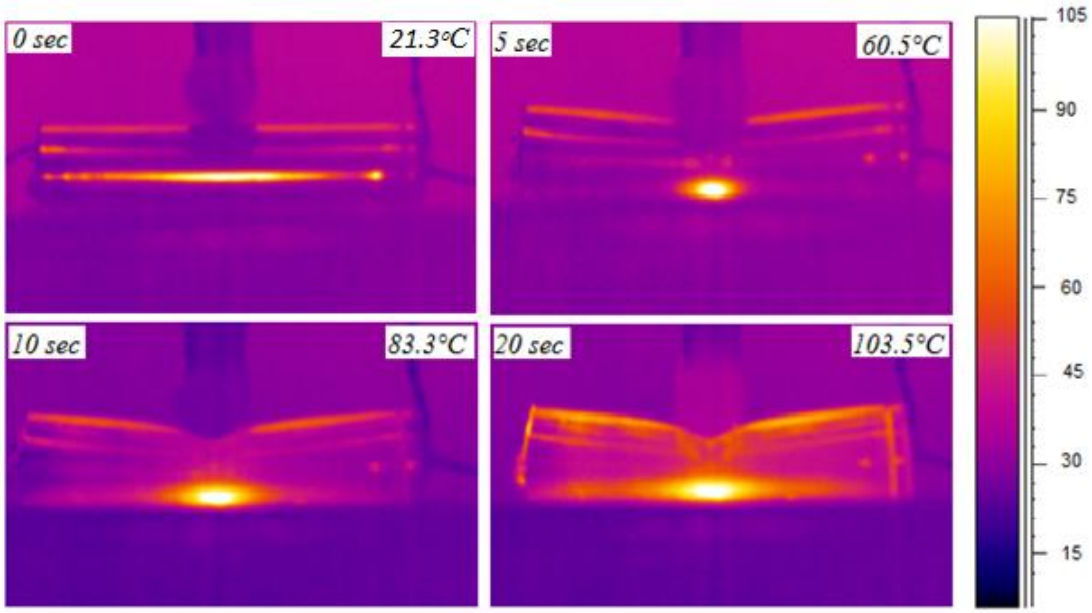

Figure 4.8: Sequential temperature variations for cell failure at 75% rod test

As shown in figure 4.8, initial hotspot shows highest temperature location is bottom mid surface but as time passes hotspot location changes and it moves to terminals (positive and negative terminals) as illustrated in figure 4.9.

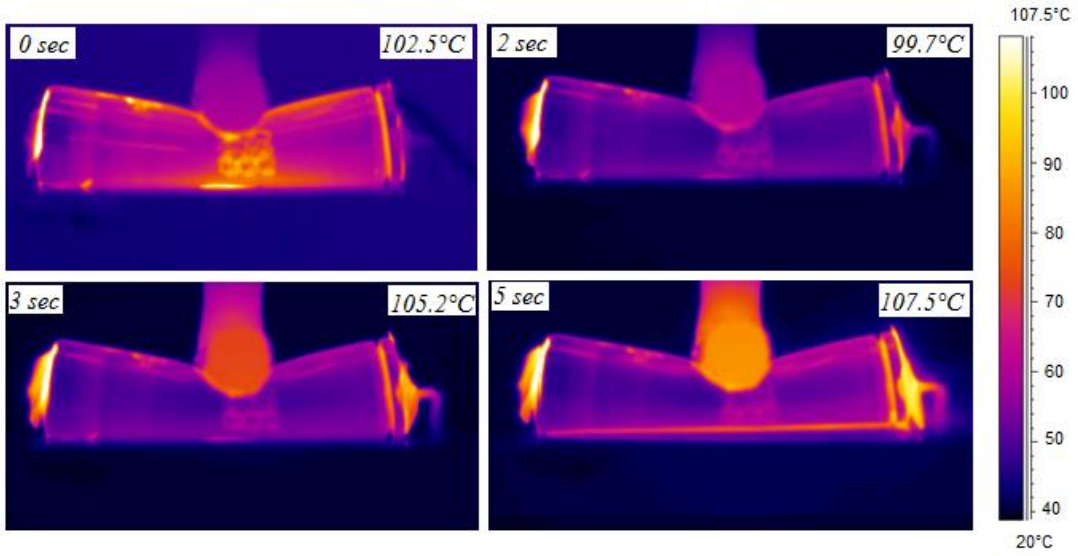

Figure 4.9: Temperature variation location for cell failure at 75% rod test

As shown in figure 4.9, temperature variation is not uniform, and change in temperature location caused the dip in temperature values which is stable after this change. Change of temperature location shows the propagation of damage in the internal electrochemistry. This thermal analysis confirms the results discussed earlier where values are given in tabular form.

4.4.2 Circular punch test

4.4.2.1 Immediate failure analysis

During circular punch and rod tests cells are not restrained using side rods and maximum compressive loading is allowed so that crack location can be monitored and ejection of compounds, if any, can be observed using the digital and infrared camera.

In circular punch test unlike other tests, slow build-up of temperature is observed, and no fracture is observed, however deformation of steel casing which also deforms internal layers is observed. The rate of temperature change is quite high compared to other cells because of variation in short circuit occurrence, which is detailed in previous sections.

As mentioned in previous sections for 0% SOC circular punch test, in one particular test temperature probe failed, which caused the discrepancy in temperature reading for that test. Repeated test also did not show any significant changes, which might be due to internal failures well before structural failure and caused the battery to respond in a strange way. Failure occurred at displacement (d_{sc0}) 5.43mm, and change in temperature (ΔT_{c0}) is 16.4^{o}C, and cell took nearly 300 sec to complete discharge. This observation is detailed in table 4.5.

Time (s) t_{c0}	Force (N) F_{c0}	Displacement (mm) d_{sc0}	Initial temp (°C) T_{ic0}	Final temp (°C) T_{fc0}	Change in temp (°C) ΔT_{c0}	Voltage V_{c0} V	Nominal failure Strain ε_{nc0}	Nominal failure stress, σ_{nc0} (MPa)
420	9.56	5.431	19.2	35.6	16.4	3.325	0.301	10.241
505						1.686		
700						0.367		

Table 4. 5: 0% SOC circular punch test results at short circuit development

At 25% SOC applied force is high compared to 0% SOC, and high-temperature change (ΔT_{c25}) of 59.7°C is observed. Voltage drop is slow and took nearly 2 minutes to drop down to zero value. Values of all the parameters and initial and final results are tabulated in table 4.6.

Time (s) t_{c25}	Force (kN) F_{c25}	Displacement (mm) d_{sc25}	Initial temp (°C) T_{ic25}	Final temp (°C) T_{fc25}	Change in temp (°C) ΔT_{c25}	Voltage V_{c25} V	Nominal failure Strain ε_{nc25}	Nominal failure stress, σ_{nc25} (MPa)
290	13.92	7.896	19.4	79.1	59.7	3.615	0.4386	12.205
355						3.51		
430						0.324		

Table 4. 6: 25% SOC circular punch test results at short circuit development

At 50%, similar results as observed in 25% SOC are achieved, however temperature change (ΔT_{c50}) is 80.1°C and complete cell failure time (t_{c50}) is 94 seconds. This is detailed in table 4.7 below.

Time (s) t_{c50}	Force (kN) F_{c50}	Displacement (mm) d_{sc50}	Initial temp (°C) T_{ic50}	Final temp (°C) T_{fc50}	Change in temp (°C) ΔT_{c50}	Voltage V_{c50} V	Nominal failure Strain ε_{nc50}	Nominal failure stress, σ_{nc50} (MPa)
454	13.20	7.459	19.8	99.9	80.1	3.697	0.414	11.936
474						3.559		
548						0.391		

Table 4. 7: 50% SOC circular punch test results at short circuit development

In 75% SOC circular punch high force (F_{c75}) is required to initiate the short circuit, where displacement at short circuit (d_{sc75}) is 7.315mm and temperature change (ΔT_{c75}) is 89°C. Cell went to complete discharge within 51 sec of short circuit occurrence. This detail is given in table 4.8. Due to high-temperature change, fast degradation and failure, 75% SOC circular punch test is further investigated for temperature variations as shown in figures 4.14 and 4.15.

Time (s) t_{c75}	Force (kN) F_{c75}	Displacement (mm) d_{sc75}	Initial temp (°C) T_{ic75}	Final temp (°C) T_{fc75}	Change in temp (°C) ΔT_{c75}	Voltage V_{c75} V	Nominal failure Strain ε_{nc75}	Nominal failure stress, σ_{nc75} (MPa)
284	13.97	7.315	21	110	89	3.913	0.406	12.766
291						1.375		
335						0.377		

Table 4. 8: 75% SOC circular punch test results at short circuit development

4.4.2.2 Nominal stress-strain analysis

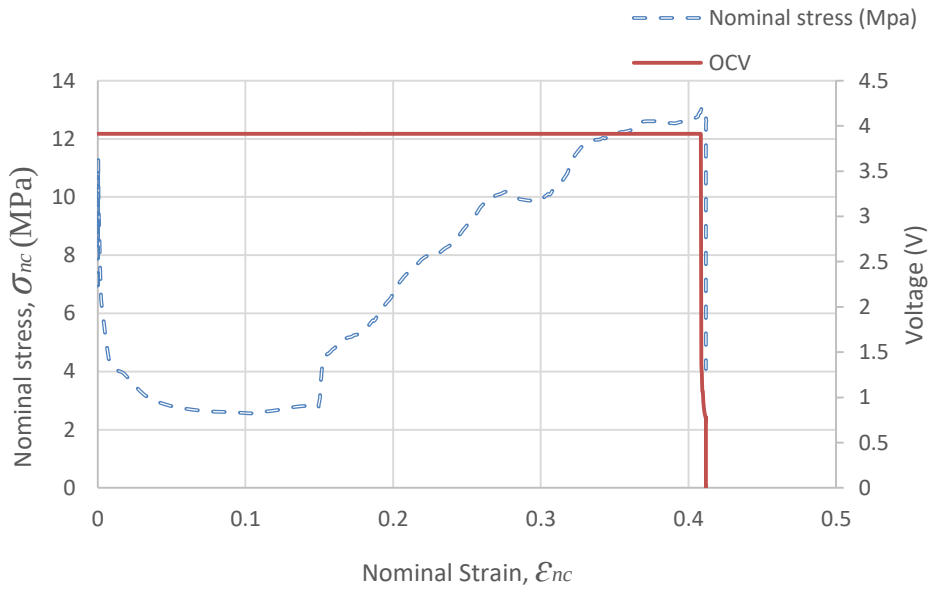

Figure 4.10: Circular punch test, Nominal stress-strain and voltage-strain curve

Circular punch stress-strain behaviour is shown in figure 4.10, where ε_{nc} denotes nominal strain for circular punch and σ_{nc} represents nominal stress for circular punch test. Linearly increasing stress-strain behaviour was observed for this test; however, failure stress-strain behaviour was identical to rod test failure; hence both tests were used for deformation at centre locations with different geometries where circular punch had the same effect as flat plate deformation except contact area which was large for flat plate test. Nominal strain failure for circular punch test is shown in figure 4.11.

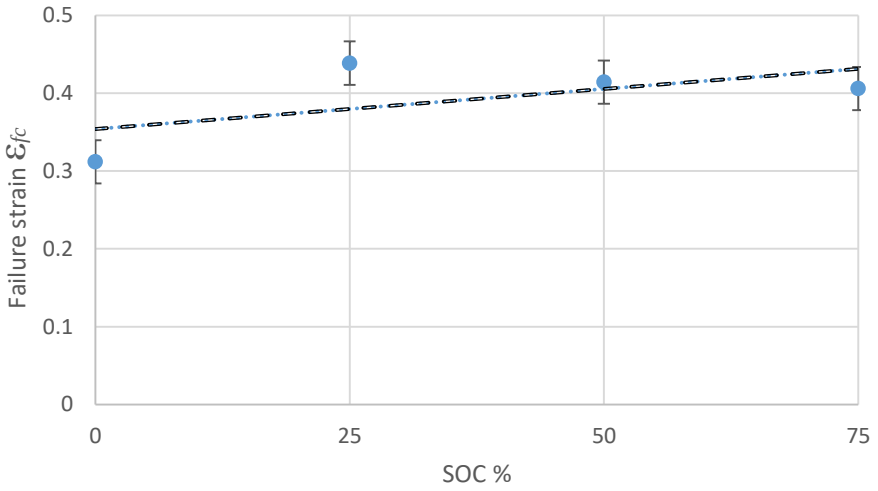

Figure 4.11: Nominal failure strain for circular punch test

Figure 4.11 shows failure strain for circular punch at various SOCs, where ε_{fc} represents failure strain for circular punch test. Although failure strain is linearly increasing with increasing SOC, increment is very much identical to 50% and 75% SOC which shows at high SOC failure strain become less relevant compared to 0% SOC where failure strain has comparatively very low value. Governing equation for circular punch failure strain is as follows.

$$\varepsilon_{fc} = 0.354 + 0.001\text{SOC} \tag{4.9}$$

Eq. (4.9) provides linear fit for circular punch failure strain where ε_{fc} represents failure strain for circular punch test. Adjusted R square fit is 0.3583.

Failure stress for circular punch is shown in figure 4.12, where σ_{fc} represents failure stress for circular punch test. With increasing SOC failure stress increases, however, compression modulus is relatively high. The significant increase in failure stress is observed for high SOCs except for 25% and 50%

SOCs which have closest values. Linear fit for failure stress is given in Eq. (4.10)

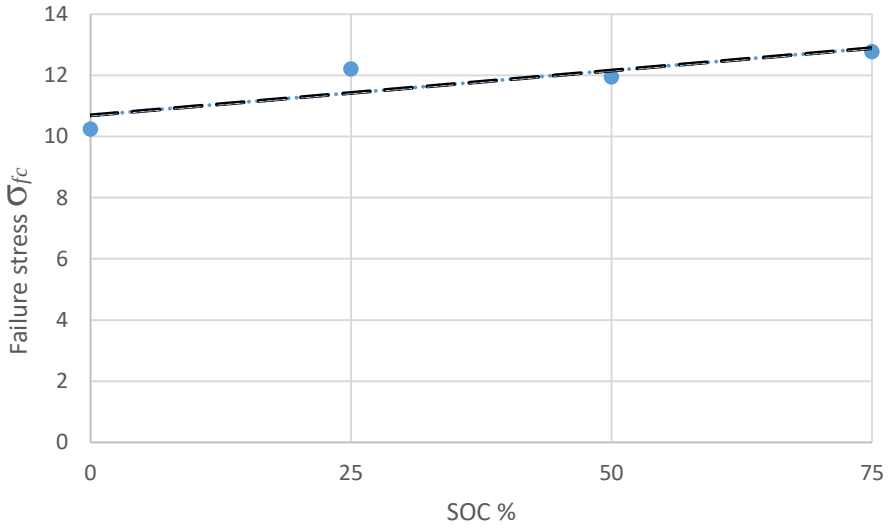

Figure 4.12: Nominal failure stress for circular punch test

$$\sigma_{fc} = 10.691 + 0 \cdot 0292\text{SOC} \quad (4.10)$$

Further analysis of temperature variations and temperature change rate with thermal analysis for circular punch is given in later section.

4.4.2.3 Post-failure structural analysis

In circular punch test, no fracture is observed but high buckling ratio compared to other tests was observed, which was mainly due to the shape of indenter as shown in figure 4.13.

(a)  (b) 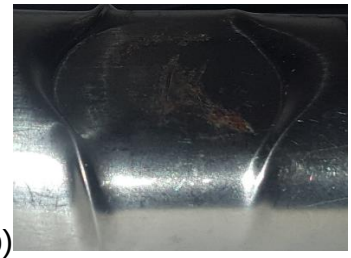

(c)  (d) 

Figure 4.13: Circular punch test, (a) side view, (b) buckling at side, (c) top view, (d) buckling at top

In circular punch test, due to buckling, cell temperature and voltage change occurred sequentially but after removing force when the cell was left to observe temperature variations, it was found that temperature change rate was very high in circular punch test which can be attributed to uneven buckling. As deflection was occurring, it means applied load did not affect cell's load carrying capability.

4.4.2.4 Post-failure temperature analysis

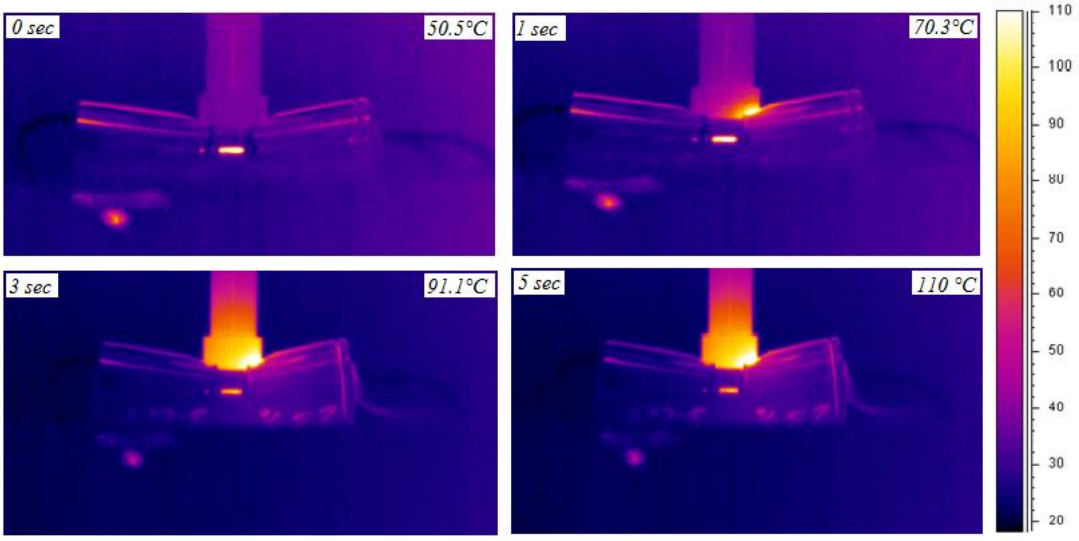

Figure 4.14: Initial temperature variations for circular punch test at 75% SOC

As shown in figure 4.14, within 5 secs cell attained 60˚C temperature, which indicates that, at this rate, thermal runaway occurrence is evident if this stay same for some time. Change of temperature rate is high, as at this ratio of temperature change cell can undergo burning within a minute and this change rate also affects test impactor which lost its protective coating and started to work as the metal heat sink as explained below.

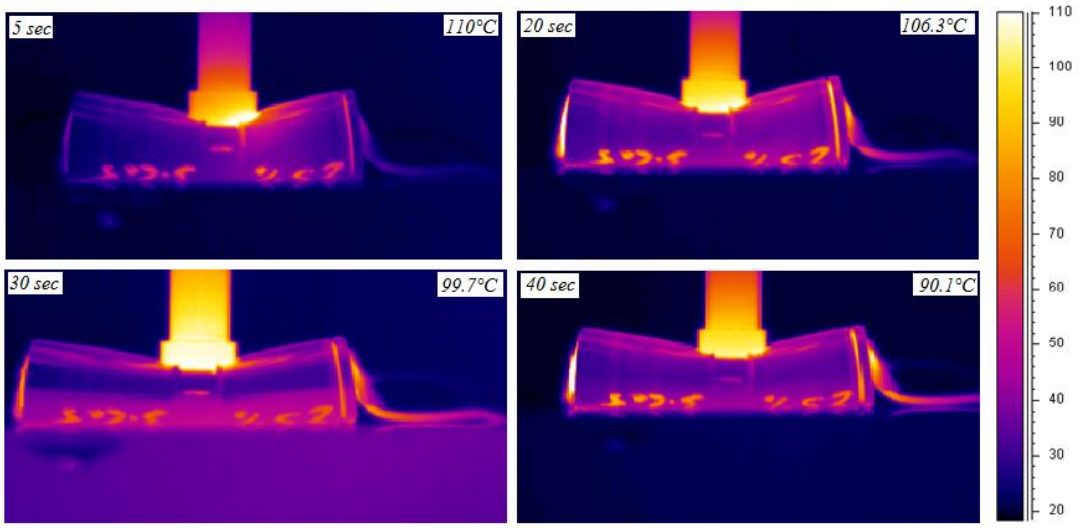

Figure 4.15: Final temperature variations for circular punch test at 75% SOC

As shown in figure 4.15, as the time progressed the cell dissipated heat to contact where contact temperature increase and cell temperatures at terminals started to decrease. This is due to the metal object which acts as a heat sink and cools down the cell where low temperatures are observed, however short circuit occurrence is observed as voltage variations are immense. To check this cell for its failure, post-failure charge test was carried out which is explained in the following sections.

4.4.3 Three-point bend test

4.4.3.1 Immediate failure analysis

Sharp edge indenter is used to investigate sharp object effect on cylindrical cells and possible thermal runaway event. At force (F_{t0}) 2.33kN short circuit occurred in 0% SOC test, where the complete discharge of cell took 110 sec. Short circuit displacement (d_{st0}) was 6.46mm, and temperature change (ΔT_{t0}) was 16.3°C. Table 4.9, gives values of all the parameters observed during the impact test.

Time (Sec) t_{t0}	Force (kN) F_{t0}	Displacement (mm) d_{st0}	Initial temp (°C) T_{it0}	Final temp (°C) T_{ft0}	Change in temp (°C) ΔT_{t0}	Voltage V_{t0} V	Nominal failure Strain ε_{nt0}	Nominal failure stress, σ_{nt0} (MPa)
390	2.33	6.46	20.9	37.2	16.3	3.31	0.344	2.2763
430						3.273		
500						0.357		

Table 4. 9: 0% SOC three-point bend test results at short circuit development

Higher force (F_{t25}) is observed for 25% SOC, where short circuit displacement (d_{st25}) is 7.94 mm and significant temperature change (ΔT_{t25}) of 91.6°C. It took 20 sec for high voltage change and 90 sec for complete discharge of the cell. Table 4.10, gives values obtained from this test.

Time (Sec) t_{t25}	Force (kN) F_{t25}	Displacement (mm) d_{st25}	Initial temp (°C) T_{it25}	Final temp (°C) T_{ft25}	Change in temp (°C) ΔT_{t25}	Voltage V_{t25} V	Nominal failure Strain ε_{nt25}	Nominal failure stress, σ_{nt25} (MPa)
450	2.55	7.94	21.1	84.5	91.6	3.608	0.326	2.229
470						3.59		
540						0.546		

Table 4. 10: 25% SOC three-point bend test results at short circuit development

At 50% SOC almost similar applied force as in 25% SOC was observed for the short circuit occurrence, however, displacement (d_{st50}) was 8.4mm and temperature change was 63.4°C, which is lower compared to 25% SOC. Cell showed significant voltage change within 10 sec of the first instance of the short circuit; however complete failure time for the cell was 135 sec. Table 4.11 gives values of all the parameters investigated.

Time (Sec) t_{t50}	Force (KN) F_{t50}	Displacement (mm) d_{st50}	Initial temp (°C) T_{it50}	Final temp (°C) T_{ft50}	Change in temp (°C) ΔT_{t50}	Voltage V_{t50} V	Nominal failure Strain ε_{nt50}	Nominal failure stress, σ_{nt50} (MPa)
465	2.577	8.4	23.1	114.7	63.4	3.663	0.321	2.184
475						3.648		
600						0.219		

Table 4. 11: 50% SOC three-point bend test results at short circuit development

Three-point bend test short circuit for 50% SOC occurred at the time (t_{t75}) 300 sec, and within 5 sec cell showed significant voltage change, however complete

cell failure occurred at 600 sec which is 300 sec after first short circuit indication. Cell temperature change (ΔT_{t75}) was 91°C. Table 4.12 provides values of all test parameters for 75% SOC three-point bend.

Time (Sec) t_{t75}	Force (kN) F_{t75}	Displacement (mm) d_{st75}	Initial temp (°C) T_{it75}	Final temp (°C) T_{ft75}	Change in temp (°C) ΔT_{t75}	Voltage V_{t75} V	Nominal failure Strain ε_{nt75}	Nominal failure stress, σ_{nt75} (MPa)
300	2.98	5.807	20.1	111.1	91	3.869	0.316	3.081
305						3.714		
600						0.17		

Table 4. 12: 75% SOC three-point bend test results at short circuit development

4.4.3.2 Nominal stress-strain analysis

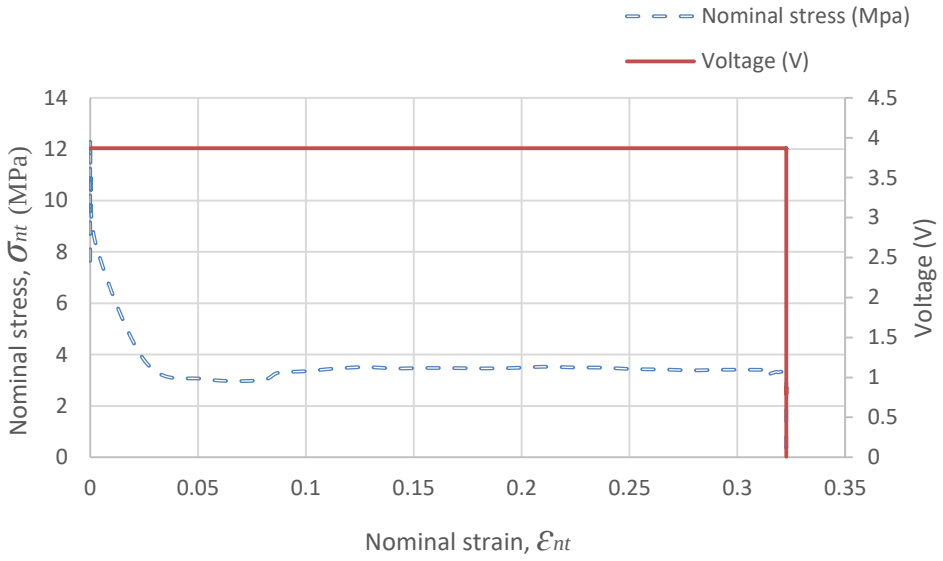

Figure 4.16: Three-point bend test, Nominal stress-strain and voltage-strain curve

As shown in figure 4.16, nominal stress and nominal strain for battery degradation in three-point bend test were observed where ε_{nt} represented

nominal strain for three-point bend test, and σ_{nt} represented nominal stress for three-point bend test. Unlike rod test in three-point bend low stress and strain values were observed, where a failure of cell occurred at the nominal strain of 0.32 and stress was 3.32 MPa. This indicates in the case of battery bending test, initial high-stress values were due to steel casing buckling which penetrates deep into the layers and failure of layers occurs. This is discussed concerning individual failure stress and strain behaviour in the following sections.

To better understand and generalise cell failure due to bending, failure strain for three-point bend test is shown in figure 4.17.

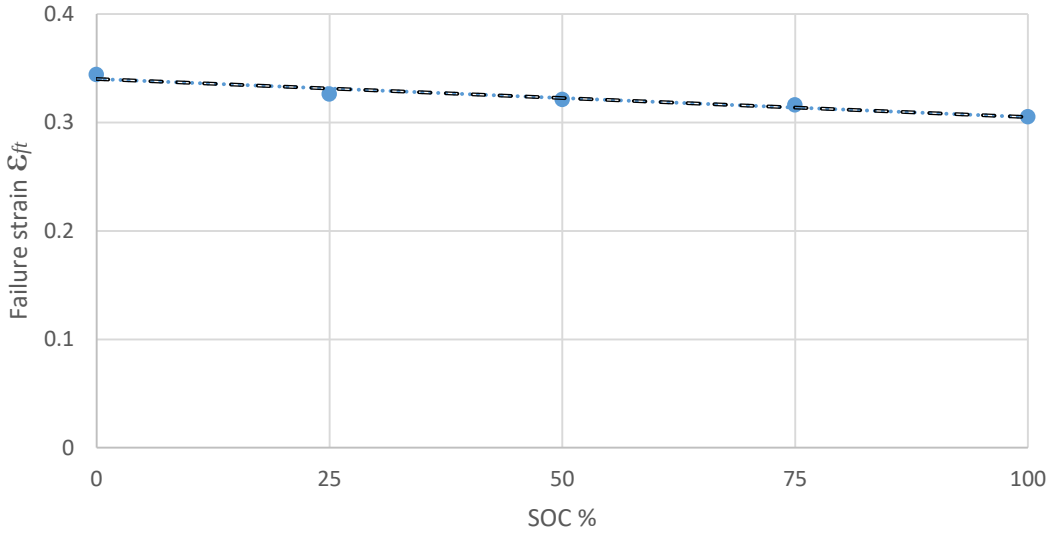

Figure 4.17: Nominal failure strain for three-point bend test

$$\varepsilon_{ft} = 0.34 - 0.0004\mathrm{SOC} \tag{4.11}$$

Eq. (4.11) shows linear fit for three-point bend test where ε_{ft} represents failure strain for three-point bend test. Eq. (4.11) has adjusted R square fit of 0.9384. As can be seen in figure 4.12, strain failure for three-point bend test has linearly decreasing function where at lower SOC high strain failure was observed, unlike rod test and circular punch test where failure strain for 25% and 50% SOCs showed similar response and was not affected by failure stress and failure strain. Linear fit for failure strain is shown in Eq. (4.11).

Figure 4.18, shows failure stress for three-point bend test where failure stresses for 0%, 25% and 50% SOCs are identical and indicate that at low SOCs failures follow same stress pattern, unlike failure strain which is high at low SOCs. Linear fit for failure stress is given in Eq. (4.12), where σ_{ft} represents failure stress for three-point bend test.

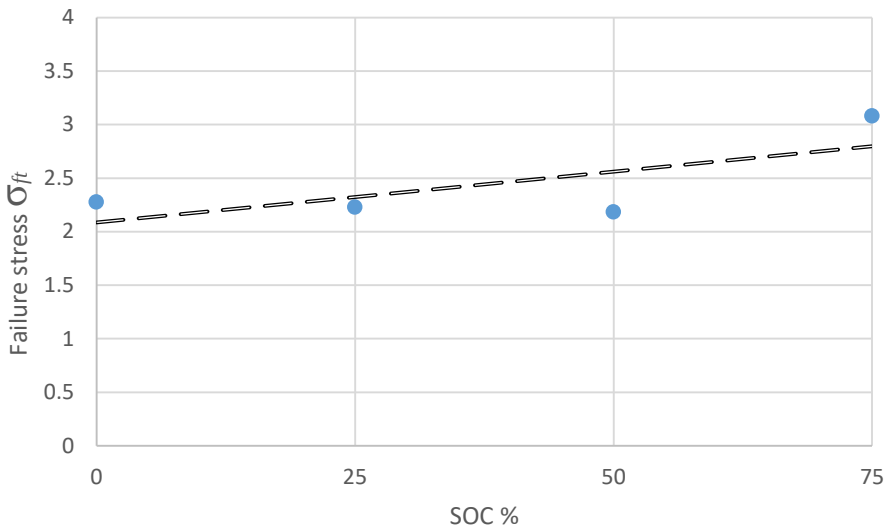

Figure 4.18: Nominal failure stress for three-point bend test

$$\sigma_{ft} = 2.0872 + 0.0095\text{SOC} \quad (4.12)$$

Further analysis for battery failures due to three-point bending is discussed in the following section; however, the stress-strain analysis provides grounds for further analysis and are useful for simulation.

4.4.3.3 Post-failure structural analysis

In three-point bend test, cell bending and rupture is observed where cell benda gradually but the formation of crack occurs where sharp edge establishes contact with the cell, this is shown in figure 4.19. Both cell fracture and buckling takes place in three-point bend test where sharp edge indenter is used. Cell terminals and end caps are intact in this testing; however, cell thinning took place at the centre of the cell. In this test, indenter travelled 40% of original cell diameter where mean displacement is 7.27mm.

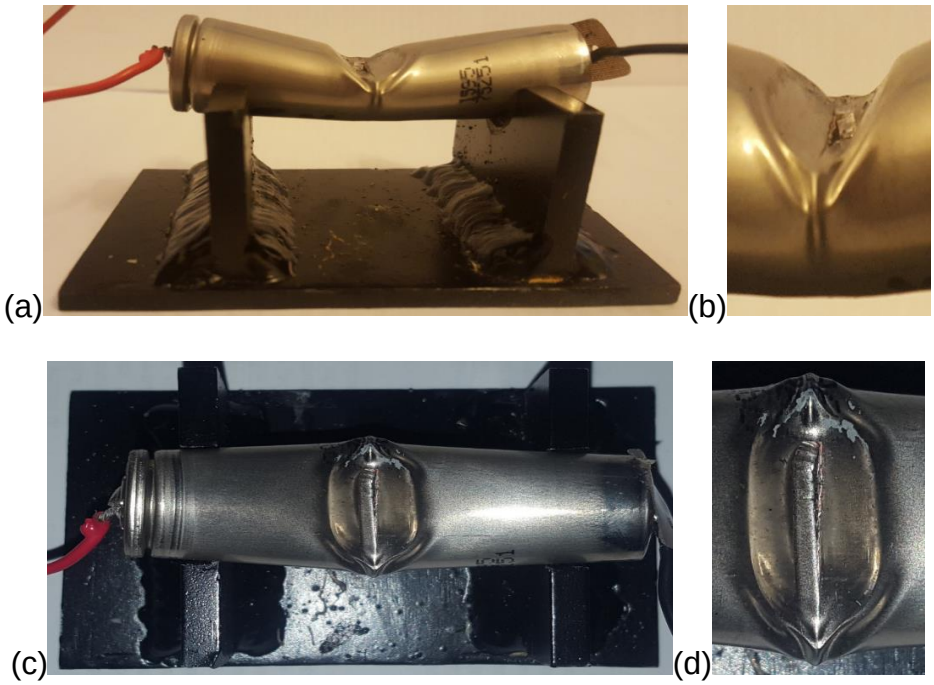

Figure 4.19: Three-point bend test, (a) side view, (b) cell fracture, (c) top view, (d) buckling and fracture of cell

Sideway deflection can be observed in three-point bend which is due to triangle shape of indenter tip. At cell failure, the fracture is observed in three-point bend test where drastic temperature and voltage variations are observed.

4.4.3.4 Post-failure temperature analysis

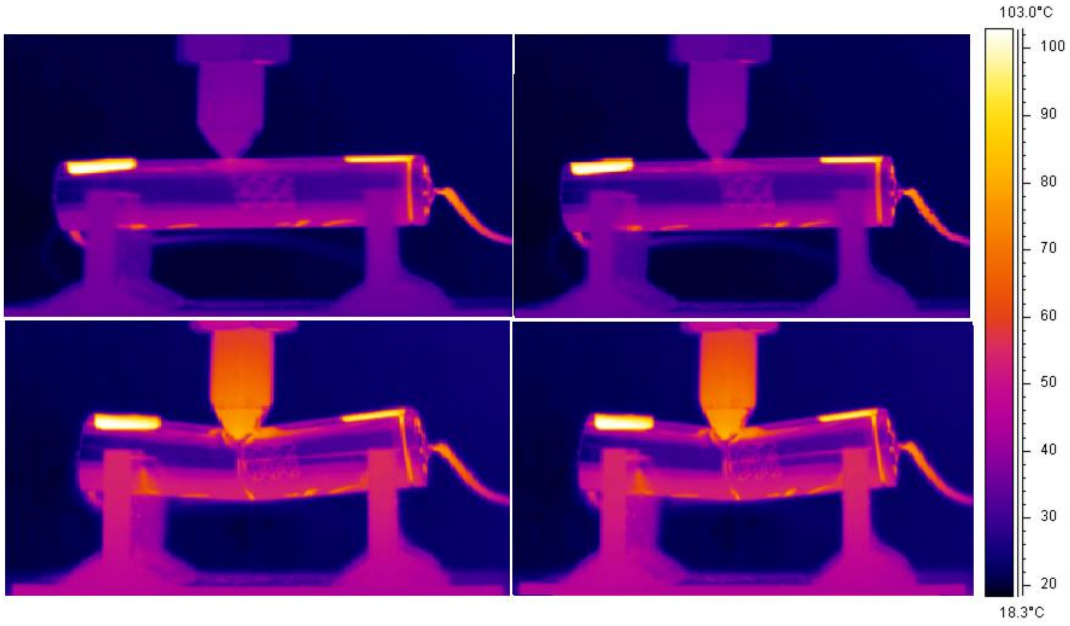

Figure 4.20: Initial results of temperature change for three-point bend test

For three-point bend test, 75% SOC is chosen for further analysis where high-temperature change (ΔT_{t75}) and short circuit failure time (t_{t75}) is observed. In the figure 4.20, hotspot development is very slow and spans the period of time, so sample time is not mentioned, which is discussed later. As shown hot spot location is the bottom of the cell where similar to circular punch after first loading indenter established contact with cell casing and started to dissipate

heat from the cell, so temperature change was observed for 1sec where heat dissipation effect is negligible.

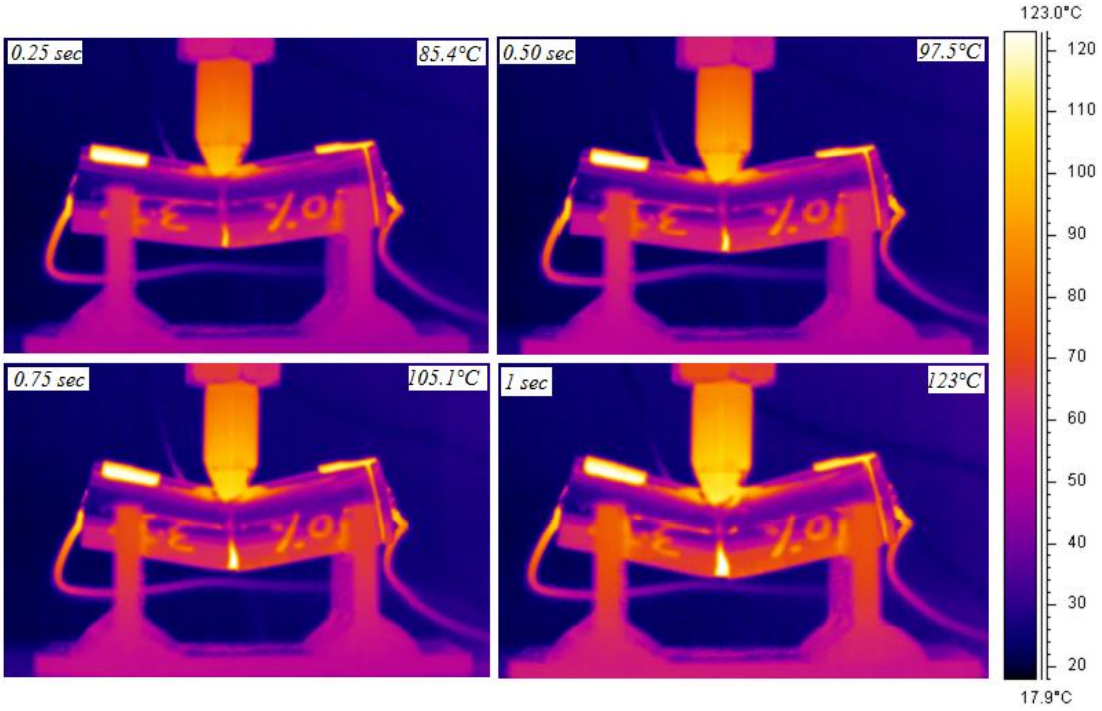

Figure 4.21: Initial temperature change with sample time for three-point bend test

In the figure 4.21, sample time with the temperature at the hotspot is shown, where the high-temperature location is bottom mid of the cell, unlike commonly reported bending and fracture pattern for three-point bend test due to indenter shape cell showed fracture on the top surface and bending at the bottom. Temperature variations immediately after short circuit show cell fracture at this loading condition go to thermal runaway earlier compared to other loading conditions.

4.4.4 Flat plate deformation test

4.4.4.1 Immediate failure analysis

Flat plate deformation is of great importance as the maximum area of a cell is in contact during these types of damage, when cell crushing occurs. In this situation, maximum test area of battery comes into effect including terminals which are intact in other tests. Results with the high indication of short circuit leading to thermal runaway are discussed here; however, each cell was analysed to find this behaviour, but high SOC cells have the high thermal impact after short circuit as shown in figure 4.27, where SOC is 75%.

Test results obtained for flat plate deformation with detailed parameter list which contributes towards short circuit are given in table 4.13 to 4.16. Low short circuit displacement (d_{sf0}) compared to other test scenarios was observed in this test. High-temperature change (ΔT_{f0}) was observed in all cases which were sequentially increasing. ΔT_{f0} for 0% SOC test was 97.90˚C. Cell complete discharge took place 360 sec after first short circuit response; this value is given in table 4.13.

Time (s) t_{f0}	Force (kN) F_{f0}	Displacement (mm) d_{sf0}	Initial temp (°C) T_{if0}	Final temp (°C) T_{ff0}	Change in temp (°C) ΔT_{f0}	Voltage V_{f0} V	Nominal failure Strain ε_{nf0}	Nominal failure stress, σ_{nf0} (MPa)
790	42.0	5.548	20	117.90	97.90	3.546	0.308	44.49
855						3.5		
1130						1.116		
1150						0.03		

Table 4. 13: 0% SOC flat plate deformation test results at short circuit development

At 25% SOC, cell had similar force and temperature response, however sudden voltage drop occurred after 15 sec of the first instance of the short circuit and then slow discharge of cell occurred which took 730 sec to get to Voltage (V_{f25}) 1V, this cell was further used for remaining useful condition assessment in the next section. Table 4.14 provides obtained values for this test.

Time (s) t_{f25}	Force (kN) F_{f25}	Displacement (mm) d_{sf25}	Initial temp (°C) T_{if25}	Final temp (°C) T_{ff25}	Change in temp (°C) ΔT_{f25}	Voltage V_{f25} V	Nominal failure Strain ε_{nf25}	Nominal failure stress, σ_{nf25} (MPa)
500	43.010	6.32	20.1	126.5	106.4	3.605	0.351	42.514
515						3.3		
1230						1.049		

Table 4. 14: 25% SOC flat plate deformation test results at short circuit development

For 50% SOC test applied force (F_{f50}) was 41.6kN, and displacement (d_{sf50}) at the short circuit was 6.367. Temperature change for 50% SOC cell was 130˚C which was quite high compared to other test where time to completely discharge was 125 sec. Table 4.15 provides obtained values for this test.

Time (s) t_{f50}	Force (kN) F_{f50}	Displacement (mm) d_{sf50}	Initial temp (°C) T_{if50}	Final temp (°C) T_{ff50}	Change in temp (°C) ΔT_{f50}	Voltage V_{f50} V	Nominal failure Strain ε_{nf50}	Nominal failure stress, σ_{nf50} (MPa)
195	41.6	6.367	20.3	150.3	130	3.714	0.35	40.958
290						3.573		
295						0.134		
320						0.032		

Table 4. 15: 50% SOC flat plate deformation test results at short circuit development

At 75% SOC, the short circuit occurred at twice the time of 50% SOC, and within 10 sec sudden voltage drop was observed. The short circuit displacement (d_{sf75}) was 7.331mm, which was higher and cell took nearly 60 seconds to completely discharge where the final voltage (V_{f75}) was 0.036V. Temperature change (ΔT_{f75}) was 136.6°C. Table 4.16 provided detail of parameters observed during this test.

Time (s) t_{f75}	Force (kN) F_{f75}	Displacement (mm) d_{sf75}	Initial temp (°C) T_{if75}	Final temp (°C) T_{ff75}	Change in temp (°C) ΔT_{f75}	Voltage V_{f75} V	Nominal failure Strain ε_{nf75}	Nominal failure stress, σ_{nf75} (MPa)
380	44.13	7.331	20.9	157.5	136.6	3.886	0.407	40.281
390						3.38		
400						3.445		
440						3.341		
445						0.036		

Table 4.16: 75% SOC flat plate deformation test results at short circuit development

4.4.4.2 Nominal stress-strain analysis

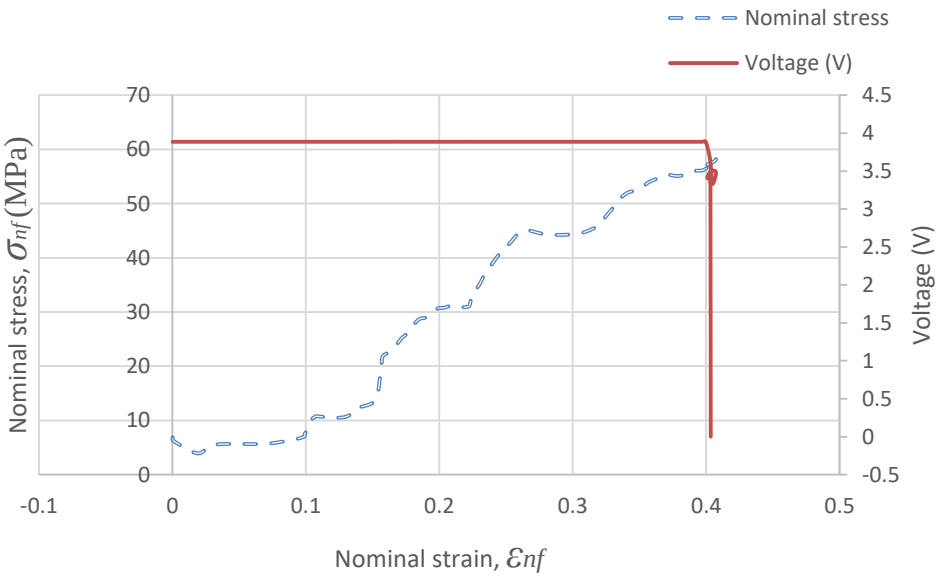

Figure 4.22: Flat plate deformation, Nominal stress-strain and voltage-strain curve

Figure 4.22 shows the stress-strain curve for flat plate deformation where ε_{nf} represents nominal strain for flat plate test and σ_{nf} represents nominal stress for flat plate deformation test. In this analysis, the stress-strain relation is studied where the voltage is used as failure indicator. High failure stress is observed, which is due to compression of internal layers which initially experience the change of shape as shown in the following sections, layers adopt elliptical shape, and due to crack development, short circuit occurrence has high intensity compared to other mechanical loads. Compression modulus for flat plate deformation (E_{cf}) is also calculated which indicates the occurrence of the

short circuit as it is the point where cell failure starts to develop and for this test E_{cf} was 205MPa.

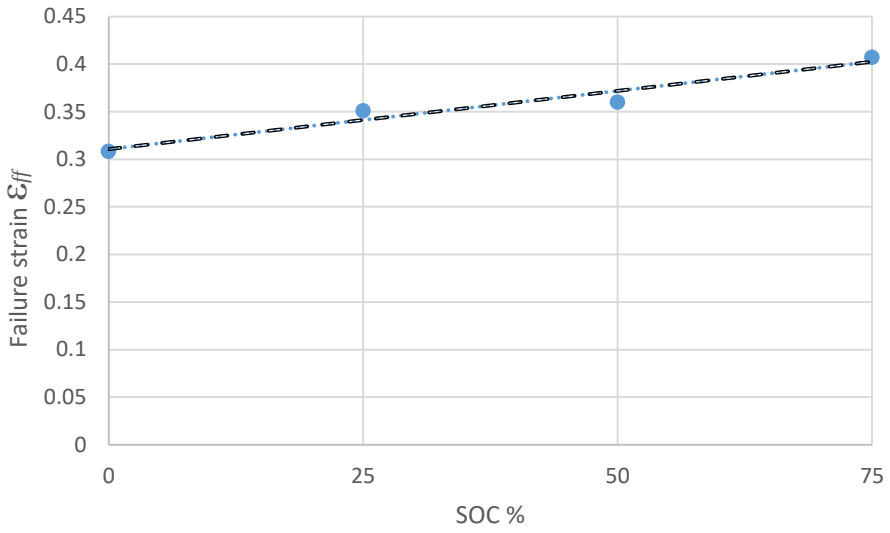

Figure 4.23: Nominal failure strain for flat plate deformation test

Nominal failure strain for flat plate deformation is shown in figure 4.23. Linear fit for flat plate deformation was obtained where adjusted R square was 0.9468. Like circular punch test, flat plate deformation had linearly increasing response where with increasing SOC failure strain has highest values. Eq. (4.13) provides linear fit for flat plate deformation.

$$\varepsilon_{ff} = 0 \cdot 3106 + 0.0012\mathrm{SOC} \tag{4.13}$$

In Eq. (4.13) ε_{ff} represents nominal failure strain for the flat plate deformation test. Failure strain for 25% and 50% SOC has very close values which are similar to rod test and circular punch test where same phenomena were observed. Flat plate deformation test is differentiated from three-point bend test

as in three-point bend test linearly decreasing response is observed, however in this test linearly increasing response for failure strain was observed. At 25% and 50%, SOCs strain failure had similar values.

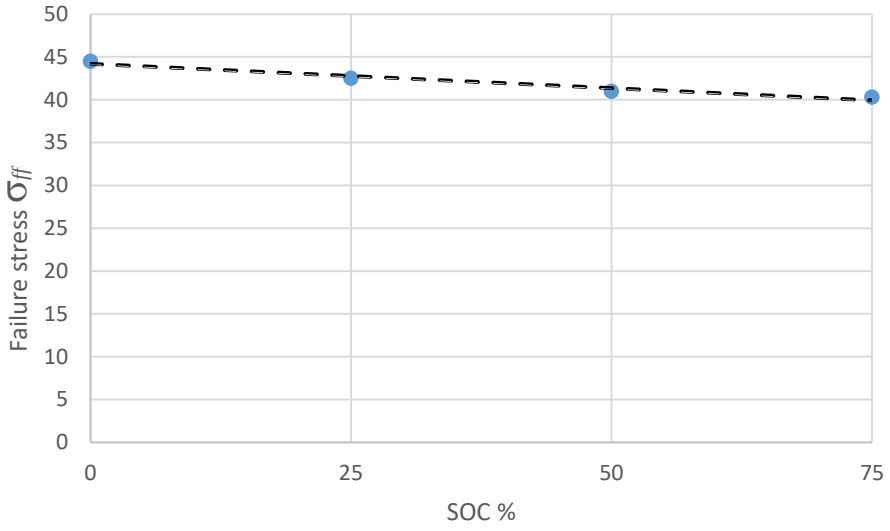

Figure 4.24: Nominal failure stress for flat plate deformation test

$$\sigma_{ff} = 44.188 - 0.0567\text{SOC} \tag{4.14}$$

Governing equation for flat plate deformation is given in Eq. (4.14), where σ_{ff} represents failure stress for flat plate deformation. Similar to nominal strain failure, stress failure is shown in figure 4.24, where linearly decreasing curve is observed and at low SOCs high-stress failure values were observed, which means flat plate deformation test has inverse relation compared to other three tests where with increasing SOC failure stress increased as well which can be attributed to large contact area of this type of testing as, for other three tests, contact area was smaller, especially for three-point bend test which showed identical response for 0%, 25% and 50% SOCs.

From failure stress and failure strain for all loading conditions, it can be concluded that failure stress and failure strain at 25% and 50% SOCs have identical values for individual tests, except flat plate deformation where failure stress is linearly decreasing with increasing SOC.

4.4.4.3 Post-failure structural analysis

In flat plate deformation due to the large contact area of flat plate impactor, cell attains elliptical shape, where no fracture occurred; however, end caps removed from the terminal which was due to high force impacts and formation of end caps. Flat plate deformation is shown in figure 4.25.

(a) 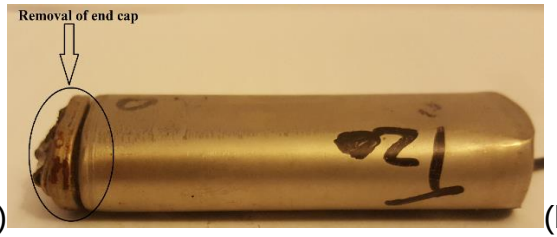

(b) 

Figure 4.25: Flat plate deformation, (a) removal of end cap, (b) top view of cell

In figure 4.25(a) removal of the end cap at positive terminal is highlighted, although there is a very narrow gap and cell internal protection layer did not allow the cell to undergo smoke or fire but this indicates that damage to end caps can cause severe electrical and thermal changes which are reported in the following sections. In this testing, however, cell undergoes the complete change of shape from cylindrical to elliptical, which caused high-temperature increase as internal layers are very thin, and evolving shape might cause layers

to develop the crack which created electrode contacts to initiate short circuit. Electron microscopy, computer tomography scan (CT scan) and X-ray scan are a few of the methods being used for cell post-failure analysis (Taiwo *et al*., 2016) where internal damage behaviour of layers are investigated. In flat plate deformation cell bears a significant amount of force before going into short circuit state, once it went to short circuit temperature rise was very high.

4.4.4.4 Post-failure temperature analysis

Propagation of temperature change is shown in figure 4.26, where initial temperature contour with high-temperature variation was observed and in figure 4.27 very high temperatures for the very short instant of time is shown, where duration for this event was 1 sec. These results are explained in detail.

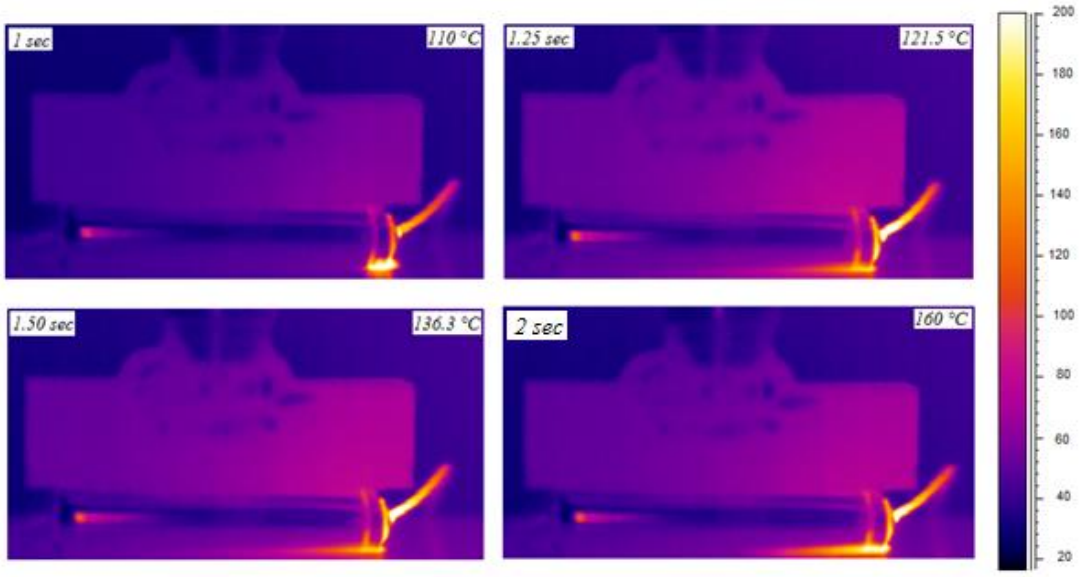

Figure 4.26: Propagation of short circuit with temperature for flat plate at 75% SOC

As shown in figure 4.26, initially high temperatures were observed at the positive terminal which propagates to negative terminal as shown in figure 4.27, where high temperatures can be seen in the cell, and once cell attains peak temperature, then negative terminal shows temperature which is due to the thermal conductivity of negative terminal and internal failures.

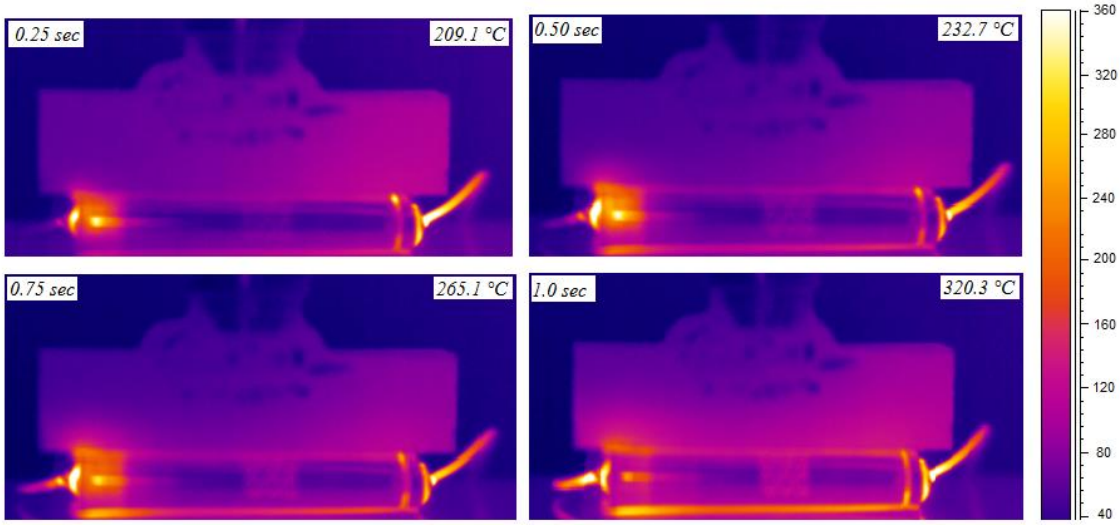

Figure 4.27: Propagation of temperature with hotspot at 75% SOC

As high temperatures occur where terminal wires are showing hotspot, no disconnection is noticed as voltage variations were observed throughout the test. Heat dissipation to surrounding and flat plate impactor was not observed which shows due to even surface of the impactor, and coating material did not come out which gave good results of temperature variations.

Once the cell reaches the temperature around 150˚C, which is also melting temperature of separator layers, the temperature change is very high. Flat plate deformation test undergo thermal runaway five seconds after short circuit occurrence which is similar to three-point bend test, where temperature variations are not as high as in flat plate deformation but the fracture is observed at the top of the cell, and the high temperature is observed at the bottom of the surface.

4.5 Conclusions of analysis

There appear to be two major patterns; the first where the temperature increase occurs as the voltage drops, and the second where the voltage drop precedes the temperature increase. In some of the cases temperatures only rise a few degrees to the mid 30ºC from the initial room temperature starting point (approximately 20ºC), but in general, temperatures spiked at above 100 degrees. Flat plate failures appear to have the highest temperature increases of all the failure scenarios tested. It seems that most failures occur after 5-7 minutes of loading, but longer periods exist for some tests. Table 4.17, shows mean displacement for each loading condition and standard deviation of displacement.

Loading condition	**Mean Displacement (mm)**	**Std. Deviation of Displacement**
Rod test	*6.900*	*1.731*

Circular Punch	*7.571*	*0.287*
Three-point	*7.272*	*1.083*
Flat plate	*6.036*	*0.971*
ALL	*6.945*	*1.202*

Table 4.17: Mean Displacement at short circuit

The average displacement that began short circuit is 6.94mm; however, it appears that flat plate deformation tests developed short circuit earlier compared to other loading conditions where mean displacement was nearly 6mm. Sahraei, *et al*. (2012a) found that displacement greater than approximately 6.5mm is associated with the outer shell of the casing fracturing which is followed by the jelly roll fracturing internally and initiation of the short circuit.

Failure stress-strain analysis was conducted in detail by Xu, *et al*. (2016) and Cannarella, *et al*., 2014. Similarly in the current research, failure strain and stress for all loading conditions, concerning SOC were calculated to formulate the nominal failure strain which is given in the next section. Similar to observations in this study, research was conducted for mechanical integrity of cells by Sahraei, *et al*. (2015); whereas, in this study detailed experimental results cover temperature variations as well. Mostly 10% SOC cells were used for abuse testing in the literature, but additional observations from this work at other SOCs support their theory and models regarding the process of

deformation leading to delamination but thermal behaviour due to structural abuse is not defined and onset of thermal runaway due to structural failure where SOC is also involved is not evident from previous research. Further analysis was conducted concerning deformation pattern, temperature change rate at different loading conditions and SOC after impact, Stress-strain analysis along with voltage-temperature variations, pre- and post-impact thermal analysis. In this study punch and rod, indenter are also used to identify compression effect on the centre of the cell which is also significant to predict any structural behaviour and the consequences.

To understand the permanent damage to a cell two cells were chosen randomly from all tested cells. All cells experience short circuit and undergo thermal runaway, where electrical, mechanical and thermal properties change. A cell with the unusual response for all loading conditions is chosen to investigate for remaining capacity in this section where initially low C-rate is applied, and then high C-rate of up to 1C is applied to check either cell undergoing sleeping mode or permanent damage condition. Results and respective observations are discussed in detail. Like in rod test only 0% and 50% initially tested SOC cells are in good condition without any crack which is appropriate to carry out the further experiment. Circular punch 0% SOC damaged the cell and flat plate 25% SOC damaged cells showed excellent charge-discharge behaviour after post-failure assessment, however other cells started to charge where 1C charge current (2.2A) was applied, but after some time, they started to loose charge and temperature increment was noticed. They are removed from charger to

observe variations where slow voltage drop was observed which shows severe internal damage occurred in these cells which does not allow charge transfer and this damage is impossible to revert. Due, however, to heat capacity and thermal conductivity characteristics it is still possible that these sufficiently damaged cells can contribute towards the temperature increase of adjacent cells in the pack because battery terminals are still in good shape which may behave the same in these events unless they come under impact in a particular loading direction. Figures 4.28 to 4.31 show tested cells, where respective voltage and temperature variations can be observed.

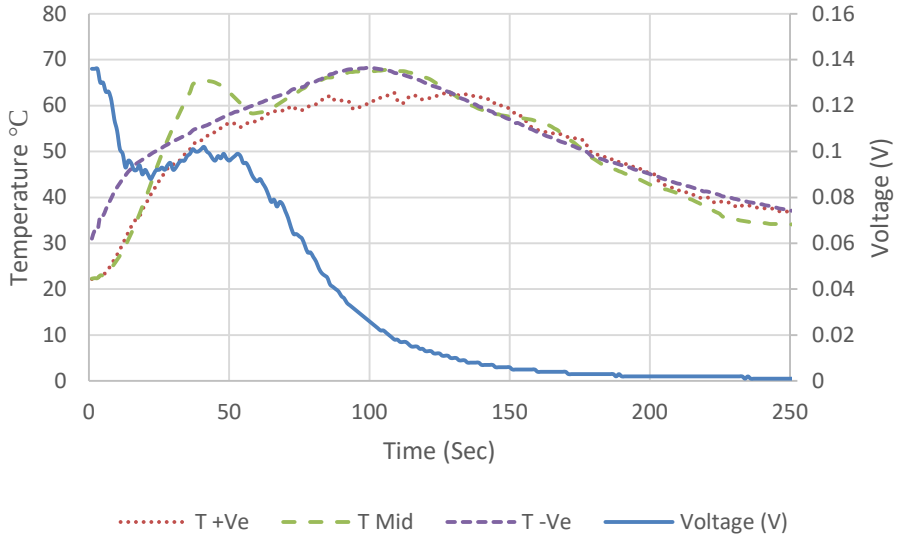

Figure 4.28: Rod test, damaged cell with 50% SOC

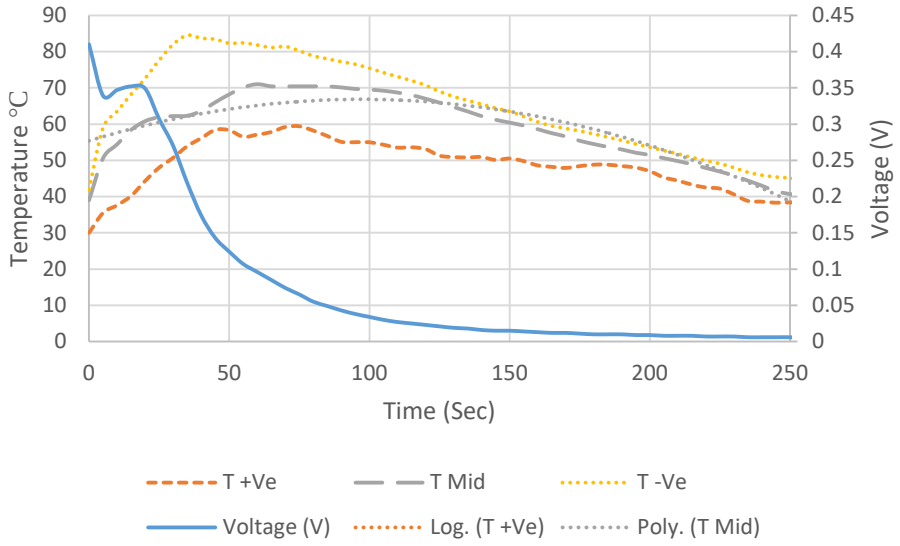

Figure 4.29: Circular punch test, damaged cell with 0%SOC

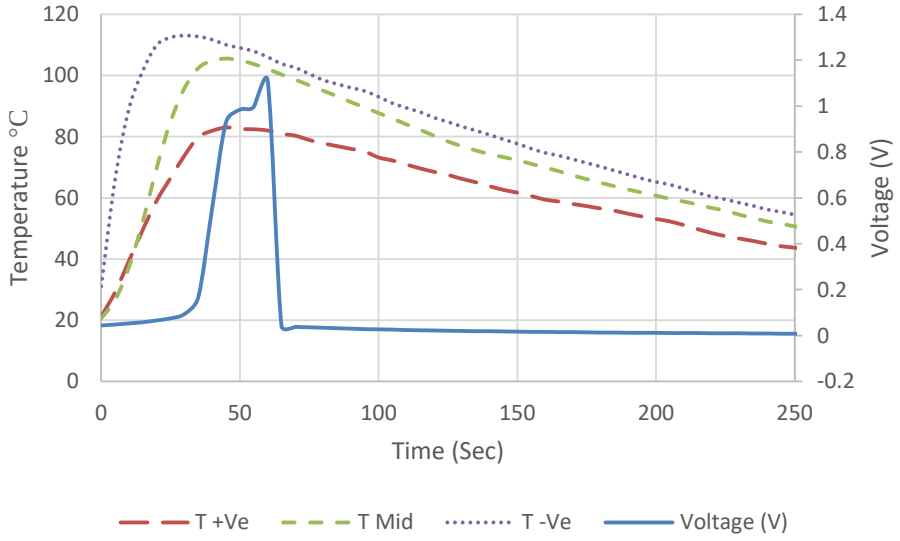

Figure 4.30: Three-point bend test, damaged cell with 75% SOC

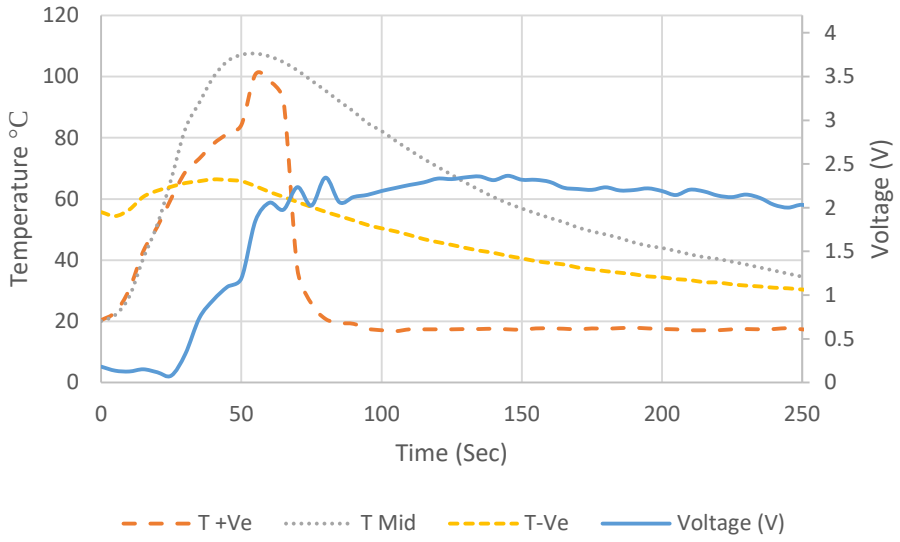

Figure 4.31: Flat plate test, damaged cell with 25% SOC

Interesting results are achieved for these tests as for circular punch and rod tests, cells showed similar voltage and temperature curves, where temperature values at each surface location were similar and showed similar curve response. Voltage increased for some time and slowly decreased to zero which shows cells were completely damaged and could not hold the charge, however at the low charge current these cells showed the same response.

For flat plate and three point bend test, cells started to hold the charge for a while but after some time while connected to power supply they started to discharge, and high ripples were observed in flat plate test, which shows internal electrochemical discrepancy due to damage. Maximum temperatures for both tests were above 100˚C and slowly dropped down to ambient temperature.

Thermal runaway process for flat plate deformation is shown in figure 4.32, where temperatures at three surface locations with voltage variations are shown. Summary of all models explained earlier is given in the summary section of this chapter.

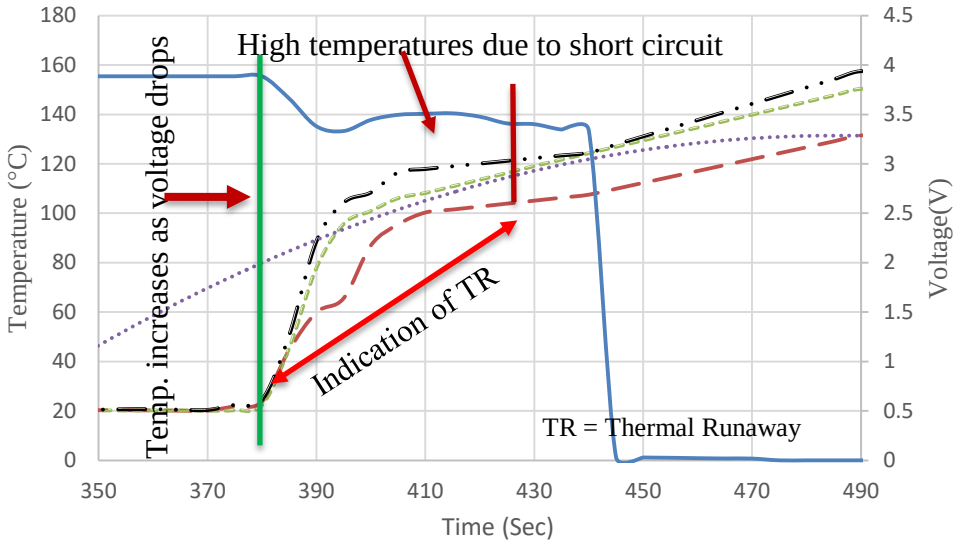

Figure 4.32: Thermal runaway indication at three surface location in flat plate deformation

In figure 4.32, temperature can be calculated using parabolic fit where governing equation is as follows, where adjusted R square is 0.8009

$$Temperature\ (T) = -0.0046t^2 + 4.4891t - 958.39 \quad (4.15)$$

In eq. 4.15, "T" is temperature and "t" denotes time in seconds for 380<t<450. High temperature change can be observed as within 10 seconds of short circuit, 12% voltage drop was observed and temperature change rate of 500°C/min was observed at surface locations. Mean temperature variations were observed at three surface locations.

4.6 Summary

After detailed analysis, various indicators of thermal runaway detection were observed and discussed in this chapter, which includes the force applied, the amount of displacement, temperature variations and voltage change. Force applied, and displacement gives an idea of indentation type and effects which can be listed as an indicator of thermal runaway detection. As mentioned in previous research, if thermal runaway does not happen it might slow progress and lead to permanent damage to the cell, so post-impact analysis was investigated where temperature change rate and voltage and temperature relationship were observed. A few of the cells did not show any fracture or the sudden drop in voltage and temperature rise, but it does not mean they were safe and behaved in the usual way. They might undergo severe conditions when used in the application and cause damage to adjacent cells as well. As mentioned by Wang, (2016), it takes 15-40 sec from instantaneous drop of voltage to temperature rise in the event of thermal runaway, current research demonstrates that thermal runaway occurrence in the case of external abuse varies with SOC and type of loading, which is shown in this chapter. Failure stress and failure strain equally contribute towards onset of thermal runaway. Sharp edge bend test has lower detection time for thermal runaway as bending of steel casing affects internal layers and immediate damage to layers causes instant temperature rise and voltage drop, where temperature change rate is higher. Flat plate deformation tests showed high mechanical strength as cells took time to deform and deformation is gradual where once cells developed the

short circuit, it went to high surface temperatures, and permanent damage occurred. Rod and circular punch tests were used to check compression effect on the centre of cells, which gave identical response for stress and strain; however, temperature variations in the rod tests are high compared to the circular punch which developed slow increase of temperatures. Initial hotspot of all tests were analysed where pre- and post-impact temperature changes with contour plot were observed, and in all cases, highest temperature locations were found around contact area except three-point bend test, where initial hotspot showed the high temperature at the bottom of the cell. In this research for mechanical abuse testing, quasi-static loading is used and mean loading speed is 1mm/min, which is in accordance with most of the loading speeds found in the literature for mechanical testing of cylindrical lithium-ion cells.

From the structural analysis, it is found that high deformation was observed for flat plate, rod and circular punch tests and buckling of casing was observed. For three-point bend tests where only three-point bend test went for cell fracture as for all test conditions, loading was suspended immediately after short circuit occurrence. All parameters useful for simulation were identified and tabulated in this chapter so that they could be used for LS-DYNA simulation in next chapter, where the structural behaviour of all loading conditions with thermal solver implementation was observed. Layered cylindrical cell model was implemented where concentric layer formation was used with solid element formulation. Delamination of layers was observed. Significant results with test cases have

been compared, and all the parameters used from experiment or literature are mentioned with their references.

Chapter 5: Numerical Simulation and Validation

5.1 Introduction

Experimental work explained earlier in this thesis brings to attention the properties of the lithium-ion battery during quasi-static mechanical loading, where due to variations of mechanical properties it is difficult to study these properties at different stages of loading. Computer simulation techniques are appropriate for these applications where to model battery, finite element analysis (FEA) methods are commonly used (Marcicki, *et al*., 2017; Wang, *et al*., 2016; Xia, *et al*., 2014; Trattnig, *et al*., 2014; Wierzbicki, *et al*., 2013; Sahraei, *et al*., 2012a; Sahraei, *et al*., 2012b; Martínez-Rosas, *et al*., 2011), which allows for the evaluation of the mechanical properties of battery specimens where material properties are known, or sensitivity analysis can be used to determine these properties.

FEA is useful for structural behaviour analysis and widely used in the automotive sector. In this chapter, a numerical simulation model of a battery is developed to validate experimental results and some of the key parameters are taken into account. Temperature variations due to abuse conditions is one of the concerns as explained in the previous chapter, where this leads to temporary and permanent damage to the battery and causes thermal runaway. In this chapter, the numerical simulation approach incorporating parameters obtained from experimental work is used to develop a single battery layer model where some assumptions are made to replicate properties of battery model. In

this research, FEA of the battery is conducted using LS-DYNA simulation tools, where LS-Pre-Post is used for initial geometry, material properties, boundary conditions and solver. The input file is executed in LS-DYNA executable, where binary d3Plot files are generated containing simulation results. Analysis is carried out at different time intervals to magnify relevant results. Major determinants to analyse battery characteristics are displacement, force, contact area, stress-strain and temperature. Series of battery models are used to develop single battery model which includes 9-layer model, complete cell model with thickness of 0.3mm. Battery layer formation, number and size of elements, step size, impactor geometries and properties are discussed in detail in this chapter.

5.2 Modelling approach

Before implementing full cell model, it is necessary to adopt an alternative technique where similar battery formation is used, for this purpose a battery layered model is chosen. The purpose of choosing an alternative model is to verify results on a small scale compared to lithium-ion cell model where the number of elements are much higher which increase computation time, and it is sometimes difficult to rectify issue if a complete cell model is encountered comprised of several settings and conditions. For initial model mainly three material types are used, where for the separator, anode and cathode MAT_63_CRUSHABLE_FOAM is used. Crushable foam material is used as it has an option of tension cut off where tension is treated as elastic-perfectly-plastic at the tension cut-off value (Material selector for LS-DYNA, 2016).

Detailed validation of crushable foam is given by Silk, *et al*., (2006). For Current collectors and steel casing MAT_24_PIECEWISE_LINEAR_PLASTICITY is used. Piecewise linear plasticity material model accounts for stress-strain behaviour where curve can be used to provide stress-strain values. For the rigid base plate, MAT_20_RIGID is used which is to turn solid element part into a rigid body. Detailed properties and relevant characteristics of materials used can be found in LS-DYNA material model manual (LS-DYNA keyword user manual, R_8.0, Vol_ii). Layered model proposed in current research consists of nine layers where eight layers represent cell stack, and additional layer represents rigid bottom plate as shown in figure 5.1. Element size selection is crucial which affects computation efficiency as well as stability of model. For layered model element size chosen was 3mm which is still an appropriate size as in complete vehicle simulation model. Marzougui, *et al*., (2014) used an element size of 4mm.

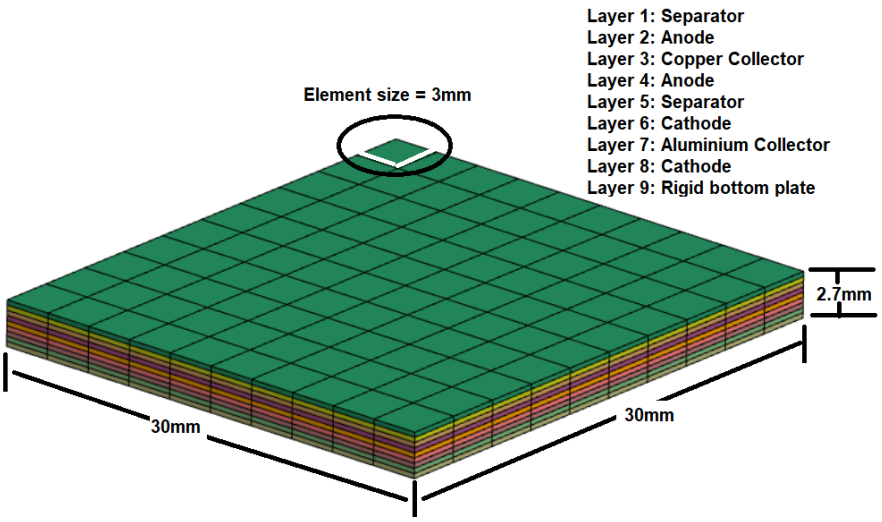

Figure 5.1: Battery layered model

Layers with thicknesses of 0.3mm and length of 30mm with square shape are modelled as shown in figure 5.1. For layered model, the rigid bottom plate is constrained; also all sides are restricted to check the loading impact on the centre of layers. Material properties for current collectors and active materials are used from (Engineering tool box, 2017; Zhang, *et al*., 2015a, Zhang, *et al*., 2015b; Sahraei, *et al*, 2014), and experimental study, which are given in table 5.1.

Material	Mass density (Tonne/mm^3)	Modulus of elasticity (MPa)	Poisson ratio	Yield stress (MPa)	% Failure strain ε_f
Copper current collector	7.94e-9	1.1e5	0.35	210	5
Aluminum current collector	2.69e-9	7e4	0.36	180	5
Anode	2.23e-9	1e4	0.3	100	10
Cathode	4.20e-9	1e4	0.3	100	10
Separator	1.179e-9	3.45e3	0.35	18	25
Steel casing	7.83e-9	2e5	0.3	450	4
Rigid plate	----	----	----	----	

Table 5. 1: Material properties used for LS-DYNA simulation (Engineering tool box, 2017; Zhang, et al., 2015a, Zhang, et al., 2015b; Sahraei, et al, 2014)

A sphere indenter with 5mm diameter is used for preliminary modelling. To facilitate layered model to exhibit their properties, various contact cards were

used to identify the differences, where initially CONTACT_AUTOMATIC_GENERAL was used, but to verify results another contact card CONTACT_AUTOMATIC_SURFACE_TO_SURFACE was also used, both gave a better approximation of layers' failure behaviour. CONTACT_AUTOMATIC_SINGLE_SURFACE was used for initial model to avoid penetration during buckling. Layered model provided good approximation of results where different types of contact entities, material cards from LS-DYNA library, termination time and time step were checked. To check delamination and individual layers' behaviour further analysis was carried out using symmetry (quarter) model where various sets of boundary conditions where used to correctly model symmetry model. Initially, high penetration was observed which affected layer properties and respective stress-strain behaviour. To verify initial model *all steel material model* was used, where only material properties were changed from original model, and all layers were considered steel material. This technique is quite effective as no penetration was observed, which means our model is correct but some properties were affecting the results. These were further investigated as contact entities, boundary conditions and element selection. Further modelling was performed with different sets of contacts and solid element formation for all layers in the model. Figure 5.2, shows (a) layered model with penetration and (b) all steel model without penetration.

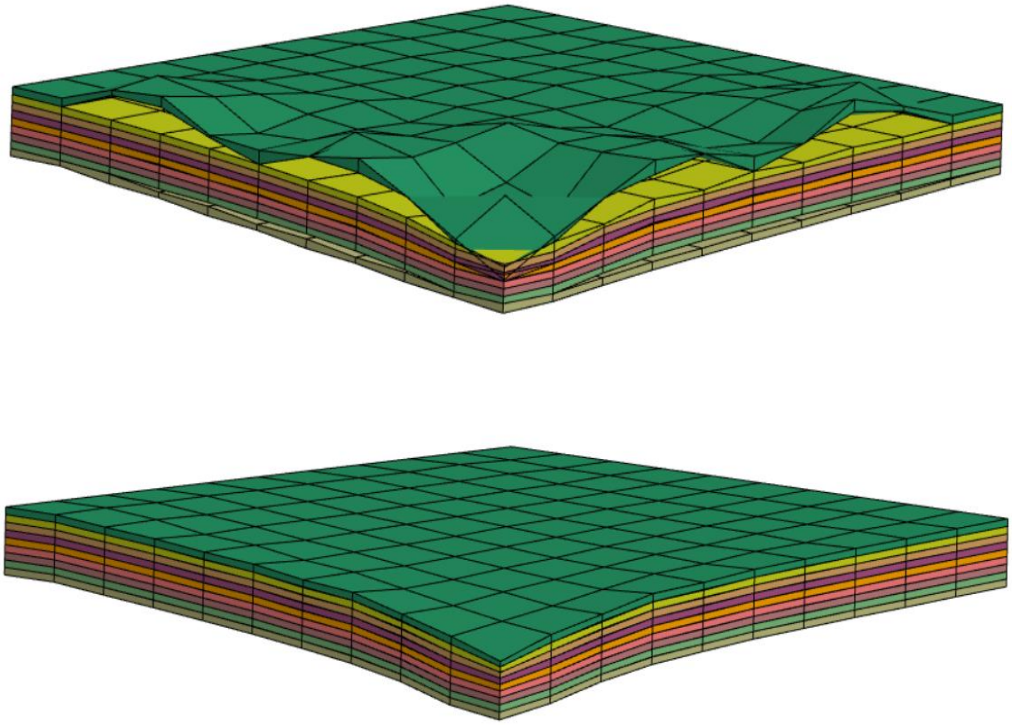

(a)

(b)

Figure 5.2: (a) layered model with penetration (b) all steel model without penetration

As shown in figure 5.2, initially layers were modelled using shell elements, which were replaced with solid elements. After using solid element formation, better accuracy was achieved for the initial test. Figure 5.3 shows symmetry model with better accuracy.

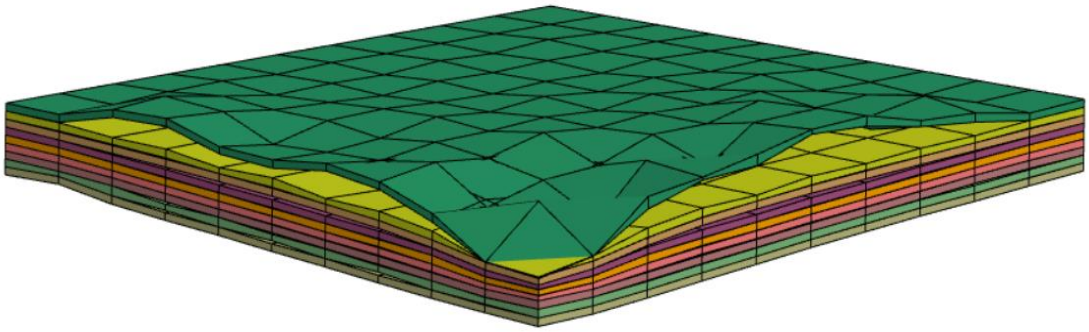

Figure 5.3: Symmetry model with better accuracy

To capture master and slave side forces, FORCE_TRANSDUCER_PENALTY card was used. Based on initial layered model few modelling decisions were made for full cell model including layer formation, element type, element size, material properties, boundary conditions, time step and initial velocities. These decisions are explained in the upcoming sections, which will lead to achieving improved results and better accuracy for all test scenarios.

5.3 Formation of concentric layered model

Concentric layers were used by Nadimpalli, *et al*., (2015), where layers had thickness accurate to 18650 cylindrical cell. as shown in figure 5.4.

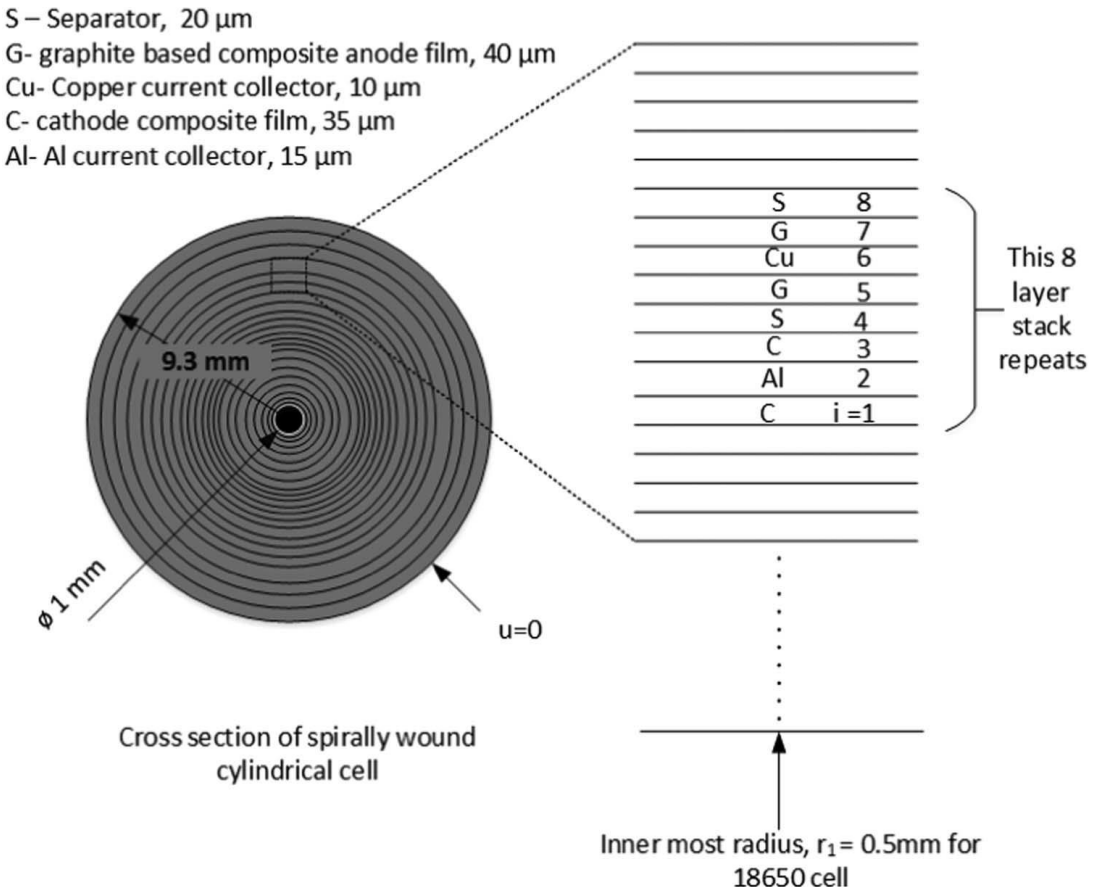

Figure 5.4: Concentric layers of 18650 cylindrical cell with original thicknesses of layers (Nadimpalli et al., 2015)

Nadimpalli, *et al*., (2015) mentioned a total of 304 layers for 18650 cell which accounts for 38 stacks, where each stack contains eight layers. To model 304 layers with exact thickness requires high computation efficiency and modelling time, where very thin layers need special modelling precautions. In this research concentric layer model formation was used to model 18650 cylindrical cell which was not found in the literature, however, jellyroll model where all the layers are lumped in jellyroll model was proposed by (Sahraei, *et al*., 2012a). As cells have spiral wound formation in general, concentric layer model represents

a different structure, where the main aim is to find an alternative way to model the battery where each layer is independent in the case of geometry; however, layers share mechanical and thermal behaviour under loading conditions. A thicker layer model is found to be the best choice to represent cells with the number of layers. Similar methods were used by Zhang, *et al*. (2015a); Zhang, *et al*. (2015b) and Sahraei, *et al*. (2012a).

In this research all layers are considered to be the same size, this assumption provides an opportunity for simplifying the model as well as, due to low thickness compared to Zhang, *et al*. (2015a) and Zhang, *et al*. (2015b), more layers can be integrated to form a complete cell., Steel casing has, however, an almost similar size to the original cell. Concentric layers can be an appropriate alternative to spiral wound layers which are complex to design and simulate due to different thicknesses of cell layers.

5.4 Simulation parameters and assumptions

Cell initial temperature was selected as 22°C, which is in agreement with single cell testing standards and SAEJ2464 standard, which sets the limit of 55°C for module level test. The battery model is modelled with fully integrated solid element formulation, where a total of 103306 elements are used. The size of elements for steel casing is 0.5mm and for all other layers is 1mm. The reason for different element size selection is to achieve accuracy, where steel housing is the first layer to experience load. All indenters and bottom plates are modelled as rigid geometry, where rigid material MAT_20_RIGID was used. A

coefficient of friction between cell and support is considered to be 0.3 as given by Saharei, *et al*. (2012). No endcaps were taken into account for this simulation, however, SPC boundary conditions were used to restrain components of the battery if required. Failure strain of separator documented by Zhang, *et al*. (2015a) was 93%; however, separator failure strain of 35% to 80% from literature is evident, which means values of 0.2 to 0.5 (50% or 80% of initial thickness) could be used for the separator. Consistent units by (LSD-DYNA consistent units) were used for all simulation models given in table 5.2. For simplification, only consistent units used in this research are considered in table 5.2.

Consistent units (Steel material)							
Mass	Length	Time	Force	Stress	Energy	Density	Young's Modulus
ton	*mm*	*s*	*N*	*MPa*	*N-mm*	*(Tonne/mm^3)*	*MPa*

Table 5. 2: LS-DYNA consistent units

5.5 18650 cell simulation model

Based on above-mentioned properties and assumptions, the simulation model is designed to understand loading impact on the cell. For simulation, all layers (steel shell casing, anode, cathode, separators, anode current collector and cathode current collector) were considered to be 0.3mm thick and innermost radius was considered to be 1mm as detailed by Croop and Lobo, (2009). It is important to understand the material properties for individual layers for

stress/strain relation and for that purpose, two foam material models were discussed by Sahraei *et al.,* (2012a) and Maleki and Al-Hallaj, (1999) with compression and three-points bend test were considered for initial investigation. True stress/strain curve from dogbone specimen for shell casing is given by Bai, *et al*. (2009) and Bai, *et al*. (2008), nominal failure stress and failure strain were used from experimental results, where for each test case values at 0% SOC were used, which is to check if the model predicts failure. Material selection (LS-DYNA keyword user manual, R_8.0, Vol_ii) was made based on the layered model analysis explained at the beginning of this chapter. Steel casing material is modelled using MAT-24-PIECEWISE-LINEAR-PLASTICITY in LS-DYNA. Separator, anode and cathode were considered to be as the MAT-63-CRUSHABLE-FOAM model, and anode current collector and cathode current collector were modelled using MAT-003-PLASTIC-KINEMATIC. Stress/strain curve for the separator, active anode material and active cathode material was used from Zhang, *et al*. (2015b) and Croop and Lobo, (2009). Li-ion 18650 cylindrical cell and finite element models of the cell are given in figure 5.5. Central core and cell terminals are not considered in this research. Wang, *et al*. (2016) and Sahraei, et al., (2012a) used jellyroll model for simulation to predict short circuit.

(a) 

(b) 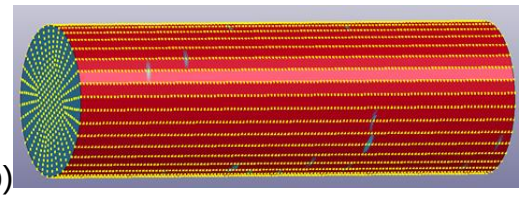

Figure 5.5: a) Li-ion 18650 cylindrical cell b) FEM model of cell

Due to the higher number of elements (103306) used for this simulation, a small termination time is used, which is still within the scope of battery testing as quasi-staic loading is achieved where kinetic energy is less than 5% of total energy. Heat capacity and thermal conductivity values used for all layers are given in table 5.3.

Scaled layered thickness of each layer is chosen where 0.1mm and 0.3mm thicknesses are found to be more accurate, but due to computation time results are concluded from 0.3mm thick layers. Material properties and failure crietaria are used from experimental work and literature. A thermal solver is used for thermal analysis of 18650 cell due to structural deformation. Coupled mechanical and thermal solver is used, where structural deformation is an input for the thermal solver. Heat capacity and thermal conductivity of individual layer along with the type of deformation contribute towards temperature variations of the cell.

Type of layer	Heat capacity $(Jkg^{-1}K^{-1})$	Thermal conductivity $(Wm^{-1}K^{-1})$
Steel shell casing	477	14.9
Separator	1978	0.334
Anode active material	700	5
Cathode active material	700	5
Anode current collector	386	400
Cathode current collector	900	200

Table 5. 3: Cell heat capacity and thermal conductivity parameters for simulation

Electrochemistry of cell is not considered in this research. The literature shows cells can be modelled without electrochemistry to perform several sets of analysis as performed by Sahraei, *et al*. (2015); Zhang, *et al*. (2015a); Zhang et al., (2015b) Sahraei et al., (2014); Shraei et al., (2012a); Sahraei et al., (2012b), where authors used finite element analysis for structural behaviour due to impact. In the current research temperature variations of contact area are considered but complete cell thermal properties are not considered for this

simulation. Figure 5.6, shows single layer and complete cell with thickness 0.3mm.

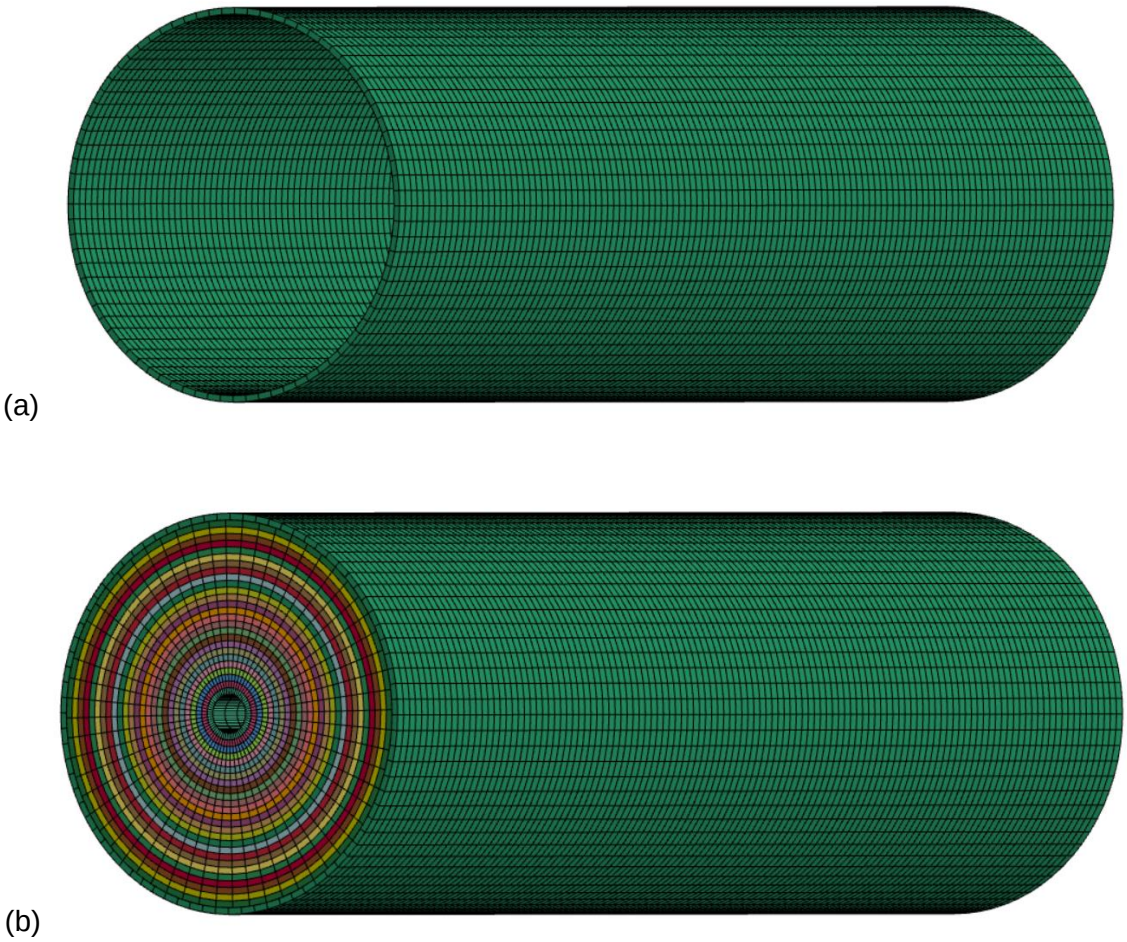

(a)

(b)

Figure 5.6: Cell layered models, (a) 0.3mm single layer, (b) 0.3mm complete cell

Boundary prescribed motion set is used in this simulation to define object motion throughout the simulation at every single time step. Due to sensitive nature of contact cards, accurate contact interface modelling is necessary which improves finite element simulation results.

5.6 Simulation results and validation

Simulation models based on parameters and methods explained earlier are discussed in this section, where results for structural and thermal behaviour and their comparison with experimental work are discussed. Both quasi-static and impact load simulation results are discussed in detail where displacement and temperature variations are used as an indicator of failure. Element erosion is used for fractures due to loading.

5.6.1 Rod test simulation

5.6.1.1 Strucutral analysis

Structural analysis was conducted on the cylindrical cell using the simulation model explained in this chapter and results were compared with the experimental study as shown in figure 5.7.

(a)  (b) 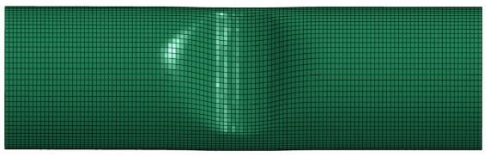

Figure 5.7: Rod test (a) loading result, (b) simulation result

As expected from the simulation model implementation, both experimental and simulation results matched for rod test simulation where, due to internal battery behaviour, this response can vary for other tests. To negate battery chemical proposition during loading, completely discharged cells are chosen to compare results, but in some cases, cell electrochemistry contributes towards cell

stiffness, thermal variations and short circuit response. In the simulation high temperature change rate was observed at around 4mm, which indicated initiation of short circuit or cell initial failure. Figure 5.8, shows simulation model of resultant displacement at the point of initial failure.

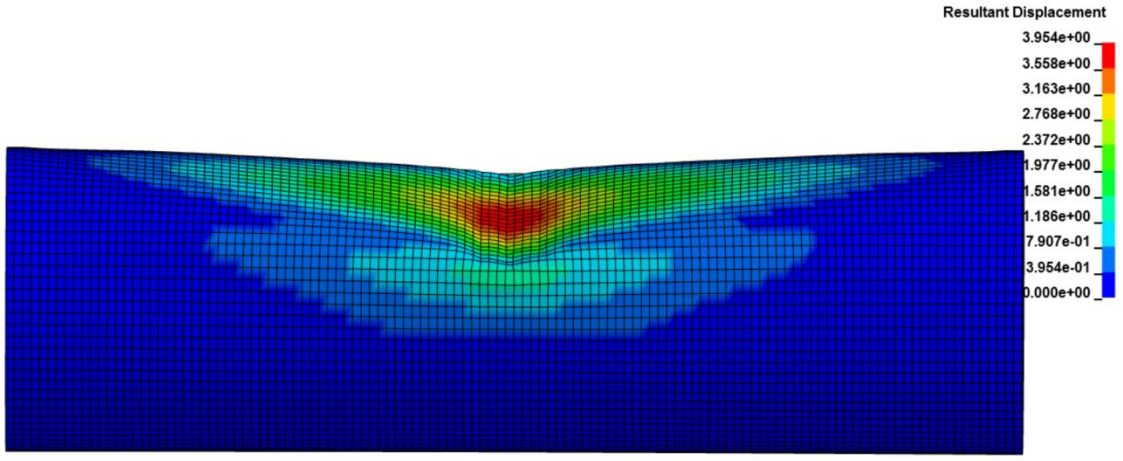

Figure 5.8: Rod test simulation, resultant displacement at initial failure

Good approximation of experimental results was achieved for structural failure due to rod test. Temperature variation for quasi-static and impact loading was discussed in detail where temperature and displacement relation shows the significance of temperature analysis for short circuit prediction and possible thermal runaway occurrence.

5.6.1.2 Temperature analysis

Temperature cut-off was considered when high temperature change rate was observed, which indicated short circuit occurrence. Temperature variations for quasi-static loading and impact loading were used in this section to analyse cell failure, where temperature changes were considered at the point of force drop.

For impact, loading speed of 6.3mm/ms was used, which is in line with Marzougui, *et al*. (2014). Figures 5.9 and 5.10, show initial temperature results obtained in this simulation.

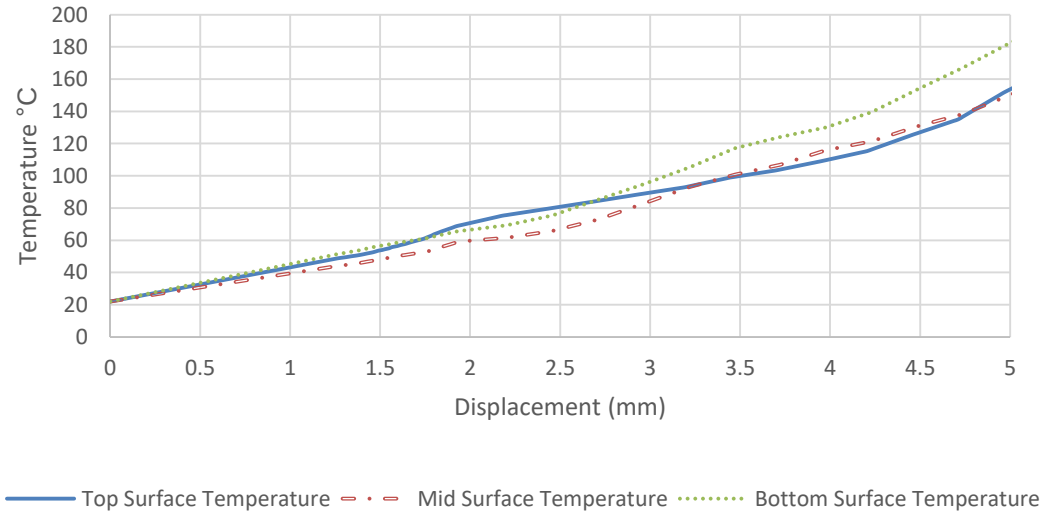

Figure 5.9: Rod test surface temperatures, impact loading

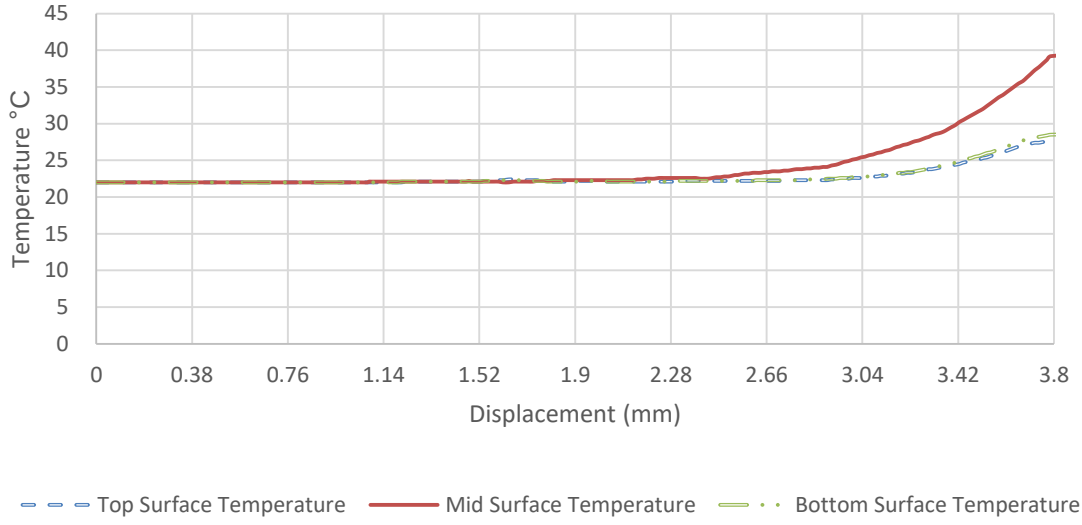

Figure 5.10: Rod test surface temperatures, quasi-static loading

Three surface locations were used to understand temperature behaviour for quasi-static and impact loading. Results show with impact load, high temperatures were observed at top, mid and bottom surfaces compared to quas-static loading conditions; however, temperature variations at the extreme end terminals for quasi-static load were similar. In the experiment, mid surface temperature at the point of short circuit was 25°C; however, results from quasi-static loading provided the closest value for simulation, which was 40°C. Contour of temperature variations at different surface locations for rod test simulation with impact load are shown in figure 5.11, where steel casing was used as temperature measurements were observed at different surfaces of steel casing.

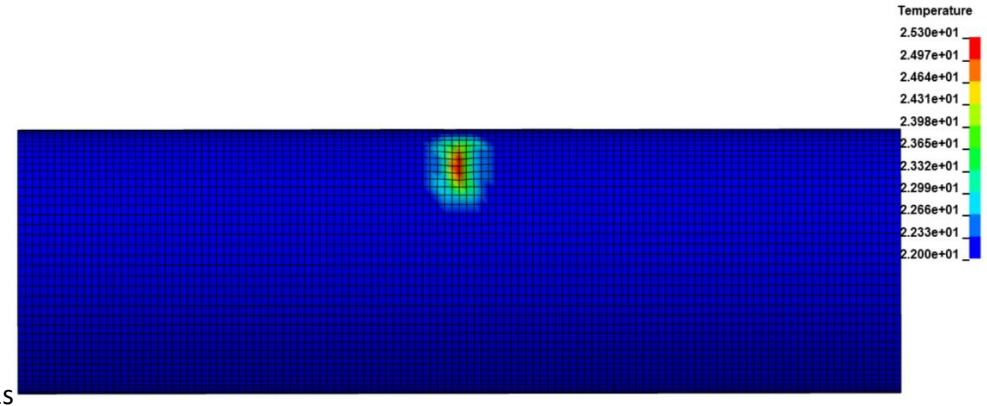

(a) t= 0.001s

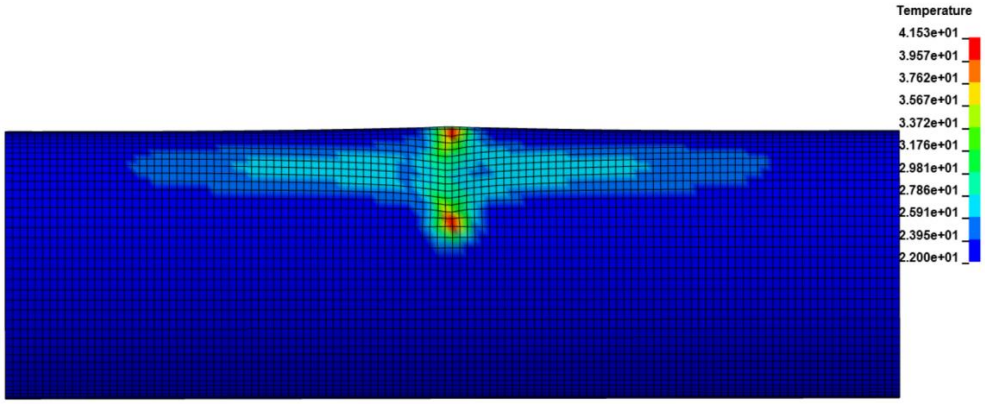

(b) t=0.003s

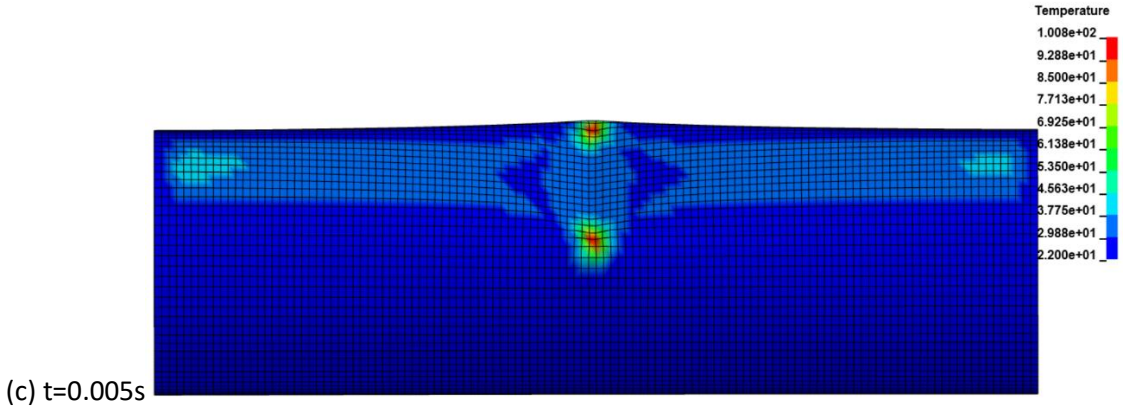

(c) t=0.005s

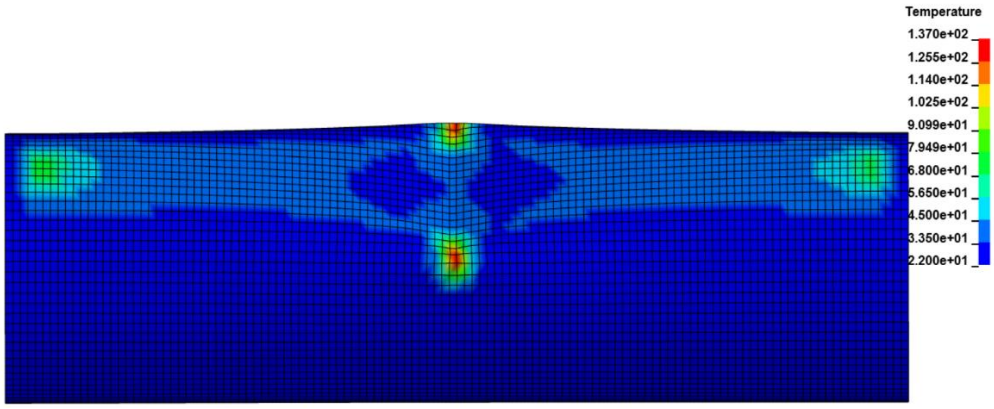

(d) t=0.01s

Figure 5.11: Contour of temperature distribution at steel casing due to rod simulation

As can be seen in figure 5.11, due to buckling and deformation of steel casing temperature at the area of buckling is high compared to other surfaces. At maximum displacement, this temperature reaches 150°C which is an indication of high short circuit temperature and separator layer failures which occur as melting point of separator layers is reached. Separator layer temperature variation analysis was conducted for circular punch and three-point bend simulation where results were used for short circuit indication and possible thermal runaway. Good correlation of experimental and numerical simulation analysis showed that rod test abuses at quasi-static loading were less

destructive compared to high speed impacts. Due to high speed, immediate failures occur at the edges of steel casing which is sufficient enough to raise overall cell temperatures and high stresses were observed at these points.

5.6.2 Circular punch test simulation

5.6.2.1 Structural analysis

Similar to rod test, simulation for circular punch is conducted to understand failure response which is detailed in this section. Experimental deformed model and simulation model are shown in figure 5.12.

(a)  (b) 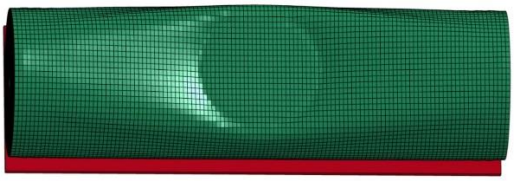

Figure 5.12: Circular punch, (a) test result, (b) simulation model

Like rod test, numerical simulation results showed similarity to experiment result for structural deformation due to circular punch. In the numerical simulation analysis the same deformation pattern as observed in experimental work was obtained where size and location of deformation is the same. Punch shape stamped on the cell, where cell buckling is clearly visible at the sides of the cell. Short circuit started to develop at 3.81mm and short circuit displacement (d_{sc0}) was found to be 5.6mm, which is slightly higher compared to experiment result. Figure 5.13, shows resultant displacement at the initiation of short circuit.

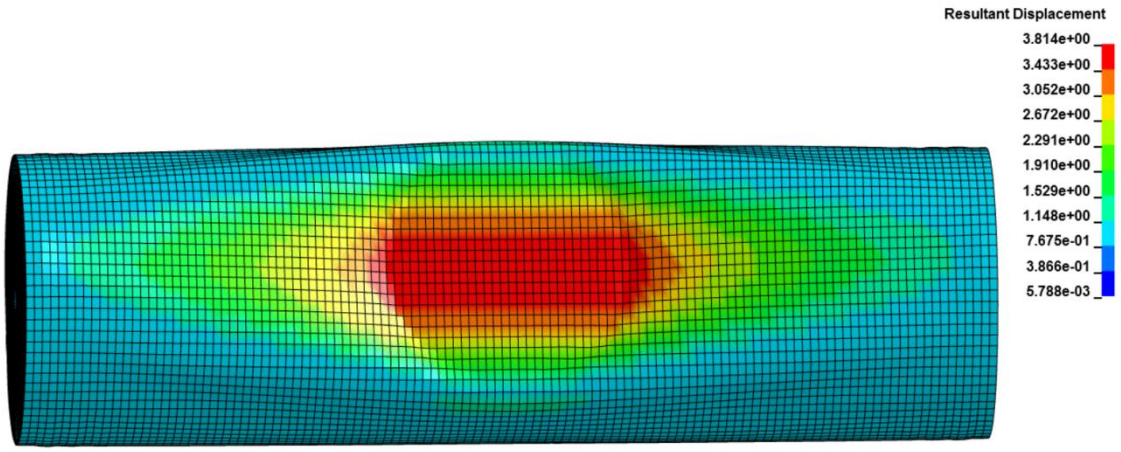

Figure 5.13: Circular punch numerical simulation resultant displacement due to quasi-static loading

Nominal failure stress for the experiment where short circuit was initiated, was 10.24 MPa; however in this simulation results showed stresses at the sides of the cell similar to rod test, which means even if cell experiences high stress, failure of the cell depends on the location and speed of impact. High speed load and quasi-static loading is compared for temperature variations to understand failures due to high speed impact. Same loading speed as used for rod simulation was used.

5.6.2.2 Temperature analysis

Temperature variations with quasi-static loading and high speed impact were observed and shown in figure 5.14 and 5.15 respectively where, for simulation, temperatures at the top, mid and bottom surfaces were observed.

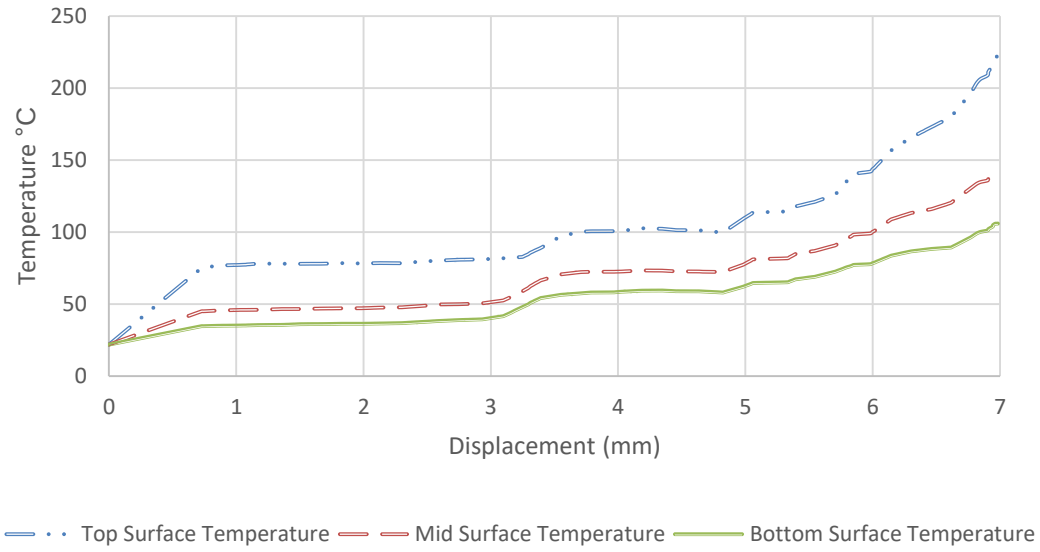

Figure 5.14: Circular punch surface temperatures, impact load simulation

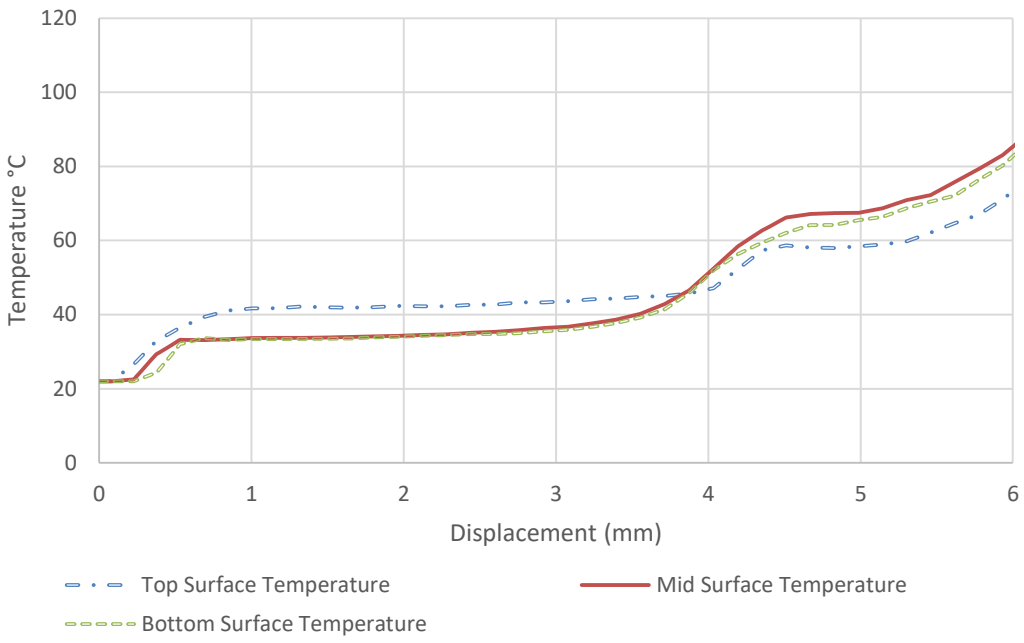

Figure 5.15: Circular punch surface temperatures, quasi-static load

As shown in figure 5.14, for impact load simulation, temperatures were between 100°C to 200°C, which is way higher than experimental values where temperature at initial short circuit was 35.6°C. Temperature at short circuit displacement for mid surface with quasi-static load was 50°C, as shown in figure 5.15; minimum temperature change was observed at the other two surface locations. Similar to rod simulation results, circular punch simulation results were close to experimental results when quasi-static simulation was used, which allows layers to attain full mechanical strength and convert plastic work into heat accurately. In the case of impact simulation, layers deformed in the unusual pattern and affected accuracy. Sudden temperature change was observed due to impact where short circuit initiated between 4 and 5mm. Resultant short circuit displacement for impact load is shown in figure 5.16.

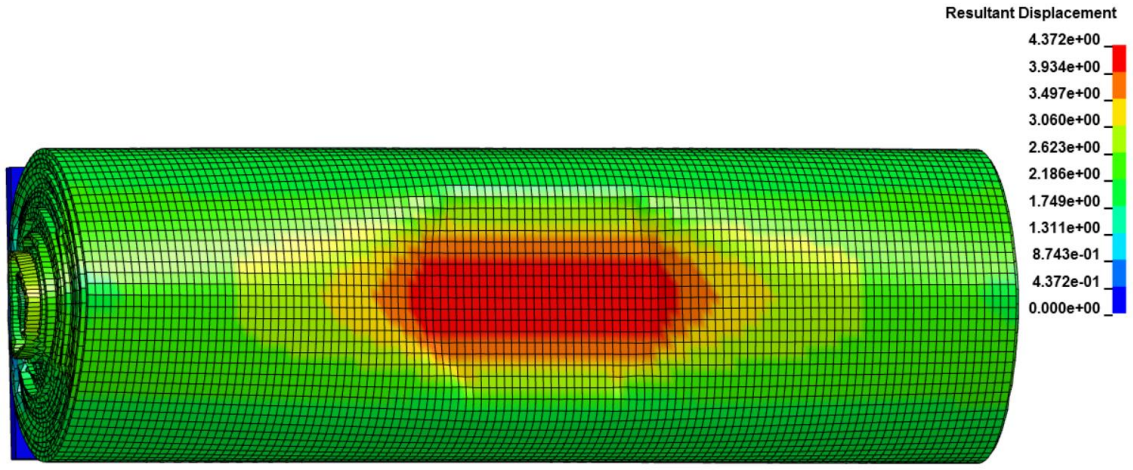

Figure 5.16: Circular punch numerical simulation resultant displacement due to impact

Separator layer failure analysis is observed for circular punch numerical simulation model, where all separator layers were considered and their respective temperature contours are shown in figure 5.17.

5.6.2.3 Separator failure analysis

In this research two of the indenter types used were different from the indenter used in the literature for short circuit and possible thermal runaway investigation. These were three-point bend test with the sharp edge and circular punch. To better understand short circuit initiation concerning separator layers, further analysis was carried out for circular punch and three-point bend test simulation results. For this analysis temperature variation locations with obtained figures and the graphical representation were used, where all the separator layers were included with applied force and temperature changes.

Sep-1:

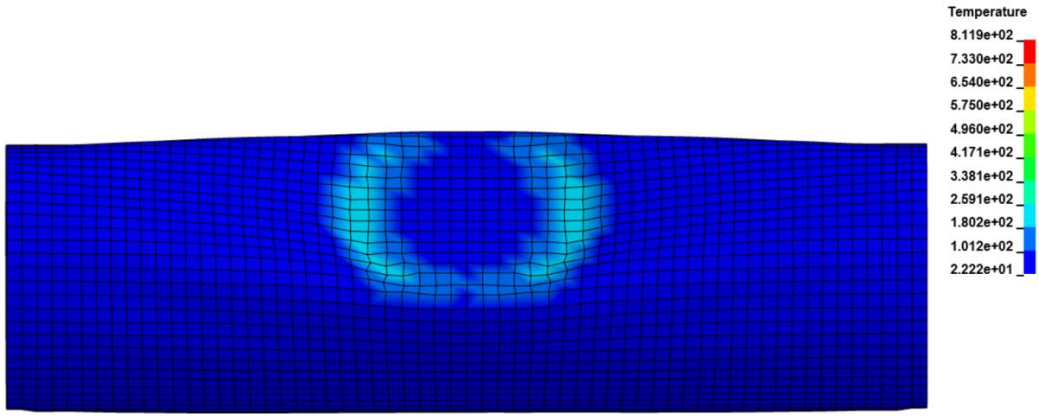

Sep-2:

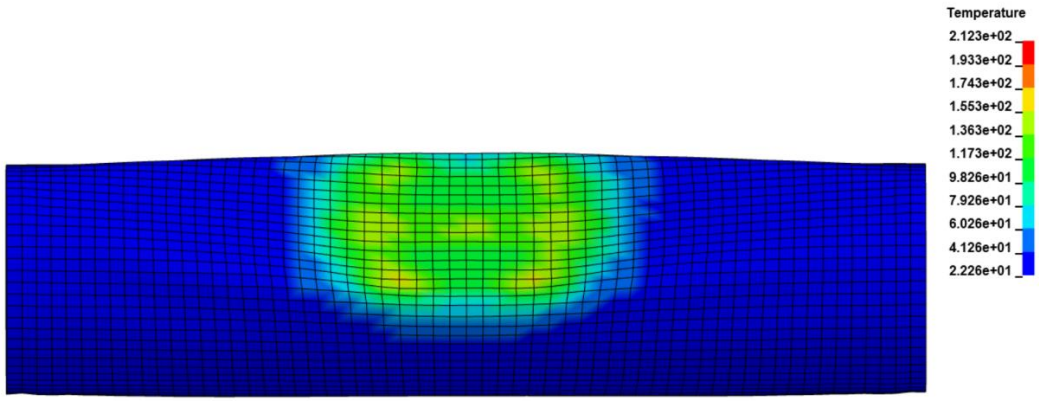

Sep-3:

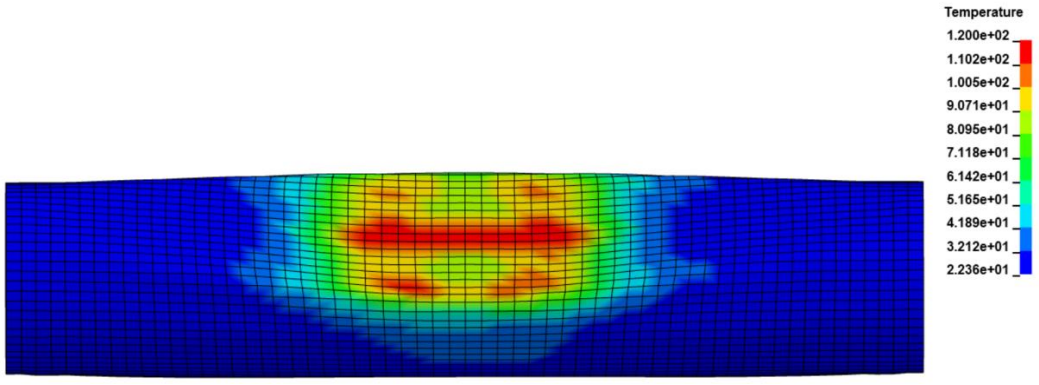

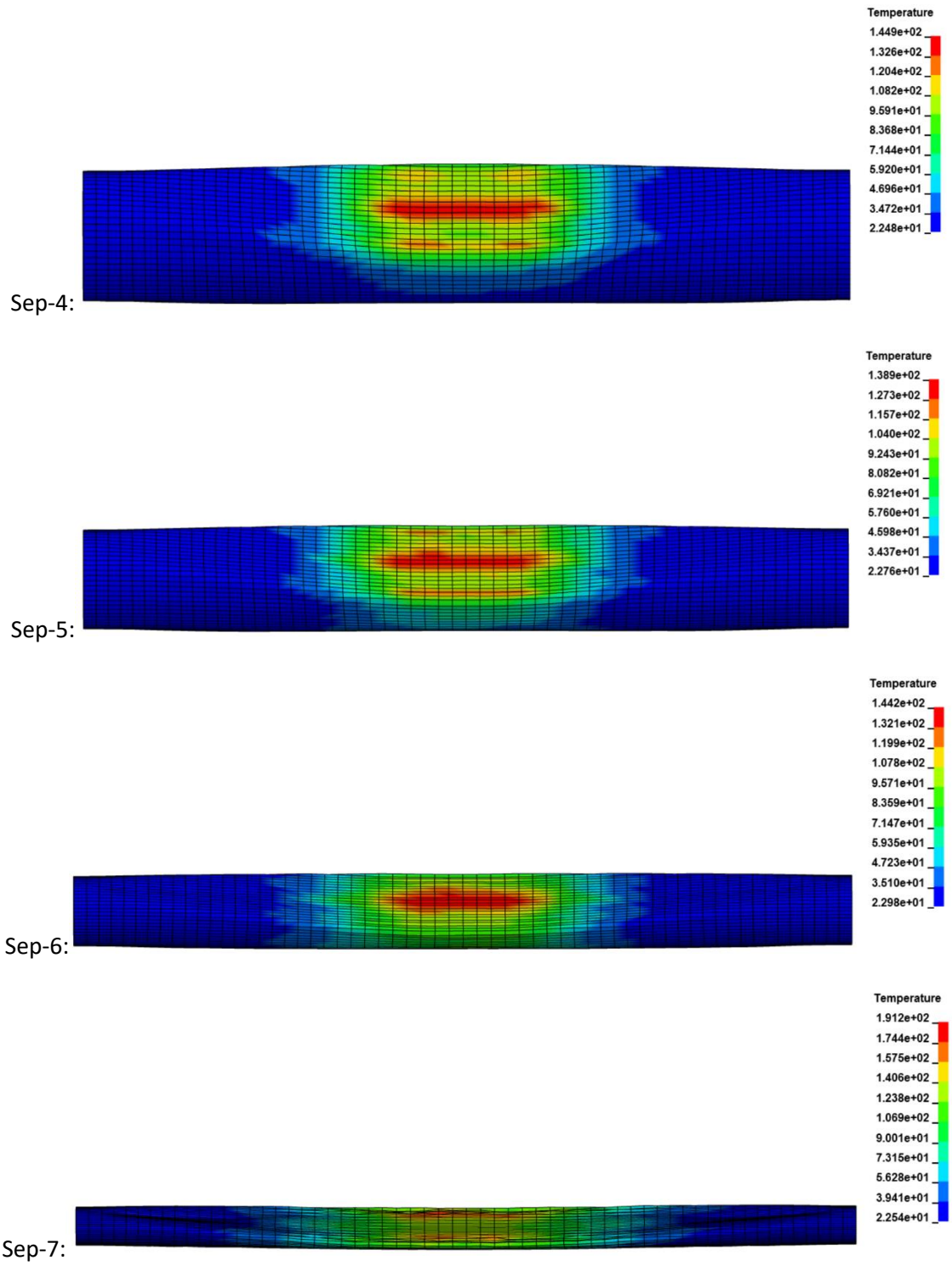

Figure 5.17: Contour of temperature variations at all separator layers

Separator layers are indicated with Sep-1 to Sep-7, where Sep-1 is first separator layer in the cell which is modelled as second layer of the cell, where first layer is steel casing. Initially, temperature distribution is around the corner of the layer where buckling of cell occurred. With the passage of time temperature distribution of separator layer varies and for sep-3 high-temperature location shift from side to the mid of the layer. For separator-5 comparatively high values were observed at mid-surface. From above figure it is shown that internal separator layers are more thermally active, which is due to the variety of reasons including forces applied from the rigid bottom plate, heat transfer inside the cell and high compression rate compared to other layers. Separator layers with temperature change and force applied are shown in figure 5.18.

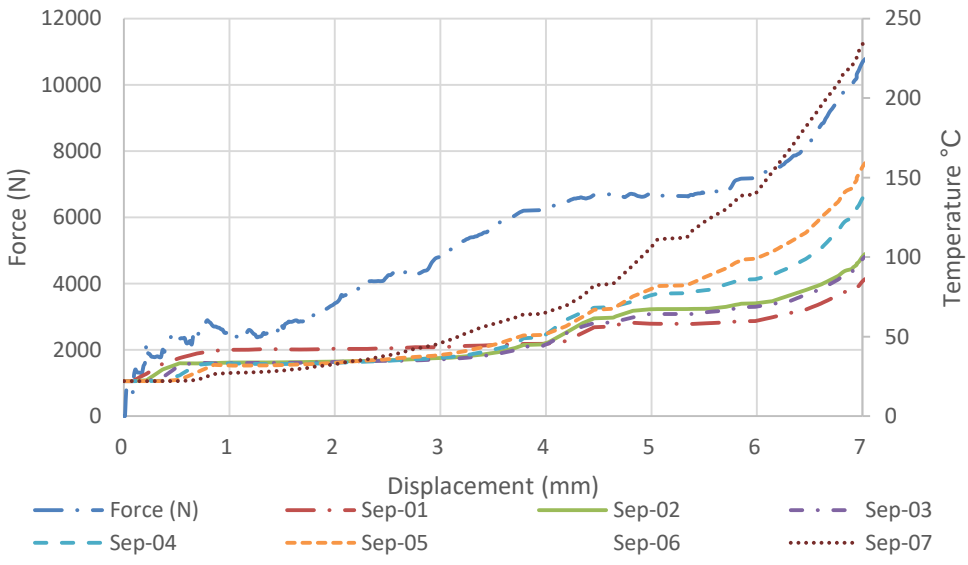

Figure 5.18: Circular punch separator layers behavior with applied force and temperature variations

As can be seen from figure 5.18, first five separator layers showed temperature variations well within the safe zone of separator melting point which is mentioned earlier. The last two layers, however, showed high temperatures which are higher than melting point. This illustrates the beginning of permanent cell failures as initial failures occurred at the time of short circuit where, due to deformation, cell temperature increased. Identical displacement values for experimental results and simulation results at the time of short circuit support this analysis.

5.6.3 Three-point bend test simulation

5.6.3.1 Structural analysis

For three-point bend test simulation, cell holders and sharp edge are modelled using rigid material. Numerical simulation model for three-point bend and experimental and simulation geometries for pre and post loading are shown in figure 5.19.

(a) 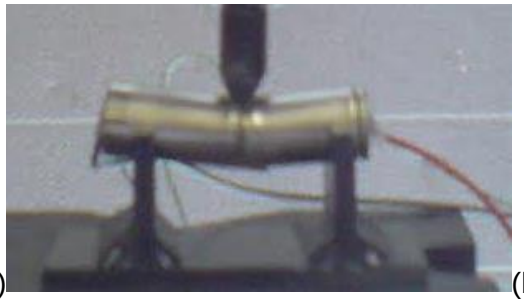 (b) 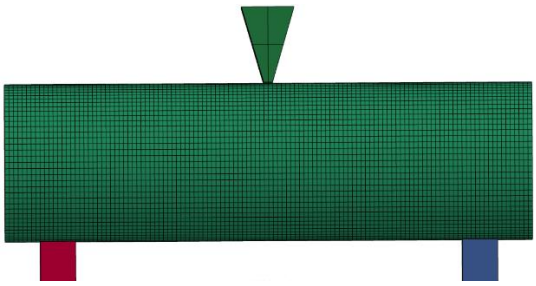

(c)  (d) 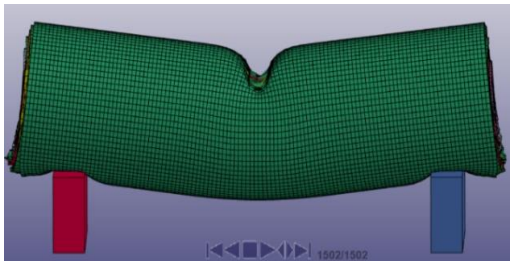

Figure 5.19: Three point bend test, (a) undeformed test, (b) undeformed simulation, (c) deformed test results quasi-static load, (d) deformed simulation resdult quasi-staic load

Due to computation efficiency, only modelled sharp edge of the indenter and cell holders without support are shown as in figure 5.19. Boundary prescribed motion is used for indenter and SPC motion set was used for cell and base plates which were fixed. Initially, when the load was applied on the cylindrical cell it used less force for compression but after some time due to material hardening excessive force was required for compression. Short circuit displacement was observed at 5.23mm for quasi-static analysis and 7.68mm for impact load. Due to sharp edge and loading speed cell fracture was observed in both quasi-static and impact load. In the case of impact load indenter penetrating deep into the layers with fracture most of the layers experienced fracture. For quasi-static loading, however, only steel casing experienced fracture but temperature at other layers also increased at the time of short circuit which is explained in the following section. Figure 5.20 shows resultant displacement due to quasi-static and figure 5.21 shows resultant displacement due to impact loading.

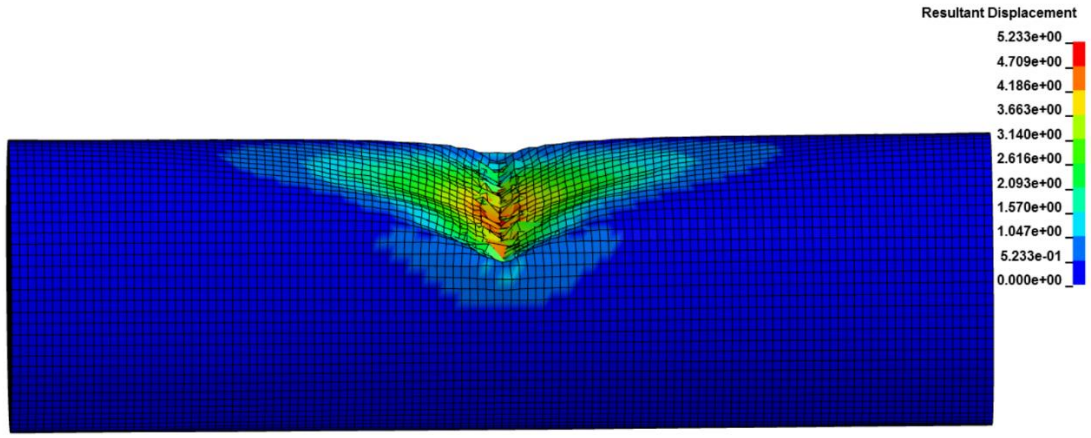

Figure 5.20: Resultant displacement due to quasi-static load

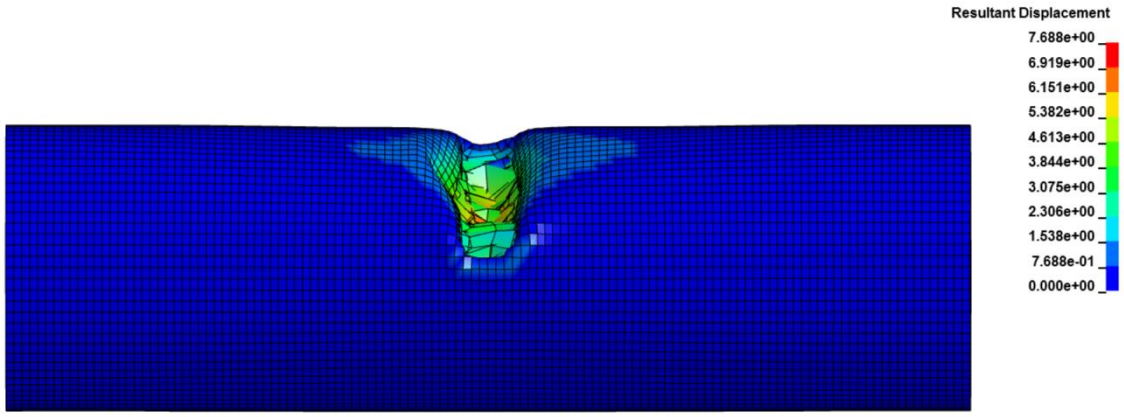

Figure 5.21: Resultant displacement due to impact load

As can be seen from figure 5.20, sideways buckling of steel casing is found but due to sharp edge cell fracture is at the point of contact of sharp edge. For impact load, cell experienced large deformation and fracture at the point of contact and layers were damaged. Temperature analysis due to quasi-static loading is discussed in the next section.

5.6.3.2 Temperature analysis

High temperatures after short circuit occurrence as shown in figure 5.22 are indicators of uncontrolled temperature, which can lead to thermal runaway. For three-point bend test simulation comparison of steel, anode current collector and cathode current collector layers are used to understand temperature distribution of cell for internal layers, where anode current collector and cathode current collector indicate first instance of short circuit. As mentioned by Doerffel, (2007) negative electrode has high thermal conductivity so the temperature change at anode current collector is high compared to cathode current collector.

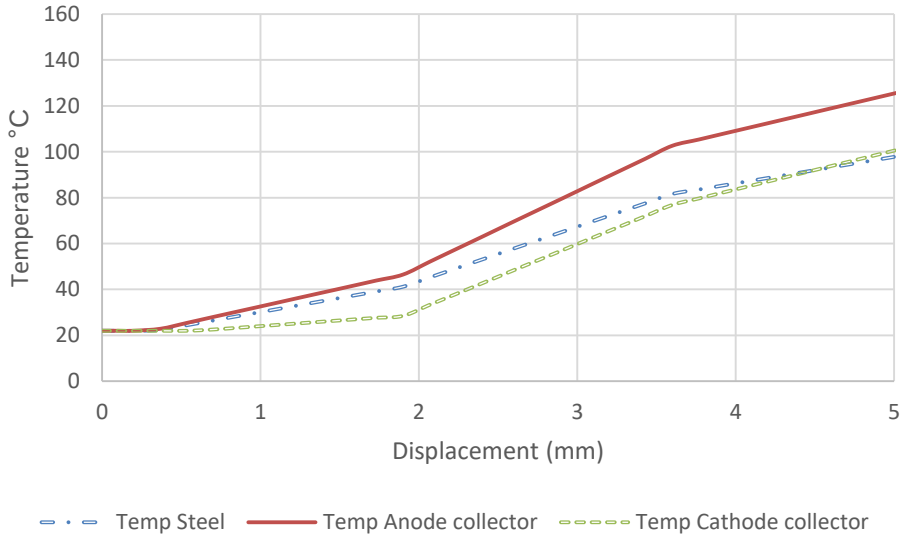

Figure 5.22: Temperature values for steel casing, anode current collector and cathode current collector

As can be seen from figure 5.22, temperature for steel and cathode current collector (aluminium) is around 100°C; however temperature for anode current

collector is around 130°C at the time of short circuit occurrence. Temperature variations at steel casing was observed and shown in figure 5.23.

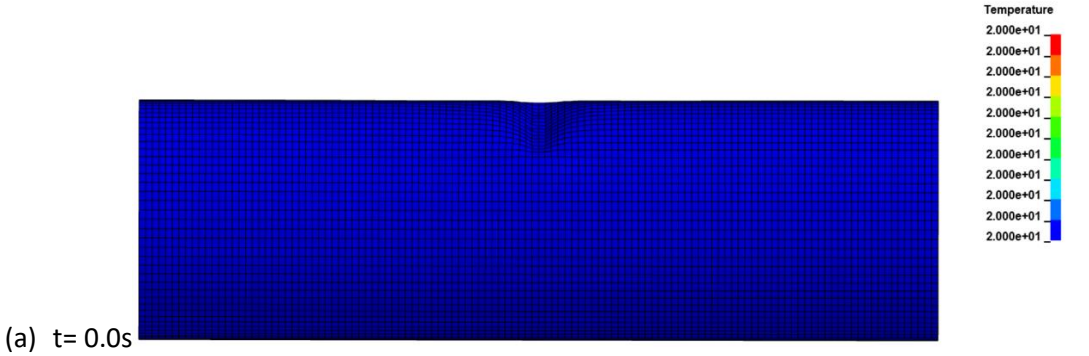

(a) t= 0.0s

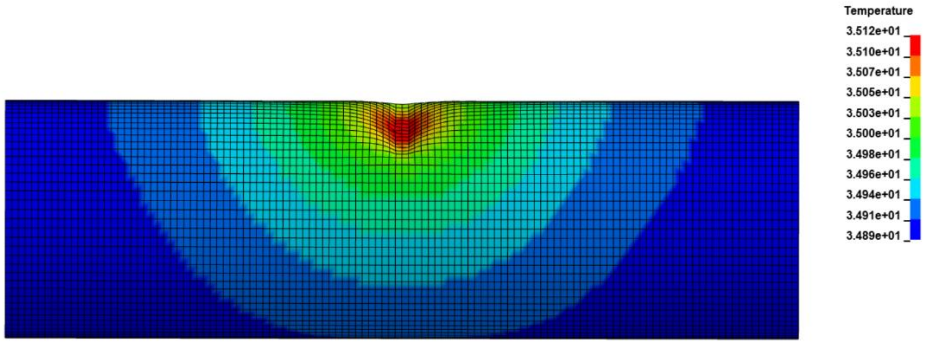

(b) t=0.001s

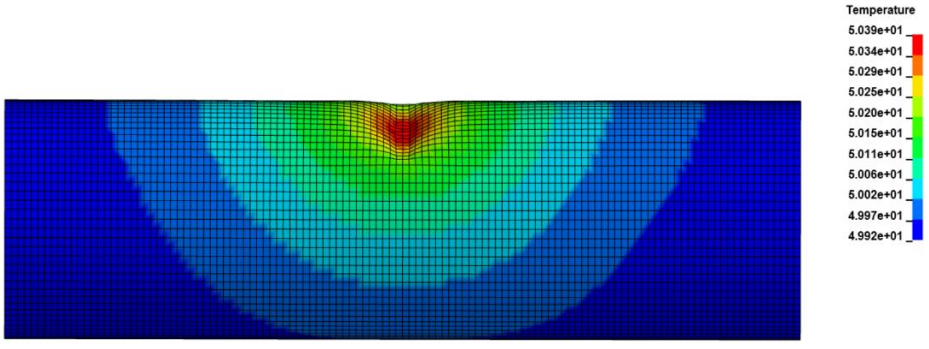

(c) t=0.003s

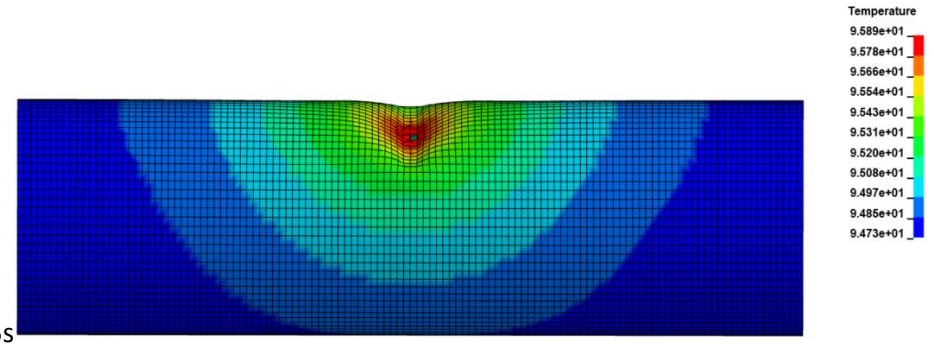

(d) t= 0.005s

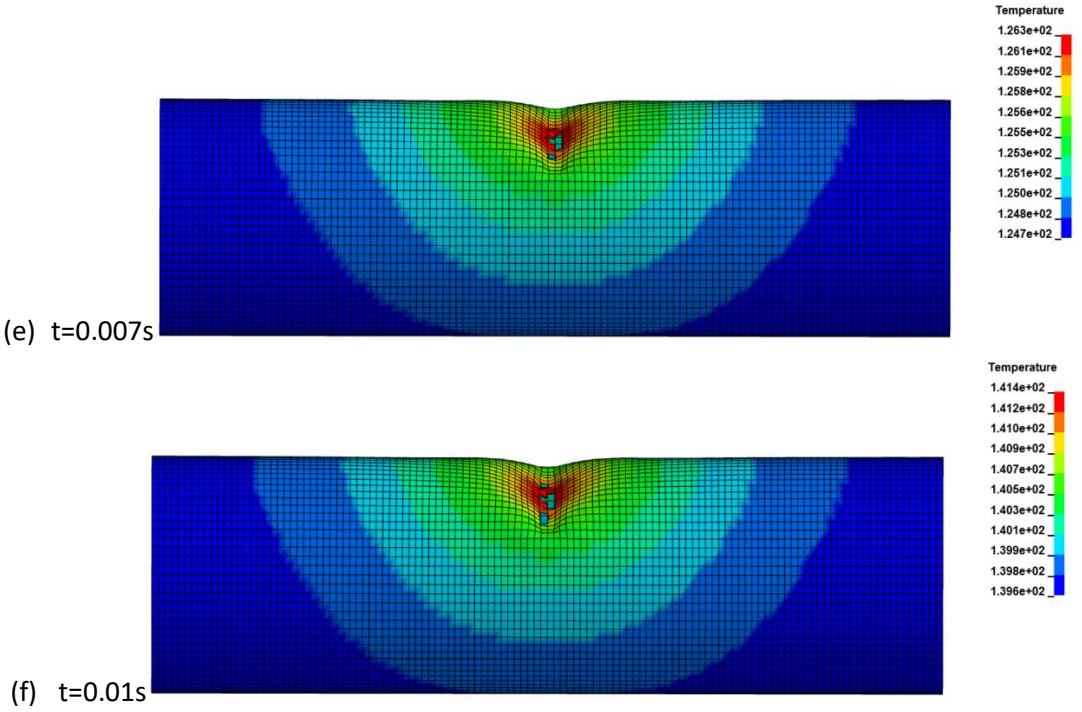

Figure 5.23: Sequence of temperature variations due to fracture for three-point bend test simulation

As can be seen from figure 5.23, temperature variations for steel casing due to impact varies with displacement and values are around 80°C before fracture of steel layer. Once the layer attains fracture then short circuit occurs with immediate change in temperature and maximum temperature was observed on the top of the cell at the point of impact. Highest temperature observed was 141°C. Further failure analysis was observed with separator layer failure.

5.6.3.3 Separator failure analysis

Three-point bend test short circuit failure was further analysed using separator failure criteria, where all separator layers were examined for their temperature variations and used to find the sequential effects of battery degradation and possible thermal runaway event. First separator layer temperature variations are shown in figure 5.24.

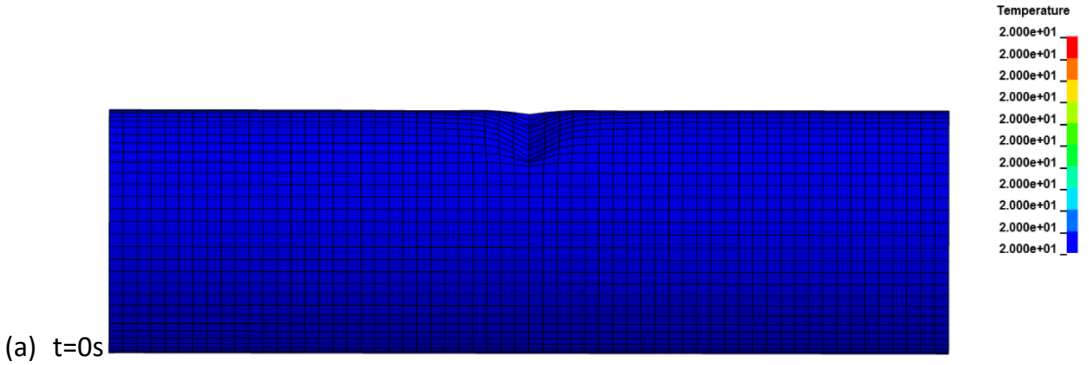

(a) t=0s

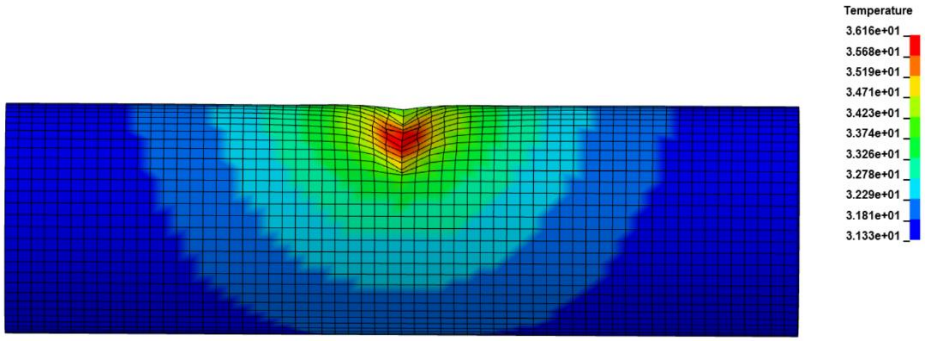

(b) t=0.002s

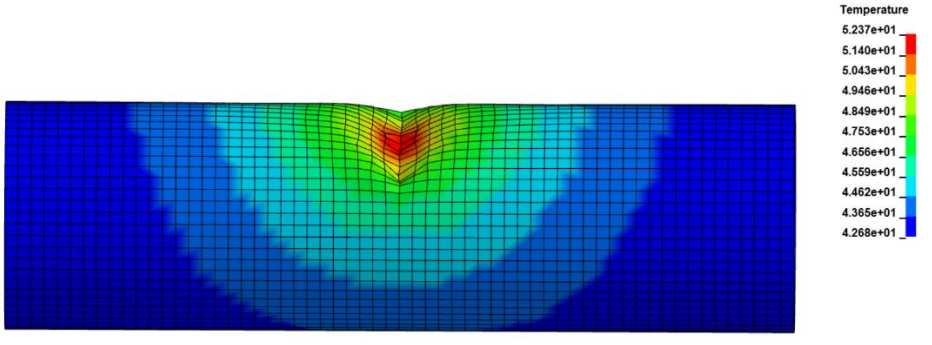

(c) t=0.003s

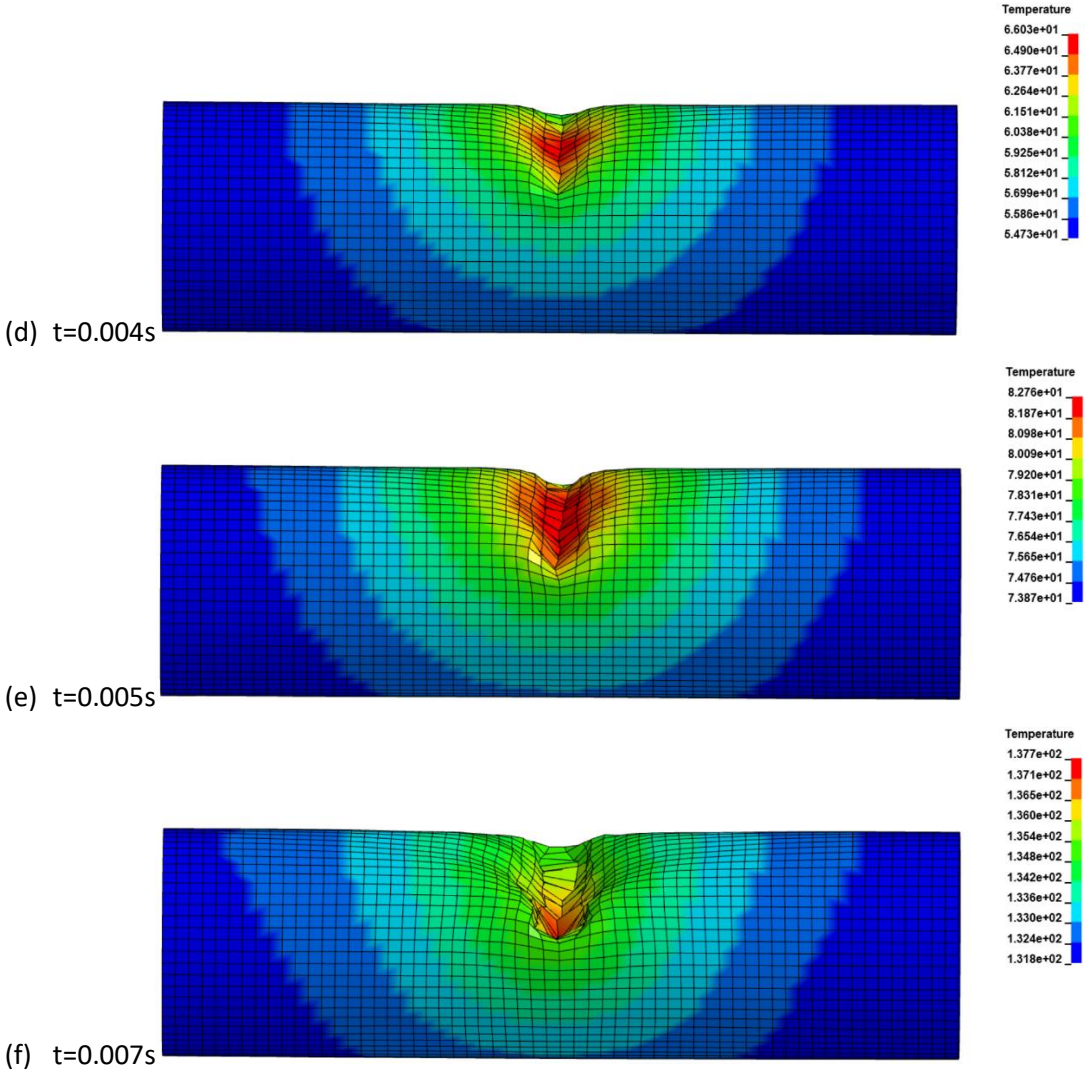

Figure 5.24: Three point bend simulation, temperature variations at the first separator layer

The top surface of separator layer 1, is shown for deformation and temperature variation with location. For separator layer 1, sideways deflection and temperature variation is shown in figure 5.24. Due to sharp edge cell damage occurs relatively early compared to other loading cases, which sequentially damage layers in the cell. Due to both tension and compression separator layer

with low mechanical strength develops brittle fracture, which occurs immediately after steel casing fracture and temperature increase drastically as shown in experiment work and this simulation model. Layers behaviour due to applied force is provided in figure 5.25.

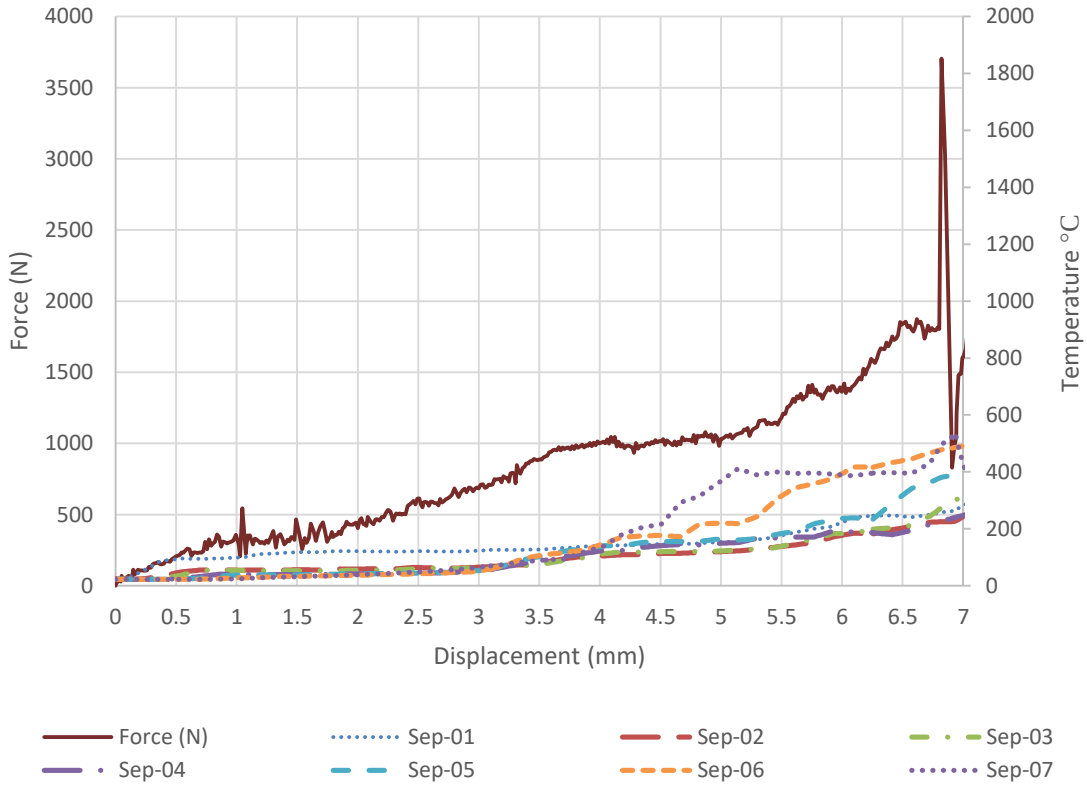

Figure 5.25: Three-point bend test simulation, separator layers behavior with applied force, displacement and temperature variations

Simulation model results show good accuracy within the cell comparison. As the only separators have the lower melting point in lithium-ion battery construction, it can melt at around 144°C (Zhang, *et al*., 2015b), so separator failure will occur earlier compared to other layers failure which have comparatively high temperatures. This separator failure is also an indication of short circuit as

contact between electrodes is established once separator layers melt. High temperature at separator layer can cause complete failure and possible thermal runaway. As shown in figure 5.25, force attains the same peak value as documented in the previous chapters for three-point bend, however sudden drop in force at around 7mm shows the point of short circuit occurrence. Temperatures of all layers started to increase after short circuit and the last separator layer which is sep-07 experiences temperature drop, which is stabilising zone or short circuit propagation. Once the thermal runaway occurred temperature started to increase in an uncontrolled manner, and temperature of all layers were around 300°C except sep-05 to sep-07 which attain temperatures of around 500°C for a short instance of time. Sep-07 layer experienced high compression and tension due to three-point bend as forces from all other layers and indenter were applied at this layer, where layer shrink and element deletion take place. Separator analysis with high-temperature variations can be used as an indicator of cell failure, which is evident from the literature but FEA of the cell for this analysis is not found in detail.

5.6.4 2 Flat plate test simulation

5.6.4.1 Structural analysis

The simulation model is used to conduct the structural analysis of flat plate deformation, where results are compared with the experimental study as shown in figure 5.26.

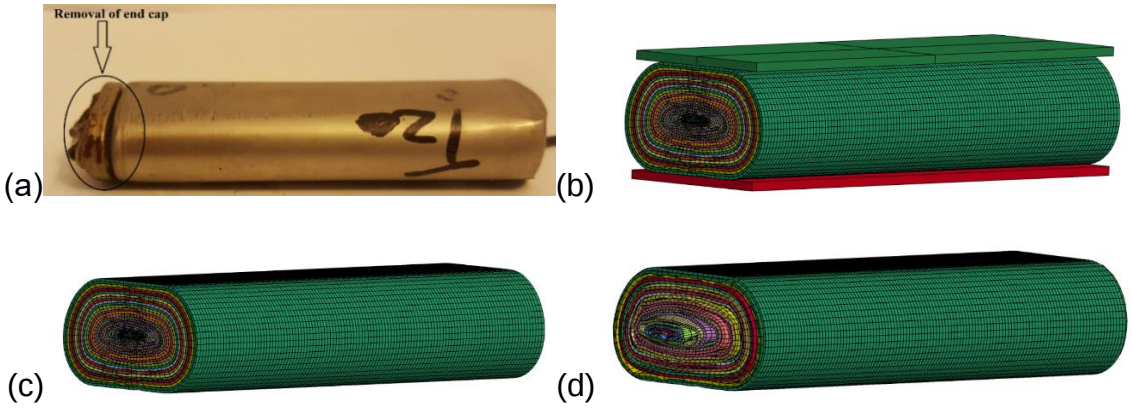

Figure 5.26: Deformed cells and simulation model, (a) Flat plate test, (b) Flat plate simulation,(c) Quasi-static loading, (d) Impact loading

Both experimental and simulation results showed identical deformation behaviour as shown in figure 5.26. Cell layers ejection can be seen in simulation model. Similar to all other simulation models, in flat plate simulation results were compared with 0% SOC experiment results. In the experimental test, short circuit displacement (d_{sf0}) was 5.5mm and short circuit stress or tensile strength was 44.49 MPa; however, force drops at 5mm in this simulation model which indicates the short circuit. Deformed geometry model exhibits layers with dense displacement behaviour at the area of the endcap, which

shows high-stress values at that point. Displacement of flat plate simulation model which is close to experimental model shows, for flat plate compression, less displacement occurs, and high force is required. This phenomenon is also explained in the experimental section where at low SOCs short circuit was slow to build and voltage drop to zero, took a long period. The contours of 1st and 2nd principal stresses are shown in figure 5.27.

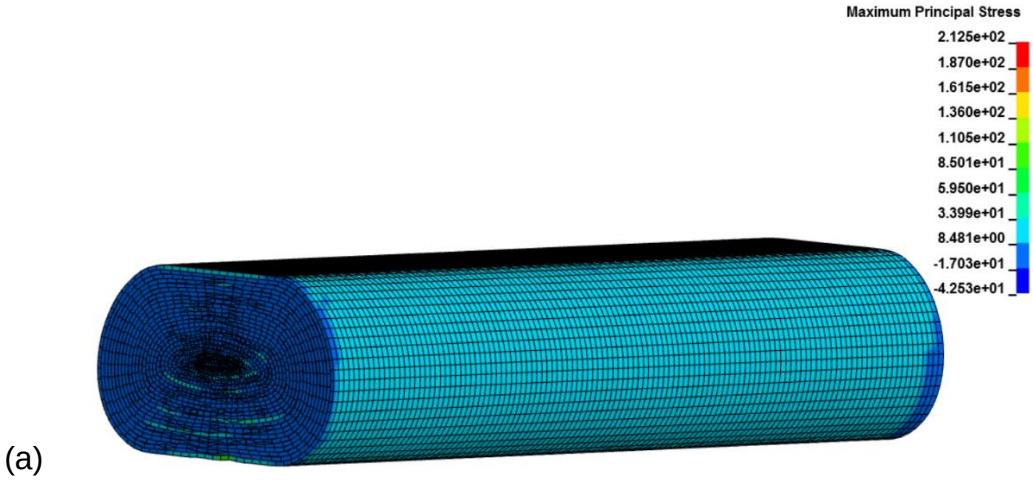

(a)

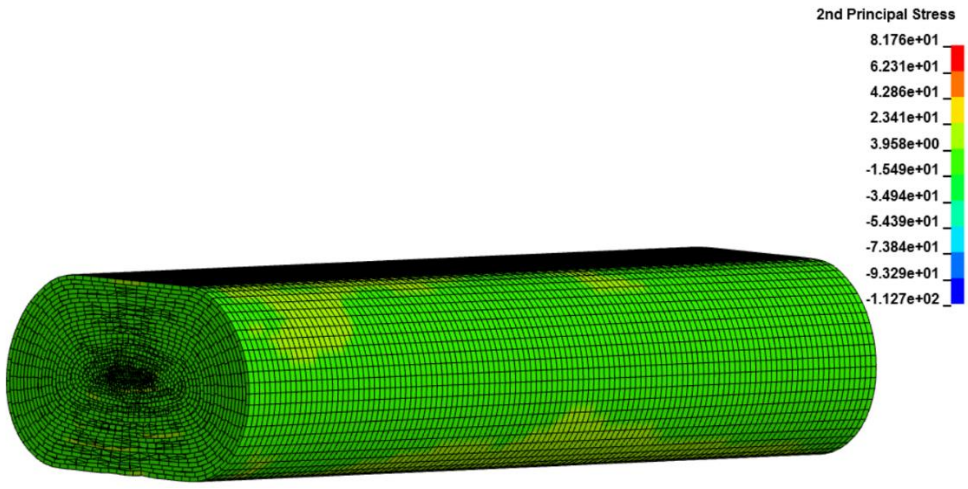

(b)

Figure 5.27: (a) 1st principlal stress for flat plate deformation simulation, (b) 2nd principal stress for flat plate deformation simulation

Both 1st and 2nd principal stress contours show good correlation with the experimental work. Stress values at the point of compression which are at the top of the layer are close to the experimental result. 2nd principle stress contour shows that these values were well within the range of experimental work where maximum stress was exerted at the bottom of the cell.

Resultant displacement at the point of short circuit show good correlation with experiemntal work and results are within 20% but for impact load despite short circuit occurrence analysis was run to understand deformation pattern. Figure 5.28, shows resultant displacement at the point of short circuit due to quasi-static loading and figure 5.29, shows resultant displacement due to impact load where delamination is also evident.

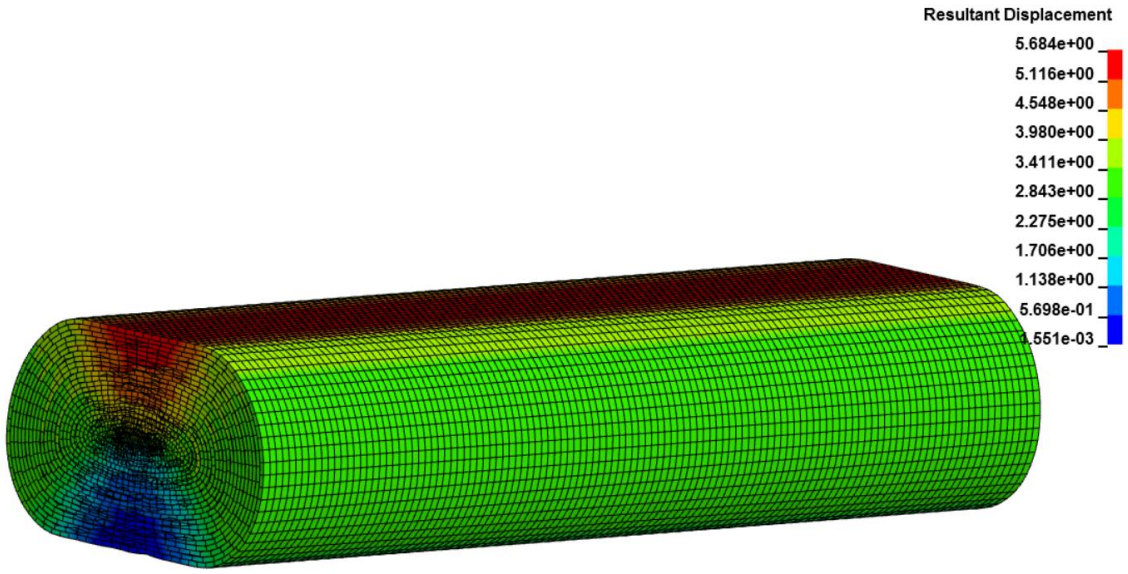

Figure 5.28: Resultant displacement for flat plate due to quasi-static load

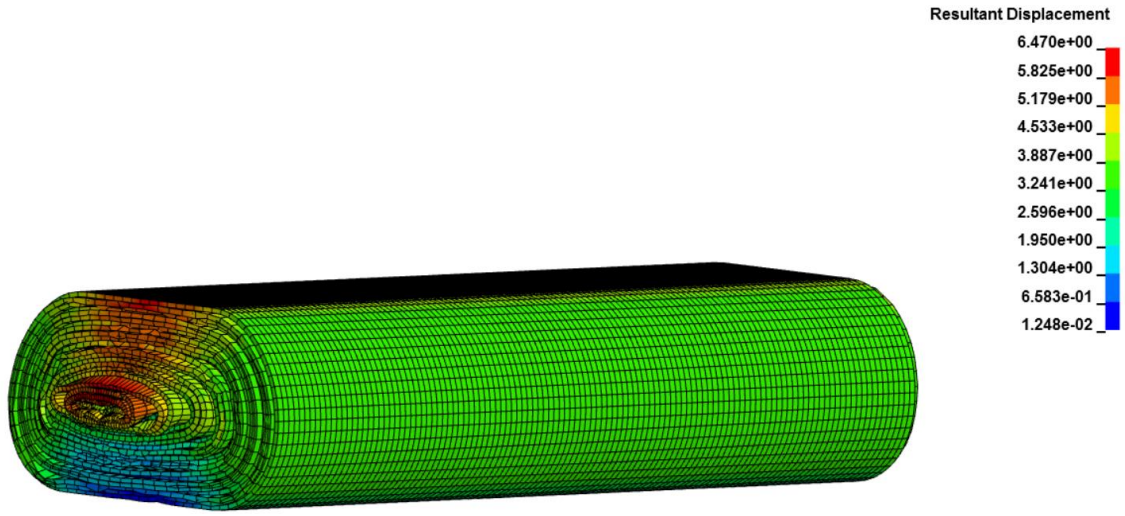

Figure 5.29: Resultant displacement for flat plate due to impact load

Delamination of layers was observed at impact loads, where simulation was run until complete failure of cell.

5.6.4.2 Temperature analysis

For flat plate simulation, it was observed when the quasi-static load is applied, that cell temperature increased slowly during compression at the mid-surface, and maximum temperature was lower than the temperature observed during the experiment. When the impact load was applied, cell temperature gradually increased and reached 170°C for mid surface and bottom surface and 250°C for top surface which is steel casing. Temperature variations for impact loading and quasi-static loading are shown in figures 5.30 and 5.31 respectively.

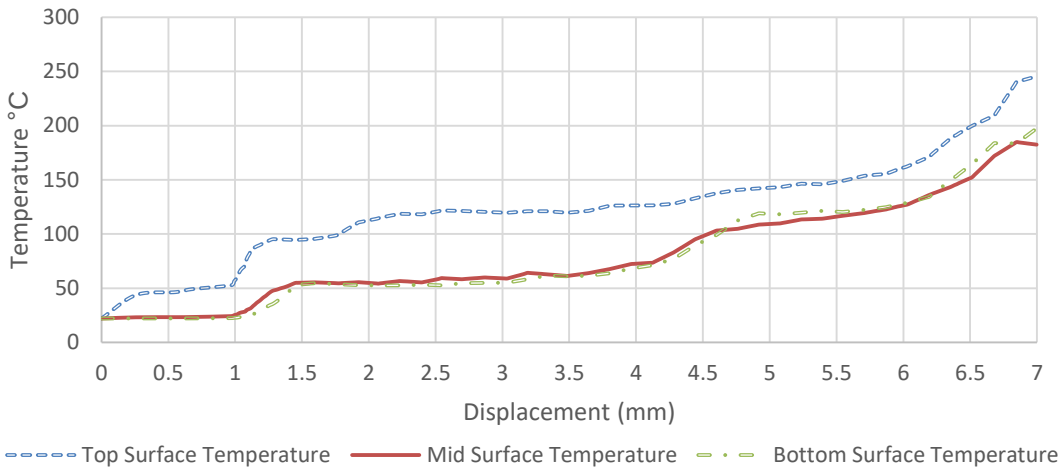

Figure 5.30: Flat plate surface temperature, impact simulation

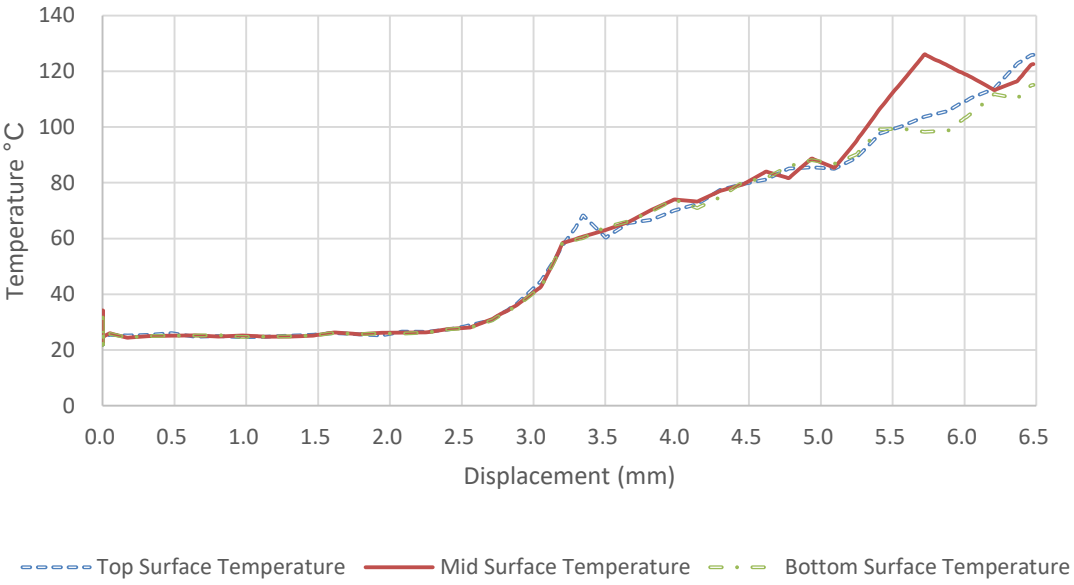

Figure 5.31: Flat plate surface temperature, quasi-static load

As can be seen from figure 5.31, due to quasi-static loading, cell exhibits values around 120°C at the time of short circuit displacement which is close to the value of experiment work and validates experimental result for flat plate

deformation at 0% SOC. Temperature variations for flat plate deformation vary at the top and bottom surfaces of the steel casing. This is shown in figure 5.32.

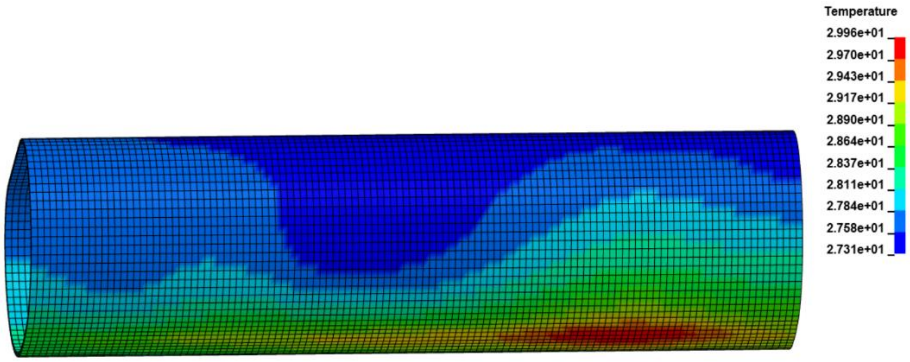

(a) t=0.001s

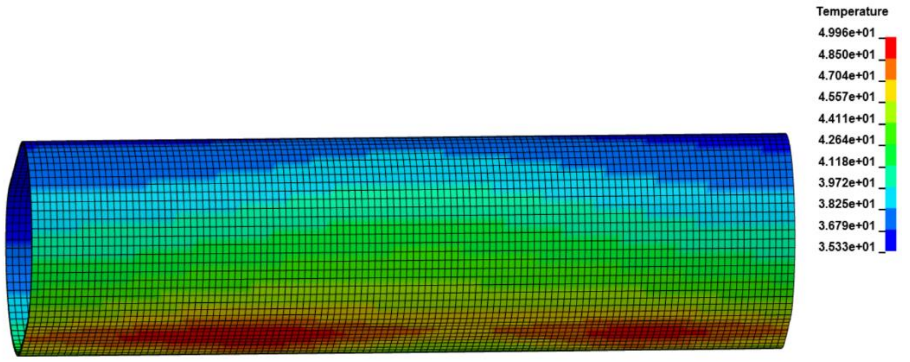

(b) t= 0.002s

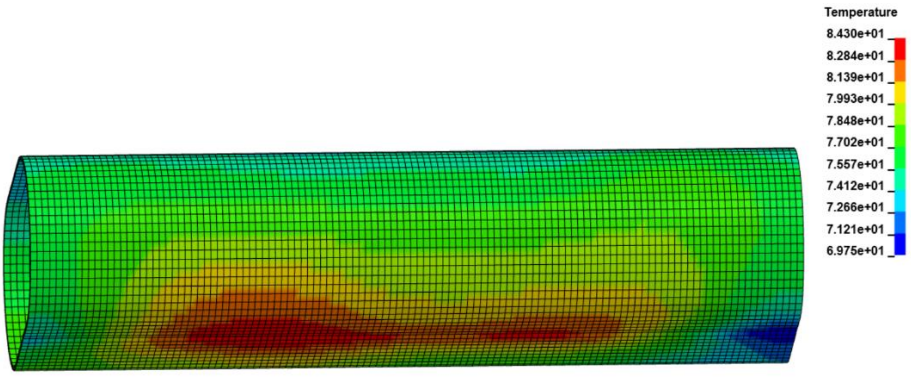

(c) t=0.005s

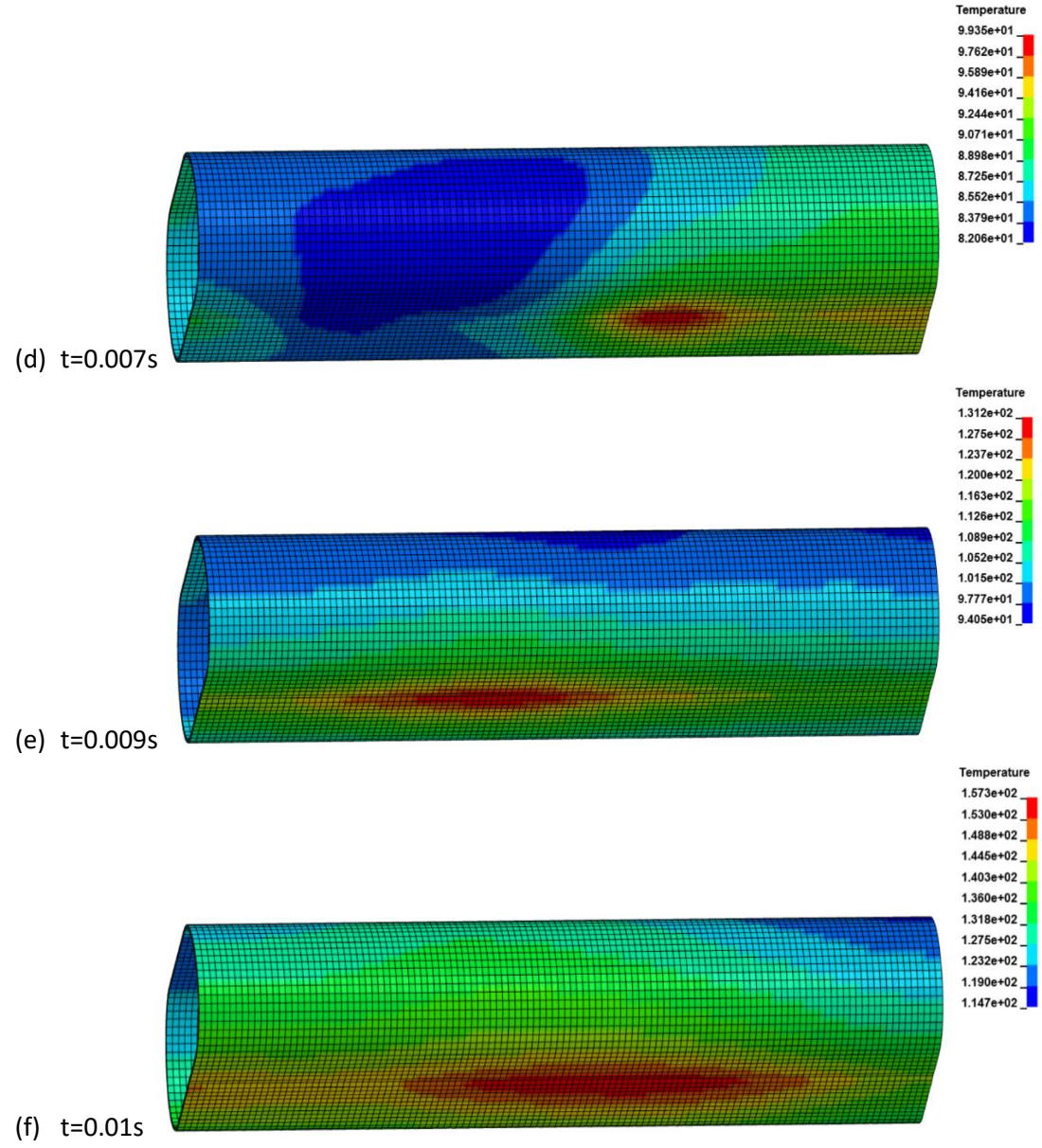

Figure 5.32: Steel casing temperature variations for flat plate simulation at quasi-static loading condition

As can be seen from figure 5.32, temperature distribution varies with the location of the steel casing and at the bottom surface temperature distribution is high compared to the top of the cell. Similar phenomenon was observed for

complete cell model. Full cell temperatures are slightly higher compared to steel housing, which shows the effect of other cell layers.

5.7 Conclusions of numerical simulation analysis

To validate experimental work, numerical simulation approach using LS-DYNA numerical simulation tool was used where focus was given to structural deformation and temperature variations due to loading conditions. To better understand cylindrical lithium-ion battery failure pattern and possible thermal runaway, quasi-static and impact loading conditions were used. Single cell model using LS-DYNA numerical simulation tool was useful for battery FEA analysis which can be further expanded for battery module and battery pack simulation where element type, element size, material properties, parameters, boundary conditions and contact cards played important roles.

In the quasi-static loading, short circuit displacement was within 20% of experimental work, whereas due to impact load large displacement values were observed. Temperature variations and displacement at which temperature suddenly increased were compared for both quasi-static and impact load. High temperatures due to impact load were observed which are due to large deformation of battery.

Separator layer temperatures were simulated for circular punch and three-point bend models, where temperature variations above melting temperatures indicated layer failure. Uncontrolled temperatures at various separator layers were indications of thermal runaway, however complete cell model with

electrochemistry and terminals will be useful to further investigate occurrence of thermal runaway.

Comparison of quasi-static and impact loading conditions showed that in the case of quasi-static loading sequential failures were useful to predict short circuit or possible thermal runaway. Due, however, to the nature of impact load it was difficult to characterize failure in detail.

5.8 Summary

Simulation results showed better approximation with the experimental results where deformed geometry and temperature variations are given. Simulation models discussed in this chapter tie the experimental work by using important parameters obtained form experiments. Values obtained in this simulation work is the result of 0% SOC, as cell electrochemistry and electrical components are not considered for current work but structural analysis was conducted. As can be seen from experimental work and simulation results, a concentric layered model with solid element formulation can be used for simulation of individual layers, where contact between layers and boundary conditions needs to be as accurate as possible. Temperature distribution for each case gives an insight on how layers are affected in case of different loading conditions. Deformation behaviour at various instances is a prime objective to introduce a concentric layered model, which can be further used for more refined layer formation. Propagation of separator failures leading to cell failure were discussed in detail, circular punch and three-point bend test simulation models were used to

understand separator layer failures, where these two simulation models showed temperature variation with respect to applied force and displacement. This criterion is useful to carry out failure analysis where failure displacement and applied force are used. Sequential failure also indicates an uncontrolled distribution of temperature which is an important determinant of thermal runaway detection in the case of abuse conditions.

Chapter 6: Conclusions and Future Recommendations

6.1 Conclusions

In the current research aims and objectives discussed in the introduction chapter have been achieved, where the main objective of this research is to challenge the mechanical integrity of lithium-ion batteries for thermal runaway detection. Battery failure analysis is carried out where the set of experiments are designed to conduct this analysis. Lack of research on SOC dependent failures of lithium-ion 18650 batteries provided the opportunity to investigate this in detail.

Location and intensity of short circuit, time for initial and complete failure of cells and structural deformation are considered in great detail, where modified test protocols which are evident from literature for detailed battery analysis are used. Temperature analysis using infrared camera and thermocouples, which was captured for the complete test data, was used. Results obtained showed SOC dependency on failure pattern, where with different test protocols this dependency varies. SOC dependency on thermal runaway is also evident from Liu, *et al*. (2017). Many indicators for the occurrence of cell failures were observed which are, force drop at the time of short circuit, temperature increase, temperature change rate, displacement and sudden voltage drop. Temperature values found by Sahraei, *et al*. (2012a) were between 40°C and 50°C at the point of short circuit occurrence, there are multiple factors for this difference from current research where temperature raised to nearly 100°C or

above. One of the reason is the initial SOC which was 10% in (Sahraei, *et al*. 2012a), however in current research SOC varies and results are explained accordingly.

Thermal runaway occurrence was observed with temperature and voltage variations, where testing was stopped immediately after the first instance of short circuit. Sequential failures of battery following short circuit leading to thermal runaway was observed, where high-temperature variations were observed for the test with high SOCs. Due to a sharp edge, three-point bend caused fracture of the cell. Structural analysis was carried out where nominal stress-strain behaviour was studied and implemented. Failure stress and failure strain at the point of the short circuit were calculated. Parameters investigated in the experimental work including displacement, cut-off stress, failure strain and force were used for the simulation model.

Numerical simulation model consisting of concentric layered model evident from Siva, *et al*. (2015) for cylindrical 18650 lithium-ion battery was used. Concentric layered numerical simulation model was not found in the literature which was new and developed using solid elements in LS-DYNA. One of the big advantages of using a concentric layered model is that layers are independent of each other which is useful for amendments or changes to one or more layers in the stack. Secondly, layer thicknesses can be changed to do more analysis without much change in the model. Starting with a layered model of the single battery stack, a complete cell model of 18650 cells was designed using LS-DYNA simulation tool.

As evident from results shown in previous chapter, the simulation model was capable of capturing cell mechanical and thermal responses, where cell electrochemistry and endcaps were not considered. Cell behaviour without endcap due to compression loading was tested by Sahraei, *et al*. (2012a), so for this research, a simulation model assuming no endcaps was used, where the primary objective was to model a single cell with maximum layers, which could be used for structural deformation behaviour and thermal response due to deformation and extendable to multiple cells in the module.

Results obtained from simulation models correlated with experimental tests, where significant improvement was observed including a number of elements and short circuit failure criteria. To improve simulation results, additional failure criteria including temperature variations and separator layer failures were implemented in this research.

Separator failures were analysed using simulation model, where at maximum displacement separator temperature increased significantly and dropped in force was observed which was also documented in the literature that, at the time of short circuit force drop, due to the internal stiffness of layers and temperature startded to increase, but high temperatures which were uncontrolled lead to thermal runaway. Another significant finding from separator layer analysis is the high-temperature locations. As from Zhang, *et al*., 2016; Zhang, *et al*., 2015b, separator failure occurs well in advance for short circuit, three-point bend test which has immediate short circuit response and circular punch test where a slow build-up of short circuit is evident from experimental

work were further analysed for separator layer failure analysis using simulation model.

Failure response of separators is in agreement with the experimental work where in circular punch, failure of layers took place at the bottom of the cell, which was due to a compression force and for three-point bend, all separator layers showed high temperatures and change in shape.

Comparison of quasi-static and impact loading are used to understand sequential failures of battery structure and temperature variations, where it was evident form simulation results that quasi-static loading was suitable to predict short circuit and possible thermal runaway. Due to impact loading it was difficult to characterise battery failure as sudden structural and temperature changes were evident from this analysis.

It can be concluded that proposed mechanical testing method was suitable for battery testing for thermal runaway detection where various criteria were used to detect early signs of thermal runaway. Numerical simulation model incorporating more layers compared to available literature was suitable choice when failure effects were investigated for every single layer in the model. Thermal runaway process varied with SOC and type of loading, where initial voltage drop and temperature rise at the time of loading were useful to predict battery behaviour. Sequential layer failure was observed in numerical simulation model where different temperature values and failure patterns were observed. Separator failure may occur well in advance of other failures investigated and

found to be correct in this research where all layers had high temperatures due to loading. Simulation models can be used for analysis of the structural and thermal behaviour of 18650 cells where electrochemistry of cell can be used to enhance these results and predictions.

6.2 Future recommendations

Based on the findings in this research where several techniques were used to investigate cylindrical lithium-ion cells for their mechanical failure behaviour and possible thermal runaway, improvements could be made in future studies by considering following recommendations.

1. Microscale testing can be used where individual layer properties are taken into account for crash analysis.

2. Improved loading conditions can be used where both quasi-static and dynamic loading scenarios can be used to challenge battery mechanical integrity for experimental and post-impact analysis.

3. The analysis should be widened to include internal resistance impact on battery failure, where this failure can be in the form of heat generation and temperature change.

4. A mathematical model representing sequential failures can be used for detailed investigation.

5. Thermocouples can be implanted inside the cell between cell casing and jellyroll to observe temperature between jellyroll and skin; however, this temperature location should be clearly mentioned.

6. Cell electrochemistry is not considered for simulation in this research which should be considered with maximum possible parameters.

7. Implementation of the concentric model for simulation is useful where battery failure response is investigated, but following improvements can be made to this model.

    a. Layer thickness should be as accurate as possible to match real-time cell properties

    b. More in-depth analysis using local failures should be considered

    c. Endcaps of the cell should be included, to better represent cell model

    d. Simulation time should be larger; however, computation efficiency should be considered in this regard

    e. More layers should be involved to set failure criteria, but these criteria should be in accordance with the experimental work and available research.

References

Abraham, D.P., Furczon, M.M., Kang, S.H., Dees, D.W., Jansen, A.N., 2008. “Effect of Electrolyte Composition on Initial Cycling and Impedance Characteristics of Lithium-Ion Cells”. *Journal of Power Sources*, 180(1), pp.612-620.

Abraham, D.P., Roth, E.P., Kostecki, R., McCarthy, K., MacLaren, S., Doughty, D.H., 2006. “Diagnostic Examination of Thermally Abused High-Power Lithium-Ion Cells”. *Journal of Power Sources*, 161, pp. 648-657.

Al-Hallaj, S., Kizilel, R., Lateef, A., Sabbah, R., Farid, M., Selman, J.R., 2005. “Passive Thermal Management Using Phase Change Material (PCM) for EV and HEV Li-ion Batteries”. *Proceedings of IEEE, Vehicle Power and Propulsion, (VPPC’ 2005) Conference*, 7 September 2005, Chicago, IL, USA.

Al-Hallaj, S., Maleki, H., Hong, J.S., Selman, J.R., 1999. “Thermal Modeling and Design Considerations of Lithium-Ion”. *Journal of Power Sources*, 83, 1–2, pp. 1-8.

Albright, G., Al-Hallaj, S., 2012. “Making Lithium-ion Safe through Thermal Management”.

http://www.battcon.com/PapersFinal2012/Greg%20Albright%20-%20Making%20Lithiumion%20safe%20through%20thermal%20management.pdf. (Accessed on 13/06/2014).

Bai, Y., Teng, X., Wierzbicki, T., 2009. "On the Application of Stress Triaxiality Formula for Plane Strain Fracture Testing". *Journal of Engineering Materials and technology*, 131(2), pp. 021002-1 to 021002-10.

Bai, Y., Wierzbicki, T., 2008. "Forming Severity Concept for Predicting Sheet Necking under Complex Loading Histories". *International Journal of Mechanical Sciences*, 50(6) 1012-1022.

Bandhauer, T.M., Garimella, S., Fuller, T.F., 2011. "A Critical Review of Thermal Issues in Lithium-Ion Batteries". *Journal of the Electrochemical Society*, 158, pp. R1–R25.

Battery University, 2014. "Safety of Lithium-ion batteries". *http://batteryuniversity.com/learn/article/safety_of_lithium_ion_batteries*. (Accessed on 14/06/2014).

Battery University, 2017. "Comparison of Lithium-ion batteries for EV applications". *http://batteryuniversity.com/learn/article/types_of_lithium_ion*. (Accessed on 18/04/2017)

Bazinski, S. J., and Wang, X., 2015. “Experimental Study on the Influence of Temperature and State-of-Charge on the Thermophysical Properties of an LFP Pouch Cell”. *Journal of Power Sources*, 293, pp. 283–291.

Bernardi, D., Pawlikowski, E., Newman, J., 1985. “A General Energy Balance for Battery Systems”. *Journal of the Electrochemical Society*, 132, 1, pp: 5-12.

Bowkett, M., Thanapalan, K., Stockley, T., Hathway, M., Williams, J., 2013. “Design and Implementation of an Optimal Battery Management System for Hybrid Electric Vehicles”. *Proceedings of IEEE, 19th International Conference on Automation and Computing (ICAC)*, 2013, London UK.

Braun, P.V., Cho, J., Pikul, J.H., King, W.P., Zhang, H., 2012. “High Power Rechargeable Batteries”. *Current Opinion in Solid State and Materials Science*, 16, pp. 186–198.

Budde-Meiwes, H., Drillkens, J., Lunz, B., Muennix, J., Rothgang, S., Kowal, J., Sauer, D.U., 2013. “A review of current automotive battery technology and future prospects”. *Proceedings of the Institution of Mechanical Engineers, Part D: Journal of Automobile Engineering*, 227, 5, pp. 761 – 776.

Cai, L., White, R.E., 2011. “Mathematical Modeling of a Lithium Ion Battery with Thermal Effects in COMSOL Inc. Multiphysics (MP) software”. *Journal of Power Sources*, 196, 14, pp. 5985-5989.

Cai, C.H., Du, D., Liu, Z.Y., Zhang H., 2002. “Modeling and Identification of Ni-MH Battery using Dynamic Neural Network”. *Proceedings of IEEE. International Conference on Machine Learning and Cybernetics*, pp. 1594–1600, 4-5 November. 2002 Beijing, China.

Cannarella, J., Liu, X., Leng, C.Z., Sinko, P.D., Gor, G.Y., Arnold, C.B., 2014. “Mechanical Properties of a Battery Separator under Compression and Tension”. *Journal of the Electrochemical Society*, 161, pp. F3117-F3122.

Cao, J., Schofield N., Emadi, A., 2008. “Battery balancing methods: A comprehensive review”. *Proceedings of IEEE, 4th IEEE Vehicle Power and Propulsion Conference (VPPC’08)*, pp.1-6, 3-5 September, 2008, Harbin, China.

Chanson, C., Wiaux, J.P., 2013. “Safety of Lithium Batteries. RECHARGE”. *The European Association for Advanced Rechargeable Batteries*, June 2013.

Chen, Y., Evans, J.W., 1996. “Thermal analysis of Lithium-Ion batteries”. *Journal of Electrochemical Society*, 143, pp. 2708–2712.

Chen, X. H., Wang, Y., Gong, M. & Xia, Y. M., 2004. “Dynamic Behavior of SUS304 Stainless Steel at Elevated Temperatures”. *Journal of Materials Science,* 39, pp. 4869–4875.

Cheng, L., Ke, C., Fengchun, S., Peng, T., Hongwei Z., 2009. “Research on Thermo-Physical Properties Identification Analysis of EV Li-Ion Battery”. *Proceedings of IEEE, Vehicle Power and Propulsion Conference, VPPC '09*. 7-10 Sept. 2009, Dearborn, MI, USA, pp. 1643-1648.

Cho, S., Jeong, H., Han, C., Jin, S., Lim, J.H., Oh, J., 2012. “State of Charge Estimation for Lithium-ion Batteries under Various Operating Conditions Using an Equivalent Circuit Model”. *Computers & Chemical Engineering*, 41. pp. 1–9.

Croop B., and Lobo, H., 2009. “Selecting Material Models for the Simulation of Foams in LS-DYNA”. *7th European LS-DYNA Conference, 2009*. DYNAmore GmbH.

Dawod, M., Omar, N., Bossche, P., Mierlo, L., 2011. “Passive and Active Battery Balancing Comparison based on MATLAB Simulation”. *Proceedings of IEEE, 7th IEEE Vehicle power and propulsion Conference, VPPC’11*, 6-9 September, 2011, Chicago, IL, USA.

Doerffel, D., 2007. “Testing and Characterisation of Large High-Energy Lithium-Ion Batteries for Electric and Hybrid Electric Vehicles (Ph.D thesis)”. *Southampton University, UK.*

Doughty, D., and Roth, E.P., 2012. “A General Discussion of Li-Ion Battery Safety”. *The Electrochemical Society Interface*, summer 2012, pp.37-44.

Doyle, M., Fuller, T.F., Newman, J., 1993. “Modeling of Galvanostatic Charge and Discharge of the Lithium/Polymer/Insertion Cell”. *Journal of Electrochemical Society*, 140, 6, pp. 1526-1533.

Drake, S. J., Martin, M., Wetz, D. A., Ostanek, J. K., Miller, S. P., Heinzel, J. M., Jain, A., 2015. “Heat Generation Rate Measurement in a Li-Ion Cell at Large C-Rates through Temperature and Heat Flux Measurements”. *Journal of Power Sources*, 285, pp. 266–273.

Dubarry, M., Liaw, B.Y., Chyan, S.S., Han, K.C., Sie, W.T., Wu,S.H., 2011. “Identifying Battery Aging Mechanisms in Large Format Li ion Cells”. *Journal of Power Sources*, 196, pp. 3420-3425.

Escobar-Hernandez, H.U., Gustafsona, R.M., Papadakib,M.I., Sachdevaa, S., Mannan, M.S., 2016. “Thermal Runaway in Lithium-Ion Batteries: Incidents, Kinetics of the Runaway and Assessment of Factors Affecting Its Initiation”. *Journal of the Electrochemical Society*, 163, 13, pp. A2691-A2701.

Feng, X., Sun, J., Ouyang, M., Wang, F., He, H., Lu, B., Peng, H., 2015. "Characterization of Penetration Induced Thermal Runaway Propagation Process within a Large Format Lithium Ion Battery Module". *Journal of Power Sources*, 275, pp. 261-273.

Finegan, D.P., 2016. "X-ray Imaging of Failure and Degradation Mechanisms of Lithium-ion Batteries (Ph.D. Thesis)". *University College London, UK.*

Finegan, D. P., Scheel, M., Robinson, J. B., Tjaden, B., Hunt, I., Mason, T. J., Millichamp, J., Di Michiel, M., Offer, G. J., Hinds, G., Brett, D. J. L., Paul, R.S., 2015. "In-Operando High-Speed Tomography of Lithium-Ion Batteries during Thermal Runaway". *Nature Communication, 6:6924.*

Forgez, C., Do, D.V., Friedrich, G., Morcrette, M., Delacourt,C., 2010. "Thermal Modeling of a Cylindrical LiFePO4/Graphite Lithium-Ion Battery". *Journal of Power Sources*, 195, 9, pp. 2961-2968.

Gao, Z., Chin, C., Woo, W., Jia, J., 2017. "Integrated Equivalent Circuit and Thermal Model for Simulation of Temperature-Dependent LiFePO4 Battery in Actual Embedded Application". *Energies*, 10, 85.

Golubkov, A. W., Fuchs, D., Wagner, J., Wiltsche, H., Stangl, C., Fauler, G., Voitic, G., Thaler, A., Hacker, V., 2014. "Thermal-Runaway Experiments on Consumer Li-ion Batteries with Metal-Oxide and

Olivin-Type Cathodes". *Royal Society of Chemistry Advances*, 4, pp.3633-3642.

Gomez, J., Nelson, R., Kalu, E.E., Weatherspoon, M.H., Zheng, J.P., 2011. "Equivalent Circuit Model Parameters of a High-Power Li-Ion Battery: Thermal and State of Charge Effects". *Journal of Power Sources*, 196, pp. 4826–4831.

Grandjean, T., McGordon, A., Jennings, P., 2017. "Structural Identifiability of Equivalent Circuit Models for Li-Ion Batteries". *Energies*, 10, 90.

Gu, W.B., Wang C.Y., 2000. "Thermal-Electrochemical Modeling of Battery Systems". *Journal of the Electrochemical Society*, 147, 8, pp. 2910-2922.

Guirong, Z., Henghai, Z., 2012. "Research of the Electric Vehicle Safety". *Proceedings of IEEE, World Automation Congress (WAC)*, 2012, pp. 1 – 4, 24-28 June 2012, Puerto Vallarta, Mexico.

Guo, G., Long, B.,Cheng, B., Zhou, S., Xu, P., Cao, B., 2010. "Three-Dimensional Thermal Finite Element Modelling of Lithium-Ion Battery in Thermal Abuse Condition". *Journal of Power Sources*, 195, pp. 2393-2398.

Guo, R., Lu, L., Ouyang, M., Feng, X., 2016. "Mechanism of the Entire Overdischarge Process and Overdischarge Induced Internal Short Circuit in Lithium-Ion Batteries". *Scientific Reports, 6:30248*.

Guo, G., Long, B., Cheng, B., Zhou, S., Xu, P., Cao, B., 2010. “Three-Dimensional Thermal Finite Element Modeling of Lithium-Ion Battery in Thermal Abuse Application”. *Journal of Power sources*, 195, pp. 2393-2398.

Haruna, H., Itoh, S., Horiba, T., Seki, e., Kohno, K., 2011. “Large-Format Lithium-Ion Batteries for Electric Power Storage”. *Journal of Power Sources*, 196, pp. 7002-7005.

He, H., Xiong, R., Guo, H., Li, S., 2012. “Comparison Study on the Battery Models used for Energy Management of Batteries in Electric Vehicles”. *Energy Conversion and Management*, pp. 113–121.

He, H., Xiong, R., Fan, J., 2011. “Evaluation of Lithium-ion Battery Equivalent Circuit Models for State of Charge Estimation by an Experimental Approach”. *Journal of Energies*, 4, pp. 582-598.

Hooper, J.M., Marco, J., Chouchelamane, G.H., Lyness, C., Taylor, J., 2016. “Vibration Durability Testing of Nickel Cobalt Aluminium Oxide (NCA) Lithium-Ion 18650 Battery Cells”. *Energies*, 9(4), pp.281.

Hu, P., Jiang, Z., Qi, C., Guo, R., Han, X., An, W., 2011. “Front Crash simulation and design improvement of a pure electric vehicle”. *Proceedings of IEEE, International Conference on Electrical and Control Engineering (ICECE)*, 16-18 Sept. 2011 Yichang, China, pp. 1085 – 1088.

Hu, X., Li, S., Peng, H., 2012. “A Comparative Study of Equivalent Circuit Models for Li-Ion Batteries”. *Journal of Power sources*, 198, pp. 359-367.

Hussein, A., 2015. “Derivation and Comparison of Open-loop and Closed-loop Neural Network Battery State-of-Charge Estimators”. *Energy Procedia*, 75, pp. 1856-1861.

Ishikawa, H., Mendoza, O., Sone, Y., Umeda, M., 2012. “Study of Thermal Deterioration of Lithium-Ion Secondary Cell using an Accelerated Rate Calorimeter (ARC) and AC Impedance Method”. *Journal of Power Sources*, 198, pp. 236-242.

Jarrett, A., and Kim, I. Y., 2011. “Design Optimization of Electric Vehicle Battery Cooling Plates for Thermal Performance”. *Journal of Power Sources*, 196(23), pp. 10359–10368.

Jasinski, L., 1974. “Rapid Battery Charging System and Method”. *U.S. Patent number 3852652*, Dec 3, 1974.

Jeon, D.H., 2014. “Numerical Modeling of Lithium Ion Battery for Predicting Thermal Behavior in a Cylindrical Cell”. *Journal of Current Applied Physics*, 14, 2, pp. 196-205.

Jeon, D.H., Baek, S.M., 2011. “Thermal Modeling of Cylindrical Lithium Ion Battery during Discharge Cycle”. *Energy Conversion and Management*, 52, 8–9, pp. 2973-2981.

Ji, Y., Zhang, Y., and Wang, C. Y., 2013. “Li-Ion Cell Operation at Low Temperatures”. *Journal of the Electrochemical Society*. 160(4), pp. A636–A649.

Jian, G., Si-Qi, S., Hong, L., 2016. “Brief Overview of Electrochemical Potential in Lithium Ion Batteries”. *Chinese Physics B*, 25(1).

Jiang, F., Peng, P., 2016. “Elucidating the Performance Limitations of Lithium-ion Batteries due to Species and Charge Transport through Five Characteristic Parameters”. *Scientific Reports 6, Article number: 32639.*

Jossen, A., Spath, V., Doring, H., Garche, J., 1999. “Reliable Battery Operation — A Challenge for the Battery Management System”. *Journal of Power Sources*, 84, pp. 283-286.

Julien, C., Mauger, A., Zaghib, K., Groult, H., 2016. “Optimization of Layered Cathode Materials for Lithium-Ion Batteries”. *Materials*, 9, pp. 595.

Kalnaus, S., Wang, Y., Turner, J., 2017. “Mechanical Behavior and Failure Mechanisms of Li-ion Battery Separators”. *Journal of Power Sources*, 348, pp. 255–263.

Kim, Y., Mohan, S., Siegel, J. B., Stefanopoulou, A. G., and Ding, Y., 2014. “The Estimation of Temperature Distribution in Cylindrical Battery

Cells under Unknown Cooling Conditions". *IEEE Transaction on Control System Technology*, 22(6), pp. 2277–2286.

Kim, G.H., Smith, K., Ireland, J., Pesaran, A., 2012. "Fail-safe Design for Large Capacity Lithium-Ion Battery Systems". *Journal of Power Sources*, 210, pp. 243-253.

Kim, G.H., Pesaran, A., 2009. *Fifth International Symposium on Large Lithium Ion Battery Technology and Application*. June 9-10, 2009, Long Beach Convention Center, Long Beach, CaliforniaL, CA.

Kim, G-H., Pesaran, A., Spotniz, R., 2007. "A Three Dimensional Thermal Abuse Model for Lithium-Ion Cells". *Journal of Power Sources*, pp. 476-489.

Kizilel, R., Sabbah, R., Selman, J.R., Al-Hallaj, S., 2009. "An alternative Cooling System to Enhance the Safety of Li-Ion Battery Packs". *Journal of Power Sources*, 194, pp. 1105-1112.

Koo, B., Goli, P., Sumant, A. V., dos Santos Claro, P. C., Rajh, T., Johnson, C. S., Balandin, A. A., Shevchenko, E. V., 2014. "Toward Lithium Ion Batteries with Enhanced Thermal Conductivity". *American Chemical Society, Nano*, 8(7), pp. 7202–7207.

Kutkut, N., and Divan, D., 1996. "Dynamic Equalization Techniques for Series Battery Stacks". *Proceedings of IEEE, International*

Telecommunications Energy Conference (INTELEC), pp.514-521, 6-10 October, 1996, Boston, MA, USA.

Lamb, J., and Orendorff, C., 2014. “Evaluation of Mechanical Abuse Techniques in Lithium ion Batteries”. *Journal of Power Sources*, 247, pp. 189-196.

Le, A., Wang, M., Shi, Y., Noelle, D.J., Qiao, Y., 2015. “Heat Generation of Mechanically Abused Lithium-Ion Batteries modified by Carbon Black Micro-Particulates”. *Journal of Physics D: Applied Physics*, Volume 48, Number 38.

Lei, B., Zhao, W., Ziebert, C., Uhlmann, N., Rohde, M., Seifert, H.J., 2017. “Experimental Analysis of Thermal Runaway in 18650 Cylindrical Li-Ion Cells Using an Accelerating Rate Calorimeter”. *Batteries* 3, 14.

Leng, F., Tan C.M., Pecht M., 2015. “Effect of Temperature on the Aging Rate of Li Ion Battery Operating above Room Temperature”. *Science Report*. August 5, 2015

L’Eplattenier, P., Caldichoury, I., 2013. “Electromagnetism (EM) Module presentation*”.https://www.dynamore.de/de/download/presentation/dokumente/2013-multiphysik/em-mp2013.pdf. March 2013*.

Li, Z., Zhang, J., Wu, B., et al., 2013. “Examining Temporal and Spatial Variations of Internal Temperature in Large-Format Laminated

Battery with Embedded Thermocouples". *Journal of Power Sources*, 241, pp. 536-553.

Lingeman, J., 2013. "Tesla Model S burns in Seattle". *Autoweek, 2013. http://autoweek.com/article/car-news/tesla-model-s-burns-seattle* (Accessed 04/2014).

Lisbona, D., Snee, T., 2011. "A Review of Hazards Associated with Primary Lithium and Lithium-ion Batteries". *Journal of Process Safety and Environmental Protection*, 89, pp.434-442.

Liu, J., Wang, Z., Gong, J., Liu, K., Wang, H., Guo, L., 2017. "Experimental Study of Thermal Runaway Process of 18650 Lithium-Ion Battery". *Materials*, 10 (3), 230.

Littlefuse, 2017. "Fuses Vs PTCs". http://www.littelfuse.com/about-us/education-center/fuses-vs-ptcs.aspx (Accessed 11/2017).

Lotfi, N., Fajri, P., Novosad, S., Savage, J., Landers, R.G., Ferdowsi, M., 2013. "Development of an Experimental Testbed for Research in Lithium-Ion Battery Management Systems". *Energies*, 6, pp. 5231-5258.

Lopez, C., Jeevarajan, J., Mukherjee, P., 2015. "Characterization of Lithium-Ion Battery Thermal Abuse Behavior Using Experimental and Computational Analysis". *Journal of Electrochemical Society*, 162, 10, pp. A2163-A2173.

"LS-DYNA Consistent units". *LS-DYNA Support, 2017. http://www.dynasupport.com/howtos/general/consistent-units*. (Accessed January 2017).

"LS-DYNA keyword user's manual, volume (ii) material models, LSTC, LS-DYNA R8.0". *http://www.dynasupport.com/manuals/ls-dyna-manuals/ls-dyna-manual-r-8.0-vol-ii*. (Accessed June 2016).

Lu, L., Han, X., Li, j., Hua, J., Ouyang, M., 2013. "A review on the Key Issues for Lithium-ion Battery Management in Electric Vehicles". *Journal of Power Sources*, 226, pp. 272-288.

Maleki, H. and Howard, J.N., 2009. "Internal short circuit in Li-ion Cells". *Journal of Power Sources*, 191, 2, pp. 568-574.

Martínez-Rosas, E., Vasquez-Medrano, R., Flores-Tlacuahuac, A., 2011. "Modeling and Simulation of Lithium-Ion Batteries". *Computers and Chemical Engineering*, 35, pp. 1937–1948.

Marcicki, J., Zhu, M., Bartlett, A., Yang, X.G., Chen, Y., Miller, T., L'Eplattenier, P., Caldichoury, I., 2017. "A Simulation Framework for Battery Cell Impact Safety Modeling Using LS-DYNA". *Journal of the Electrochemical Society*, 164(1), pp. A6440-A6448.

Marcicki, J., Bartlett, A., Yang, X.G., Mejia, V., Zhu, M., Chen, Y., L'Eplattenier, P., Çaldichoury, I., 2016. "Battery abuse case study using LS-DYNA". *14th LS-DYNA user conference, June 2016*.

Marzougui, D., Brown, D., Park, H.K., Kan, C.D., Opiela, K.S., 2014. "Development & Validation of a Finite Element Model for a Mid-Sized Passenger Sedan". *13th International LS-DYNA Users Conference, 2014*.

"Material selector for LS-DYNA, 20162. *LSTC website, http://www.lstc.com/dynamat/*. (Accessed on June 2016)

Mayyas, A.R., Omar, N., Pisu, P.,Al-Ahmer, A., Mayyas, A., Montes, C.,Dongri, S., 2011. "Comprehensive Thermal Modeling of a Power-Split Hybrid Powertrain using Battery Cell Model". *Journal of Power Sources* 196, 15, pp. 6588-6594.

Melcher, A., Ziebert, C., Rohde, M., Lei, B., Seifert, H.J., 2016. "Modeling and Simulation of the Thermal Runaway in Cylindrical18650 Lithium-Ion Batteries". *Proceedings of the 2016 COMSOL Conference, Munich, Germany*.

Mendoza-Hernandez, O.S, Taniguchi, S., Ishikawa, H., Tanaka, K., Fukuda, S., Sone, Y., Umeda, M., 2017. "Accelerating Rate Calorimetry Tests of Lithium-ion Cells before and after Storage Degradation at High Temperature". *E3S Web of Conferences 16, 07001*.

Mendoza-Hernandez, O.S., Ishikawa, H., Nishikawa, Y., Maruyama, Y., Umeda, M., 2015. "Cathode Material Comparison of Thermal

Runaway Behavior of Li-Ion Cells at Different State of Charges including Over Charge2. *Journal of Power Sources* 280, pp. 499-504.

Miller J.M., 2009. “Energy Storage System Technology Challenges facing Strong Hybrid, Plugin and Battery Electric Vehicles”. *Proceedings of IEEE, Vehicle Power and Propulsion Conference, VPPC '09*. 7-10 Sept. 2009, Dearborn, MI, USA.

Moloughney, T., 2013. “Another Model S fire. Tesla Motors Club, 2013”. *https://teslamotorsclub.com/tmc/threads/ugh-another-model-s-fire-2013-11-06.23581/* (Accessed 03/2014).

Moore, S., and Schneider, P., 2001. “A Review of cell equalization methods for Lithium Ion and Lithium polymer battery systems”. *Proceedings of the SAE World Congress*, 5th March, 2001.

Morris, C., 2013. “Mitsubishi finds cause of battery fires”. https://chargedevs.com/newswire/mitsubishi-finds-cause-of-battery-fires/ (Accessed 11/2017).

Musk, E., 2014. “Tesla Adds Titanium Underbody Shield and Aluminium Deflector Plates to Model S. Tesla Motors Inc., 2014”. *http://www.teslamotors.com/blog/tesla-adds-titanium-underbody-shield-and-aluminum-deflector-plates-model-s*. (Accessed 2017).

Nadimpalli, S.P.V., Sethuraman, V.A., Abraham, D.P., Bower, A.F., Guduru, P.R., 2015. “Stress Evolution in Lithium-Ion Composite

Electrodes during Electrochemical Cycling and Resulting Internal Pressures on the Cell Casing". *Journal of the Electrochemical Society*, 162(14), pp. A2656-A2663.

Onda, K., Ohshima, T., Nakayama, M., Fukuda, K., Araki, T., 2006. "Thermal Behavior of Small Lithium-Ion Battery during Rapid Charge and Discharge Cycles". *Journal of Power Sources*, 158, 1, pp. 535–542.

Orendorff, C.J., Lamb, J., Steele, L., Anna, M., Spangler, S.W., Langendorf, J., 2016. "Quantification of Lithium-ion Cell: Thermal Runaway Energetics" *SANDIA REPORT, Report Number, SAND2016-0486*.

Orendorff, C.J., Lamb, J., Anna, M., Steele, L-A., Spangler, S.W., 2014. "Propagation Testing Multi-Cell Batteries". *SANDIA REPORT, SAND2014-17053, October 2014*.

Rad, M.S., Rad, Danilov, D.L., Baghalha, M., Kazemeini, M., P.H., Notten, P.H., 2013. "Adaptive Thermal Modeling of Li-Ion Batteries". *Journal of Electrochimica Acta*, 102, pp.183-195.

Ramadesigan, V., Northrop, P.W.C., De, S., Santhanagopalan, S., Braatz, R.D., Subramanian, V.R., 2012. "Modeling and simulation of Lithium-Ion Batteries from a Systems Engineering Perspective". *Journal of the Electrochemical Society*, 159, pp. R31–R45.

Richardson, R. R., Ireland, P. T., Howey, D. A., 2014. “Battery Internal Temperature Estimation by Combined Impedance and Surface Temperature Measurement”. *Journal of Power Sources*, 265, pp. 254–261.

Roscher, M.A., Bohlen, O., Vetter, J., 2011. 2OCV Hysteresis in Li-Ion Batteries including Two-Phase Transition Materials2. International *Journal of Electrochemistry*, pp.6.

Roth, E.P., Doughty, D.H., 2004. “Thermal Abuse Performance of High-Power 18650 Li-ion Cells”. *Journal of Power Sources*, 128, pp. 308-318.

Sabbah, R., Kizilel, R., Selman, J.R., Al-Hallaj, S., 2008. “Active (Air-Cooled) vs. Passive (Phase Change Material) Thermal Management of High Power Lithium-Ion Packs: Limitation of temperature Rise and Uniformity of Temperature”. *Journal of Power Sources*, 182, 2, pp. 630-638.

Sahraei, E., Bosco, E., Dixon, B., Lai, B., 2016. “Microscale Failure Mechanisms Leading to Internal Short Circuit in Li-ion Batteries under Complex Loading Scenarios”. *Journal of Power Sources*, 319, pp. 56-65.

Sahraei, E., Campbell, J., Wierzbicki, T., 2012a. “Modeling and short circuit detection of 18650 Li-ion cells under mechanical abuse conditions”. *Journal of Power Sources*, 220, pp. 360-372.

Sahraei, E., Hill, R., Wierzbicki, T., 2012b. “Calibration and Finite Element Simulation of Pouch Lithium-Ion Batteries for Mechanical Integrity”. *Journal of Power Sources*, 201, pp. 307-321.

Sahraei, E., Kahn, M., Meierc J., Wierzbicki, T., 2015. “Modelling of Cracks Developed in Lithium-Ion Cells under Mechanical Loading”. *Royal Society of Chemistry Advances, 5:80369*.

Sahraei, E., Meier, J., Wierzbicki, T., 2014. “Characterizing and Modeling Mechanical Properties and Onset of Short Circuit for Three Types of Lithium-Ion Pouch Cells”. *Journal of Power Sources*, 247, pp. 503–516.

Sahraei, E., Wierzbicki, T., Hill, R., Luo, M., 2010. “Crash Safety of Lithium-ion Batteries towards Development of a Computational Model”. *SAE Technical Paper 2010-01-1078, Detroit, Michigan USA*, April 13- April 15, 2010.

Santhanagopalan, S., Ramadass, P., Zhang, J., 2009. “Analysis of Internal Short-Circuit in a Lithium ion Cell”. *Journal of Power Sources*, 194, pp. 550-557.

Saw, L.H., YYe, Y., Tay, A.A.O., 2014. “Electro-Thermal Characterization of Lithium Iron Phosphate Cell with Equivalent Circuit Modelling”. *Journal of Energy conversion and management*, 87, pp. 367-377.

Scapin, M., Peroni, L. & Fichera, C., 2014. “Investigation of Dynamic Behaviour of Copper at High Temperature”. *Journal Materials at High Temperatures*, 31, 2 pp. 131–140.

Selman, J.R., Al-Hallaj, S., Uchida, I., Hirano, Y., 2001. “Cooperative Research on Safety Fundamentals of Lithium Batteries”. *Journal of Power Sources*, 97-98, pp. 726-732.

Seppala, T.J., 2013. “Tesla Model S Catches Fire after Battery Puncture, Musk Responds”. *https://www.engadget.com/2013/10/04/tesla-model-s-battery-fire-musk-response*. (Accessed on April 2017).

Shah, K., Drake, S. J., Wetz, D. A., Ostanek, J. K., Miller, S. P., Heinzel, J. M., Jain, A., 2014. “An Experimentally Validated Transient Thermal Model for Cylindrical Li-Ion Cells”. *Journal of Power Sources*, 271, pp. 262–268.

Shan, M.X., 2016. “Analysis on Thermal Runaway of Lithium Ion Battery”. *Proceedings of International Conference on Applied Mechanics, Mechanical and Materials Engineering (AMMME 2016)*.

Sheikh, M., Elmarakbi, A., Rehman, S., 2017. “Thermal and Electrical Failure Analysis of Lithium-Ion Battery after Crash”. *Proceedings of*

2nd International Electrical Engineering Conference (IEEC). May 19th-20th, 2017, at IEP Centre, Karachi, Pakistan.

Sheikh, M., Baglee, D., Knowles, M., Elmarakbi, A., Al-Hariri, M., 2015. "A Novel Approach for Predicting Thermal Runaway in Electric Vehicle Batteries when Involved in a Collision". *Proceedings of ASME, International Mechanical Engineering Congress & Exposition (IMECE)*, November 13-19, 2015, Houston, Texas, USA.

Shi, Y., Noelle, D.J., Wang, M., Le, A.V., Yoon H., Zhang M., Meng, Y., Qiao, Y., 2016. 1Exothermic Behaviors of Mechanically Abused Lithium-ion Batteries with Dibenzylamine". *Journal of Power Sources*, 326, pp. 514-521.

Siguang, L., and Chengning, Z., 2009. "Study on Battery Management System and Lithium-ion Battery". *Proceedings of IEEE, International Conference on Computer and Automation Engineering (ICCAE '09)*, 8-10 March 2009, Bangkok, Thailand.

"Single Cell Thermal Runaway Initiation (SCTRI)". *Report of NHTSA, Pages 168 – 289, www.nhtsa.gov*. (Accessed on 27/04/2017).

Slik, G., Vogel, G., Chawda, V., 2006. "Material Model Validation of a High Efficient Energy Absorbing Foam". *5th LS-DYNA forum, 12-13 October 2006, Ulm, Germany.*

Smith, B., 2012. “Chevrolet Volt Battery Incident Summary Report”. *Washington, DC, 20 January 2012, (Downloaded 04/2017).* *https://wwwodi.nhtsa.dot.gov/acms/cs/jaxrs/download/doc/UCM399393/INRP-PE11037-49880.pdf*.

Smith, K., Kim, G.H., Darcy, E., Pesaran, A., 2010. “Thermal/Electrical Modeling for Abuse-Tolerant Design of Lithium Ion Modules”. *International Journal of Energy Research*, 34, 2, pp.204-215.

Smith, K.A., Rahn, C.D., Wang, C.Y., 2007. “Control oriented 1D electrochemical model of lithium ion battery”. *Energy Conversion and Management*, 48, 9, pp. 2565-2578.

Somasundaram, K., Birgersson, E., Mujumdar, A.S., 2012. “Thermal-electrochemical model for passive thermal management of a spiral-wound lithium-ion battery”. *Journal of Power Sources*, 203, pp. 84-96.

Soylu, E., Soylu, T., Bayir, R., 2017. “Design and Implementation of SOC Prediction for a Li-Ion Battery Pack in an Electric Car with an Embedded System”. *Entropy*, 19, 146.

Spinner, N. S., Field, C. R., Hammond, M. H., Williams, B. A., Myers, K. M., Lubrano, A. L., Rose-Pehrsson, S. L., Tuttle, S. G., 2015a. “Physical and Chemical Analysis of Lithium-Ion Battery Cell-to-Cell Failure

Events Inside Custom Fire Chamber". *Journal of Power Sources*, 279, pp. 713–721.

Spinner, N. S., Mazurick, R., Brandon, A., Rose-Pehrsson, S. L., Tuttle, S.G., 2015b. "Analytical, Numerical and Experimental Determination of Thermophysical Properties of Commercial 18650 LiCoO2 Lithium-Ion Battery". *Journal of the Electrochemical Society*, 162(14), pp. A2789–A2795.

Spotnitz, R., Franklin, J., 2003. "Abuse Behavior of High-Power Lithium-ion Cells". *Journal of Power Sources*, 113, pp. 81-100.

Sung, W., Shin, C., 2015. "Electrochemical Model of a Lithium-ion Battery Implemented into an Automotive Battery Management System". *Computers & Chemical Engineering*, 76, pp. 87-97.

Taiwo, O., Finegan, D., Gelb, J., Holzner, C., Brett, D., Shearing, P., 2016. "The use of contrast enhancement techniques in X-ray imaging of lithium–ion battery electrodes". *Journal of Chemical Engineering Science*, 154, pp. 27-33

Tang, L., Zhang, J., Cheng, P., 2017. "Homogenized Modeling Methodology for 18650 Lithium-ion Battery Module under Large Deformation". *PLOS ONE 12(7): e0181882*.

Taylor, M., 2014. "Joule Counting Correction for Electric Vehicles Using Artificial Neural Networks". *Proceedings of the Twenty-Eighth,*

Association for the Advancement of Artificial Intelligence (AAAI) Conference on Artificial Intelligence.

The Engineering tool box, 2017. *http://www.engineeringtoolbox.com/young-modulus-d_417.html*. (Accessed on May 2017).

Tobishima, S., Yamaki, J., 1999. "A consideration of lithium cell safety". *Journal of Power sources*, 81-82, 882-886.

Tourani, A., White, P., Ivey, P., 2014. "A Multi Scale Multi-Dimensional Thermo Electrochemical Modelling of High Capacity Lithium-Ion Cells". *Journal of Power Sources*, 255, pp.360-367.

Trattnig, G. and Leitgeb, W., 2014. "Battery Modelling for Crash Safety Simulation". *Virtual Vehicle Research Center, Graz, Austria, Automotive Engineering. Simulation and Validation Methods, DOI: 10.1007/978-3-319-02523-0_2.*

Viswanathan, V.V., Choi, D., Wang, D., Xu, W., Towne, S., Williford, R.E., Zhang, J.G., Liu, J., Yang, Z., 2010. "Effect of Entropy Change of Lithium Intercalation in Cathodes and Anodes on Li-ion Battery Thermal Management". *Journal of Power Sources*, 195, 11, pp. 3720–3729.

Wang, H., Lara-Curzio, E., Winchester, C., Rule, E.T., Helmer, J., 2017a. "Thermal Runaway Risk Assessment by Mechanically Induced Internal Short Circuit". *January 2017, http://www.prba.org/wp-*

content/uploads/Internal-short-circuit-BatterySafetyCouncil-Jan2017.pdf. (Accessed on April 2017).

Wang, H., Lara-Curzio, E., Rule, E.T., Winchester, C.S., 2017b. 2Mechanical Abuse Simulation and Thermal Runaway Risks of Large-Format Li-ion Batteries". *Journal of Power Sources*, 342, pp. 913-920.

Wang, Q., He, Y.J., Shen, J., Ma, Z., Zhong, G., 2017. "A Unified Modeling Framework for Lithium-ion Batteries: An Artificial Neural Network based Thermal Coupled Equivalent Circuit Model Approach". *Energy*, 138, pp. 118-132.

Wang, M., Le, A.V., Shi, Y., Noelle, D.J., Yoon, H., Zhang, M., Meng, Y.S., Qiao, Y., 2016. "Effects of angular fillers on thermal runaway of lithium-ion battery". *Journal of Materials Science and Technology*. 32, 11, pp. 1117-1121.

Wang, S., 2016. "Entropy and heat generation of lithium cells/batteries". *Chinese Journal of Physics: B*, 25, 1.

Wang, W.W., YANG, S., Lin, C., 2016. "Clay-like Mechanical Properties of Components for the Jellyroll of Cylindrical Lithium-ion Cells". *Energy Procedia*, 104, pp. 56 – 61.

Wang, T., Tseng, K. J., Zhao, J., Wei, Z., 2014. "Thermal Investigation of Lithium-Ion Battery Module with Different Cell Arrangement

Structures and Forced Air-Cooling Strategies". *Applied Energy*, 134, pp. 229–238.

Wang, Z., Shi, S., Liu, P., 2011. "Research progress on collision safety of electric vehicles". *Proceedings of the Third International Conference on Measuring Technology and Mechatronics Automation (ICMTMA)*, 2011. 6-7 Jan. 2011, Shangshai, China.

Wang, Q., Sun, J. and Chu, G., 2005. "Lithium Ion Battery Fire and Explosion. Fire Safety Science". *Proceedings of the eighth international symposium*, 18-23 September 2005, Beijing, China, pp. 375-382.

Westerhoff, U., Kurbach, K., Lienesch, F., Kurrat, M., 2016. "Analysis of Lithium-Ion Battery Models Based on Electrochemical Impedance Spectroscopy". *Energy Technology*, 4, pp. 1620–1630.

Wierzbicki, T., Sahraei, E., 2016. "Homogenized mechanical properties for the jellyroll of cylindrical Lithium-ion cells". *Journal of Power Sources*, 241, pp. 467-476.

Wong, Q., Ping, P., Zhao, X., Chu, G., Sun, J., Chen, C., 2012. "Thermal Runaway caused Fire and Explosion of Lithium-ion Battery". *Journal of Power Sources*, 208, pp. 210–224.

Woodbank Communications Ltd 2005. “Battery and energy technologies. Battery management systems”. http://www.mpoweruk.com/bms.htm#top. (Accessed 05/01/2014).

Wu, Z., Weng, R., Zhang, Z., Li, J., 2016. “A Novel Equivalent Circuit Model for Lithium-ion Battery with Complex Electrical Element Parameters”. *Proceedings of SAE 2016 World Congress and Exhibition*, Technical Paper 2016-01-119.

Xia, Y., Wierzbicki, T., Saharei, E., Zhang, X., 2014. “Damage of Cells and Battery Pack due to Ground Impact”. *Journal of Power Sources*, 267, pp. 78-97.

Xu, J., Liu, B., Wang, X., Hu, D., 2016. “Computational Model of 18650 Lithium-Ion Battery with Coupled Strain Rate and SOC Dependencies”. *Applied Energy*, 172, pp. 180–189.

Xu, J., Liu, B., Hu, D., 2016. “State of Charge Dependent Mechanical Integrity Behavior of 18650 Lithium-ion Batteries”. *Scientific Reports* 6, 21829; doi: 10.1038/srep21829 (2016).

Xu, D., Wang, L., Yang, J., 2010. “Research on Li-ion Battery Management System”. *Proceedings of the International Conference on Electrical and Control Engineering (ICECE)*, 25-27 June 2010, Wuhan, China.

Yang, Q., Xu, J., Cao, B., Li, X., 2017. “A simplified fractional order impedance model and parameter identification method for lithium-ion batteries”. *PLOS ONE*, 12(2): e0172424.

Yang, H; Amiruddin, S; Bang, H.J; Sun, Y-K; Prakash, J., 2006. “A review of Li-ion cell chemistries and their potential use in hybrid electric vehicles”. *Journal of Industrial and Engineering Chemistry*, 12(1), pp.12-38.

Yang, H., Bang, H., Amine, K., Prakash, J., 2005. “Investigations of the Exothermic Reactions of Natural Graphite Anode for Li-Ion Batteries during Thermal Runaway”. *Journal of the Electrochemical Society*, 152, 1, pp. A73-A79.

Yeow, k., Teng, H., Thelliez, M., Tan, E., 2012. “3D Thermal Analysis of Li-Ion Battery Cells with Various Geometries and Cooling Conditions using Abaqus”. *Proceedings of the SIMULIA Community Conference 2012*. May 15-17, 2012, Providence RI, USA.

Yiu, K., 2011. “Battery Technologies for Electric Vehicles and Other Green Industrial Projects”. *Proceedings of IEEE, 4th International Conference on Power Electronics Systems and Applications (PESA)*, 8-10 June 2011, Hong Kong, China.

Zhang, Z., Jin, Z., Wyatt, P., 2017. “Electrochemical Modeling of Lithium Plating of Lithium Ion Battery for Hybrid Application". *SAE International Journal of Alternative Powertrains*, 6, 2.

Zhang, X., Sahraei E., Wang, K., 2016. “Li-ion Battery Separators, Mechanical Integrity and Failure Mechanisms Leading to Soft and Hard Internal Shorts”. *Scientific Reports*. 6:32578.

Zhang, J., Su, L., Li, Z., Sun, Y., Wu, N., 2016. “The Evolution of Lithium-Ion Cell Thermal Safety with Aging Examined in a Battery Testing Calorimeter”. *Batteries*, 2, 12.

Zhang, C., Santhanagopalan, S., Sprague, M.A., Pesaran, A.A., 2015a. “Coupled Mechanical-Electrical-Thermal Modeling for Short-Circuit Prediction in a Lithium-Ion Cell under Mechanical Abuse”. *Journal of Power Sources*, 290, pp. 102–113.

Zhang, C., Santhanagopalan, S., Sprague, M.A., Pesaran, A.A., 2015b. “A Representative-Sandwich Model for Simultaneously Coupled Mechanical-Electrical-Thermal Simulation of a Lithium-Ion Cell under Quasi-Static Indentation Tests”. *Journal of Power Sources*, 298, pp. 309–321.

Zhang, G., Cao, L., Ge, S., Wang, C. Y., Shaffer, C. E., Rahn, C. D., 2014. “In Situ Measurement of Radial Temperature Distributions in

Cylindrical Li-Ion Cells". *Journal of the Electrochemical Society*, 161(10), pp. A1499–A1507.

Zhao, W., Luo, G., Wang, C.H., 2015. "Modeling Nail Penetration Process in Large-Format Li-Ion Cells". *Journal of the Electrochemical Society*, 162 (1), pp. A207-A217.

Zhao, R., Gu, J., Liu, J., 2014. "An Investigation on the Significance of Reversible Heat to the Thermal Behavior of Lithium Ion Battery through Simulations". *Journal of Power Sources*, 266, pp. 422–432.

Zheng, W., Lan, F., Cheng, J., LI, Z., 2017. "Compression Experiment and Simulation on Prismatic Lithium-ion Batteries". *Proceedings of International Conference on Energy, Power and Environmental Engineering (ICEPEE 2017)*.

Appendix A: Author's Publications

Sheikh, M., Elmarakbi, A., Elkady, M., 2017. "Thermal runaway detection of cylindrical 18650 lithium-ion battery under quasi-static loading conditions". Journal of Power Sources, 370, pp. 61–70.

Sheikh, M., Elmarakbi, Elkady, M., 2017. "A combined experimental and simulation approach for short circuit prediction of 18650 lithium-ion battery under mechanical abuse conditions", under review in Journal of Applied Energy.

Elkady, M., Sheikh, M., Elmarakbi, A., 2017. "Numerical Analysis for Vehicle Collision Mitigation and Safety Using Dynamics Control Systems", Advances in System Dynamics and Control. (Accepted)

Sheikh, M., Elmarakbi, A., Rehman, S., 2017. "Thermal and Electrical Failure Analysis of Lithium-Ion Battery after Crash". Proceedings of 2nd International Electrical Engineering Conference (IEEC). May 19th-20th, 2017, at IEP Centre, Karachi, Pakistan.

Sheikh, M., Elmarakbi, A., 2017. "State of Charge (SOC) dependent separator failure analysis of lithium-ion battery", Submitted to Journal of Applied Material Today.

Sheikh, M., Elmarakbi, A., Rehman, S., 2017. "Numerical simulation model for short circuit prediction under compression and bending of 18650 cylindrical lithium-ion battery". IET conference PEMD 2018.

Sheikh, M., Baglee, D., Knowles, M., Elmarakbi, A., Al-Hariri, M., 2015. “A Novel Approach for Predicting Thermal Runaway in Electric Vehicle Batteries when Involved in a Collision”. Proceedings of ASME, International Mechanical Engineering Congress & Exposition (IMECE), November 13-19, 2015, Houston, Texas, USA.

Sheikh, M., Elmarakbi, A., 2017. “Numerical simulation model of Graphene based electrode for energy storage devices to enhance safety and performance”. To be submitted in Elsevier journal of Power Sources or Applied Energy.

Sheikh, M., Elmarakbi, A., 2017. “Temperature distribution of cylindrical 18650 lithium-ion battery due to various loading conditions”. To be submitted in Energies.